Nucleation of polypropylene: synthesis and characterization of organo functionalized nanosilica particles

K. Venkatakrishna, K. Sreenivas, K. Vijayamohanan* and C. Ramesh

Divison of Polymer Science and Engineering and Division of Physical Chemistry National Chemical Laboratory,
Pune-411 008, Maharashtra

Email: c.ramesh@ncl.res.in

Abstract:

The aim of the present work was to study the nucleation effect of Organo functionalized silica nanoparticles on Polypropylene (PP). To that end, monodisperse nanosilica particles were prepared by hydrolysis and condensation of tetraalkoxysilanes according to the method developed by Sto-ber, with tetraethoxy silane (TEOS), deionized water, and ammonia (NH_4OH) as a catalyst in the presence of ethanol (C_2H_5OH). Nanosilica particles having different particle size were prepared by changing the molar ratio of ammonia. The nanoparticles were organo functionalized with octadecyl trichlorosilane (OTS), octadecyl trimethoxysilane (OTDMS), aminopropyl trimethoxysilane (APTMS), mixture of OTS-APTMS (1:1), oleic acid (OA) and γ-methacrloxypropyl trimethoxysilane (KH-570). The nanoparticles were characterized using Fourier Transform Infrared spectroscopy (FTIR), Thermo Gravimetric Analysis (TGA) and SEM. The nucleating efficiency of these particles on PP was studied using optical microscopy and differential scanning microscopy.

Introduction:

Polypropylene (PP) is one of the most widely used thermoplastic both domestic and industrial purposes. Nucleating agents are used not only because they can significantly increase the crystallization rate of polymers and therefore the rate of production of artifacts, but also because they would dramatically and alter the structure and morphology and therefore, modify the physical, mechanical, and optical properties. A variety of nucleating agents are known to nucleate PP.[1, 2] Talc, mica, sodium2, 2'methylenebis (4, 6-di-tert-butylephenylene) phosphate (NA-11), silica, calcium carbonate and Millad 3988 (Benzene sorbitol derivative) are well known nucleators for PP. The addition of nucleating agent molecules into polymer will modify the crystallization process and the morphology that subsequently forms.[2, 3] In this present work we study the nucleation of polypropylene using surface modified nano silica particles.

Experimental Section:

Materials:

Tetraethoxy orthosilane (TEOS), 95% Octadecyl trichlorosilane (OTS), Octadecyl trimethoxy silane (ODTMS), Amino propyl trimethoxy silane (APTMS), Oleic acid and (OA) were purchased from Aldrich Chemicals. γ-methacrloxy propyl trimethoxy silane (KH-570) was purchased from fluka chemicals. Ethanol (99%), Ammonia solution (25%), toluene, and O-xylene were purchased from Merck specialities private Ltd. The isotactic polypropylene was purchased from RIL India.

Monodisperse, nanosilica particles were synthesized by Sto-ber[4] method. In brief, 1.5 ml of tetraethyl orthosiline (TEOS) was added to 25 ml of ethanol (C_2H_5OH) and stirred for 10 min. To this 1ml of deionized water was added. After completion of 10 min, the mixture of 25ml

C_2H_5OH and 1.7ml of NH_4OH (25%) was added in drop wise to the above reaction mixture. The total reaction was carried out at 40°C for 3hrs with continuous stirring. Then another 1ml of TEOS was added after being stirred for another 3hrs in presence of the same conditions. The particles obtained were separated by centrifuge and washed several times with C_2H_5OH and water to remove the excess amount of unreacted chemicals and dried at 65°C under nitrogen atmosphere.

Surface modification of nanosilica particles was performed by the method prior to silaniation[5]. Silica particles were dried for 5 hrs in a vacuum woven at 65°C in the presence of nitrogen atmosphere and were used immediately for silanization process. In this distinctive synthesis procedure, 25 mg of nanosilica particles (60-80 nm) were dispersed in 30 ml of dry toluene with continuous reflection for 30 min. To this mixture 1% OTS (w/w) solution in dry toluene was added drop wise. In order to ensure a complete monolayer formation of OTS on silica, the mixture was refluxed for 24 h under nitrogen atmosphere at 80°C. This solution was then allowed to stand for few hours the particles were separated and washed several times with toluene and ethanol in order to remove the unreacted OTS. The obtained particles were consequently dried in a vacuum oven at 65°C for 5 hrs under nitrogen atmosphere and then used for further characterization. Similarly, the silanization was carried out by changing the % of OTS (w/w) in toluene (i.e., 0.2, 0.5, 1, 2 and 5%) and also by using different silane reagents such as OTS, ODTMS, APTMS, OA, KH570 and mixture of OTS: APTMS to get mixed mono/multilayers on silica.

The nanoparticles were incorporated in PP by melt blending method. The samples were melt blended in DSM micro twin-screw compounder at 200°C at 100 rpm. The typical batch size was ~5g and mixing time was 5minutes. The samples were initially dried in a vacuum oven for 10-12 hours at 65°C before melt blending. About 2000PPM of nanoparticles was added in the PP.

The morphology of the particles was characterized by Scanning electron microscopy (SEM). The surface chemistry of nanosilica was studied using Fourier transform infrared spectroscopy (FTIR) at a resolution of $2cm^{-1}$ in the range 4,000 - 400 $cm^{-1.}$ Thermo gravimetric analysis was carried out on TA Instruments TGA-Q 5000. The non-isothermal crystallization and melting behavior of PP/ Organo-functionalized SiO_2 was investigated using TA Q10 DSC. The Spherulitic morphology of the pristine PP and the PP with nanosilica was studied by using OLYMPUS polarized optical microscope under crossed polarizer.

Results and Discussions:

The preparation of nanoSiO_2 particles has been carried out using well-known method; "stober.[4]" The particle size mainly depended on the amount of ammonia solution and the deionized water. Here ammonia solution acts as a catalyst and called as base catalyzed reaction. When the concentration of ammonia solution is decreased particle size also decreased. However, In order to improve the interface in-between polymer matrix and nanoSiO_2 particles, it is necessary to do the surface modification of nanoSiO_2 particles with organic compounds (organo alkoxy silanes and organo halide silanes). In this present work, nanoSiO_2 particles were surface modified with organoalkoxy silanes and organo halide silanes (silane coupling agents) such as OTS, ODTMS, APTMS, OA, KH-570 and mixture of OTS: APTMS.

The Scanning electron micrographs of nanosilica particles surface modified and unmodified are presented in Figure 1a shows the spherical and agglomerated particles. Figure 1b shows the surface modified particles, which are spherical and non-agglomerated. The size has slightly

increased (2-5nm) and may due to the surface modification and has been observed in all samples surface modified with OTS, ODTMS, APTMS, mixture of OTS: APTMS, OA and KH-570.

Both modified and unmodified nanoSiO_2 particle showed the bands at 1090, 800 and 468cm^{-1}, which could be assigned to –Si-O-Si- vibration modes[7]. In the case of unmodified SiO_2, the band peak at 1660 cm^{-1} could be due to physically/ chemically absorbed water on the surface and the band peak at 3439 cm^{-1} due to –OH group on the SiO_2 surface[8,] The organo functionalized nanoSiO_2 particles shows new peaks at 1645-1623, 2854 and 2926 cm^{-1} and due to –O-Si-C- and stretching vibration modes of $–CH_2$ respectively. The nanoSiO_2 particles surface modified with OTS, OA, KH-570 and ODTMS shows absorption peaks at 2854 cm^{-1} and 2926 cm^{-1} due to symmetrical and asymmetrical $–CH_2$ stretching respectively and the absorption band at 2958 cm^{-1} correspond to asymmetrical $–CH_3$ stretching (Figure 2a) [6,] The new peak had been observed in the case of nanosilica particles surface modifaied with APTMS and mixer of APTMS:OTS between1600-1700 cm^{-1} due to –NH stretching [8], the absorption peak at 3640cm^{-1} due to the N-H stretching. KH-570 shows peaks at 1718cm^{-1} and 1738cm^{-1} and assigned to C=O [9] and the absorption peaks at 1507 cm^{-1} and 1559cm^{-1} may due to C=C on the nanoSiO_2 surface. The new peaks has observed in nanoSiO2 particles were organo-functionalized with oleic acid (OA) at 1521cm^{-1} and 1712cm^{-1} as a result of C=C and –Si-OOC- [10.]

TGA curve Figure 3 shows the moderate weight loss (>5%) before 150°C due the loss of physically absorbed water on the surface of nanoSiO_2 particles and also exhibited a weight loss (< 4%) at 250-600°C, which might be due to chemically bonded water and residual organics typically ethanol of the nanoSiO_2 synthesis. The organo-functionalized nanoSiO_2 particles having two steps of weight loss, one is at about 50-150°C due to the physorbed water, which is of very less percentage. The weight loss from 200-600°C is ascribed to the removal of residual surfactants due to the organic functional groups de-bonding and degradation of grafted silane functional groups on the surface [11]. After 600°C the surface modified nanoSiO_2 particles shows similar to basilica. The thermal stability of the various modified nanosilica is shown in the Table 1.

Figure 4 and Table 2 show that the crystallization temperatures of PP nucleated with nanosilica modified with APTMS. The crystallization temperature varies 114.7°C to 121.6°C by the addition of organo-functionalized nanoSiO_2 particles with different percentages of APTMS. It is clearly indicating that the silica particles act as a nucleating agent for the polymer matrix. All the samples show a melting temperature of ~163°C which is the characteristic melting point of α-phase of PP[12] indicating that the APTMS modified silica acts as an efficient α nucleator. The crystallization temperature increases with increasing amount of modifier on the silica and observed with all the samples modified with OTS, ODTMS, APTMS, OA, KH-570 and mixture of OTS: APTMS.

The nucleation effect of organo-fuctionalized nanoSiO_2 particles on the crystalline structure of PP was observed by Polarized Optical Microscopy. Figure 5 shows that the PP without nucleating agents showing spherulite size of 60 to 90 μm but reduces to very small size on the addition of APTMS modified silica particles and in consistent with thermal data.

Summary and conclusion:

The inorganic silica particles were prepared in nano-scale level by using the ammonia as a base catalyst and these particles were organo-functionalized with different silane coupling agents such as APTMS, KH-570, OA, ODTMS and OTS. The structure and morphology of nanosilica particles were observed through SEM. The thermal degradation of organo-functinalized SiO_2 particles were investigated by TGA, the organo-functionality on silica surface was identified by

FTIR. The result of FTIR and TGA provided a clear evidence of surface modification. Polypropylene nucleated with organo functionalized SiO_2 showed enhanced nucleation indicating that surface modified nanosilica can be an efficient nucleator for PP.

References:

1. Kurja, J.; Mehl, N. A. In Plastics Additives Handbook, 5th ed.; Zweifei, H., Ed.; Hanser: Munich, Germany, 2001.
2. Blomenhofer, M.; Ganzleben, S.; Hanft, D.; Schmidt, H.; Kristiansen, M.; Smith, P.; Stoll, K.; Mader, D.; Hoffmann, K. Macromolecules.2005, 38, 3688.
3. Alootta, F.; Di Marco, G.; Ober, R.; Pieruccini, M. J. Appl. Phys. 2003, 93, 2039.
4. W. Stöber, A. Fink, E.J. Bohn, J. Colloid Interface Sci. 1968, 26, 62.
5. Kulkarni SA, Ogale SB, Vijayamohanan KP. J. Colloid Interface Sci. 2008, 2, 318.
6. R. Y. Hong, H. P. Fu, Y. J. Zhang, L. Liu, J. Wang, H. Z. Li, Y. Zheng, J. Appl. Polymer Sci.2006, 105, 2176.
7. X. J. Xiang, J. W. Qian, W. Y. Yang, M. H. Fang, X. Q. Qian, J. Appl. Polymer Sci.2006, 100, 4333.
9. Indra K. Varma, Anil K. Tomar, R. C. Anand, J. Appl. Polymer Sci.1987, 33, 1377.
10. Z. F. Zhou, H. Huang, N. C. Liu, European Polymer Journal.2001, 37, 1967.
11. Yangyang Sun, Zhuqing Zhang, C.P. Wong, J. Colloid Interface Sci.2005, 292, 436.
12. Wunderlich B. Macromolecular physics, vol.2. New York: Acadamic Press; 1976.

Figures & Tables:

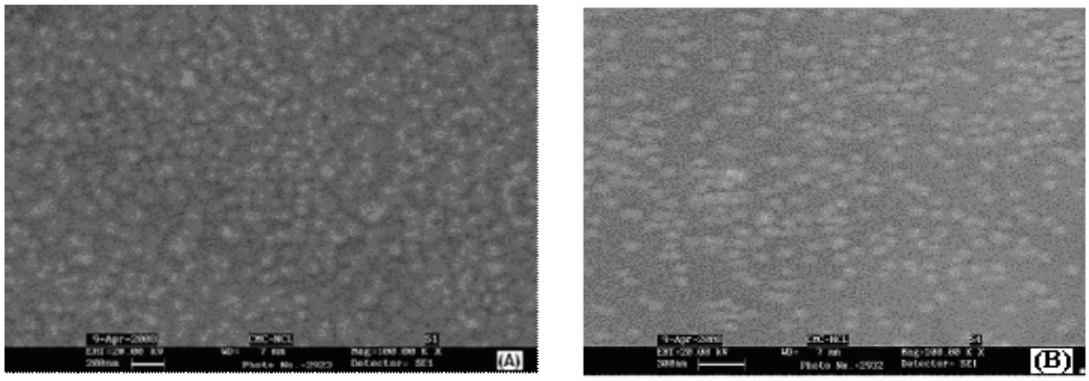

Figure1: (a) Bare silica (b) Organofunc-tionalized SiO_2

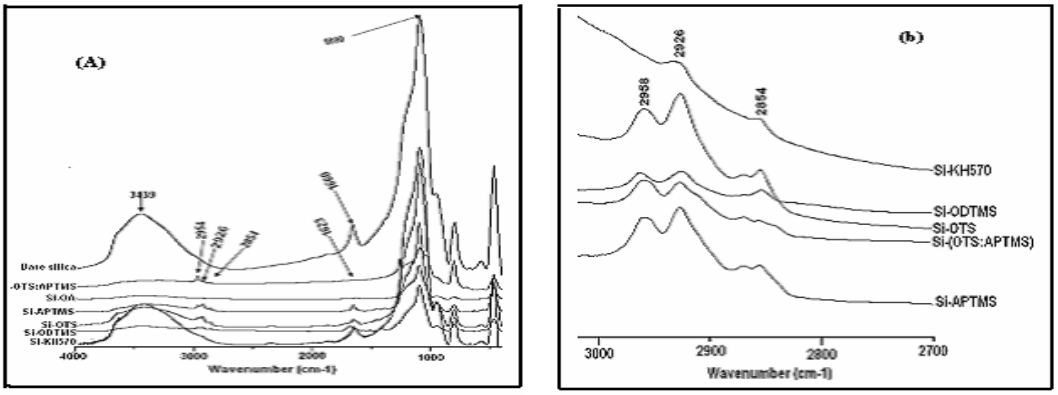

Figure 2: (a) FTIR spectrum of surface modified SiO_2 with OTS, ODTMS, OA, and KH-570
(b) In the frequency region 3000-2700 cm^{-1}

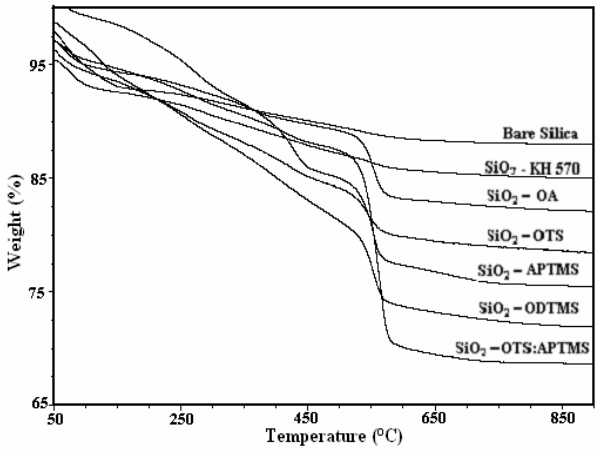

Figure 3: TGA curves of bare silica and surface Modified with different silane coupling agents.

Sample configuration	Maximum degradation temperature °C (T_{max})	Residue at 900°C (Wt %)
Bare silica	130.00	88.27
SiO_2-KH570	551.00	87.37
SiO_2-OA	553.70	83.00
SiO_2-OTS	554.50	82.00
SiO_2-APTMS	553.00	73.60
SiO_2-ODTMS	554.00	72.00
SiO_2-OTS: APTMS	563.50	70.40

Table: 1: Thermal stability of modified and Unmodified nanoSiO_2 particles

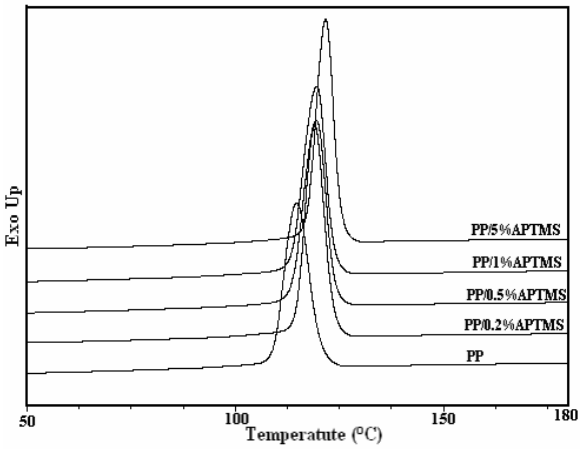

Figure 4: DSC cooling curves of PP/SiO_2 modified with APTMS

Sample configuration	Peak maximum Tc (°C)	Onset Tc (°C)
PP	114.7	120.4
PP /SiO_2 0.2%APTMS	119.1	123.5
PP /SiO_2 0.5%APTMS	119.4	123.7
PP /SiO_2 1%APTMS	119.5	123.6
PP /SiO_2 5%APTMS	121.6	125.3

Table 2: Crystallization temperatures of PP and SiO_2 modified with APTMS

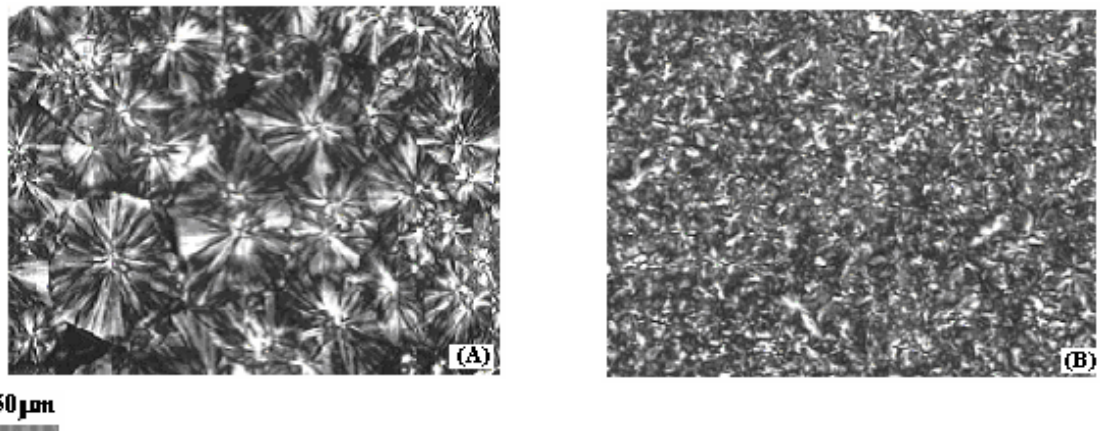

Figure 5: POM images of (a) PP and (b) Organofunctionalized SiO_2 with 0.2%APTMS nanocomposite at room temp after cooling from the melt at 10°C/min.

Droplet orientation and its morphology in polymer dispersed ferroelectric liquid crystal composite films

K K Raina* and Shikha Kapila

Materials Research laboratory, School of Physics and Materials Science, Thapar University, Patiala 147 004 India
*Email: kkraina@gmail.com, kkraina@thapar.edu

Abstract

Multiwalled carbon Nanotubes (CNT) have been dispersed in a chiral smectic c liquid crystal mixture in the ration of 0.05% and 0.1% (wt/wt). Morphological investigations were carried out which shows uniform distribution of the CNT in the liquid crystal matrix. The transition temperature of the liquid crystal increases slightly after dispersing CNT in it. The dielectric constant (measured in the frequency range 50Hz to 1 MHz) increased by about ~ 27%.

1. Introduction

Composites based on liquid crystals (LCs) have attracted much attention in the recent past due to their modified properties with respect to dielectrics, morphological and electro- optic effects and then giving rise to novel display applications. Typical examples of these systems are polymer dispersed liquid crystals [1], suspensions of aerosils in LC matrices [2] and suspensions of nanotubes in ferroelectric LCs [3, 4]. The inclusions in known composite LC systems produce director distortions that extend over macroscopic scales. A new approach, by based on the idea of controlling the properties of the composites by adding a low concentration of nanotubes into a LC matrix, however, has been proposed recently [5]. The earliest attempts to employ the LC orientational order to align CNTs were all done using standard thermotropic nematic hosts [6-9].

Due to their exceptional mechanical, electronic and electromechanical properties, carbon nanotubes are very promising for a wide range of applications [10]. The nanotubes are so small that they do not disturb the LC orientation and thus macroscopically homogeneous structures are obtained. At the same time, the nanotubes are sufficiently large to maintain the intrinsic properties of the materials from which they are made and share these properties with the LC matrix due to anchoring with the LCs [11-14].

Carbon nanotubes (CNT) occur in two general morphologies, single-wall (SWCNT) and multiwall carbon nanotubes (MWCNT). The latter are chemically more resistant and their high aspect ratio together with their flexibility leads to physical entanglement, while attractive Vander Waals interactions between individual nanotubes invariably results in their association in bundles. The latter is also responsible for the generally poor solubility of nanotubes in most solvents.

The research efforts on chiral smectic c liquid crystals (also refered as ferroelectric smectic c liquid crystals) have shown exponential growth soon after their discovery by Meyer et al. in 1975. It is due to the fact that these materials are very interesting for understanding the soft condensed matter and also their practical applications suited for fast electro-optical displays [15, 16]. The dielectric spectra of multiwalled carbon nanotube dispersed ferroelectric liquid crystal gives useful information about the static and the dynamic properties of these compounds. The dielectric spectroscopy behavior of multiwalled carbon nanotube dispersed ferroelectricliquid crystals can also be described by two relaxation processes: the dominant Goldstone mode (GM) due to the phase fluctuations and the softmode (SM) due to the fluctuation in the amplitude of the tilt angle. It appears in the vicinity of SmC*-SmA phase transition temperature (T_{C*A}).

Here we report on the studies of the dielectric properties of a ferroelectric liquid crystal containing carbon nanotubes and the effect of frequency and temperature parameters on the dielectric spectra of material. We found that embedding the carbon nanotubes in LC material results in the change of the dielectric spectra of the matrix, caused by the strong interaction between LC and carbon nanotubes.

2. Experimental

2.1 Materials

The dispersing liquid crystal is an eutectic mixture of ferroelectric liquid crystal(ZLI-4237-100) obtained from E-Merck Darmstadt. Its phase sequence is given by

$$\text{Cryst} \xrightarrow{-20^0C} \text{SmC} \xrightarrow{61^0C} \text{SmA} \xrightarrow{73^0C} \text{N*} \xrightarrow{83^0C} \text{Isotropic}$$

Multi-wall carbon nanotubes (with dimensions 110-170 nm, length between 5-9 micron) used in the experiment was purchased from M/S ALDRICH with reported purity of 90+ %. All materials were used as received without further chemical treatment.

2.2 Methods

One of the most challenging tasks was to uniformly disperse the CNTs in the liquid crystal matrix due to their tendency for aggregate formation. These CNTs aggregates generally form micrometer scale agglomerates that can be seen under optical microscopy. To achieve a finer dispersion of CNTs, sonication at 42 kHz (60^0C) was applied to the CNT mixture. We employed mixing of CNTs in ferroelectric liquid crystal (FLC) at ambient temperature. To ensure proper and uniform dispersion of CNTs, few drops of chloroform were added and further sonificated at isotropic temperature.

The planer cell of 5μm thickness (obtained from M/S Linkam Instruments, UK) was filled with this mixture by capillary action at the isotropic temperature. It consists of two aligned, indium tin oxide (ITO) coated, glass substrates. The alignment was confirmed by viewing the cell through the polarizing microscope (OLYMPUS BX-51P) interfaced to LINKAM-TP94 and THMS600 temperature programmer coupled to hot stage at an accuracy of ±0.1° C. The dielectric measurements were carried out using a programmable automatic RCL meter (FLUKE PM 6306) in the frequency range 50Hz to 1MHz. The cell was calibrated using air and benzene as standard references. The frequency and bias dependence of the real and imaginary parts of the complex dielectric permittivity have been studied in detailed.

3. Results and discussions

3.1 Morphological studies of CNT dispersed FLC

Fig. 1(a) shows optical micrographs exhibiting large CNTs aggregates in the continuum of FLC prepared by simply shaking the compound. Optical micrograph shown in Fig. 1(b), exhibit CNT dispersed through sonification and suggestive of a finer dispersion. The concentration of the CNT-FLC mixtures was diluted by decreasing the concentration of CNTs and the diluted procedure was repeated to achieve very dilute solutions down to about 0.05%wt/wt.

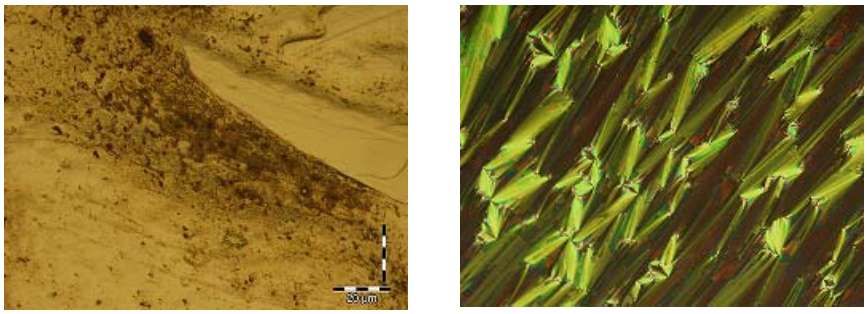

(a) (b)

Fig.1 Optical micrographs of 0.1% MWCNT in FLC (a) with shaking (b) after sonification at 10 X

Fig 2 shows micrographs of a 0.1% CNT concentration obtained under crossed polarizer at an above the smectic–isotropic transition temperature (T_{SI}). Fig 2(a) represents the isotropic state whereas birefringent domain structures appeared at 103^0 C

The structure continues to grow at the expense of the smaller domains (at 99^0C) and then evolves to larger chiral nematic domains exhibiting disclination line (at 95 ºC). The growing chiral nematic domains eventually coalesce at 78^0C and the interface disappears, exhibiting Smectic A phase at ambient temperature. Our textural study confirms that the Smectic A – Smectic C* transition temperature of the mixed CNT-FLC is about 68 ºC higher by about 7 ºC over the undispersed medium. This enhanced T_{NI} in the CNT-FLC mixture may be attributed to the preferred alignment of FLC induced by the CNT bundles [17].

A similar enhanced behavior of transition temperature from N* to isotropic phase can be seen in the 0.05% CNTs concentration. On decreasing to, 0.05%, the transition temperature of N* to isotropic is decreased to 90 ^{0}C. This transition eventually approaches to that of the FLC with further decrease of the nanotube concentration and then declines further to 83 ^{0}C at 0% CNT (FLCs).

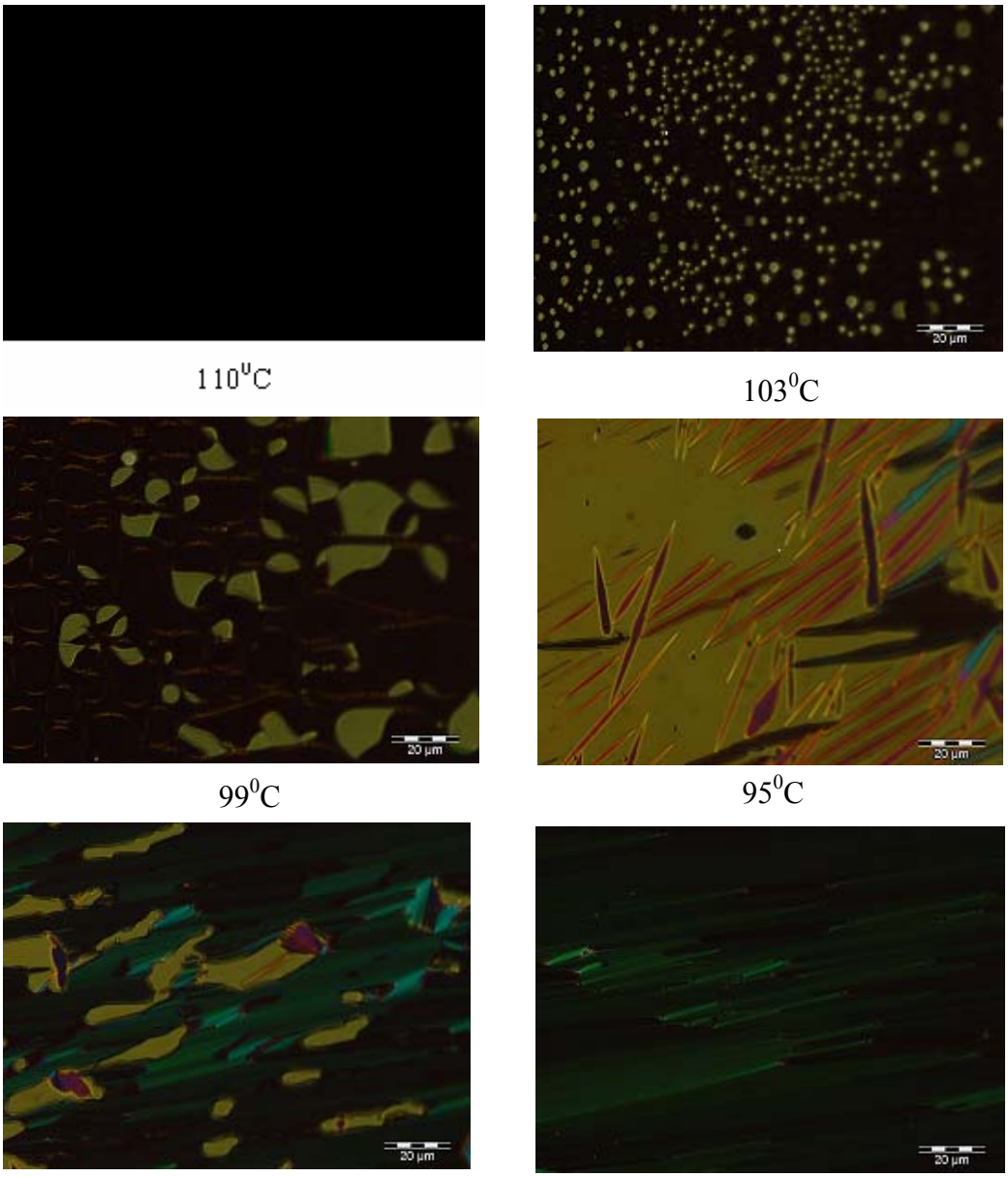

Fig.2. Micrographs showing structural evolution during cooling from the isotropic (110^{0}C) to 78^{0}C at 10X.

3.2 Dielectric spectroscopy constant

3.2.1 Temperature dependence of permittivity (ε')

Fig 3 shows that dielectric permittivity decreases with increasing temperature and then tends to attain saturation beyond 50 ^{0}C as shown in fig. 3. At high temperature, the thermal agitation became more dominant over intermolecular interactions which resulted in collisions between molecules and hence randomization of dipoles. This randomization results in decreased dielectric permittivity.

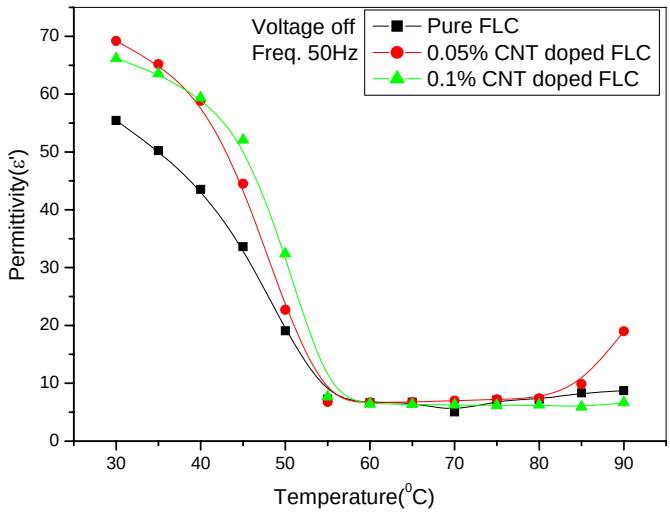

Fig. 3 Dielectric permittivity ε' as a function of temperatures for FLC and CNT dispersed FLC, at 50 Hz.

Fig. 3 shows the effect on the dielectric permittivity of MWNT in ferroelectric liquid crystals at zero biasing and frequency 50 Hz. It was observed that dielectric permittivity increased on dispersing CNT in ferroelectric liquid crystals at lower temperatures but at higher temperatures there was no significant variation in dielectric permittivity values. Such kind of behavior shown by CNT-FLCs composite might be due to the high conductivity and high anisotropic nature of CNT [18] and they had given alignment to liquid crystal molecules results in enhanced dielectric permittivity.

3.2.2 Frequency dependence of permittivity and dielectric loss

The permittivity decreased exponentially up to some frequency at all temperatures in the SmC* phase. At higher frequencies dipoles do not show simultaneous response to electric field and hence they do not align along the field direction. Thus dielectric permittivity was

decreased on increased frequency. Similar effects were seen at SmA phase except that the values were a smaller.

Fig 4 shows the effect on the dielectric permittivity of CNT dispersions in ferroelectric liquid crystals with out any bias voltage at room temperature. It was observed that dielectric permittivity increases on dispersing CNT in ferroelectric liquid crystals at lower frequencies but at higher frequency no significant variation in dielectric permittivity values was noticed

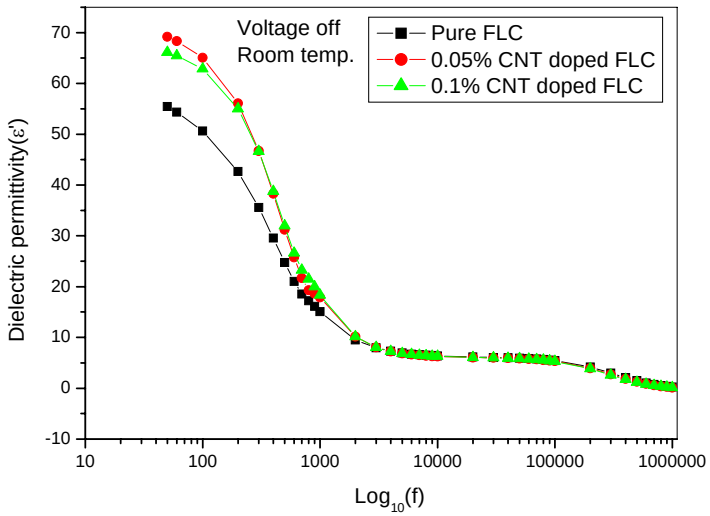

Fig 4 Dielectric permittivity ε' as a function of frequency for FLC and CNT dispersed FLC, at 30° C.

Fig 5 also shows the effect on the dielectric loss of CNT dispersions in ferroelectric liquid crystals at room temperature and zero bias voltage. It was observed that dielectric loss was increased on dispersing CNT in ferroelectric liquid crystals at lower frequencies but at higher frequencies there was no significant variation in dielectric loss. As CNT are conducting in nature, thus on adding the CNT in FLC there should be increased lattice vibration of molecules and hence there would be more dissipation loss. Fig. 5 shows the same behavior as defined in theory.

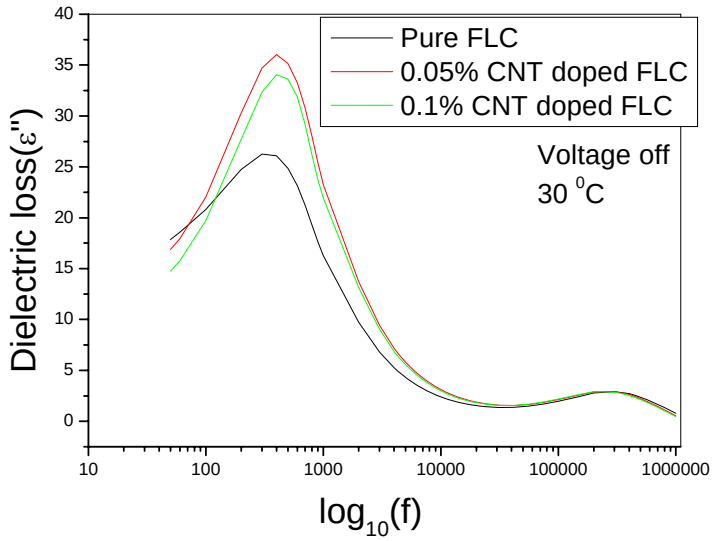

Fig 5 Dielectric loss ε" as a function of frequency for FLC and CNT dispersed FLC at 30 °C.

3.2.3 Relaxation spectra

This relaxation phenomena was also reflected in Cole- Cole plot as shown in Fig 6 The smaller semi- circle in this figure represents the relaxation due to the Soft Mode where as, bigger semi circle represents the contribution due to Goldstone Mode. In the vicinity of the $T_{c^*\text{-}A,}$ SM followed the Currie-Weiss law. The relaxation frequency (f_i) can be evaluated using an expression

$(v/u) = (\omega\tau)^{1-\alpha}$,

where

$v = [(\varepsilon_0\text{-}\varepsilon'(\omega))^2 + \varepsilon''(\omega)^2]^{1/2}$,

$u = [(\varepsilon'(\omega) - \varepsilon'(\infty))^2 + \varepsilon''(\omega)^2]^{1/2}$, $\varepsilon'(\omega)$ is dielectric permittivity at particular frequency.

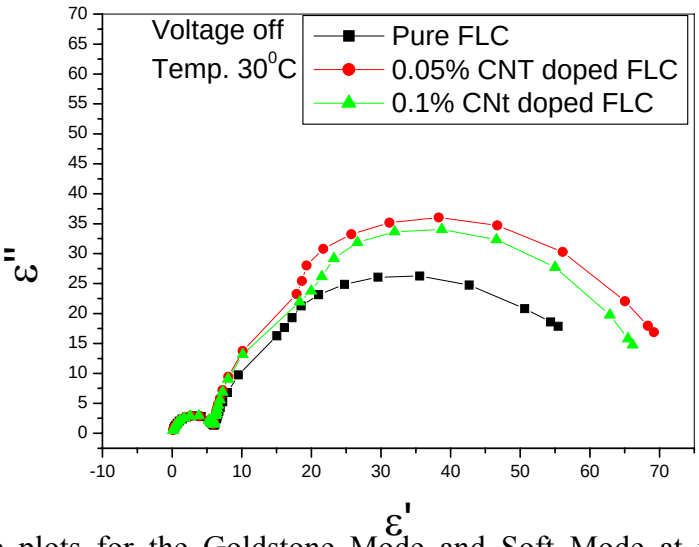

Fig 6 Cole-Cole plots for the Goldstone Mode and Soft Mode at room temperature for mixtures FLC and CNT dispersed FLC.

4.2.4 Effect of Bias voltage

The dielectric permittivity in SmC* phase was dominant due to the Goldstone mode contribution, so it became difficult to detect the other collective dielectric process. The Goldstone mode can be suppressed by applying a dc bias field, being strong enough to unwind the helicoidal structure. The effect of bias voltage on the Goldstone mode in the form of dispersion is shown in Fig. 7(a) and 7(b). We saw that the loss was highest without any bias (0V) voltage but decreased with bias voltage e.g. at 10V in the 0.1% CNTs dispersed FLCs. The Goldstone mode can be suppressed by applying a dc bias field, being strong enough to unwind the helicoidal structure.The voltage at which dielectric permittivity and losses become minimum, is called critical voltage. This voltage was sufficient to unwind the helical structure and suppress the Goldstone mode. The Goldstone mode can be suppressed by applying a dc bias field, being strong enough to unwind the helicoidal structure. But there was no significant variation in permittivity in FLCs. On adding the CNTs in FLCs, the molecules got aligned along CNT and were unable to follow the electric field and hence FLC lost their helical structure. Thus dielectric permittivity and dielectric losses got decreased on increasing dc bias field.

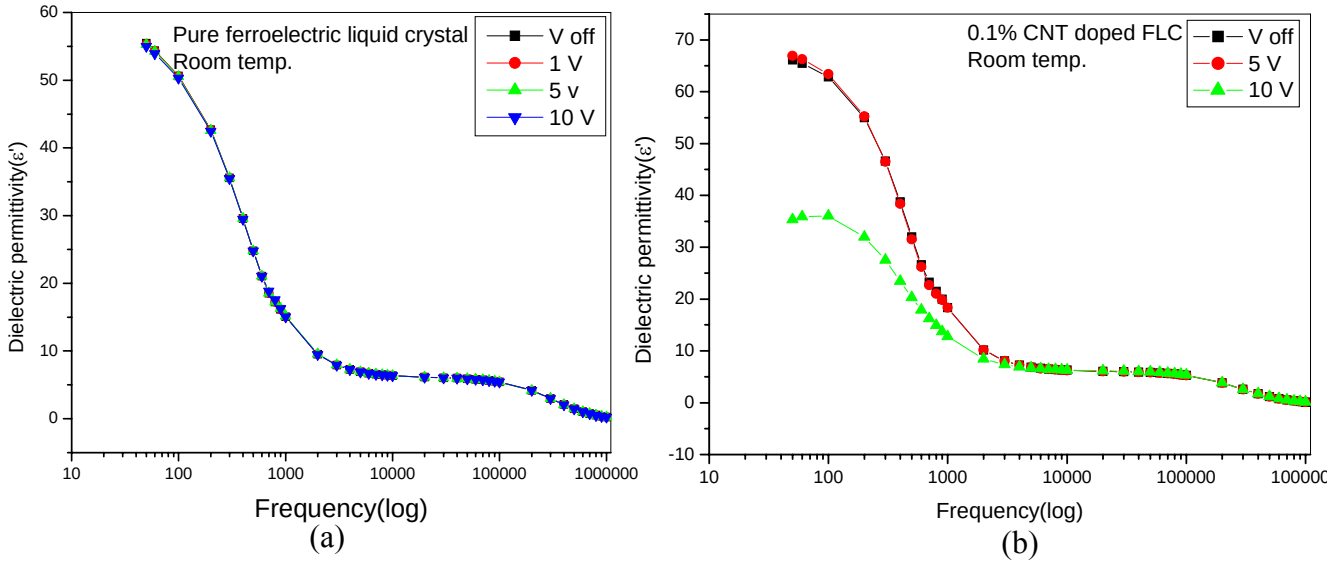

Fig.7 Dielectric permittivity as a function of frequency at different voltage for (a) FLC (b) 0.1% CNTs dispersed FLC

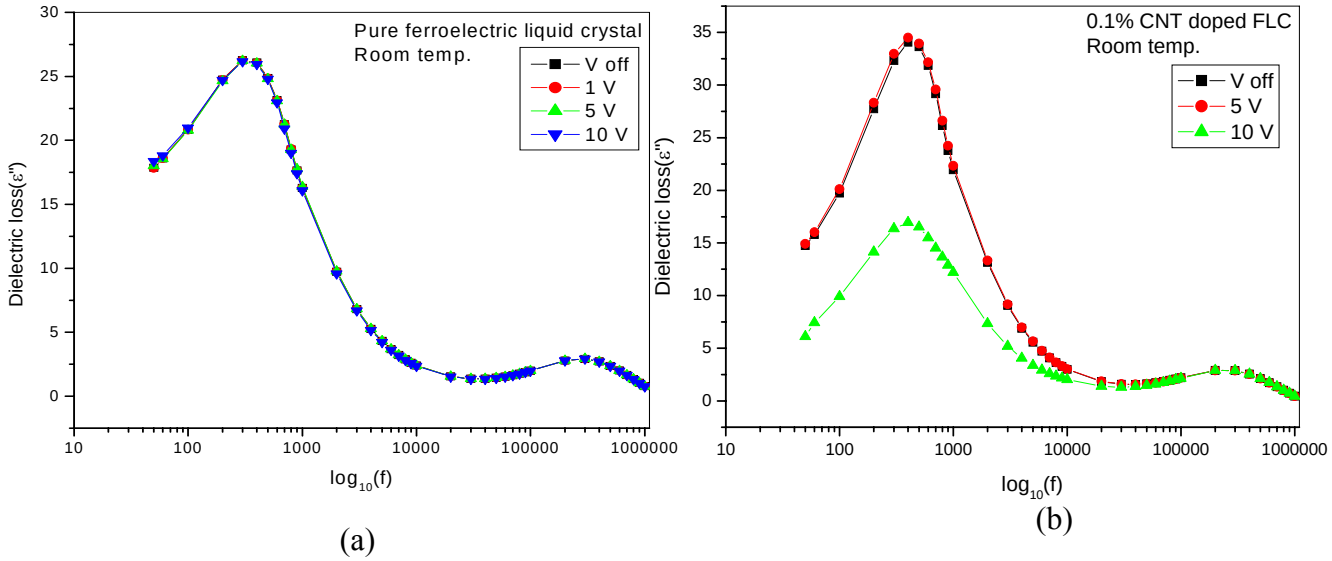

Fig 8 Dielectric loss as a function of frequency at different voltage for (a) FLC (b) 0.1% CNT dispersed FLC

Fig 8(a) shows the dielectric loss (ε") as a function of frequency at different voltages for pure FLC. It was observed that there was no effect of biasing on FLC. Fig 8(b) shows the dielectric

loss (ε”) as a function of frequency at different voltages for multiwalled carbon nanotube dispersed FLC. Two relaxation peaks at 500Hz and 500 kHz were observable. The first peak corresponds to a domain mode structure where as the second one corresponds to the soft mode. This was also reflected in the form of Cole-Cole plot.

5. Conclusions

- dispersed nanotubes in LC, enhanced the alignment of the LC molecules and thus macroscopically homogeneous structures was obtained. The inherent conductivity and spontaneous self- alignment properties of CNTs make them an attractive alternative as an alignment layer.
- transition temperature increased by 7% and 17% after addition of 0.05% and 0.1% wt/wt carbon nanotubes in FLC.
- dielectric permittivity got increased almost by 27% on dispersing CNT in ferroelectric liquid crystals at lower temperatures and frequencies values but at higher temperatures and frequency, there was no significant variation in dielectric permittivity values.
- relaxation peaks at 300Hz and 500 kHz were observable that corresponds to Goldstone mode and Soft mode respectively. This was also reflected in the form of Cole-Cole plot.

References

1. J. W. Doane., N. A., Wu, B. G. Vaz., And S. Zumer., Appl. Phys. Lett., **48**, 269 (1986), .
2. M. Kreuzer., T. Tschudi., And R. Eidenschink., Appl. Phys. Lett., **62,** 1712 (1993),.
3. F. Brochard , And P. G. De Gennes., J. Phys., **31**, 691(1970).
4. B. J. Liang., And S.H. Chen., Phys. Rev., **39**, 1441 (1989),.
5. Yu. Reznikov., O. Buchnev., O. Tereshchenko., V. Reshetnyak., A. Glushchenko., And J. West., Appl. Phys. Lett., **82**, 1917 (2003).
6. Jan P. F. Lagerwall and Giusy Scalia, J. Mater. Chem., **18**, 2890 (2008).
7. Dierking, G. Scalia and P. Morales, J. Appl. Phys., **97**, 044309 (2005).
8. I. Dierking, G. Scalia, P. Morales and D. Leclere, Adv. Mater., **16**, 865 (2004).
9. M. Lynch and D. Patrick, Nano Lett., **2**, 1197 (2002).
10. M. Endo, T. Hayashi, Y.A. Kim, H. Muramatsu. Jap. J. of Appl. Phys, **45**, 4883 (2006).
11. H.Y. Chen, N.A. Clark, W. Lee. Appl. Phys. Lett, **90**, 033510 (2007).
12. C.Y. Huang, H.C. Pan, C.T. Hsieh. Jpn J. Appl. Phys. Part 1, **45**, 6392 (2006).
13. S.Y. Jeon, S.H. Shin, S.J. Jeong, S.H. Lee, S.H. Jeong, Y.H. Lee, H.C. Choi, K.J. Kim. Appl. Phys. Lett, **90**, 121901 (2007).
14. I.S. Baik, S.Y. Jeon, S.J. Jeong, S.H. Lee. J. Appl. Phys, **100**, 074306 (2006).
15. A.M. Birader, S.S. Bawa, C.P. Sharma, Subhas Chandra, Ferroelectrics **122**,81(1991).
16. K. Kondo, T. Kitamura, M. Isogai, A. Mukoh, Ferroelectrics **132,** 99 (1988).
17. Giusy Scalia, Clemens von Bu¨hler, Constanze Ha¨gele, Siegmar Roth, Frank Giesselmann and Jan P. F. Lagerwall, Soft Matter, 4, 570,(2008).
18. CECILE ZAKRI, Liquid Crystals Today, **16**, 1, (2007).

Zinc powder filled coatings for corrosion protection

A.Mathiazhagan, Rani Joseph and K.P.Narayanan

Cochin University of Science and Technology, Kochi-682022, Kerala, India.

Email: alagan@cusat.ac.in

Abstract:

Epoxy based coatings were prepared with metallic Zinc powder and the Zinc content was varied from 50% to 80% w/w. Nanoclay was used as a filler. The filler content was varied from 10 to 40 wt %. This coating was tried on mild steel substrates. The substrates were found to have superior corrosion protection over zinc rich coating as observed by chemical and electrochemical measurements . The corrosion potential, limiting current, mass loss , water uptake and coating defects by salts spray in 3 wt % sodium chloride solution for different time duration etc showed the superiority of the Zinc rich coating . Mechanical properties of the coatings (100μm) were also evaluated by scratch hardness and cross hatch hardness tests and results indicated the enhanced mechanical properties of the coating.

Keywords: zinc, nanoclay, epoxy, corrosion protection

Introduction:

The possibility of effecting cathodic protection by means of paint containing metal pigments, which are anodic to the materials to which they are applied, has drawn considerable attention in recent years. Zinc-rich coatings have zinc powder as filler and binder may be one of the organic resins. The primary action of mechanism of the zinc coating has always been explained in the past on the basis of electrochemical theory-Cathodic protection. Zinc-rich coating has many problems associated with formulation, physico-mechanical properties, sedimentation of zinc dust in cans, loss of adhesion due to blistering and solubility of zinc corrosion product [1, 2, 3]. This fact together with the relatively high cost of zinc has been the reason for search of alternative filler in zinc rich coating formulation.

Incorporation of inorganic nanoparticles can be a way to improve corrosion resistant properties [4].

Nanoparticles are generally considered to be a number of atoms or molecules bonded together with radius of 100nm. A cluster of one nanometer radius has approximately 25 atoms, but most of them are on the surface of the cluster [5]. Substances with high surface areas have enhanced physical, chemical, mechanical, optical and magnetic properties and this can be exploited for a variety of structural and non-structural application. Nanoparticle /fillers find application in wear-resistant, erosion-resistant and corrosion resistant [6]. Studies on preparation of epoxy-clay nanocomposite coating by M.R.Bagherzadeh et al [7] shown that incorporating nanoclay particles into organic coatings improves anti-corrosive properties of

coating. It was found that as the clay loading increases the barrier and anti-corrosive properties increases and the best anti-corrosive performance of coatings was obtained at 3 and 5 wt % clay concentrations.

Nanocomposite materials in the form of coatings with low loading of nanoclay (e.g., 5 wt.%, CLMA5) on cold rolled steel (CRS) were found much superior in corrosion protection over those of neat PMA based on a series of electrochemical measurements of corrosion potential, polarization resistance, corrosion current and impedance spectroscopy in 5 wt.% aqueous NaCl electrolyte [8] .

This study reports modification of zinc-rich protective coatings using nanofillers that make the coatings more durable and corrosion resistant and study the effect of nano clay in zinc filled epoxy coating for corrosion protection. The coating's performance has been assessed by corrosion potential, limiting current, weight loss, and water uptake measurements and salts spray. Gloss, scratch hardness, cross-hatch adhesion tests for the coating has also been performed.

Materials and methods:

Sample preparation: Bakelite Hylam-India through Ms.Sharon Engineering Enterprises, Kochi, Kerala supplied Epoxy resinB11 and hardener K59 and zinc duct was obtained from metal powder company Ltd, Madurai, Tamil Nadu. Nanoclay was supplied by southern clay products, Inc. The mild steel coupons of the dimensions (6cm x3.4 cm x1.6cm) were prepared. The corrosion products were mechanically removed from the surface of the steel specimens by emery paper (200 grit) and also by immersion in hydrochloric acid for 15 min and finally they were washed with distilled water and dried.

Coating formulation:

The coating was prepared by incorporating zinc powder in a content of 80%,70%,60%,50% w/w and nanoclay with various concentration ranging from 10 to 40 %w/w in the ethanol/water mixture under vigorous mechanical stirring followed by addition of epoxy (B11) resin and hardener (K59) in 1:0.5 by weight .The coating was applied on pre treated mild steel substrate by a brush and allowed to cure at 30^0 C to get dry film thickness of 100 +_ µm .This coating procedure is based on method described by Hasmuhk et.al [9] .

Potential measurements:

During the exposure of the specimen in the corrosive environment of 3.5% w/w NaCl solution, their half-cell potentials were measured viruses a saturated calomel Electrode (SCE).The potential measurements were based on procedure prescribed by N.Koulumbi et al[10].

Electrochemical method: Series of mild steel sample were coated with the coating and the experiment was carried out using the three-electrode configuration for polarization. The working electrode, the coated mild steel panel were fixed with a glass tube with M-seal compound .The working electrode was kept as 50 cm^2, a platinum gauge was used as a auxiliary electrode and a saturated calomel electrode was used as a reference electrode. A 3 % sodium chloride was prepared and used as the electrolyte. Cathodic

polarization experiments were carried out using potentiostate (model 600A). The potential was varied from the open circuit potential to –1.1 V and the resultant current was recorded. From these plots the limiting current was determined and it was utilized in evaluating the coatings. This measurement is based on procedure prescribed by S.Syed et al[11].

Weight loss method:

The specimens of the different types (uncoated and coated with different types of coatings) were immersed in the 3.5% NaCl solution for about 2 months. At the end of each exposure period, the coatings were removed first by the epoxy diluents (dodecyl / tetradecyl glycidyl ether) and then mechanically (using an acrylic knife). Finally the specimens were immersed in hydrochloric acid to eliminate the corrosion products formed during the exposure, washed with distilled water, dried and weighed to obtain the weight loss. This measurement is based on procedure prescribed by Th.Skoulikidis et al[12].

Measurements of coating water uptake:

The evaluation of the water up take process into a coating immersed in a solution is important and this can be obtained by measuring weight difference before and after immersion of the coated specimens in liquid medium for a predetermined time. The prepared coatings were applied over 2 inc x3inc glass plates for determining water uptake. This measurement was made according to procedure prescribed by S.Syed et al[11].

Salt spray test:

This test was performed to assess the corrosion resistance ability of coated steel panels under marine environment by using servo salt spray chamber as per ASTM B117 Specification[13]. The neutral sodium chloride solution of concentration 3% was used for spraying. The conditions of salt spray testing were as follows: 5 wt% NaCl, $_{P}$H 6.5-7,Temperature 35%,air pressure 15 Psi and relative humidity RH=95-98%.

The coated mild steel specimens were kept inside the spry chamber in such a way that the surfaces of the specimens were exposed freely to the fog. The experiments were carried out for 1000 hrs and observations were made periodically till failure of coating.

Physical properties:

The dry film thickness was kept at 100 μ for all experiments and gloss; Crosshatch adhesion (2mm) and Scratch hardness were measured for all coated samples as per ASTM-D-3359 standard [14] .

Surface morphology studies: The pigments and nanofillers as used for coating formulation were observed by a scanning electron microscope (SEM) JEOL 6390 LV with operating voltages ranging from 5kV-30 KV.

Results and Discussion:

The corrosion tendency of the steel substrate was estimated in all types of coated specimen, by the half-cell potential development versus the exposure time to the corrosive environment. In all cases as shown in Table.2, the potential of the coated panels move to more positive values with time. The results indicate that corrosion resistance behavior of coating increased with increase of nanoclay. In a research carried out by N.Kouloumbi et al[10] , the specimen coated with composites of epoxy resin and aluminum, iron or zinc powder, immediately after in solution, exhibit a potential value which corresponds closely to that of the specimen coated with pure epoxy and they concluded that the particulate composite coatings with Fe, Al, Zn powder provide systems with similar anticorrosive behavior in chloride environment as the coating of pure epoxy resin. According to Leidheiser[16], the corrosion potential in combination with other methods can provide information about the mechanism of the reaction and the rate controlling process. It is concluded that the movement of the corrosion potential in the active (i.e. more negative) direction indicates that the cathodic/anodic areas ratio decreases and as a consequence the under film corrosion process may be significant, denoting a limited coating life.

Ole Qystein et al [17] reported that only the zinc particles in direct contact with the steel will contribute to the cathodic protection and too few particles will give too low electrical continuity and on the other hand too much zinc particles will result in a porous film with poor mechanical properties.

The potential of zinc in sea water is approximately -1.050 $V_{SCE,\ while}$ the steel substrate used here has a potential of approximately -0.65$V_{SCE.}$ The measured potentials are mixed potentials between the steel substrate and the active zinc-pigments and will depend on the area ratio between the two. If only few zinc-pigments are active, the anode area will be small, and the potential will be close to that of the steel. On the other hand, if the area of active pigment is large, the potential will be close to that of zinc.

As the zinc particles corrodes, the contact to the steel will gradually be lost and the potential will have to move to active sites but in this work the potential moves to passive sites due to the fact that other mechanisms must also contribute to the protection of steel, in addition to the galvanic effect. Zinc corrosion products may inhibit corrosion (t.k.ross et al[18]), e.g. by increasing the PH under the coating (S.Lindquist19). Corrosion products from the zinc particles may also seal pores in the coating, improving the barrier properties (C.Hare et al[20]). In this work addition of nanoclay moved potential to passive site which is due to enhanced barrier properties offered by presence of nanoclay in corrosion products.

From the cathodic polarization experiments, the resultant current for each applied voltage was measured and the same was used for calculating the limiting current as shown in fig 1 for all five coatings. Similarly the experiment was carried out up to 62 days. It is a well-known fact that the limiting current is a measure of diffusion of anions. The lower the limiting current the lower will be the diffusion rate of anions into the

coating film. The dissenting order of the limiting current density shown by the coating with nanoclay attributes higher corrosion resistance compared to zinc rich coating with out nano-fillers.

S. Syed Azim et al [12] evaluated the various grades of iron oxide as main pigments in epoxy paint and their finding says cathodic polarisation method can be used along with conventional methods to evaluate anticorrosive coatings.

The results of the mass-loss measurements for coated and uncoated samples in corrosive environments, of a 3.5%W/W NaCl solution and at several time intervals are shown in Table.1. From the test result, it is observed that corrosion resistance of coating is increased with increase of nanofiller (nanoclay) in the formulation.

When coated metals are exposed to wet corrosion environments, the first process causing the onset of corrosion could be up take of water by the coating-metal interface and evaluation of the water uptake process into an organic coating immersed in a solution is important because this phenomenon is related to the corrosion protection properties[16] . The results of the coating water uptake measurement of coated samples in corrosive environments, of a 3.5%W/W NaCl solution at several time intervals are shown in Table 2. From the test result, it is observed that water resistance of coating is also increased with increase of nanofiller content in the formulation.

Table 3 shows result of neutral salt spray after 1000 hours (as per test as ASTMB117).

The salt spray chambers specimens of different formulation shown that there was no propagation of rust on the surface with increase of nanofiller (nanoclay) content up to 30%. While in other coatings, the rust penetrates into the surface and lifting of the coating was observed. Blistering numbers 6, 4, and 2 represented progressively larger sizes. Frequency of occurrence was presented as dense (D), medium dense (MD), medium (M), few (F), and very few (VF). This salts spray test result is also comparable with the half-cell potential of the coated samples. It was also noted that adhesion was better (noticed during scraping of the film after salt spray test) for all formulation.

The results of the various film parameters tested are given in Table 4 .It was observed that all coating systems passed the scratch hardness test with 2000g except system 1 but only system 4 and 5 passed the crosshatch adhesion (2x2 mm square). SEM micrograph of zinc dust with nanoclay as used for coating formulation indicates the fused pattern of nanoclay in zinc powder. The image was taken at 10000 X to view include the fused form of zinc particle with nanoclay.

Conclusion:

The corrosion potential of mild steel coated with ZFE coating shifted to more positive value with time as nanoclay percentage increased from 10%-40% . The ZFE coating containing nanoclay showed a reduction in the limiting current with time as nanoclay percentage was increased. Weight loss of steel coated ZFE with nanoclay and water uptake by the coating was found to decrease with time as nanoclay

percentage increased. ZFE with nanoclay up to 30% showed no propagation of rust on the coated surface while the rust penetration into surface and lifting of coating was seen on ZFE coating with 40% nanoclay. The gloss of ZFE coating was found to vary between 62 to 72 on addition of nanoclay. All nanoclay % in ZFE coating with film thickness 100μ showed better scratch hardness but only two coating with nanoclay 30% and 40% shown better cross-hatch adhesion. In zinc-rich coating, the replacement of part of the zinc (even as little as 10 percent in weight) with nanoclay increases possibilities of cathodic protection of these types of coatings and the barrier effect.

References:

1.M.Selvaraj and S.Guruviah ' The Electrochemical aspects of the influence of different binders on the corrosion protection afforded by zinc- rich paints' Surface coatings international, January 1997.

2. A.Kalenddova, Mechanism of the action of zinc powder in anticorrosive coatings, Anticorrosivemethods&materials, Vol49, 3, 2002.

3. M.Morcillo and M.Svoboda.A new pigment to be used in combination with zinc dust in zinc rich anti-corrosive paints, Pigments &resin technology Vol27Number3.1998, pp161-167.

4. Zheludkevich, M. L., Miranda Salvado, I. M. and Ferreira, M. G.S., Sol–gel coatings for corrosion protection of metals. J. Mater.Chem., 2005, 15, 5099–5111.

***5.** P.Poole Jr.Frank J.Owens 'Introduction to nanotecnology,' John Wiley sons (Asia) Pvt Ltd, Singapore.*

6. Mick Wilson, Kamali Kannangara, "Nanotechnology-basic science and emerging technologies", Overseas press India pvt Ltd New Delhi.

***7.** M.R.Bagherzadeh, F.Mahdavi, Preparation of epoxy –clay nano-composite coating, Progress in Organic Coating, Vol-60 pp-117-120, issue 2, Sep-2007.*

8.Jui-Ming Yeh, Tai-Hung Kuo, Hou-Ju Huang, Kung-Chin Chang, Mei-Ying Chang and Jen-Chang Yang 'Preparation and characterization of poly (o-methoxyaniline)/Na^{+}MMT clay nanocomposite via emulsion polymerisation: Electrochemical studies of corrosion

9. Hasmukh A.Patel, Rajesh S. Somani, Hari C, Bajaj and Raksh.V.Jasra "Nanoclays for polymer composites" Bull.Mater Sci, Vol: 29, No2, April 2006.PP.133-145.

10. N.Kouloumbi, G.M.Tsangaris, S.Kyvelidis "Metal filled composites as protective coating against marine corrosion" J.Coat.Technol.66, 1994,839.

11. S.Syed Azim, M.Dhanalakshmi, P.Jayakrishnan and N.S.Rengasamy "Evaluation of various grades of micaseous iron oxide (MIO) as main pigment in epoxy undercoat" Eighth National congress on corrosion control, September.9-11, 1988, Kochi, Kerala.

12. Th.Skoulikidis, P.Vassilious, S.Vlachos " New anticorrosive pigments" , 9th International Congress on marine fouling and corrosion held at the university of Portsmouth,17-21 July 1995.

13. G.S.Haynes and R.Baboian "Laboratory corrosion tests and standards"ASTM, Philadelphia, 1985, PP.496-503

14. Charles G.Munger "Corrosion prevention by protective coatings"NACE, Houston 1986.

15.P.L.Bonora,F.Deflorian,L.Fedrizzi,S.Rossi Electrochemical Evaluation of coatings for marine corrosion control, 9th International Congress on marine fouling and corrosion held at the university of Portsmouth,17-21 July 1995.

16.H.Leidheiser, Corrosion Control by coatings, P.143,SciencePress, NY(1979)

17. Ole Qystein Knudsen, Unni Steinsmo, Marit Boreal,"Zinc rich primers –Test performance and electrochemical properties" Progress in organic coatings 54(2005)224-229

18. T.K.Ross, J. Wolstenholme, Corros. Sic., 17(1977) 341-351

19. S.Lindquist, L.Meszaros, L.Svenson, J. Oil XColour.Chem.Assoc.68 (1989)10-14

20. C. Hare, m.Steele, S.Collins, J.Prot.Coat.Lining 18(2001)54-72

Table1. Mass loss Vs Time

Time (hrs)	Plain steel-Mass loss (gm)	Epoxy-Zinc90%Mass Loss (gm)	Epoxy -Zinc80% Nanoclay10% Mass loss(gm)	Epoxy-Zinc70%-Nanoclay20% -Mass loss(gm)	Epoxy-Zinc60%-Nanoclay30 %-Mass loss (gm)	Epoxy-Zinc50%-Nanoclay40 %-Mass loss (gm)
7	0.09	0.04	0.02	0.02	0.01	0.01
14	0.14	0.08	0.02	0.02	0.01	0.01
21	0.19	0.09	0.03	0.02	0.02	0.01
28	0.27	0.1	0.03	0.02	0.02	0.02
35	0.32	0.13	0.05	0.03	0.02	0.02
41	0.37	0.17	0.05	0.03	0.02	0.02
49	0.41	0.19	0.06	0.03	0.02	0.02
55	0.45	0.2	0.09	0.04	0.03	0.03
62	0.48	0.25	0.1	0.04	0.03	0.03

Table2. Result of various coating performance in salt water

Time in days	Coating System	Potential (mv)	Water-uptake (mg/sq.cm)
1	Epoxy-Zinc90%	-670	0.04
7		-657	0.04
15		-635	0.03
30		-625	0.02
45		-616	0.01
60		-602	0.01
Time in days	Coating system	Potential (mv)	Water-uptake (mg/sq.cm)
1	Epoxy -Zinc80% -Nanoclay10%	-590	0.04
7		-572	0.03
15		-557	0.02
30		-533	0.02
45		-529	0.01
60		-513	0.01
Time in days	Coating system	Potential(mv)	Water-uptake (mg/sq.cm)
1	Epoxy-zinc70%- Nanoclay20%	-520	0.03
7		-502	0.02
15		-496	0.02
30		-480	0.01
45		-460	0.01
60		-457	0.01
Time in days	Coating system	Potential (Mv)	Water-uptake (Mg/sq.cm)
1	EpoxyA-zinc60%- Nanoclay30%	-512	0.03
7		-503	0.02
15		-487	0.02
30		-479	0.01
45		-458	0.01
60		-442	0.01
Time in days	Coating system	Potential (mv)	Water-uptake (mg/sq.cm)
1	Epoxy-zinc50%- Nanoclay40%	-505	0.02
7		-494	0.02
15		-484	0.02
30		-469	0.01
45		-446	0.01
60		-440	0.01

Table.3 result of neutral salt spray after 1000 hours (as per ASTMB117).

Sl.No	Coating system	Rating as per ASTMD714 Blistering Rating	
1	Epoxy-zinc90%	6	dense
2	Epoxy-zinc80%-Nanoclay10%	4	Few
3	Epoxy-zinc70%-Nanoclay20%	2	Few
4	Epoxy-zinc60%-Nanoclay30%	2	Medium
5	Epoxy-zinc50%-Nanoclay40%	2	Very few

Table 4. Result of various paint film parameters (as perE-6, ASTM D-3359, relevant parts)

System No.	Paint system	DFT (Microns average)	Gloss (60^0)	Scratch hardness 2000G load	Crosshatch adhesion (2x2 mm)
1	Epoxy-Zinc90%	100	75	Failed in 2 stroke	2B
2	Epoxy-Zinc80%-Nanoclay 10%	100	70	Passed in 2 stroke	3B
3	Epoxy-Zinc70%-Nanoclay20%	100	72	Passed in 2 stroke	4B
4	Epoxy-Zinc60%-Nanoclay30%	100	65	Passed in 2 stroke	5B
5	Epoxy-Zinc50%-Nanoclay40%	100	62	Passed in 2 stroke	5B

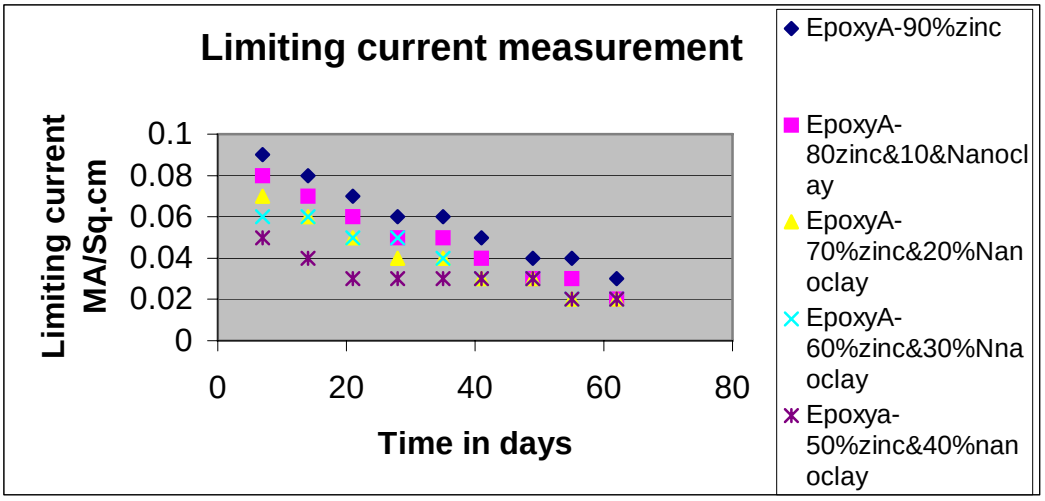

Fig.1. Limiting current Vs time duration

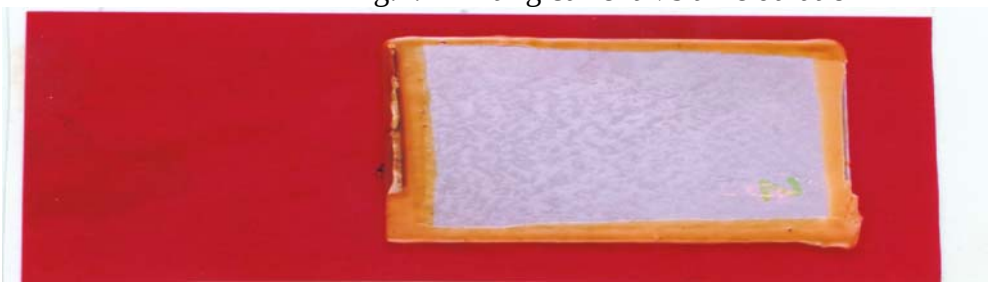

Fig.2 Zinc rich coating with nanoclay filler on mild steel

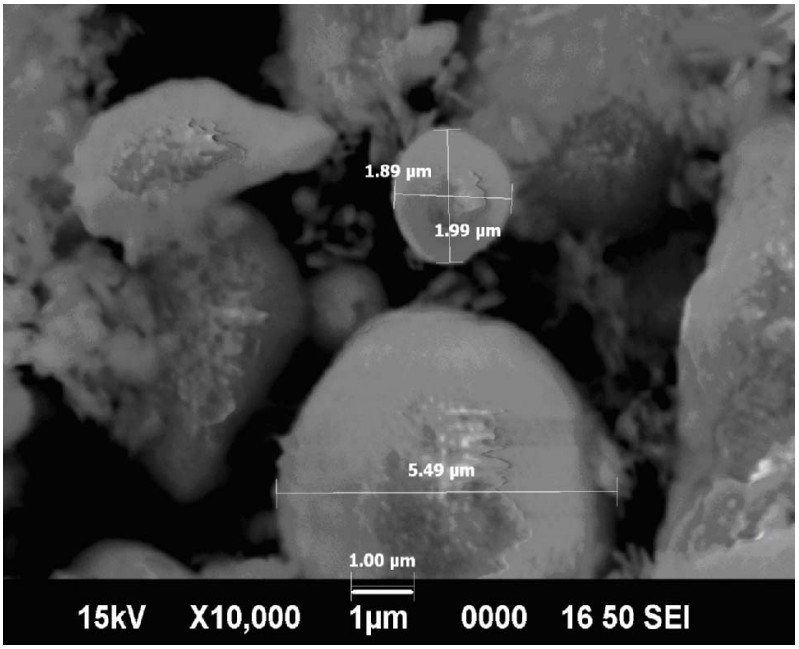

Fig.3 .SEM micrograph of zinc dust with nanoclay as used for coating formulation taken at 10000 X

Studies on adhesive properties of vinyl acetate-butyl acrylate copolymer for coating applications

Suma K.K[*], Sinto Jacob and Rani Joseph[#]

Department of Polymer Science and Rubber Technology, Cochin University of Science and Technology, Cochin- 682 022, India

Email-rani@cusat.ac.in

Introduction

Coatings are used to protect the substrate from the environment. The coating must adhere to the surface that has been coated because to decorate or protect any surface, the coating must remain in position[1]. Performance of the film depends on their adhesion properties. Adhesion involved whenever solids are brought into contact, as in coatings, paints, and warnishes; multilayered sandwiches; polymer blends; filled polymers; and composite materials. Since the final performance of these multi component materials depends significantly on the quality of the interface that is formed between the solids. Poly vinyl Acetate is widely used as an adhesive for porous materials; particularly wood, paper and cloth. For many other applications copolymer of Vinyl acetate with other monomers like n-Butylacrylate, MMA, Vinylchloride, Vinylversatate etc. are used due to its poor hydrolytic stability under alkaline condition, poor weathering stability, poor wet adhesion and high water sensitivity. It has only limited application in exterior coating because of high Tg(30^0C) and MFT(20^0C) making its film too hard and inflexibility limits its use in paint application[2].

In the paper we report the properties of copolymer of vinyl acetate-n-butyl acrylate with varying composition and solid content. The polymer was prepared using semicontinuous emulsion polymerization method[3]. The shear and peel strength of the resulting copolymers were investigated at different temperatures to evaluate its adhesion property.

Experimental

Materials

Both monomers, Vinyl acetate(VAc) and n-butyl acrylate(BuA), were distilled under vacuum to remove the inhibiter. Distilled, deionized and deoxygenated water was used in all polymerization reactions. Ammonium persulphate and Sodium carbonate were reagent grade(Merck), Sodium dodecyl benzene sulphonate surfactant and Rexol(N-300) were used.

Preparation of copolymer latex

The lattices were prepared by emulsion polymerization. A semicontinuous process of monomer addition was used. The polymerization was carried out in one litre four necked reactor immersed in a constant bath at 80^0Cand equipped with water condenser, a two bladed Teflon coated stirrer and 25ml graduated dropping funnel. DDI water, emulsifiers and buffer were initially charged and maintained under constant agitation of 150rpm under nitrogen atmosphere for half an hour. The monomers were mixed and then slowly added to stirred solution of surfactant and DDI water to obtain pre-emulsion. The pre-emulsion was fed to the reactor over a period of separation of 2.5hours through a droping funnal at a rate of 0.30 and 0.40ml/min respectively. No phase separation of pre-emulsion was noticed over the feed period. The initiator was in two stages. The first stage was added prior to the addition of the monomer feed. The second portion of the initiator dissolved in demonized water to form concentrated solution. The initiator solution was added to the reactor concurrently with the monomer. After the addition of all the ingredients the reaction mixture was further heated for 1hr at 80^0C. The reactor contents were cooled and then filtered to remove any residual coagulum.

The latex of varying solid content was prepared by changing water content and concentration of stabilizer.

Lap shear and peel strength studies

The adhesive property of copolymer latex investigated by lap shear strength. Mild steel substrate used for bonding. Metal strips of size 100 × 25 mm were machined from 0.60-mm-thick sheets to serve as metal substrates for lap-shear-strength studies on metal-to-metal bonds. Metal strips of size 100 × 25 mm were machined from 0.11-mm-thick sheets to serve as metal substrates for peel strength studies on metal-to-metal bonds. Mechanical cleaning (surface roughening) was done with a No. 100 emery paper. Solvent degreasing with trichloroethylene followed mechanical cleaning. The copolymer latex with different compositions by varying the solid content was used for metal to metal bonding. After applying the copolymer latex, the substrates were kept aside for half an hour to evaporate the solvent. The copolymer latex was applied to a thickness of 0.1 mm on both substrates. The substrates were then subsequently bonded together and the copolymer latex cured at room temperature for two weeks and at 70^0C for 24hours.

Results and discussion

Figure 1 shows the effect of varying the solid content of 85/15 VAc-BuA copolymer on the metal-to-metal shear strength at room temperature (30^0C) kept for two weeks and at 70^0C kept for 24hours.

Figure 2 shows the effect of varying the solid content of 74/26 VAc-BuA copolymer on the metal-to-metal shear strength at room temperature (30^0C) kept for two weeks and at 70^0C kept for 24hours.

Figure 3 shows the effect of varying the solid content of 70/30 VAc-BuA copolymer on the metal-to-metal shear strength at room temperature (30^0C) kept for two weeks and at 70^0C kept for 24hours.

All above studies shows that the shear strength value increases with increasing the solid content at different temperatures. As the solid content increases, the modulus of the copolymer increases. Furthermore, the copolymer has a high affinity towards metal surfaces, and this result in better metal–metal bonds.

Figure 4 shows the effect of varying the solid content of 85/15 VAc-BuA copolymer on the metal-to-metal peel strength at room temperature (30^0C) kept for two weeks and at 70^0C kept for 24hours.

Figure 5 shows the effect of varying the solid content of 74/26 VAc-BuA copolymer on the metal-to-metal peel strength at room temperature (30^0C) kept for two weeks and at 70^0C kept for 24hours.

Figure 6 shows the effect of varying the solid content of 70/30 VAc-BuA copolymer on the metal-to-metal peel strength at room temperature (30^0C) kept for two weeks and at 70^0C kept for 24hours.

The peel strength also found to increases with increasing solid content. The higher peel strength was obtained at higher solid content. As the BuA content increases the flexibility of the latex film increases, which leads to inferior peel strength values.

Conclusions

For metal-to-metal bonding, Vinylacetate-Butylacrylate copolymer latex shows high shear strength. At higher temperature VAc/BuA copolymer latex showed better shear and peel strength compared to room temperature. This shows the thermal stability of VAc/BuA copolymer latex for bonding applications. Both the peel and shear strength values increased with increasing solid content. Hence higher solid content VAc/BuA latex is more suitable to use as binder for water based surface applications.

References

1. Arthus A.Tracton; Coatings technology handbook, taylor and Francis group, Boca Raton

2. K.O. Calvert; Polymer lattices and their applications, Applied science publishers Ltd, London

3. Grald A, Vandezande and Alfred Rudin; Properties of Vinyl acetate-Butyl acrylate copolymer latexes of narrow particle size distribution, American chemical society, 1992

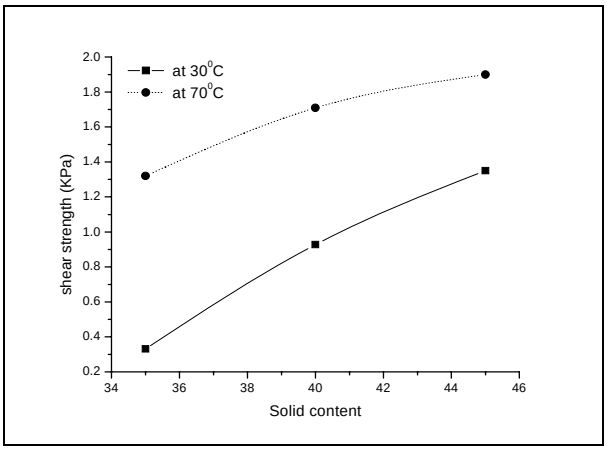

Figure 1: Effect of varying the solid content of 85/15 VAc-BuA copolymer on shear strength

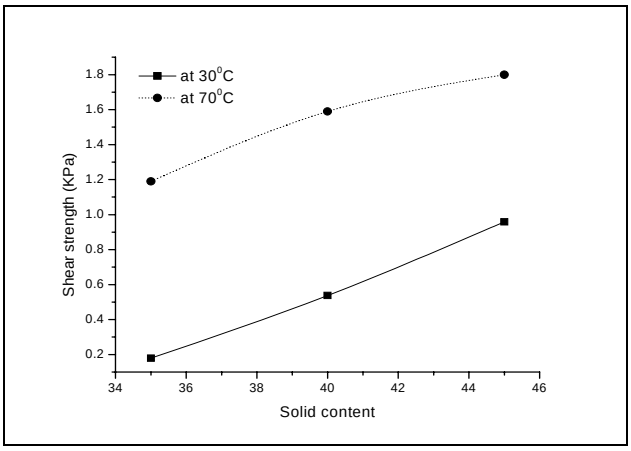

Figure 2: Effect of varying the solid content of 74/26 VAc-BuA copolymer on shear strength

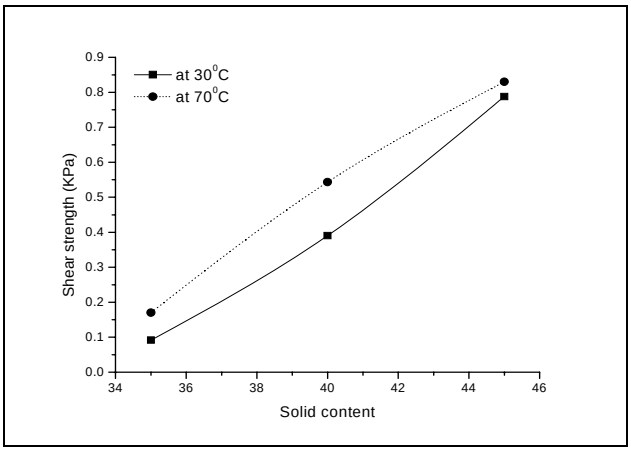

Figure 3: Effect of varying the solid content of 70/30 VAc-BuA copolymer on shear strength

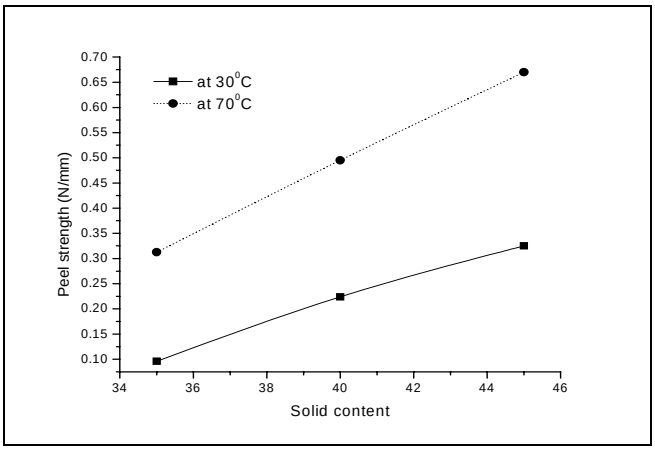

Figure 4: Effect of varying the solid content of 85/15 VAc-BuA copolymer on peel strength

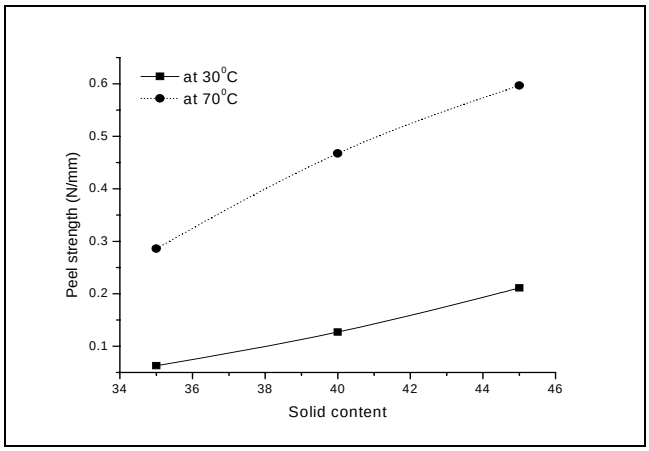

Figure 5: Effect of varying the solid content of 74/26 VAc-BuA copolymer on peel strength

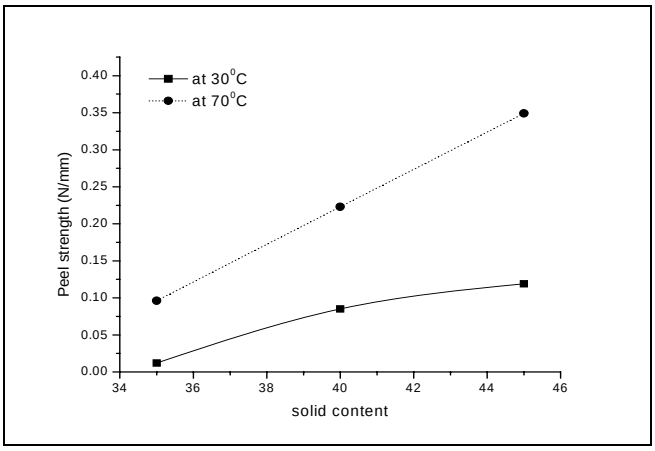

Figure 6: Effect of varying the solid content of 70/30 VAc-BuA copolymer on peel strength

Polymer blends, alloys and their application

Ridhi Kaushik* & Rajni Lakhani#

Organic Building Material Division, Central Building Research Institute, Roorkee-247667, (U.K.) India.

E-mail: rlakhani_cbri@rediffmail.com

Abstract

The unbelievable advances in science and technologies have resulted in the emergence of new products and processes which have in turn accelerated the pace of industrialization. One such group of products are polymeric systems. The system when converted in to solid state is called plastic. Plastics are the products of twentieth century and can be expected to perform a major role as materials of next century.

Many new materials were introduced into the family of plastics during the last forty years, but the direction of polymer research and development has been changing gradually in the recent years. In the last decade, the pace of introduction of new polymers has slowed down due to huge expenses involved in the development and testing of totally new polymers. Therefore, now the trend is to fulfill the gaps in the existing array of plastics materials by modifying them through blending, reinforcing, grafting and other methods such as polymer alloys/ interpenetrating polymer systems which can improve the properties and/ or appearance.

Much attention is currently being diverted to the simplest route for combining outstanding properties of different existing polymers that is the formation of polymer blends. Although an increasing no. of miscible blends are reported in the literature, most polymer pairs are none the less immisible., thus leading to heterophase polymer blends. In the formation of blends many useful propreties characteristics of single phase, may be preserved in the blend while other properties may be averaged according to the blend composition. Proper controle of overall blend morphology and good adhesion between phases are in any case required in order to achieve good mechanical properties. Examples of few blends such as Rubber-phenolic blend,Epoxy / liquid polysulphide polymer blends, interpenetrating type network has been highlighted in this paper alongwith their properties.

Introduction

In the last decade, the pace of introduction of new polymers has slowed down due to huge expenses involved in the development and testing of totally new polymers. Therefore, now the trend is to fulfill the gaps in the existing array of plastics materials by modifying them through blending, reinforcing, grafting and other methods such as polymer alloys/ interpenetrating polymer systems which can improve the properties and/ or appearance.

Polymer Blends

Much attention is currently being diverted to the simplest route for combining outstanding properties of different existing polymers that is the formation of polymer blends. Although an increasing no. of miscible blends are reported in the literature, most polymer pairs are none the less immisible., thus leading to heterophase polymer blends. In the formation of blends many useful propreties characteristics of single phase, may be preserved in the blend while other properties may be averaged according to the blend composition. Proper control of overall blend

morphology and good adhesion between phases are in any case required in order to achieve good mechanical properties. Examples of few blends are highlighted below :

Rubber – Phenolic Blends

Rubber – phenolic blends were prepared in the laboratory by using natural rubber (Isoprene) and nitrile rubber. While assessing the adhesive properties, it was observed that these blends have much improved properties as compared to unmodified phenols. Rate of attainment of strength property is also fast. The results are given in Table 1.

Epoxy / Liquid Polysulphide Polymer Blends

Liquid polysulphide polymers are usually used for the manufacture of high performance sealants for buildings. Epoxy / polysulphide blends were developed for developing the protective coating to be used in highly aggressive conditions with slight modifications structural and semistructural adhesives were also developed by using the above blends. The coatings and adhesives thus developed have improved adhesive and protective property as compared to epoxy resin. These are presently being used as a corrosion protection coating as well as patch and crack repair composition and grouting compounds.

Development of IPN Coating System

Inter penetrating polymer networks(IPNs) are relatively novel, involving special type of chemical combination of different polymer networks in which permanent entaglements are formed by simultaneous or sequential cross linking of component networks.
A process for the production of anticorrosive coatings from epoxy/ phenolic IPN systems has been developed. In this process the prepolymer of epoxy and phenolic resins were made to polymerize with their respective hardeners in such a manner that the prepolymers crosslinks simultaneously with their respective hardners by a separate non- interfering mechanism. Coatings were prepared by using this polymer with various additives, such as reactive diluents, pigments, fillers, flow controlling agents, wetting agents, thicking agents ets. To assess the suitability of the coating system from end use application point of view, the properties of the coating were determined are as follows:
(1) Properties of the free film / sheet.

(2) Properties of the coating after applying on the substrate.

Properties of the free coating Film / Sheet

In order to determine the characteristics of the free paint film, tensile strength, modulus of elasticity, elongation, specific permeability, coefficient of thermal expansion, hardness and chemical resistance against urea, diammonium phosphate, sulphuric acid, phosphoric acid, sodium hydroxide, distilled water etc. were determined and have been compared with epoxy resin under the similar test conditions. Result are reported in Table 2.

Characteristics of the coatings when applied on the substrate:

To assess the suitability of the coating systems when applied on the substrate –salt spray test , impact test, scrub resistance test, adhesion test , scrach hardness test etc. have been performed. Results are reported in the Table-3.

Corrosion of Reinforcement in RCC

Epoxy / phenolic coating can provide an excellent protection to steel reinforcement in concrete against aggressive environment. R& D work in this direction has been carried out at CBRI, Roorkee.For evaluating the coating system chemical resistance, accelerated corrosion test by weight change method and bond strength test by pull out test method were performed. Results are reported in Tables 4 and 5.

Chemical Resistance Test

Specimens for this test were prepared by applying two coats of epoxy / phenolic IPN coating and epoxy / phenolic IPN coating and epoxy coating on cleaned mild steel sheets. After curing these specimens for three days at RT, these were immersed in distilled water, an aqueous solution of 3 M calcium chloride, an aqueous solution of 3M NaOH and saturated solution of calcium hydroxide. Visual observations were recorded at different intervals of time upto a period of six months. Both type of specimens were found to be intact after immersion in these chemicals.

Accelerated Corrosion Test By Weight Change method

The accelerated corrosion studies on coated and uncoated mild steel bars embedded in 100mm cubes of 1:2:4 concrete for two cover thickness of 15 mm and 25mm were carried out. Loss in weight of these bars were determined after 10, 30 and 60 cycles. One cycle consists of one day dipping of these cubes in 3% NaCl solution followed by three days drying at room temperature ($27\pm 2^{o}C$) and then two days at $60^{o} \pm 3^{o}$ C. The results are reported in Table 4.

Bond Strength With Concrete By Pull Out Test Method

Bond strength of coated and uncoated bars were determined as per IS:2770. Results obtained are tabulated in Table-5.
It is evident from Table-4 that upto 10 cycles there was negligible corrosion in uncoated bars but no corrosion in coated bars. Upto 30 cycles corrosion was there in case of uncoated bars but not sufficient to cause cracking in concrete while no corrosion in the coated bars. After 45 cycle fine hair crack was seen in the case of uncoated bars which was further widened after 60 cycles while negligible corrosion was seen on the edges of the coated bars. This might be due to improper coating on the edges. On the basis of the preliminary studies, it may be concluded that IPN coating provides adequate protection to the reinforcement.
For bond strength data it may be concluded that IPN coated reinforcing bars developed acceptable bond strength with concrete. Hence can be used as reinforcement.

Conclusions

From the tests conducted so far, it has been observed that the IPN coating has better adhesion than epoxy with mild steel and very good adhesion with concrete. It has also been observed that IPN coating has better chemical resistance, better durability than the epoxy coating. Since in IPN coating, a part of the epoxy resin has been replaced by low cost phenolic resin, due to this it is estimated to be 20 percent economical than epoxy resin system. IPN coating system satisfies all the requirements of a good protective coating and hence an ideal material for protecting concrete, steel and reinforcement.

References

1. M.S. Khan, Corrosion state of reinforcing steel in concrete at early age, ACI Mater J 88 (1991) 37-40
2. S.R. Yeoman, Comparative studies of galvanised and epoxy coated steel reinforcement in concrete, Durability of Concrete- Second International Conference SP-126, ACI Detroit 1991, pp. 335-370.
3. IS 13620-1993, Fusion bonded epoxy coated reinforcing bars- Specification, 1993.
4. Akihiro Matsumoto, Kiichi Hasegawa and Akinori Fukuda, "Studies on modified phenolic resin. IV: Properties of phenolic resin modified with 4-hydroxy phenyl-maleimide / name-butyl acrylate copolymers" Polymer International, 1993, 65 (30)
5. Gabriele Perego, Gian, Domenico Cella and Catia Bastioli, "Effect of molecular weight and crystallinity on poly (lactic acid) mechanical properties" J.of applied polymer science, 1996, 37 (59)
6. Doo Sung Lee etal., "Thermal stability and compatibility of epoxy / polycarbonate and epoxy / tetramethyl polycarbonate blends" J. of Applied Polymer Science, 1996, 1639 (59)

Table-1

Sl. No.	Curing condition	Tensile bond strength kg/cm^2		
		Rubber Phenolic		Unmodified
		A	B	
1.	At 27 ± 2 ^{o}C For 6 days	43.2	27.0	7.20
2.	For 15 days	51.2	48.00	16.00
3.	For 30 days	66.4*	70.40*	25.50
4.	For 90 days	70.4*	70.40*	42.30

*wooden strips fails, adhesive bond remains intect.

(Phenols- used for this studies are based on cashew nut shell liquid (CNSL), a biproduct of cashew industries)

A – nitrile rubber

B – Isoprene rubber

Table – 2: Properties of Free Coating Films

Name of Tests	**Type of Coating Systems**	
	Epoxy	**Epoxy / Phenolic (IPN)**
Tensile strength N/mm^2	22.4	24.4
Elongation,(%)	8.0	21.0
Modulous of elasticity N/mm^2	1244.4	1031.0
Specific permeability $Mg/cm^2/mm/24hrs$	0.2043	0.1354
Glass Transition Temp.(^oC)	107.0	94.0
Coeff. of Linear Expansion $^oC\ 10^{-5}$ (30-80)^oC	1.714	0.835

Table-3: Characteristics of the Coatings after applying on substrate

Name of Tests	**Type of Coating**	
	Epoxy	**Epoxy/Phenolic (IPN)**
Shear strength (Kg/cm^2)	58.0	77.00
Bond Strength (Kg/cm^2) with Concrete Substrate*	30.00*	30.00*
Scrub resistance(10,000cycles)	No failure	No failure
Impact Resistance (falling weight method)	No failure	No failure
Salt Fog (720 hrs)	No failure	No failure
Scratch Hardness (1500gm load)	No failure	No failure

Table-4 : Results of Loss in Weight of Reinforcement Bars after Accelerated Corrosion Test

Sl. No.	Number of Cycles	Weight Loss(%)			
		Uncoated Bars Cover, mm		Coated Bars Cover,mm	
		15	25	15	25
1.	10	0.16	0.08	0.00	0.00
2.	30	2.46	1.91	0.31	0.21
3.	60	6.69	5.36	0.75	0.55

Table-5 :Bond Strength with Concrete (Pullout Test Method)

Dia of the Bar (mm)	Condition of bar	Bond Stress 0.25mm slip (Kg/cm^2)	Bond stress at rupture(kg/cm^2)
12	Uncoated rebar	44.5	113.00
12	IPN coated rebar	42.5	110.00
12	Plain uncoated bar	-	67.00
12	Plain IPN coated	-	82.00*

* After curing the first coat second coat was applied immediately.After the second coat, sand was sprinkled on the coated surfaces.

Modification of resol phenolic resin by unsaturated polyester for improved mechanical properties

Parameswaran PS[1,2], Eby Thomas Thachil[1*]

[1]Department of Polymer Science and Rubber Technology,Cochin University of Science and Technology, Kochi, Kerala, India
[2]Department of Chemistry, S D College, Alappuzha, Kerala, India.

Email: pspeswaran@cusat.ac.in

***Abstract*: Cured phenol formaldehyde resol resin is a brittle material due to an extensive three dimensional structure. Formation of microvoids in the cured structure results in inferior mechanical properties. In this study, unsaturated polyester (UP) is used as a modifier for phenolic resol resin. The tensile and impact strengths of the modified resin are compared with that of the neat resin. The SEM pictures of the fractured surface are used to investigate the morphological changes on modification. The modified resin has fewer voids after crosslinking and possesses superior mechanical properties, especially impact strength**.

Introduction:

Phenol formaldehyde resol resin is a thermoset resin and forms a three dimensional network structure on curing. The methylene bridges formed between the individual phenolic units make it a brittle material. Another drawback of resol resin is the formation of microvoids in the cured resin due to the escape/trapping of condensation byproducts in the materia[l]. The normal method of reducing the microvoids is by carrying out the cure process by heat and pressure. Open molding of phenolic resin creates a large number of microvoids even if the cure process is done in a controlled manner. Reinforcements like saw dust, cotton linters, glass fibers, particular fillers etc. have also been employed for reducing microvoids and improving the properties of phenolic resin. Polyols like ethylene glycol, glycerol etc have been used as modifiers for microvoids and give transparent nature to the cured resin[2]. Dicarboxylic acids with 6-10 carbon atoms can improve the properties of resol phenolic resin by introducing these into the network structure[3]. Unsaturated polyester (UP), prepared from a glycol and a dicarboxylic acid, containing an alcoholic part and an acid part, can combine with phenolic resin during curing. It is expected that the UP can reduce the microvoids and also introduce soft segments to improve the brittle character of phenolic resin.

Experimental:

1,2 propylene glycol, maleic anhydride , phthalic anhydride, xylene, triphenyl phosphate and glacial acetic acid were laboratory reagent (LR) grade supplied by E. Merck India Ltd, Bombay. Commercial resol resin in alkaline condition (solid content ~ 50%) was obtained from M/S.Polyformalin (P) Limited, Thripunithura, Kerala, India

Resol resin was neutralised with glacial acetic acid until the pH reached a value of ~7.0. It was then kept overnight for phase separation and the water layer was decanted off. The resin was subsequently dried for 12 hours using a vacuum oven to completely remove the water.

Synthesis of unsaturated polyester (UP):

* Corresponding author. Tel.: +91 484 2575723; fax.: +91 484 2577747
E-mail address: ethachil@cusat.ac.in (Eby Thomas Thachil)

Cherian et al[4] have observed that the optimal procedure for synthesis of UP is to initially react PA with the total stoichiometric amount of PG and subsequently react the product with MA. This procedure has been adopted for the synthesis. UPs with four different maleic anhydride to phthalic anhydride (MA/PA) ratios (90/10, 70/30, 50/50 & 30/70) designated as UP1, UP2, UP3 & UP4 respectively were synthesised (acid value~26).

Sample preparation:

Dried phenolic resol resin (R) was mixed with varying proportions of UP dissolved in methyl ethyl ketone using a mechanical stirrer for 20 minutes. The solvent was then removed by applying vacuum for about 45 minutes. The modified resins were designated as RUP1, RUP2, RUP3 and RUP4 corresponding to each MA/PA ratio. Since UP2 corresponding to an MA/PA ratio of 70:30 was observed to give the best properties when blended with phenolic resin, subsequent studies using polyesters of different acid values were limited to UP2 only. RUP2a - d represent various blends containing UP of different acid values namely 93, 70, 60 and 50. The dried and degassed samples were then poured into a teflon mold fabricated as per ASTM standards and cured in an air oven according to the following temperature schedule: 60°C-2hours, 70°C-15hours, 80°C-2 hours, 90°C-1hour, 100°C-1hour, 110°C-1hours and 120°C-2hours.

Mechanical properties: Tensile strength of the cured samples were tested in a Shimadzu Autograph AGI Universal Testing Machine. Impact strength of the cured samples was tested in a Resil Impact Analyser (Junior). The specimens were tested using a hammer with 4J capacity at a speed of 3.46m/s.

SEM Analysis:The morphology of the fractured surface was studied using JOEL JSM 840A Scanning Electron Microscope in order to find the extent of microvoids in the cured phenolic resin.

Results and Discussions:

The variation in tensile strength and impact strength of modified phenolic resin with the proportion UP having varying ratios of MA/PA is shown in Table I

Both the tensile strength and impact strength of the resin increased on modification with UP and show a maximum at 7.5% of UP content. Phenolic resin modified with UP2 shows comparatively better properties. Higher number of unsaturation in UP may give more flexibility to the cured resin. But the properties show a maximum at MA/PA ratio=70/30. This may be due to greater compatibility bequeathed by PA to the resin by virtue of more benzene rings in the structure. But as can be expected, still higher amounts of PA in UP slightly decreased the mechanical properties due to lessened possibility of a 'Diels Alder' type addition reaction between quinanoid structures of phenolics and unsaturated bonds in UP. Hence UP with MA/PA ratio 70/30 is preferred.

The influence of acid value on the properties of phenolic resin is shown in Table II. Both the tensile and impact strength values of the modified resin show variation with the acid value of UP2. An acid value of ~60 shows a maximum in the properties. This indicates that a UP with a medium chain length is a better modifier for phenolic resin. As can be seen from the SEM pictures of the modified resin (Fig.1), the microvoids in the cured resin tremendously decreased as a result of modification.

The micrographs clearly indicate the reduction in the microvoids. Broader fracture paths on modification also indicate greater energy absorption. These factors lead to overall improvement in the properties of phenolic resin.

Conclusion:

Phenolic resin can be successfully modified by UP resin. UP resin with MA/PA ratio=70/30 shows the best properties. The acid value of UP resin has also an influence on the properties. The SEM picture of the fractured surface indicate that the the modification leads to reduction in the microvoids as well as greater energy absorption.

Reference:

1. Wolfrum, J., Ehrenstien, G. W. J Appl. Polym.Sci. 1999,74,3173-3185.
2. Singh, K. P.; Palmese, G. R. J Appl. Polym.Sci. 2004,91,3096-3106.
3. Kaynak, C.; Tasan, C. C. Euro Poly Jnl 2006,42,1908-1921.
4. Benny, C.; Eby, T. T. Polym. Plast. Techn. Eng. 2005,44,931-938.

Table I. Tensile and Impact strength of modified resin by UP with varying MA/PA ratio

Modifier	Tensile Strength(MPa)					Impact Strength(KJ/m^2)				
	0	2.5	5.0	7.5	10.0	0	2.5	5.0	7.5	10
UP1(90/10)	26.0	29.2	31.8	33.2	29.1	47.4	56.4	75.7	114.4	110.4
UP2(70/30)		28.3	30.9	34.0	31.2		63.5	78.2	117.8	115.3
UP3(50/50)		28.5	30.8	31.8	30.6		60.2	74.8	111.6	109.1
UP4(30/70)		27.0	31.1	29.9	27.2		58.3	68.3	106.2	105.4

Table II: Tensile and Impact strength of modified resin by UP2 with varying acid values

Modifier	Tensile Strength (MPa)					Impact Strength(KJ/m^2)				
	0	2.5	5.0	7.5	10.0	0	2.5	5.0	7.5	10
UP2a(93)	26.0	29.1	32.2	34.1	30.6	47.4	68.5	89.1	118.8	115.1
UP2b(70)		28.1	31.2	34.0	29.0		70.9	91.3	122.0	121.6
UP2c(60)		30.3	32.6	35.3	31.9		69.3	97.8	133.8	125.9
UP2d(50)		29.6	31.4	32.4	27.5		65.2	93.6	120	117.9

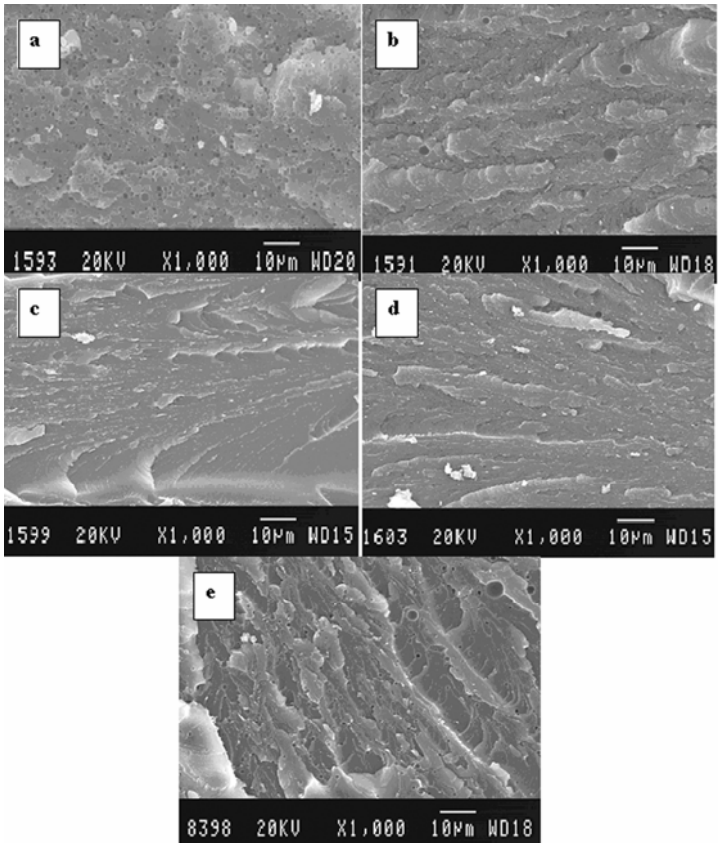

Fig.1. SEM micrographs of fractured surface of modified phenolic resin with 7.5% of UP2(a)RUP2a (b)RUP2b (c)RUP2c (d)RUP2d and (e)RUP2

Effect of blend composition on the tensile behaviour of PS/HIPS blends

Deviprasad Varma P.R [1 *], Sreejith P.S [2], George K.E [3 #]

1. Department of Mechanical Engineering, M.A.College of Engineering, Kothamangalam-686 666, Kerala, India..
2. Division of Mechanical Engineering, School of Engineering, CUSAT, Kochi-22, Kerala, India.
3. Dept. of Polymer Science and Rubber Technology, CUSAT, Kochi-22, Kerala, India.

E mail: kegeorge@ cusat.ac.in

Abstract

The tensile behaviour of un-notched and notched polystyrene / high impact polystyrene blends was evaluated at slow speed. Both the tensile modulus and maximum strain remain more or less constant upto about 40% HIPS and thereafter show a drastic change indicating changes in the morphology at this composition. The notched specimens also follow a comparable trend even though the notch sensitivity marginally increases with HIPS content.

Introduction

Polymers are now widely employed in engineering and other fields to replace conventional materials because of their attractive properties like light weight, easy processability, corrosion resistance etc. Polymer blends are widely used to optimize the processing and performance characteristics [1, 2].In many applications, their mechanical behaviour especially the fracture characteristics and notch sensitivity is important [3].

Polystyrene (PS) is one of the most widely used thermoplastics due to its transparency, easy processibility and low cost. Because of the brittleness of PS, its impact resistant counterpart high impact polystyrene (HIPS) is also widely used. However, the improvement in impact strength is achieved with reduction in stiffness and transparency. The objective of the present study is to explore the effect of blend composition on the tensile behaviour of PS/HIPS blends.

Experimental

The materials used were,

1. Polystyrene (PS)

PS grade LGG104 was supplied by LG Plastics with MFI 18 gm/10 min.

2. High Impact Polystyrene (HIPS)

HIPS grade LGH 302 was supplied by LG Plastics with MFI 18 gm / 10 min.

Melt mixing in Thermo Haake Torque Rheometer

PS and HIPS were melt mixed in different proportions in a torque rheometer (Thermo Haake Torque Rheometer 600P) for 8 minutes at 180 ^{0} C and 50 RPM with continuous torque monitoring.

Specimen preparation

Dumbell specimens were prepared (according to ASTM D 638 specification) by injection moulding the blends at 180 ^{0} C in a semi automatic injection moulding machine. To conduct notch sensitivity test, the specimens were notched to 1 mm depth before testing.

The tensile properties of the specimens were determined using a universal testing machine (Schimadzu UTM) at a crosshead speed of 5 mm/mim.

Results and discussion

The variation of tensile modulus with HIPS content is shown in Fig.1. The figure shows that the blend retains its mechanical stiffness upto about 40% of HIPS and thereafter the stiffness drastically reduces.

The variation of maximum strain with HIPS content is shown in Fig.2.This behaviour is also similar to that of Fig.1. The maximum strain remains more or less constant upto 40% of HIPS and thereafter improves significantly.

The variation of tensile modulus with HIPS content for notched samples is shown in Fig.3. The difference in tensile modulus between notched and un notched specimens gradually increases with HIPS content. The variation of maximum strain with HIPS content for notched samples is shown in Fig.4.

Conclusion

1. Polystyrene fails under brittle mode and HIPS under ductile mode.

2. The fracture behaviour of PS/HIPS blends was investigated. Upto 40% concentration of HIPS, the blend was found to fail under brittle mode and thereafter under ductile mode.

3. The notch sensitivity of PS/HIPS blends is found to increase marginally with HIPS content under slow speed testing.

References

1. Karger-Kocsis, J., Ed.; *Polypropylene – structure, Blends and Composites*. Chap.7. Chapman and Hall, London, 1995.

2. Paul D.R., Bucknall C.B. (Ed) *Polymer Blends,* John Wiley, New York, 2000

3. Takayuki Murayama, *Dynamic Mechanical Analysis of Polymeric Materials*, Elselvier Scientific Publishing Company, Amsterdam, 1978

4. Vishu H. Shah, *Handbook of Plastics Testing Technology*, John Wiley & Sons, New York, 1984

5. Brydson J.A, *Plastic Materials* 7th Ed.., Butterworth, Oxford, 1999

6. Sperling L.H., *Introduction to Physical Polymer Science*, Wiley & Sons, New York, 1986

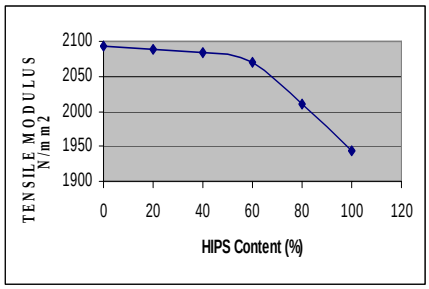

Fig:1 The variation of tensile modulus with HIPS content.

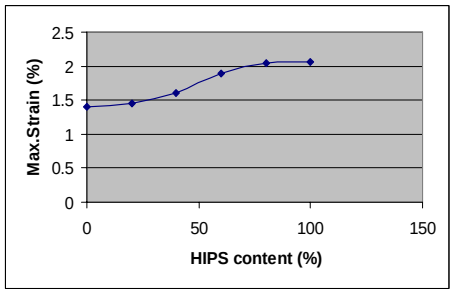

Fig:2 The variation of Max. strain with HIPS content.

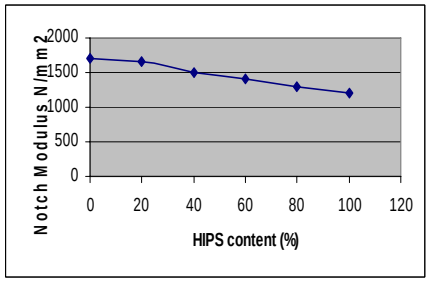

Fig:3 The variation of tensile modulus with HIPS content for notched samples.

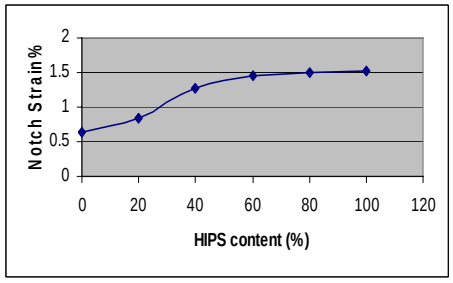

Fig:4 The variation of max. strain with HIPS content for notched samples.

Surface energy and water uptake behavior of PVA/SSA proton conducting membranes

P. Kanakasabai , P.Vijay, Abhijit P. Deshpande, Susy Varughese*
Department of Chemical Engineering, Indian Institute of Technology Madras,
Chennai-600036, Tamilnadu, India

Email: susy@iitm.ac.in

Abstract

The surface and interfacial properties of proton-conducting ion exchange membranes are important in their application as solid polymer electrolytes in fuel cells. Poly(vinyl alcohol)(PVA)/ sulfosuccinic acid (SSA) membranes of different crosslink densities were prepared by varying the SSA content (0-30 wt.%) and the drying temperature. These membranes were characterized for their surface energy and wetting characteristics using the contact angle method under dry and wet conditions. Contact angles were measured using the sessile drop method. The total surface energies of the membranes varied as a function of the membrane condition (wet and dry) and the degree of crosslinking. For varying SSA content, the proton conductivity and water uptake of these membranes were measured. Wetting and surface energy of these membranes were found to vary with crosslinking time and SSA content. Wetting characteristics of these membranes affect the proton conductivity, water uptake and ion exchange capacity. For comparison purposes commercial Nafion 117 membranes were also analyzed.

Keywords: Surface energy, Proton conductivity, PVA/SSA membranes

1. INTRODUCTION

Proton exchange membrane fuel cells (PEMFC) are promising energy converters for stationery and portable applications as well as for applications in automobiles. The proton conducting membrane is a vital component of any PEMFC [1]. Protons are transported through the polymer electrolyte when the humidification of the polymer is high enough. Nafion membrane, a perfluorinated sulfonated ionomer shows high proton conductivity (~0.1 S/cm) at fully hydrated state [2, 3]. The main limitations of Nafion are its poor barrier properties and cost .Hence, novel proton conductive membranes with low cost and better barrier properties are needed. To meet these objectives, many kinds of proton exchange membranes have been developed. Among these membranes, poly (vinyl alcohol) (PVA) based membranes show good protonic conductivity with low methanol permeability. Introduction of negatively charged ion groups in PVA membrane using sulfo succinic acid (SSA) can chemically modify and also can crosslink PVA [2, 3].

The wetting characteristics of proton conducting membranes are important in understanding the water uptake features of the membranes. When hydrophilicity and hydrophobicity are studied, contact angle measurement is one of the most used experimental methods [5]. The wetting properties of proton–conducting membranes were investigated by Zawodzinski et al. [4]. They studied the contact angles of water on the surface of perfluorosulfonic acid (Nafion) membranes in pre-hydrated state and also a function of drying time or water content of the membrane. They found out that contact angles of water on nafion membranes decreased as the water content in the membrane increased. Brack et al [6] investigated the surface properties of selected proton conducting membranes using contact angle measurements with several different liquids. The surface energy of a material determines how it is wet by the liquids. The change in the surface energy of ion-conducting polymers may result from the contributions of the polar and dispersive components. In this study, we investigate the effects of crosslink density and drying time on the surface energy, water uptake and proton conductivity of PVA/SSA membranes.

2. EXPERIMENTAL

2.1 Materials

Polyvinyl alcohol (PVA) (<Mw> = 1, 25,000, degree of hydrolysis - 88 %) and formamide were obtained from Sd Fine Chemicals Ltd Mumbai, India. Sulfosuccinic acid (SSA, 70 wt% solution in water), and Nafion 117 were obtained from Aldrich Chemicals, USA. Glycerol was obtained from Sisco Research Laboratories Limited (Mumbai, India).

2.2 Membrane preparation

PVA solutions were prepared by dissolving required amount of PVA in water [2]. SSA solution (in water) was added to the PVA solution in varying amounts (10-30 wt %) at room temperature and stirred for 24 h. The solutions thus obtained were used to cast films and allowed to dry at 60 °C in an air oven for 24 h (pre-processed membranes). The fully dried membranes were then heated for 2 h in an air oven at 120 °C for increasing the cross-linking reaction (fully processed membranes). Thickness of the membranes was in the range of 150-200 μ_m.

2.3 Contact angle and surface energy

The PVA/SSA membranes were placed on a level surface and the contact angle was measured using Goniometer (GBX Digidrop contact angle meter). The contact angle with each test liquid was measured a minimum of 5 time on different films. Solid surface energy is determined from the contact angle measurements using equation (1) [7]:

$$(1+\cos\theta)\gamma_L = 4\left(\frac{\gamma_s^d\gamma_L^d}{\gamma_s^d+\gamma_L^d}+\frac{\gamma_s^p\gamma_L^p}{\gamma_s^p+\gamma_L^p}\right) \quad (1)$$

where θ - contact angle between solid and liquid, γ_L - surface energy of liquid, γ_s^d - dispersion component of surface energy of solid, γ_L^d - dispersion component of surface energy of liquid, γ_s^p - polar or non-dispersive component of surface energy of solid, γ_L^p - polar or non-dispersive component of surface energy of liquid. The total surface energy can be expressed by two separate components, one is the dispersion force and the other is the polar or non-dispersive force based on a theoretical consideration of attractive forces at the interface suggested by Fowkes [8]:

$$\gamma = \gamma^d + \gamma^p \quad (2)$$

If two test liquids are used to measure the contact angles on a solid, the surface energy and non-dispersiveity of the solid can be determined by means of equations (1) and (2).

2.4 Swelling studies

The water uptake in the PVA/SSA membranes were determined by immersing the membrane samples in distilled water at 25 °C for 24h. The membranes were taken out and dried using tissue paper and weighed immediately on a microbalance. The water uptake in the membranes is given by equation (3)

$$W = \frac{W_{wet} - W_{dry}}{W_{dry}} \quad (3)$$ (3)

where, W_{dry} and W_{wet} are the weights of dry and corresponding water-sorbed membranes.
Cross linking density (ρ mol/cm^3) of the membranes was determined using equation (4) [9].

$$\rho = 1/(vM_c) \quad (4)$$

where M_c - molecular weight between crosslinks was determined using the Flory-Rehner equation [10] and ν is the specific volume of PVA.

2.5 Proton conductivity

Impedance measurements on PVA/SSA membranes were carried out using an impedance analyzer in combination with an electro chemical interface (GILL ACM Instrument) in the frequency range 30-30 KHz using circular films of 10 mm diameter at room temperature. The proton conductivity, σ (S/cm) can be obtained from equation (5)

$$\sigma = l/RS \tag{5}$$

where *R* is the bulk resistance or ohmic resistance of the membrane sample, *l* is the thickness of the membrane (cm) and *S* is the cross sectional area (cm^2) of the membrane.

3. RESULTS AND DISCUSSION

PVA membranes of different crosslink densities were prepared by varying the SSA content (10, 20 and 30 wt %) and the drying temperature (at 60°C and 120°C). Membranes dried at 60 °C are considered as pre-processed and the membranes dried at 120 °C are considered as fully processed. Contact angle measurements were carried out on the membranes to determine the total surface energy and the contributions of the non-dispersive and dispersive components to the total surface energy**.** Proton conductivity, water uptake and ion exchange capacity (IEC) were also determined for these membranes. The liquids used to determine surface energies of the membranes are given in Table 1.The non-dispersive, dispersive components, total surface energies, water uptake and ion exchange capacities of membranes under dry and wet condition are given in Tables 2, 3 and 4. Total surface energy values of Nafion (dry membrane - 25.44 mN/m, wet membrane 38.21 mN/m) and PVA are similar to that reported earlier [5, 6]. Cross linking density of PVA increases with the increase in SSA content and the drying temperature as shown in Table 2 and 3. This in turn affects the surface wetting properties of the membranes. Crosslink density values are high for fully processed membranes in comparison with pre-processed ones. Similar behavior is observed in the case of total surface energy. Surface energy is found to increase with increase in crosslink density upto 20% SSA content and then decreases in the case of 30% SSA content. The increase in surface energies are mainly due to contributions from the non-dispersive component as can be seen in Tables 2 and 3. The contribution of the sulfonic acid groups to non-dispersive (non-dispersive component) interactions is expected to be high because of their ability to act as both a strong donor and acceptor in hydrogen bonding interactions [6].

The surface energy of PVA/20%SSA is high in comparison with PVA/10% SSA and PVA/30% SSA for dry and wet membranes. This indicates that 20% SSA gives an optimum in spreading of water over the membranes. For pre-processed membranes under wet conditions, the total surface energy is mainly due to the polar component and it is higher than fully processed membranes. This could be due to the higher water uptake in the pre-processed membranes and its contribution to the polar component in comparison with fully processed membranes as can be seen from Table 4.

Table.1. Surface energies (mN/m) of study liquids with dispersive and polar components

Liquid	Non-dispersive (polar) component	Dispersive component	Total surface Energy
Water	51	21.8	72.8
Glycerol	30	34	64
Formamide	19	39	58

Water uptake in membranes decreases with increase in the SSA content and the cross linking temperature. It indicates that more cross linking in the PVA/SSA membrane might lead to more rigid and compact polymer [2]. In all the cases proton conductivities of dry membranes were much lower than the hydrated membranes indicating the role of water in the proton transport. Faster mobility of H^+ ions is possible in hydrated state than in dried state.

Table 2: Crosslink density, surface energy, water uptake and ion exchange capacity for pre-processed, dry membranes

SSA content (wt%)	Crosslink density x 10^4 (mol/cm^3)	Surface energy (mN/m)			Water uptake (%)	Ion Exchange Capacity (mmol/g)
		Polar	Dispersive	Total		
0	0.00	24.22	23.69	47.91	0	0
10	2.18	12.56	27.82	40.39	399.67	0.23
20	2.58	25.92	22.37	48.29	399.18	0.5
30	6.35	29.68	9.03	38.72	252.56	1.3

Table 3: Crosslink density, surface energy, water uptake and ion exchange capacity for fully processed, dry membranes

SSA content (wt %)	Crosslink density (mol/cm^3)	Surface energy (mN/m)			Water uptake (%)	Ion Exchange Capacity (mmol/g)
		Polar	Dispersive	Total		
10	0.003	43.34	9.90	53.24	130.50	0.89
20	0.132	57.10	6.43	63.53	6.56	1.4
30	0.281	30.67	13.66	44.32	1.47	0.5

Table 4: Surface energy, proton conductivity and water uptake for pre-processed membranes and fully processed, wet membranes

SSA content (wt %)	Surface energy (mN/m)					
	Pre-processed membranes			Processed membranes		
	Polar	Dispersive	Total	Polar	Dispersive	Total
10	50.97	1.40	52.38	23.46	20.50	43.97
20	50.19	8.55	57.74	27.89	16.50	44.39
30	50.10	3.40	53.50	21.55	17.64	39.20

Fig. 1 and 2 show the proton conductivities of PVA/SSA membranes as a function of cross link density, temperature and level of hydration. The proton conductivities of PVA/SSA membranes are found to be dependent upon the degree of crosslinking which is affected by the amount of crosslinking agent and the drying temperature. The increase in SSA content in the PVA membrane could lead to significant improvement in the proton conductivity owing to the presence of more sulfonic acid groups ($-SO_3H^+$) as a proton donor and carrier when the membranes are in the hydrated condition. Membranes under hydrated condition showed good proton conductivities (10^{-2} S/cm) at 20% SSA irrespective of the cross linking temperature. Similar behavior is observed in the case of surface energy. Hence, higher the surface energy, higher will be the wetting. Ion exchange capacity increases with increase in the crosslink density for pre-processed membranes. Whereas for processed membranes it increases up to 20%SSA beyond that it decreases. This is due to higher brittleness of the

30%SSA processed membranes. Similar behavior is also observed for proton conductivity of 30%SSA processed membranes.

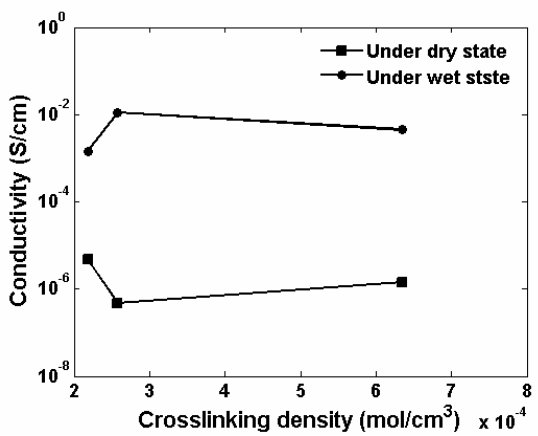

Fig.1. Proton conductivities of PVA/SSA membranes dried at 60°C

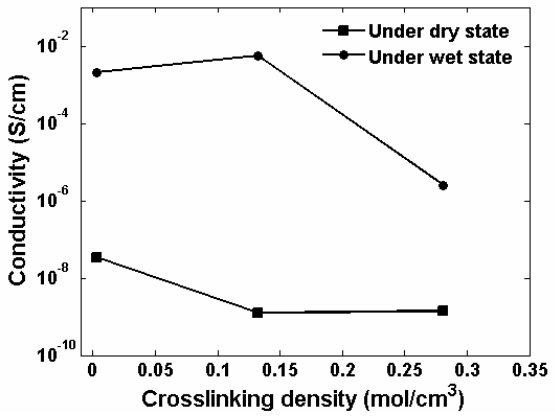

Fig.2. Proton conductivities of PVA/SSA 60°C (???!) dried membranes

CONCLUSIONS

PVA crosslinked membranes containing sulfosuccinic acid were prepared by varying the amount of SSA and the drying temperature. Cross linking density increases with the increase in SSA content and drying temperature. Total surface energy of the 20% SSA crosslinked membranes showed higher values in comparison with other membranes. PVA/SSA membranes show better protonic conductivity under hydrated conditions than dry membranes. Protonic conductivity of 20% SSA crosslinked PVA membranes was in the range of 10^{-3} to 10^{-2} S/cm irrespective of the drying temperature, under hydrated conditions. Wetting and conductivity properties are good for 20% SSA crosslinked membranes. When the total surface energy increased, the membranes showed higher wetting and hence higher proton conductivity. However, this is due to the polar contributions to the total surface energy in the case of wet membranes.

REFERENCES

1. Rhim, J.W., Park, H.B., Lee, C.S.,Jun J.H., Kim, D.S., Lee, Y.M., J. Memb. Sci., 2004, 238, 145
2. Kim, D. S., Park, H.B., Rhim, J.W., Lee, Y.M., J. Memb. Sci., 2004, 240, 37
3. Yan, O., Toghiani, H., Wu, J., J Power Sources 2008, 158, 316
4. Zawodzinski, T.A., Gottesfeld, S., Shoichet, S., McCarthy, T.J., J. Appl. Electrochem., 1993, 23, 86
5. Yu, H.M, Ziegler, C., Oszcipok, M., Zobel, M., Hebling, C., Electochemica Acta, 2006, 50, 1199
6. Brack, H. P., Wyler, M., Peter, G., Scherer, G.G., J. Memb. Sci., 2003, 214, 1
7. Wu, S., J. Polym. Sci., Part C, 1971, 34, 19
8. Fowkes, F.M., Ind. Eng. Chem., 1964, 56, 40
9. Matsuyama, H., Teramoto, M., Urano, H., J. Memb., Sci. 1997, 126, 151
10. Yarimikaya, S., Basan, H., J. Macromol. Sci., 2007, 44, 699

Modification of epoxy by addition of thermoplastic polymers

Anupam S. Shiwach[*] & Rajni Lakhani [#]

Organic Building Material Division, Central Building Research Institute, Roorkee-247667, (U.K.) India

E-mail: anupam_shiwach@yahoo.co.in

Abstract

In civil engineering constructions, cement-bonded materials have a major contribution. Improvement of performance and durability of cement bonded materials has been the continued efforts since long. Nevertheless, such structures deteriorate with time due to various reasons such as moisture, temperature, load, chemical attack, fatigue and many other factors. For repair and restoration of these structures, the requirement of properties of repair materials varies according to the properties of the base concrete and form of the repair. Fresh plain cement mortar or concrete may not meet the desired properties. Polymers are often used for most of the repair works to meet the required properties.

Currently latexes or emulsions of polymers are used either as monomer or as copolymer of various combinations like polyvinyl acetate, vinyl acetate-ethylene, styrene-butadiene, styrene-acrylic, and styrene butadiene rubber emulsions. However, in spite of several useful characteristics, these polymers have their own limitations.

Multicomponent polymeric system (polymeric blend) is now one of the advance domains in modern polymer science. Various physical properties of such polymer blends are of particular interest because the same are related to the composition, inter components interaction, phase structure as well as processing conditions.

In view of the above, studies have been carried out on modification of the epoxy polymer by blending thermoplastic polymers. Acrylic & Styrene Butadiene Rubber (SBR) are used in different ratios to take advantage of strong points of both the polymers. Thermal, chemical and physico-mechanical properties of developed blends have been studied. It has been inferred from the work that the polymer blend improve the properties remarkably as compared to neat epoxy system. The developed polymer blend would be used for the formulation of different types of repair materials for building applications.

Introduction

Epoxy resin have been used as an adhesive since the 1950s due to their wetting ability, low cure shrinkage, superior mechanical properties and excellent chemical resistance (Potter[1]; May *et al* [2]; Bouer [3]). However when cured with stoichiometric amounts of polyfunctional amines, the high degree of crosslinking makes epoxy resin a brittle material. This weakens the peeling and impact strength of epoxies and therefore limits their applications. The use of long chain hardener, and compatible blendings is reported in the literature as solution to this problem (Peters and Logan [4]; Ratna *et al* [5]). Blending is an important way to develop new polymers. Through blending the advantages of different polymers can be combined and new kind of material with special property can be developed (Utracki [6]; Feng *et al* [7]). The most successful method is blending with suitable reactive liquid rubbers (McGarry and Wilner [8]; Reiw [9]). Initially, the liquid rubber remains compatible with the epoxy hardener mixture, but with the advancement of curing reaction it undergoes phase separation at a certain stage leading to the formation of a two

phase microstructure (Reiw [9]; Verchere *et a*l[10]). The beauty of this method is that the improvement of impact and adhesive strength is achieved without significant deterioration of thermomechanical properties (Bitner *et al* [11]; Achary *et al* [12]).
A liquid rubber toughened epoxy, often shows outstanding fracture properties and this technology is exploited in the field of engineering adhesives (Kinloch [13]). But most of the reported rubber toughened epoxy formulations suffer from the problem of heat cure. Heat curing is difficult and impractical for fabrication of certain structures and requires significant amounts of energy. Ambient curing saves energy and is advantageous for application of surface coating and adhesive onto an intricate structure. Acrylate based liquid rubber can be a substitute for butadiene based rubber for toughening epoxy resin because of its comparatively better oxidative and thermal stability (Ho and Wang [14]).
The aim of the present work is to prepare styrene-acrylate of different formulation by varying the ratios of styrene and acrylic emulsion and examine its effect on the mechanical properties of epoxy resin.

Experimental

Materials

Styrene Butadiene Rubber (Pidilite) was used with Acrylic emulsion for the formation of Styrene-Acrylate. Epoxy resin was a liquid diglycidyl ether of bisphenol A type (Ciba Geigy, Araldite GY-250) with an equivalent weight per epoxide group of 230± 8. An ambient temperature hardener, Polyaminoimidazoline (Ciba Geigy, Aradur HY-140) was used as a curing agent. Additives like water based defoamer and emulsifier etc. were of analytical grade.

Preparation of Styrene acrylate

Three formulations of styrene-acrylate has been prepared by varying the ratio of Acrylic and SBR (Table 1) and observed for pot life after 1month, 3 month and 6 month.

Preparation,Optimization and curing of polymer blend

Now each formulation PB-4 (60:40), PB-7 (40:60) and PB-10 (20:80) of styrene-acrylate (1 part) was mixed with epoxy resin (1 part) at room temperature. This styrene acrylate modified epoxy also has been observed for pot life after 1month, 3 month and 6 month. The modified sample is liquid and no solidification or gelling was observed after mixing. The diluted mixture was then cured with Aradur (HY-140). It has been observed that prepared modified epoxy is capable of reacting with the hardener in the same way as epoxy. The gel time of unmodified and modified epoxy with HY-140 at room temp. was compared and it was found that the gel time of the modified epoxies are longer than that of the unmodified epoxy. This developed system has been characterized by various test methods.

Characterization of modified Polymer

Tensile Test

Tensile Tests were performed on dumb-bell shaped type IV samples according to ASTM D-638. The dumb-bell shaped samples were prepared by casting polymer blends directly in prespex mould. The samples were allowed to cure for 7 days at room temperature. The tensile strength was measured using Universal Testing Machine (UTM-Shimadzu). The cross head speed was 1 mm/min. and the gauge length was 55 mm. The results are being calculated by dividing the load at break by the cross sectional area of the dumb-bell centerpiece. The quoted result is the average of the results from five dumb-bells.

Flexural test

The flexural properties were measured with rectangular sample according to ASTM-790, using the same UTM at a crosshead speed of 1mm/min. The fracture strength (FS) was determined from

the following formula:

$$FS = (3 \times \text{peak load} \times \text{span}) / 2 \times \text{width} \times (\text{thickness})^2$$

The results are the average of five samples

Compression Test

Compression test were performed on cubes according to ASTM D695-02a. Cubes were prepared in teflon mould at room temperature and compressive properties were measured using UTM at a crosshead speed of 5mm/min. Results are expressed in MPa.

Fracture Surface Analysis

An optical microscope was used to analyse the fracture surface (broken in Flexural test) of the toughened epoxy networks. All the photographs were taken at 30 X magnification.

Results and Discussion

Evaluation of modified networks

In order to study the effect of styrene-acrylate modification on properties, various formulations were prepared incorporating different ratio of SBR and acrylic. All the formulations were evaluated with respect to their Tensile strength, Flexural strength and Compressive strength. The evaluation was carried out for each sample after curing according to the test method described in the Experimental section.

Table 2 shows the result of tensile tests carried out for modified and unmodfied epoxy samples after curing. It is evident that tensile strength and strain increases as concentration of SBR increases in Styrene-Acrylate. A representative tensile stress versus strain curve for pure epoxy and modified epoxy is shown in Fig1. As the concentration of SBR in styrene-acrylate increases, the tensile strength decreases and the percentage elongation at break increases. This increase in flexibility is due to the presence of rubber particles (low modulus) in the epoxy matrix. Similar observations have been reported by many authors (Manternal *et al* [15]; Pearson and Yee [16]; Bascom *et al* [17].

A similar trend was observed for flexural fracture strength and deformation (Table 2). A flexural stress versus deformation curve for pure epoxy and modified epoxy is shown in Fig.2. This indicates higher deformation and lower strength for modified epoxy. The decrease in flexural strength was also observed by lijjima *et al*[18,19] for epoxy terminated acrylic rubber modified epoxy.

Compressive properties reported in Table 2. shows that samples follow similar trend under compression.

Optical microscopy analysis

To study the morphological properties of the modified epoxy, the microstructure of the fracture surfaces of polymer blends were analyzed by optical microscopy. The micrographs for unmodified and modified networks are shown in Fig. 3. The fracture surface of pure epoxy is homogeneous without any dispersed particles, whereas the surface of blends consists of two distinct phase; globular particles are dispersed in a continuous epoxy matrix. The number of particles increases with an increase in the concentration of SBR and aggregation starts at high concentration.

Conclusions

Different formulations of styrene-acrylate has been prepared by varying the ratios of SBR and Acrylic emulsion. These formulations are compatible with epoxy resin at room temperature. No gelling was observed after mixing. The modified resin undergoes curing reaction in the same way

as pure epoxy resin. Modified resin has lesser strength under tension, compression and flexural mode in comparison to the pure epoxy. But improvement in toughness and elasticity was observed as a result of the incorporation of styrene-acrylate in to the epoxy matrix which is important criteria for repair materials. Due to this, developed blends will be used with cement to prepare polymer modified cementitious repair materials for building applications in our further studies.

References

1. Potter W G, Epoxide Resins, Springer, New York 1970.
2. May C A and Tanka G Y, Epoxy Resin Chemistry and Technology, Marcel Dekker, New York 1973.
3. Bouer R S, Epoxy Resin Chemistry, Advances in Chemistry Series 114, American Chemical Society, Washington DC 1979.
4. Peters R A and Logan TJ, Adhesive Age (Apr) 1975; 17.
5. Ratna D, Chakraborty B C and Deb PC, Journal of Polymer Materials 1997; 14: 189
6. Utracki, L.A. Polymers Alloys and Blends: Thermodynamics and Rheology, Carl Hanser Verlag, Munnich 1989.
7. Feng, J. Winnik, M.A. Shivers, R.R. Clubb, B. "Polymer blend latex films: Morphology and transparency" Macromolecules 1995; 28 (23): 7671-7682.
8. McGarry FJ and Wilner A M, Toughening of an Epoxy Resin by an Elastomer Second Phase, Report R 68-8, Massachusetts Institute of Technology, March 1968.
9. Reiw C K, Rubber Chem Technol 1981; 54: 374
10. Verchere D, Pascault JP and Sautereau H, Moschair SM, Riccardi CC and Williams RJJ, J Appl Polym Sci 42: 701 (1991).
11. Bitner JL, Rushford JL, Rose WS, Hunston DL and Riew CK, J Adhes 1981; 13:3.
12. Achary PS, Latha PB and Ramaswamy R, J Appl Polym Sci 1990; 41:151.
13. Kinloch AJ, Adhesion and Adhesive; Science and Technology, Chapman Hall, London 1987.
14. Ho C and Wang C-s, J Appl Polym Sci 1993; 50: 447.
15. Manternal S, Pascault J P and Sautereau H, in Rubber Toughened Plastics, Ed by Riew CK, Advances in Chemistry Series 222, American Chemical Society, Washington DC. 1989.
16. Pearson RA and Yee AF, J Mater Sci 1989; 24: 2571.
17. Bascom WD, Ting RY, moulton R J, Riew CK and Siebert AR, J Mater Sci 1981; 16: 2657.
18. Iijima T, Naoto y and Masao T, Eur Polym J, 1992 ; 28 :573 .
19. Iijima T, Tomoi M, Yamaski J and Kakiuchi H, Eur polym J 1990; 26:145 .

Table 1. Different formulations of styrene-acrylate

Formulation	*Part of Acrylic Emulsion*	*Part of SBR*
PB-4	60%	40%
PB-7	40%	60%
PB-10	20%	80%

Table 2. Effect of styrene-acrylate modification on the mechanical properties

Type of samples	*Tensile strength (MPa)*	*Elongation at break (%)*	*Flexural strength (MPa)*	*Deformation at break (%)*	*Compressive strength (MPa)*	*Compression at break (%)*
Epoxy	28.8	5.0	54.0	4.9	62.5	6.7
PB-4 –Epoxy	7.9	3.6	14.4	7.7	13.9	34.4
PB-7 –Epoxy	10.6	8.7	13.2	5.0	13.7	27.5
PB-10 –Epoxy	11.0	15	10.9	7.4	34.0	49.9

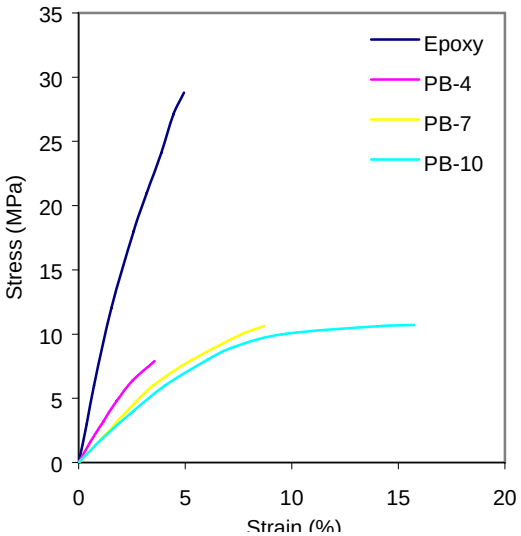

Figure 1. Tensile stress versus strain curve of pure epoxy and modified epoxy

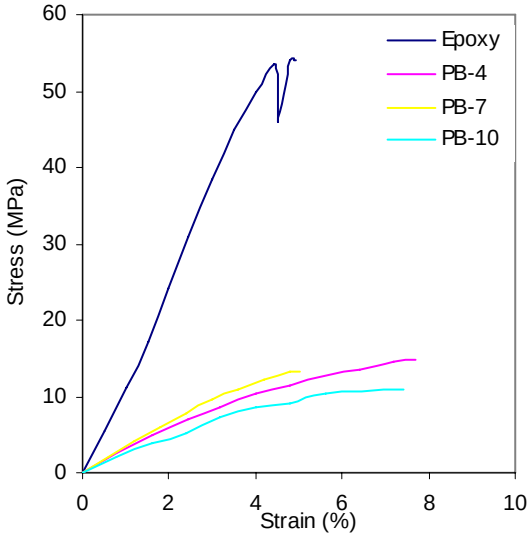

Figure 2. Flexural stress versus strain curve of pure epoxy and modified epoxy

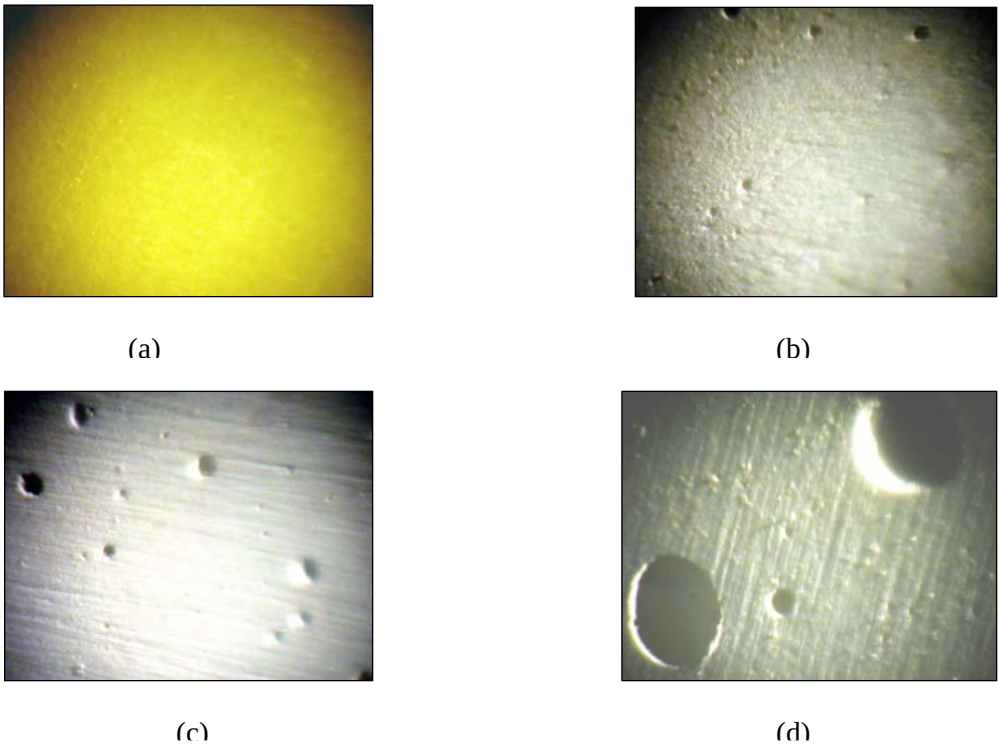

Figure 3. Micrographs of the fracture surfaces (a) Unmodified Epoxy, (b) PB-4-Epoxy (c) PB-7-Epoxy (d) PB-10-Epoxy.

WELD LINE BEHAVIOUR OF PP, HDPE AND PP/HDPE BLEND COMPOSITES.

Newly Joseph*and Dr. K. E. George#
Department of Polymer Science and Rubber Technology,
Cochin University of Science and Technology,
Kochi-682022, Kerala, India. Ph:0484-2575723.
e-mail:kegeorge@cusat.ac.in

Abstract

Incorporation of glass fibres in the commodity plastics like PP and HDPE enhances the mechanical properties of polymers but it weakens the moulded part at weld lines. The study envisages to find out the extent of weld line weakness in PP, HDPE and PP/HDPE blend composites and to determine the optimum fibre length for maximum mechanical strength. The optimum fibre length for PP, HDPE and PP/HDPE blend composites were found to be 6mm, 4mm, 4mm for specimens with weld lines and 8mm, 8mm, 4mm for specimens without weld lines respectively.

Introduction

Short fibre composites are widely used for applications in engineering and in consumer goods.They offer a unique combination of properties and are more economical than competing materials. Short fibre reinforcement improves the stiffness, strength, toughness, dimensional stability, design flexibility and can be processed in a manner similar to the matrix**.** The most common fibre is glass, usually E-glass. Glass fibres are usually 5-20 μm in diameter and are round and fairly smooth, though their surfaces are never completely defect free[1]. Properties such as low cost, high production rate, high strength and stiffness, relatively low density ,resistance to heat and chemicals ,good electrical insulation have made E-glass popular in fibre glass industry and other glass fibre reinforced composites. Short fibre composites are often manufactured through injection moulding process. The injection moulding of large and complex parts requires the use of multi-gated moulds which results in the formation of weld lines. Weld lines are the visual and structural defects that occur when two flow fronts meet due to either multi-gated moulds (type I) or the splitting and rejoining of flow that occurs around inserts (type II). Even a sudden change in wall thickness can cause weld line formation. These structurally weak points in the moulded parts causes serious difficulties in design and long term durability of the processed polymer composites. Process and material parameters, diffusion times, v-notch sharpness and depth, molecular orientation, voids, and contaminants have all been cited as the main reason for weld line weakness in different systems[2-6].

Experimental

Materials used for the composite study are

(a)Polypropylene (PP): REPOL H110MA, with a melt flow index of 20g/10min,supplied by Reliance Industries Limited , Mumbai,India

(b)High Density Polyethylene(HDPE): HDPE Grade Indothene HD50MA180 ,supplied by Indian Petrochemicals Limited (IPCL),Baroda,India,with density 0.950g/cm^3 and MFI 20g/10min

(c)Glass fibre: E-Glass with grade RP10

Melt mixing in Brabender Plasticorder: Short fibre composites of PP and HDPE with 10% fibre content of 2,4,6,8and 10mm were prepared by melt mixing and blending of 36g of the matrix and 4g of fibre at the set temperature in an internal mixer, Brabender Plasticorder, at a rotor speed of 52 rpm for 8 minutes .The temperature was kept at 180^{0}C for PP and 140^{0}C for HDPE to ensure proper melting of the matrix. For the preparation of 50% PP/HDPE blend, 18g each of PP and HDPE and 4g of fibre were melt mixed and blended at 180^{0}C for 8 minutes.

Fabrication of moulds:Moulds were fabricated with single gating for samples without weld lines (fig.1) and with double gating for samples with weld lines (fig2).Here the weld lines are formed by the direct impingement of two opposing melt fronts (fig3).Tensile test samples of size conforming to ASTM-D-638 with and without weld lines were moulded using the moulds which were fabricated.

Preparation of Test Specimens: The hot mix from the mixing chamber was immediately passed through hydraulic press and the resulting sheets were cut to small pieces. The test specimens with and without weld lines were moulded using semi-automated plunger type injection moulding machine

at identical conditions. The mould was preheated to 80^0**C** and the temperature was set according to the melt temperature of the material and the injection pressure and holding time was adjusted to get the desired properties.

Testing: The tensile properties of the samples were determined using dumbbell shaped specimens with Universal Testing Machine (Shimadzu AGI) at a cross speed of 50mm/min according to ASTM-D-638. The length between the jaws at the start of each test was fixed to 40mm and at least 5 measurements were taken to represent each data point.Young's modulus is determined from the stress-strain curve by taking the slope of the initial tangent, ie the steepest portion of the curve.

Results and discussion

(a)Studies on PP-SGF composites: Variation of Young's modulus with different fibre length for 10% fibre content for NWL(Non weld line) and WL(weld line) samples is shown in fig.4.It is obvious that modulus of pure sample of PP increases from 384.14MPa to 641.99MPa when reinforced with 2mm glass fibre(GF). It is found to increase linearly with increasing fibre length till 8mm and declined thereafter. A significant increase of 91% is recorded with 8mm GF for the NWL specimen. The moduli of WL specimens also follows the same trend ie., modulus increases from 339.54MPa of pure PP to a maximum of 763.95MPa with 6mm GF and decreases further with higher fibre lengths (fig.4).From the determined values of modulus, it can be ascertained that reinforcement with E-glass fibres improves the modulus of weld line specimen of PP matrix. When compared to NWL specimen the formation of weld lines decrease the modulus of pure PP by 11.6%.The low moduli of WL specimens when compared to corresponding NWL specimen except for the optimum fibre length of 6mm indicate that WL did significantly weaken the composite.(Table1)

The tensile strength of NWL specimen shows an increase of 2% when pure PP is reinforced with 2mm GF, the maximum being 16% for 8mm fibre length. For WL samples, an initial dip in tensile strength is noticed for 2mm GF. Then it increased until a peak is reached for 6mm GF and again decreased for 8mm and 10mm fibre length. (fig .5).

The extent of weld line weakness is calculated with respect to tensile strength measurements of WL and NWL specimens(Table2).The results indicate that % of WL weakness decreases to a minimum of 4.6% for 6mm fibre length.. On comparing the unreinforced WL and NWL specimens, it is seen that WL decreases the tensile strength by 6.4%.

Several studies have attributed the causes of WL weakness of homopolymers to different reasons. Hobbs[7] studied the WL behaviour of PP and reported that morphology of PP at WL is different and established that it is due to fountain flow. Malguarnera[8,9] reported increasing tensile strength for higher melt temperatures for PP and has attributed this to better molecular entanglement at higher melt temperatures. Hence it may be assumed that WL weakness is due to the weak entanglement of molecular chains as these chains at the melt front are stretched parallel to the weld line. These observations point out that fibre length is an important system property which ultimately influences the strength and elastic modulus of composites. The initial dip in tensile strength for WL specimens is due to the fact that a minimum fibre length is necessary for the matrix to effectively grip the fibre to take the strain. If the fibre length is below this critical length, the fibre will be pulled out instead being broken under tension..The behaviour of very short fibres is dominated by end effects and they do not act as good reinforcing agents. It may be inferred that even though weld lines are structurally weak points, a noticeable improvement in weld line strength is achieved when PP is reinforced with an optimum fibre length of 6mm and for PP-SGF composites without weld line it would be 8mm.

(b)Studies on HDPE-SGF composites: When HDPE with a modulus of 258.01MPa is reinforced with varying fibre lengths (viz., 2, 4, 6, 8, 10) the modulus is found to increase gradually from 505.42 MPa for 2mm to a maximum of 710.75 MPa for 8mm and then reduced to 684.34 MPa for 10 mm for NWL samples(fig .6).For weld line specimen modulus increased to 184% of the initial value at 6mm (Fig 7).

Weld lines decreases the modulus of pure HDPE by 20.5%. The extent of weld line weakness is less for HDPE specimens when reinforced with short glass fibre (Table 3) and is the lowest with fibre length of 4mm. It may be assumed that effective load transfer mechanism is taking place between matrix and fibre at this particular fibre length. Since weld line specimen of HDPE shows a high value of modulus at 4 mm, it may be taken as optimum fibre length for the weld line specimen. Increase in tensile strength of composites with different fibre length is not substantial when compared to the

unreinforced sample(fig.8)The low value of mechanical strength can be attributed to the low interfacial adhesion between matrix and reinforcement which in turn is due to low wetting of fibres by the HDPE matrix.From table 4 it can be seen that only 0.4% weakness is observed with 4mm fibre length. So 4mm is the optimum fibre length for which maximum mechanical strength can be achieved for a HDPE-SGF composite with weld line.

(c)Studies on HDPE/PP blend-SGF composite: HDPE/PP blends are immiscible. From a mechanical point of view they are generally considered as very unsatisfactory materials[10].They show very poor ultimate mechanical properties in comparison with those of components. The formation of weld lines will still weaken the properties. Weld lines in injection moulded polymer blends is not a well documented subject. The present study envisages to find out the variation of mechanical properties of HDPE/PP blend composites when it is reinforced with different lengths of SGF.

The effect of varying fibre lengths on the tensile strength for the NWL specimens of blend and its composites is shown in fig.9.The tensile strength is increased to 16.7% when blend is doped with 2mm SGF.Then a slight increase of only 5% is seen with 4mm and afterwards tensile strength showed a decreasing trend for 6,8,10mm fibre lengths.For the WL specimen(fig.10) of pure blend ,a decrease of 31% is observed as expected .An improvement in tensile strength of 8.7% is noticed with 2mm. A marginal increase is seen for 4mm and thereafter it is decreased. Since a maximum value of 16.93MPa is recorded for 4mm which is 11.4% of the initial, it is considered as the optimum fibre length.The moduli of NWL and WL specimens (fig11 and 12)followed the same trend. The maximum values of 771.07 MPa and 722.64 MPa are obtained for the NWL and WL specimens respectively with 4mm fibre length which amount to an increase of 116% and 85% corresponding to the pure blend with NWL and WL.

Conclusion: Eventhough weld lines are structurally weak points, the weld line strength is significantly enhanced by the reinforcement of the polymer matrix with short glass fibre. At the optimum fibre length the extent of weld line weakness is found to be the least. The optimum fibre length for PP, HDPE and PP/HDPE blend composites were found to be 6mm, 4mm, 4mm for specimens with weld lines and 8mm, 8mm, 4mm for specimens without weld lines respectively.

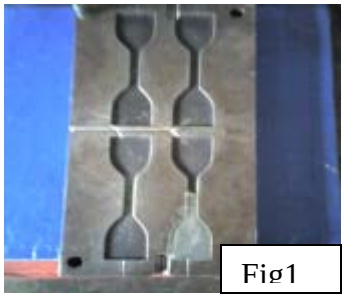

Fig1

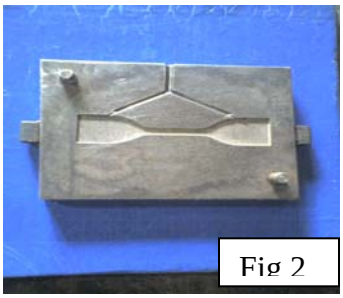

Fig 2

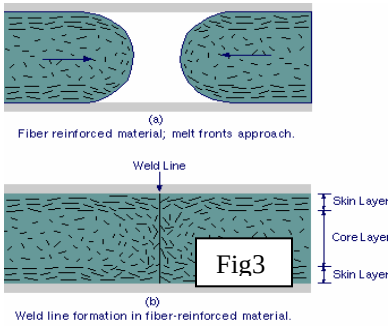

Fig3

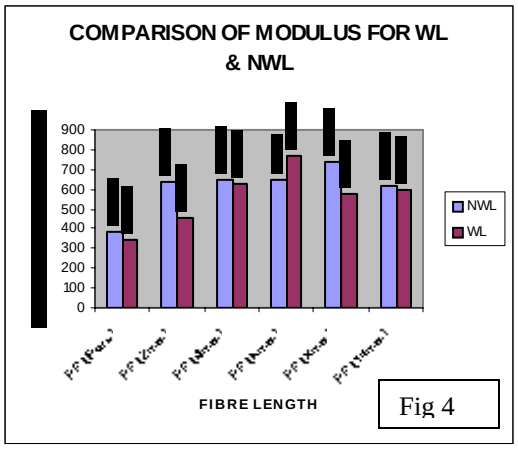

Fig 4

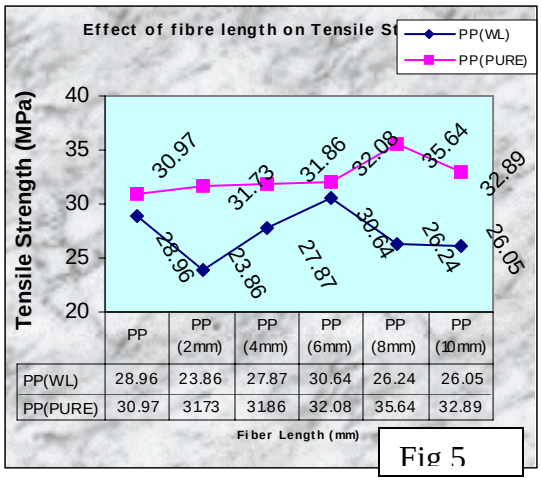

	PP	PP (2mm)	PP (4mm)	PP (6mm)	PP (8mm)	PP (10mm)
PP(WL)	28.96	23.86	27.87	30.64	26.24	26.05
PP(PURE)	30.97	3173	3186	32.08	35.64	32.89

Fig 5

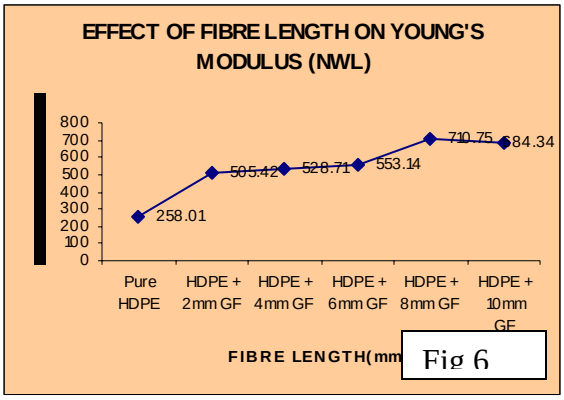

Fig 6

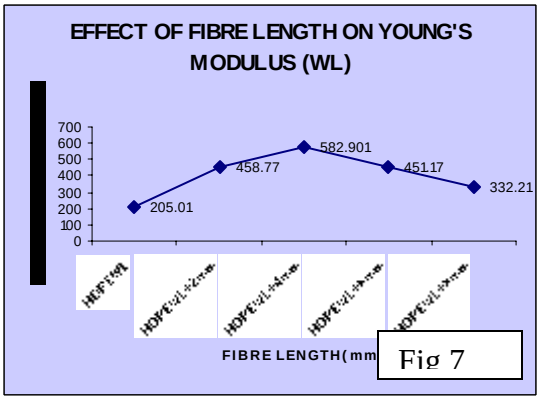

Fig 7

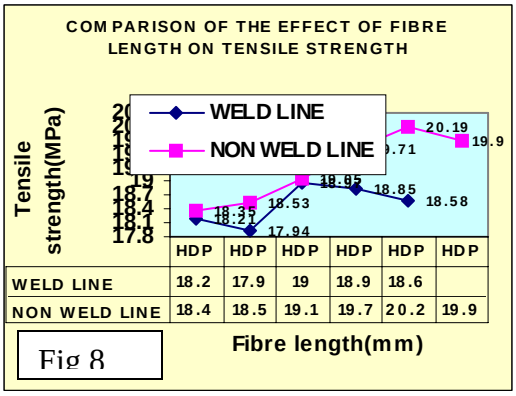

Fig 8

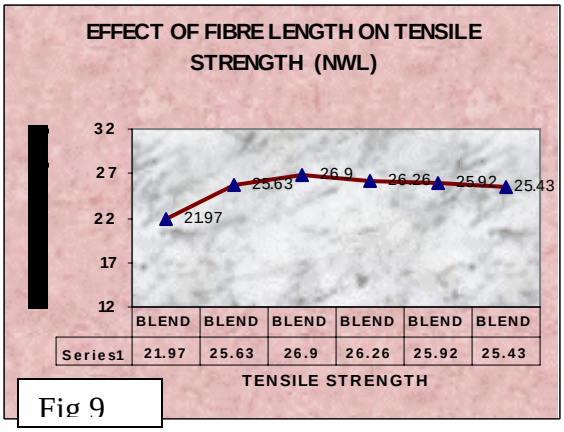

Fig 9

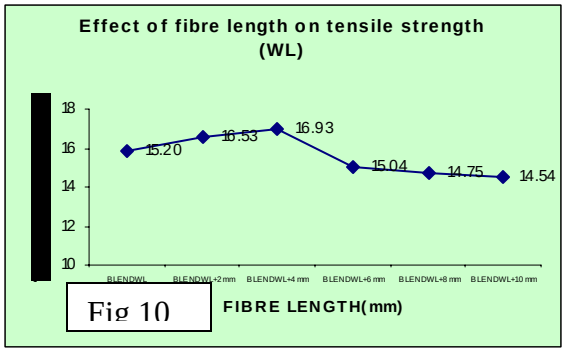

Fig 10

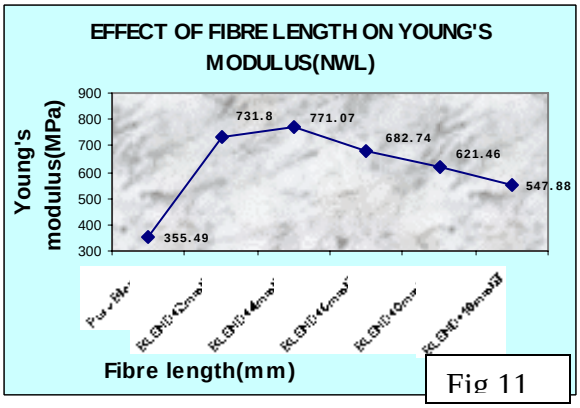

Fig 11

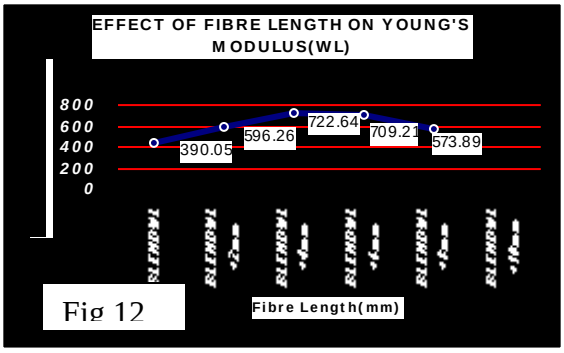

Fig 12

Table 1

Fibre length	Young's modulus of PP-SGF composite		Extent of weld line weakness (%)
	NWL MPa	WL MPa	
Pure	384.14	339.54	11.60
2mm	641.69	452.82	29.40
4mm	643.72	631.29	1.9
6mm	650.2	763.95	-17.50
8mm	733.85	579.67	21.00
10mm	618.48	592.65	4.20

Table 2

Fibre length	Tensile strength of PP-SGF composite		Extent of weldline weakness(%)
	NWL MPa	WL MPa	
Pure	31.97	28.96	6.40
2mm	31.51	23.86	24.30
4mm	31.06	27.87	10.30
6mm	32.12	30.64	4.60
8mm	35.99	26.24	27.00
10mm	32.89	26.05	20.80

Table 3

Fibre length	Young's modulus of HDPE-SGF composite		Extent of weldline weakness(%)
	NWL MPa	WL MPa	
Pure	258.01	205.01	20.50
2mm	505.42	458.77	9.00
4mm	528.71	582.9	-10.20
6mm	553.14	451.17	18
8mm	710.75	332.21	53
10mm	684.34	_	_

Table 4

Fibre length	Tensile strength of HDPE-SGF composite		Extent of weldline weakness(%)
	NWL MPa	WL MPa	
Pure	18.35	18.21	0.76
2mm	18.53	17.94	3.00
4mm	19.05	18.97	0.4
6mm	19.71	18.85	4.00
8mm	20.19	18.58	7.90
10mm	19.9	_	

References:

1.De S.K and J.R. White(1996) Short fibre polymer composites, Woodhead Publishing Limited,2-3

2.Tomari K., S. Tonogai and T. Harada, (1990) Poly. Eng. Sci., 30, 15

3.Hobbs S.Y (1974). Poly. Eng. Sci., 14, 9

4.Malruarnera S.C., A. I. Manisali, and D. C. Riggs,(1981) Poly. Eng. Sci., 21, 17

5.Gook S and N. P. Sub(1986) Poly. Eng. Sci., 26, 1200 .

6.Rosato D.V (1986) Injection Molding Handbook, Van Nostrand Reinhold Company, New York

7.Hobbs S.Y. (1974) Poly.Eng Sci,14:621

8.Malguarnera S.C., A.T.Manisali.(1981) Poly .Eng Sci ,21,1149

9.Malguarnera S.C., A.T.Manisali.(1981) Poly .Eng Sci ,21,586

10.D'Orazio L, Greco R; Martucelli E and Ragosta C.(1982)Polymer Blends,Plastics and Rubber Institute, ACS symposium series,127

……

Polymer blends and thermoplastic elastomer

M.Uma, S.Myvizhi

Amrita School Of Engineering, Ettimadai, Coimbatore

Email: uma_moh1@yahoo.co.in

ABSTRACT:

We all know that elastomers are wonderful. Cross linking makes this all possible. But crosslinked polymers can't be recycled very easily. So in the interests of keeping the earth from becoming a giant landfill, we've come up with a new approach, the thermoplastic elastomer. The idea behind thermoplastic elastomers is the notion of a reversible crosslink. In this paper we are going to discuss about the thermoplastic elastomers properties, different grades, advantages, disadvantages and also about their application.

INTRODUCTION:

The formal definition of a thermoplastic rubber or elastomer - TPE - is "a polymer blend or compound which, above its melt temperature, exhibits a thermoplastic character that enables it to be shaped into a fabricated article and which, within its design temperature range, possesses elastomeric behavior without cross-linking during fabrication. This process is reversible and the products can be reprocessed and remolded."

The idea behind thermoplastic elastomers is the notion of a *reversible crosslink*. Normal crosslinked polymers cannot be recycled because they don't melt. They don't melt because the crosslinks tie all the polymer chains together, making it impossible for the material to flow. This is where the reversible crosslink comes in. Normal crosslink are covalent, chemically bonding the polymer chains together into one molecule.

The reversible crosslink uses noncovalent or secondary interactions between the polymer chains to bind them together. These interactions include hydrogen bonding and ionic bonding. The beauty of using noncovalent interactions to form crosslinks is that when the material is heated, the crosslinks are broken. This allows the material to be processed, and most importantly, recycled. When it cools again, the crosslink reform.

TYPES:

TPE'S can be broadly classified as follows. They are

- styrenic block copolymers
- thermoplastic olefinic elastomers
- thermoplastic vulcanizates
- thermoplastic polyurethanes
- thermoplastic amide elastomers

STYRENIC BLOCK COPOLYMERS:

A copolymer is a polymer made from more than one kind of monomer, that is, made out of two or more *co monomers.* A block copolymer is a copolymer in which the co monomers are separated into long sections of the polymer backbone chain.

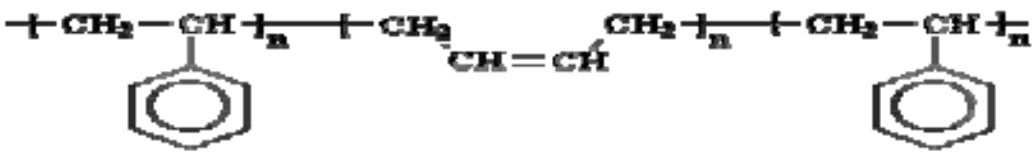

Poly(styrene-butadiene-styrene), otherwise known as SBS rubber

A very common thermoplastic elastomer that is a block copolymer is SBS rubber. SBS stands for styrene-butadiene-styrene, because SBS is made up of a short chain of polystyrene, followed by a long chain of polybutadiene followed by another short chain of polystyrene. If we could stretch out a chain of SBS, it would look like the picture below.

In styrene block copolymer the polystyrene blocks tend to clump together and the polybutadiene blocks tend to clump together. The clusters formed by the polystyrene blocks tie the polybutadiene blocks together. Remember each polybutadiene block has a polystyrene block at each end, and the different polystyrene blocks of the same SBS molecule aren't necessarily in the same cluster. This means that the different polystyrene clusters will be tied together by the polybutadiene blocks.

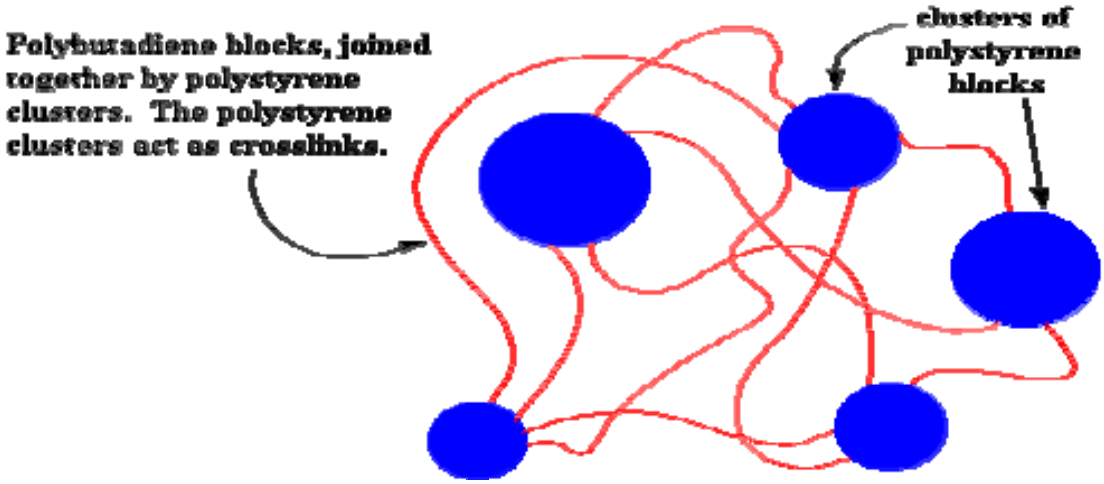

So the polystyrene clusters act as crosslinks for the polybutadiene blocks. And just like the ionic clusters of the ionomers, the polystyrene clusters break up when the SBS is heated, so it can be processed and recycled like a non-crosslinked polymer.

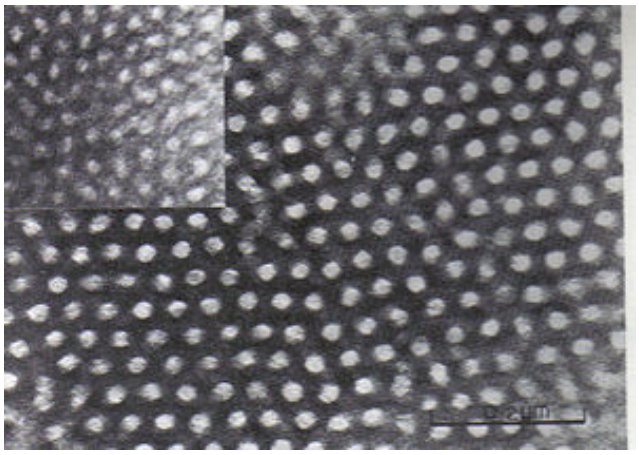

SBS block copolymer in TEM

SBS is based on two-phase block copolymers with hard and soft segments. The styrene end blocks provide the thermoplastic properties and the Butadiene mid-blocks provide the elastomeric properties.

APPLICATIONS:

TPE-S material produced and is commonly used in footwear, adhesives, bitumen modification and lower- specification seals and grips, where resistance to chemicals and aging a lower priority.

THERMOPLASTIC OLEFINIC ELASTOMER:

There are various grades of the thermoplastic olefinic elastomer available, ranging from soft grades like vulcanized rubber to semi hard grades such as RIM urethane. Unlike conventional rubber, this elastomer does not need compounding or vulcanization once it has reached the end user. Additionally, all grades of the Thermoplastic Olefinic Elastomer can be molded or extruded

similar to polyethylene and polypropylene and, like PVC, they offer excellent moldability when processed on calendaring machines.

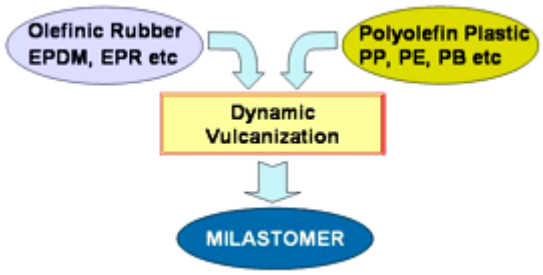

Milastomer is a recyclable Thermoplastic Elastomer which is comprised of Olefinic Rubber(s) and Olefinic Plastics.

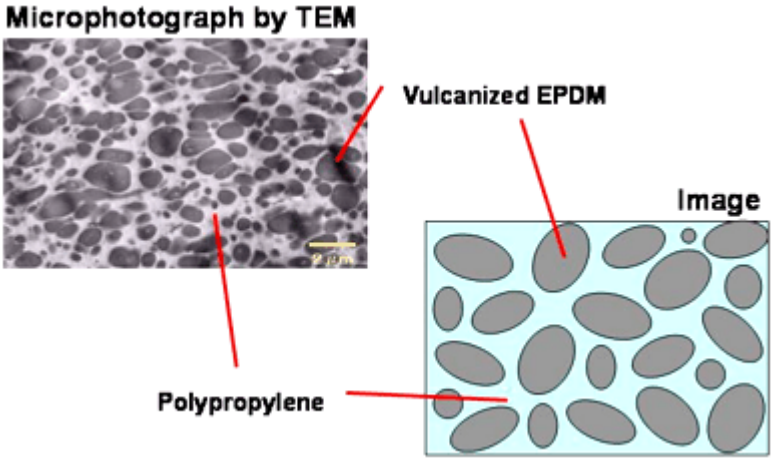

An olefin-based thermoplastic elastomer composition comprising a thermoplastic elastomer blended with other resins and rubbers is provided. The thermoplastic elastomer contains polypropylene resin and an olefin-based copolymer rubber, and optionally, a linear polyethylene resin, and the thermoplastic elastomer has been crosslinked to a gel content of 95% or higher. A polyolefin resin, an olefin-based copolymer rubber and a softening agent are further blended with optional inorganic filler to provide the olefin-based thermoplastic elastomer composition. This composition is excellent in oil resistance and extrudability, and well-adapted for use as an energy-saving, resources-saving elastomer.

THERMOPLASTIC OLEFINIC ELASTOMER CHARACTERISTICS:

- Excellent chemical resistance
- Excellent long-term stability
- Excellent mechanical strength
- Superb heat resistance
- Excellent mold ability, especially for composite molding with other polyolefins
- High weatherablity
- Light weight and recyclable
- Low temperature stability

- Non-halogenated emissions when disposed of by combustion
- Superb electrical characteristics

APPLICATIONS:

Automotive parts:
Sheeting with leather like surfaces for automotive interior trims, including dash boards, doors and headliners
Glass run channels and weather strips
Waterproof sheets, gaskets, home window weather strips, frames, etc.

THERMOPLASTIC VULCANIZATES:

These vulcanized TPE are commonly referred to as thermoplastic vulcanizates (TPV), which are commonly produced by dynamic vulcanization. Dynamic vulcanization refers to the process whereby rubber is vulcanized during its melt-mixing with molten non-crosslinking plastic.
A process for making a thermoplastic vulcanized includes blending a thermoplastic first polymer, an electrometric second polymer, a carboxylic anhydride, a free radical generator, and a particulate reinforcing material to provide a first blend containing the thermoplastic first polymer and grafted elastomeric second polymer with the particulate reinforcing material dispersed therein, the particulate reinforcing material having sufficient surface moisture to permit coupling to the thermoplastic first polymer and the elastomeric second polymer upon reaction with a coupling agent; then, combining a coupling agent with the first blend for coupling the thermoplastic first polymer and/or grafted elastomeric second polymer with the particulate reinforcing material and/or crosslinking the grafted elastomeric second polymer.

Thermoplastic vulcanizates, or TPV's, are a special class of TPE that contains a crosslinked rubber phase dispersed within a thermoplastic polymer phase. TPV's offer many of the product features of crosslinked rubbers, coupled with the processability of thermoplastic polymers. They are outstanding in their low compression set and high extensibility in addition to their solvent resistance. TPV's do not need drying, can be filled with various fillers, can be used as impact modifiers, and can be colored, as they are white opaque in color.

APPLICATIONS:

Some applications for TPV's include gaskets and seals, boots, tubing, medical stoppers, sporting equipment, automotive seals, and damping pads.

THERMOPLASTIC POLYURETHANE ELASTOMER:

The basic structure of TPU is described in Fig.1. TPU consist of two basic segments, viz.: hard segment and soft segment. Hard segment is formed by addition of the chain extender like, butanediol, to the diisocyanate. The soft segment consists of long flexible polyether or polyester chain that interconnects the hard segments. Usually, the soft segments form an elastomer matrix which gives an elastic properties and low temperature properties of TPU, with the hard segments acting as multifunctional tie points that function both as physical crosslinks and reinforcing fillers. Thermoplastic polyurethanes have excellent tear strength, abrasion resistance, and flex fatigue resistance.

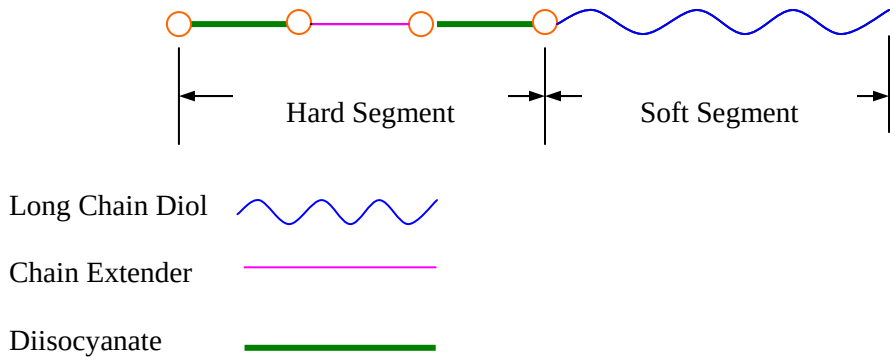

Figure 1: Basic Structure of TPU.

TPU is blended with PO to improve PO's properties e.g. impact strength, adhesion and paint ability /printability), abrasion, flexibility at low temp.

APPLICATIONS:

They are used for making shoe soles, industrial belting, ski boots, and wire and cable.

THERMOPLASTIC AMIDE ELASTOMER:

Pebax® is an Arkema trade name for its polyether block amides. Pebax® is a thermoplastic elastomer or a flexible polyamide without plasticiser consisting of a regular linear chain of rigid polyamide segments and flexible polyether segments. The general formula of the product is:

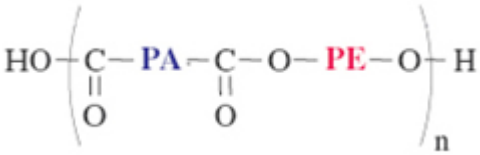

Where PA represents the polyamide segment and PE the polyether segment.

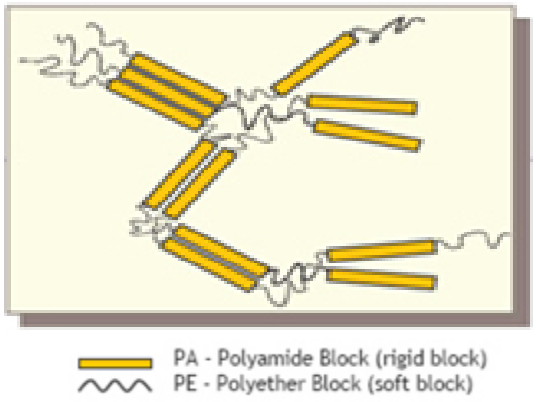

Pebax® MP 1878 is a thermoplastic elastomer with a glass transition temperature beLow -50° C. Pebax® MP1878 Added to PA6 brings even at low temperature and low humidity content

- Excellent tear resistance.
- Excellent pinhole resistance.
- High flexibility.

No modification of the film transparency. Pebax® MP1878 can be used with all kind of PA6 films: oriented (BOPA films) and non-oriented (cast blown fims).

ADVANTAGES OF TPE:

TPE materials have the potential to be recyclable since they can be molded, extruded and reused like plastics, but they have typical elastic properties of rubbers which are not recyclable owing to their thermosetting characteristics. TPE also require little or no compounding, with no need to add reinforcing agents, stabilizers or cure systems. Hence, batch-to-batch variations in weighting and metering components are absent, leading to improved consistency in both raw materials and fabricated articles. TPEs can be easily colored by most types of dyes. Besides that, it consumes less energy and closer and more economical control of product quality is possible.

DISADVANTAGES OF TPE:

The disadvantages of TPEs relative to conventional rubber or thermoset are relatively high cost of raw materials, general inability to load TPEs with low cost fillers such as carbon black (therefore preventing TPEs from being used in automobile tyres), poor chemical and heat resistance, high compression set and low thermal stability.

CONCLUSION:

TPEs are a unique class of engineering materials combining the look, feel and elasticity of conventional thermoset rubber with the processing efficiency of plastics. The melt-processability of TPEs makes them very suitable for high-volume injection moulding and extrusion. They can also be reclaimed and recycled. As elastomers, TPEs exhibit high elasticity. TPE materials are capable of exhibiting elastomeric properties without undergoing compounding and curing process. TPEs encompasses rubber like properties and offer a wide range of durometers, low compression set, and high elongation. Thus we have discussed about the different grades and specialty of thermoplastic elastomer.

Effect of amylase producing vibrios from the benthic environment on the biodegradation of low density polyethylene-starch blends

Anna Dilfi K. F[1*], Zeena P. Hamza[1], Raghul Subin[2], Thomas Kurian[1#] and Saritha G. Bhat[2]

[1]Department of Polymer Science and Rubber Technology, Cochin University of Science and Technology, Kochi – 682 022, India.
[2]Department of Biotechnology, Cochin University of Science and Technology, Kochi – 682 022, India.

E-mail: tkurian@cusat.ac.in

Abstract
Low-density polyethylene was mixed with different grades of tapioca starch namely low-grade starch and high-grade starch. Various compositions were prepared and their mechanical and thermal studies have been carried out. Biodegradability of these samples has been checked using culture medium containing Vibrios, an amylase producing bacteria. Soil burial test and reprocessability of these samples were checked. The studies on biodegradability show that these blends are partially biodegradable.

Key words: Low density polyethylene, tapioca starch, biodegradability.

Introduction

Research on degradable synthetic polymers began in the early 1980's. As a consequence of extensive discussions on better waste management strategies biodegradable polymers have recently attracted a great deal of public and industrial interest [1]. Low-density polyethylene, which is hard to degrade in landfills, is currently one of the most commonly used thermoplastic for packaging applications [2]. The resistance of polyethylene to biological attack is related to its hydrophobicity, high molecular weight, and lack of functional groups recognizable by microbial enzymatic systems. These entire properties limit the applications in which biodegradability is a desirable attribute [3].

Because of its low cost and biodegradability, starch has been extensively used with other polymers to improve the biodegradability of resulting blends [4–7]. The blending of biodegradable polymers, such as starch, with inert polymers, such as polyethylene, has received considerable attention because of the possible application of this technique in the waste disposal of plastics. The logic behind this approach is that if the biodegradable component is present in sufficient amount, and if it is removed by microorganisms in the waste disposal environment, then the base inert plastic should slowly disintegrate and disappear [8].

Low-density polyethylene is defined by a density range of 0.910-0.940 g/cm^3. The high degree of short and long chain branches characteristic of low-density polyethylene molecule inhibit their ability to crystallize. This result in a flexible product with a low molecular weight, and these has lower tensile strength and increased ductility [9]. The high degree of branching with long chains gives molten LDPE unique and desirable properties.

Starch is a polymer of glucose. Glucose units are linked together by α-1, 4 and α-1, 6 linkages. Starch occurs in two forms-amylase and amylopectin. Amylopectin is a branched chain of α-1, 4 linkages with α-1, 6 linkages at the branch point whereas amylase is a straight chain of α-1, 4 linkages [10].

In this study, LDPE was mixed with different grades of tapioca starch, namely low grade starch and high-grade starch. Various compositions (5, 10 and 15 weight %) were prepared and their mechanical properties, thermal properties and biodegradation studies have been carried out.

Experimental

Materials

The film grade LDPE (24FS040) used in this study was provided by Reliance Industries Limited, Mumbai, India. Low-grade starch and high-grade starch were supplied by Jemsons Starch & Derivatives, Aroor, Alapuzha, Kerala. These fillers were oven dried at 120^0C for 1h prior to mixing.

Mixing

The compounds were prepared in a Thermo HAAKE Polylab System equipped with roller type rotors. The mixing was done at a rotor speed of 30 rpm and at a temperature of 150^0C. Initially the LDPE was allowed to melt for 2 minutes, and then the filler was added. Mixing was continued for another 4 minutes. The neat polymer was also masticated under the same conditions. Three compositions with each filler and polymer were prepared.

Preparation of test specimens

The test specimens were prepared from the compounds by moulding in an electrically heated hydraulic press for 5 minutes at 150^0C under a pressure of 20 MPa. After moulding the samples were cooled under pressure.

Mechanical testing

The mechanical properties were measured according to ASTM D 882 (2002) in a Shimadzu Autograph AG-I series at a crosshead speed of 50 mm/min. At least five samples were tested for each composition and the average was taken.

Thermal studies

Thermogravimetric analysis

Thermo gravimetric analyses of the samples were carried out in a TGA Q-50 thermal analyzer (TA Instruments) under a nitrogen atmosphere. The samples were heated from room temperature to 800^0C at a heating rate of 20^0C/min and a nitrogen gas flow rate of 40-50 cm^3/min. Sample weight varied from 10-15 mg. Thermograms were recorded from room temperature to 800^0C. The onset of degradation temperature, the temperature at which weight loss is maximum (T_{max}), the maximum rate of degradation and residual weight in percentage were evaluated.

Differential scanning calorimetry

Crystallinity of the samples were studied using a TA Q-100 thermal analyzer (TA Instruments) performed under nitrogen at a heating rate of 10^0C/min. Sample 5-10mg was heated in a nitrogen atmosphere from -50^0C to 170^0C at a heating rate of 10^0C/min, and kept at 170^0C for 3 min in order to erase thermal history. Then a cooling was performed at a rate of 10^0C/min from 170 to -50^0C followed by a second heating from -50 to 170^0C at the same rate. Polymer crystallinity was calculated from the melting enthalpy obtained by endothermic peak integration and as reference the melting enthalpy of a perfect LDPE crystal (277.1J/g) was used.

Biodegradability

Biodegradability of the blends was tested using a liquid culture medium containing the selected amylase producing *Vibrios. Vibrios* with the ability to produce amylase enzyme were selected for checking the

biodegradability of the samples. 15 amylase producing bacteria were grown until 1 OD (10^8 CFU/ml). These cultures were inoculated into starch minimal medium, followed by plastic strips. Appropriate positive and negative controls were also kept. The conical flask containing plastic strips and cultures were kept on shaker at 120 rpm at room temperature. Strips were retrieved at the end of every week. Weight loss and tensile strength were checked to measure the degree of degradation. Biodegradability in soil was also checked by placing the samples in soil for 8 weeks. After 8 weeks the tensile strength and weight loss were measured for determining the degree of degradation.

Results and Discussion

Mechanical properties

Figures 1a, 1b and 1c show the variation of tensile strength, elastic modulus and elongation at break of starch-LDPE blends. The tensile strength, elastic modulus and elongation at break were found to decrease both in case of LDPE-LS and LDPE-HS blends. The decrease in tensile strength, elongation at break and elastic modulus may be due to weakness of interfacial adhesion of hydrophilic starch with hydrophobic matrix of LDPE. As the starch concentration increases, there is less effective cross-sectional area of LDPE towards the spherical starch. The tensile strength of LDPE-LS blends is lower compared to LDPE-HS blends whereas the elastic modulus and elongation at break show an opposite trend. The decrease in tensile strength of the blends suggests that the fillers do not reinforce LDPE.

Starch exhibits hydrophilic properties and strong intermolecular association via hydrogen bonding due to hydroxyl groups on the surface. This hydrophilic nature and strong intermolecular hydrogen bonding make these fillers less compatible with hydrophobic LDPE [10].

Thermal studies

Thermo gravimetric analysis

Figures 2a and 2b show typical thermograms of LDPE and LDPE-HS (15 weight %) blends respectively. For LDPE-HS, there is considerable decrease in weight during the temperature range 250-350^{0}C. This corresponds to the loss of starch as this is the decomposition temperature for this filler. Above this temperature, a gradual loss in weight occurs. The onset of degradation temperature, the temperature at which weight loss is maximum (T_{max}), the maximum rate of degradation and residual weight in percentage are given in Table 1. T_{max} showed a slight decrease which indicates a decreased thermal stability of LDPE-HS blends.

Differential scanning calorimetry

DSC thermograms of LDPE and LDPE-HS (15 weight %) blends are showed in figures 3a and 3b respectively. Table 2 shows the average values for the melting temperature (T_m), crystallisation temperature (T_c), enthalpy of fusion (ΔH_f), enthalpy of crystallization (ΔH_c) and % crystallinity for LDPE and LDPE-HS (15%).

ΔH_f and ΔH_c values for the blends are lower compared to virgin LDPE. There is no significant decrease in crystalinity of LDPE in the mixes which indicated that LDPE and starch are incompatible. i.e., LDPE-HS interactions were weak. In addition to this, the melting and crystallization temperature of LDPE and blends were almost similar. This also suggests the incompatibility of LDPE and the fillers [11].

Biodegradability

The Figure 4 shows the decrease in tensile strength of LDPE-starch blends after immersing the strips in culture medium for 8 weeks. There is significant variation in tensile strength of the samples indicating higher degree of biodegradation. Figure 5 shows the variation in tensile strength of LDPE-starch blends

after the soil burial test. Tensile strength decreases considerably indicating the increase in rate of biodegradation.

Tables 3 and 4 show the weight loss of starch-LDPE after biodegradability test in culture medium and soil burial test. There is considerable loss of weight for these blends after immersing the strips in culture medium and soil burial test for 8 weeks. These results confirm the partial biodegradability of the starch-LDPE blends.

Conclusions

The study suggests that the LDPE-starch blends are partially biodegradable. The tensile properties of the blends were lower suggesting that the filler has no reinforcing nature on the blends. The thermogravimetric studies indicated a decreased thermal stability of the blends. There is no significant decrease in crystallinity of LDPE in the blends which indicated that LDPE and starch are incompatible.

References

1. Steinbuchel, Alexander, *Journal of Macromolecular Science*, Part A, 32:4, 653-660, (1995).
2. A. G. Pedroso and D. S. Rosa, *Polym. Adv. Technol.*, 16: 310-317, (2005).
3. Emo Chiellini, Andrea Corti, Graham Swift, *Polym. Degrad. Stab.* , 81:341-351, (2003).
4. Ya-Jane Wang, Wanjun Liu, Zhenhua Sun, Journal of Materials Science Letters 22, 2003, 57– 59.
5. A. D. Sagar and E. W. Merrill, *J. Appl. Polym. Sci.* 58 (1995) 1647-1656.
6. S. Lim, J. L. Jane, S. Rajagopalan and P. A. Seib, *Biotechnol. Prog.* **8** (1992) 51-57.
7. G. Zhou, J. L. Willett, C. J. Carriere and Y. V. Wu, *Polym. Mater. Sci. Eng.* 83 (2000) 480.
8. Chandra R, Rustgi R, *Prog. Polym. Sci.*, 23:1273-1335, (1998).
9. Andrew. J. Peacock, Handbook of Polyethylene: Structure, Properties and Applications, CRC Press, 2-24, (2000).
10. Sangeeta Garg and Asim K. Jana, *Indian Chem. Engr.*, Section A, Vol.48, No.3, (2006).
11. A. G. Pedroso and D. S. Rosa, Carbohydrate Polymers, 59, 1-9, (2005).

Figures

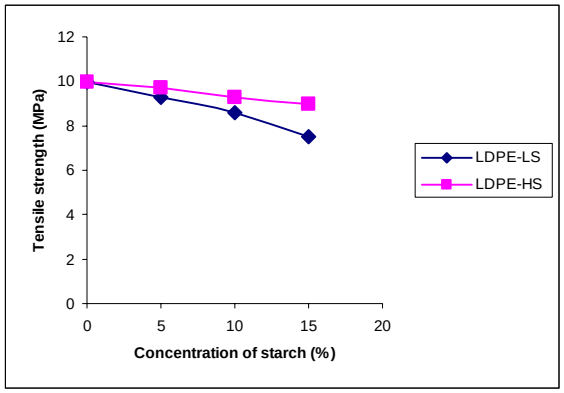

Fig 1a. Variation of tensile strength with respect to concentration of starch in starch-LDPE blends

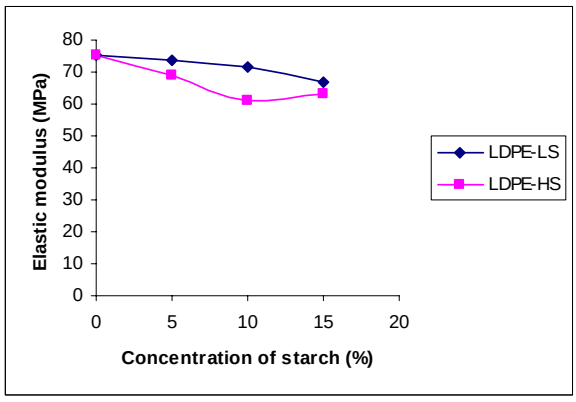

Fig 1b. Variation of elastic modulus with respect to concentration of starch in starch-LDPE blends

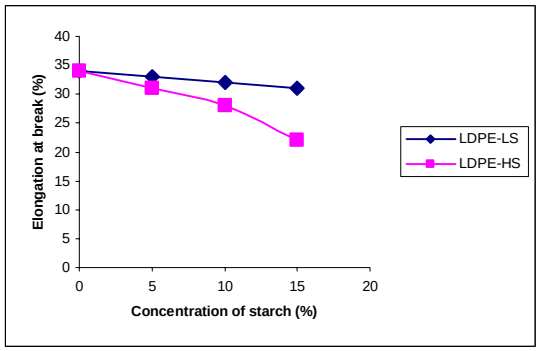

Fig 1c. Variation of elongation at break with respect to concentration of starch in starch-LDPE blends

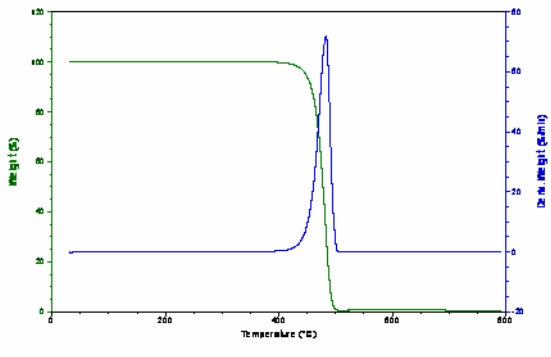

Fig 2a. TGA thermogram of LDPE

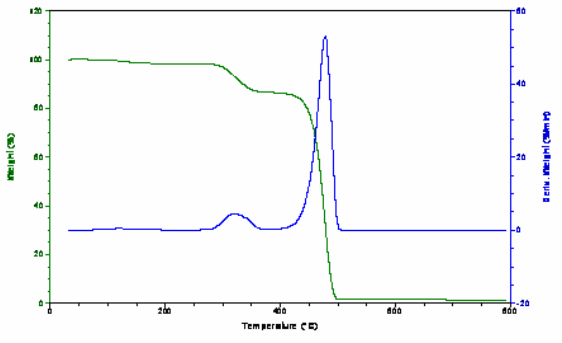

Fig 2b. TGA thermogram of LDPE-HS (15 weight %)

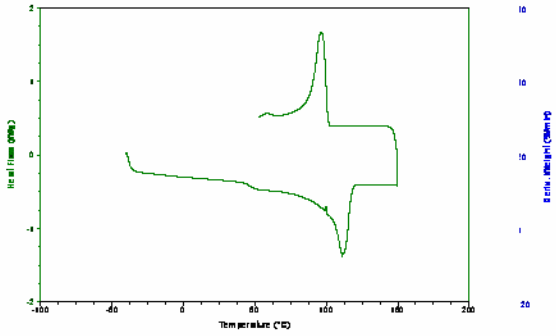

Fig 3a. DSC thermogram of LDPE

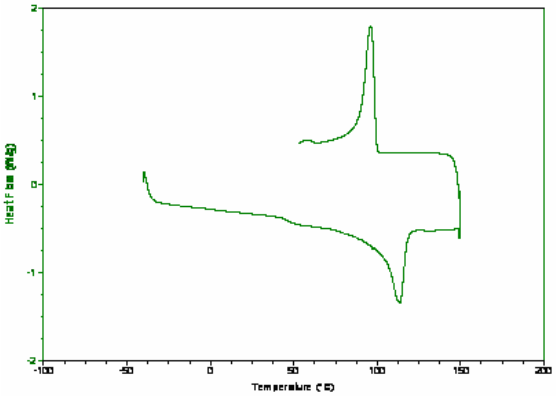

Fig 3b. DSC thermogram of LDPE-HS (15 weight %)

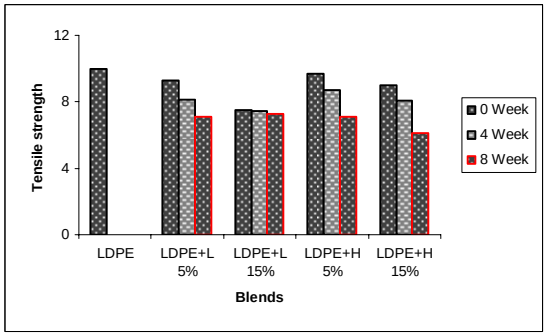

Fig 4. Biodegradability of starch-LDPE blends with respect to tensile strength in culture medium

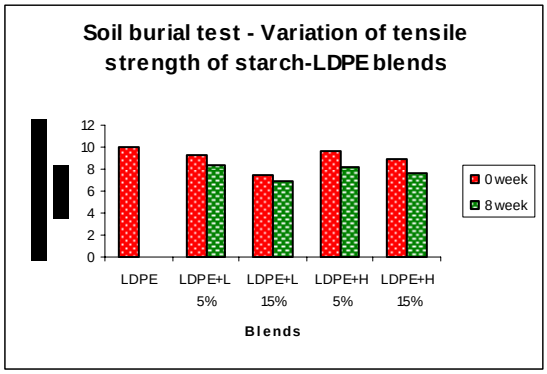

Fig 5. Soil burial test-Biodegradability of starch-LDPE blends with respect to tensile strength

Tables

Table 1. Thermo gravimetric analysis

Sample	Temperature of onset of degradation (^{0}C)	T_{max} (^{0}C)	Residual weight (%)
LDPE	420	482	0.6023
LDPE-LS (15%)	414	477	1.207
LDPE-HS (15%)	416	477	1.285

Table 2. Differential scanning calorimetry

Sample	T_m (^{0}C)	ΔH_f (J/g)	T_c (^{0}C)	ΔH_c (J/g)	% Crystallinity
LDPE	110	67	96	79	24
LDPE-HS (15%)	113	59	96	65	21

Table 3. Weight loss of LDPE- starch blends – biodegradability in culture medium

Sample	Initial weight (g)	Weight after 8 weeks (g)	% Weight loss
LDPE	0.1868	0.1776	4.92
LDPE-LS 15%	0.2137	0.2019	5.52
LDPE-HS 5%	0.2143	0.1784	16.75
LDPE-HS 15%	0.2333	0.2200	5.70

Table 4. Weight loss of LDPE- starch blends – Soil burial test

Sample	Initial weight (g)	Weight after 8 weeks (g)	% Weight loss
LDPE	0.8353	0.8346	0.08
LDPE-LS 5%	0.6603	0.6591	0.18
LDPE-LS 15%	0.2925	0.2871	1.85
LDPE-HS 15%	0.4113	0.4072	1.00

Studies on the mechanical properties and water absorption of siloxane modified epoxy resin

Jenish Paul[1], Neethumol Varghese[2], A. Benny Cherian[2], K.P.Unnikrishnan[2] and Eby Thomas Thachil[1]

[1]- Department of Polymer Science and Rubber Technology, Cochin University of Science and Technology, Kochi – 682 022, Kerala, India.
[2]- Chemistry Department, Union Christian College, Aluva, Kerala, India.

Email: jenishpaul@gmail.com

Abstract:

In the present work we were studying the modification of DGEBA with poly dimethylsiloxane (PDMS). The PDMS was blended with commercial epoxy resin (DGEBA) at various ratios using polyamine as curing agent. Their thermal, tensile and impact properties were also determined. Water absorption of the various blends was studied. Water absorption of siloxane modified DGEBA at maximum uptake of water was also studied and compared it with that of neat DGEBA. Morphology of the fractured surfaces were studied using scanning electron microscopy. The results show that the impact strength, resilience energy, energy absorption and elongation at break increase with the concentration of PDMS with out much deterioration in tensile properties. The blends show sufficient decrease in modulus indicating enhanced flexibility. The DGEBA/PDMS blends show substantial improvement in thermal stability as evident from TGA data. Siloxane modified epoxies show appreciable water resistance also.

1. Introduction

Epoxy resin has excellent mechanical, electrical and adhesion properties and is widely utilized as a high performance thermosetting material in many industrial and engineering fields (1-6). Epoxy resins based on bis phenol A-epichlorohydrin(DGEBA) exhibit brittleness and low elongation after cure. This leads to low resistance to crack initiation and propagation. The usefulness of epoxy resins in many engineering applications is often limited by these properties. The most common approach to toughen thermosets is by dispersing a rubbery phase in the epoxy matrix. One way to modify DGEBA resin by using poly dimethylsiloxanes .Among the different elastomeric materials used for toughening of epoxy resin, it is found that the hydroxyl terminated polydimethylsiloxane is the most suitable because of it's versatile behavior like flexibility due to-Si-O-Si- linkage, high thermal and thermo oxidative stability, high moisture resistance, good dielectrical properties, excellent UV and chemical resistance (7-12). Organosiloxanes exhibit important characteristics such as very low glass transition temperature (-120^0C), moisture resistance, good electric properties, low stress, high flexibility, good weatherability and good thermal and oxidative stabilities. In addition, because of their low surface energy and nonpolar structure polysiloxanes tend to migrate to the air-polymer interface and provide a very hydrophobic surface for the substrate (13)

2. Experimental

2.1 Materials

Epoxy resin GY 250 and amine hardener HY951 were procured from Petro Araldite Pvt. Ltd. Chennai. TSHF PDMS [Poly (dimethyl siloxane) hydride terminated] (M_W 3363, M_n 580)], was supplied by Aldrich. Methanol was supplied by Merck India Ltd.

2.2 Curing of neat resin

Epoxy resin was mixed with 12wt% hardener and stirred well to make it uniform. The resin was degassed in vacuum, poured into Teflon moulds and allowed to cure for 24 hrs at room temperature. Post curing was done at 100^oC for 4 hours.

2.3 Curing of siloxane modified epoxy resin

Epoxy resin was mixed with 1-10 wt % siloxane and stirred well to make it uniform. 12wt % hardener was added, stirred and degassed in vacuum. The mixture was poured in Teflon moulds and cured for 24 hrs at room temperature. Post curing was done at 100^0C for 4 hours.

2.4 Testing Methods

a) Thermal studies

Thermal stability of the neat and modified cured resin samples was determined using thermo gravimetric analyser (TGA Q 50, TA Instruments) over a temperature range of room temperature - 800^oC at a heating rate of 10^oC/min. The damping qualities were measured by dynamic mechanical analysis (DMA-Q800, Universal V4.0C TA Instruments) using dual cantilever mode over a temperature range of room temperature to 200°C at a heating rate of 3°C/ min and a frequency of 1 Hz.

b) Mechanical Properties

The samples, after post curing, were tested for tensile strength, modulus and impact strength, taking six trials in each case. The tensile properties were tested on a Schimadzu Autograph Universal Testing Machine (ASTM D 638-89) and Izod impact strength was measured on a Zwick impact tester as per ASTM D 256 specifications.

3 Results and Discussion

3.1 Thermal studies

The thermal stability of the cured blends was investigated by TGA. Onset temperature, temperature at maximum rate and temperature of half loss and residue are given in table **1.**

Table-I: TGA characteristics of blends of DGEBA, PDMS and functionalised PDMS

Resin	Onset temperature (°C)	Temperature of maximum rate (°C)	Temperature of half loss (°C)	Residue (%)
DGEBA	343	364	378	6.68
5% TSHF PDMS/ DGEBA	344	366	379	7.89

The thermograms show that there is only one decomposition stage in the heating process. There is no deterioration in thermal properties when DGEBA is blended with polydimethylsiloxanes.

3.2 Dynamic Mechanical Analysis

The storage modulus of the blend and that of neat DGEBA are given in Fig.1. The PDMS/DGEBA blends have lower crosslink density resulting in lower values of storage modulus

The tan δ (loss factor) for the modified and unmodified DGEBA is shown in Fig.2. The tan δ_{max} for neat DGEBA decreases on blending with siloxane . The glass transition temperature T_g determine by the tan δ peak of neat DGEBA decreases when functionalized siloxanes are incorporated. The lowering of T_g is due to the flexible siloxane segments in the co- polymer.

3.3 Mechanical properties

The impact strength increases with increase in concentration as. Beyond 5% the increase is marginal. The increase is impact strength is due to the energy dissipation by the soft siloxane segments which occurred during the fracture of propagation surface. The Resilience energy also increases with increase in concentration of PDMS due to greater flexibility of the matrix

Tensile strength decreases with increase in concentration of PDMS. This is due to the presence of flexible siloxane segments in the cross linked networks of blended epoxy resin

The modulus decreases with increase in concentration of PDMS due to the soft segments of siloxanes.

3.4 Water Absorption

The water absorption of the PDMS/DGEBS are given in Fig.3. Siloxanes lowered the water absorption of epoxy resin due to the hydrophobic nature of silicon molecule and its surface enrichment character there by exhibiting lower permeability to water molecules.

Table 3.1 summarizes the effect of adding varying amounts of PDMS in the base resin. The maximum improvement acquired in each property and the corresponding concentrations are tabulated.

Properties	% Improvement / composition (wt %)	
	DGEBA	PDMS/DGEBA
Tensile strength (MPa)	65	-26.15/10
Modulus ($x10^2$ MPa)	24	-25/10
Energy Absorption(J/mm^2)	5.00	6/ 5
Elongation at Break (%)	3.00	8.33/5
Impact strength J/m	111.04	46.61/10
Water Absorption	0.2003	-12.64/10

3.5 Morphological studies

SEM micrograph of the unmodified epoxy resin and modified epoxy resin are given in Fig.14. Fracture SEM micrograph of the unmodified epoxy resin (Fig. 5 a) paths are mostly straight and constitute failure bands. It is a typical case of brittle fracture. Multilevel fracture paths with ridges and wavy crests indicate energy absorption on a large scale during failure in the case of PDMS modified epoxy resin (Fig. 5 b).

4. Conclusions

PDMS blends show appreciable water resistance .The PDMS blends don't show deterioration in thermal properties as evident from TGA and damping data. There is no considerable deterioration in the mechanical properties also due to the addition of PDMS derivatives. The impact strength and resilience energy increase with the concentration of PDMS up to 5 %.

References

1. H. Li, L.Wang, K. Jacob and C. P.Wong, *J. Polym. Sci. Part A: Polym.Chem.*, 2002,**40**, 1796.
2. K. C. Cheng, S. Y. Yu and W. Y. Chiu, *J. Appl. Polym. Sci* 2002., **83**, 274 .
3. Gouri C, Reghunadhan Nair CP, Ramaswamy R. J Appl Polym Sci 1999; 73:695-705
4. Vabrik R, CZajlik I, Tury G, Rusznak I, Ille A , Vig A. J Appl Polym Sci; 1998 68:111-119
5. Denq B-L, Hu Y-S, Chem L-W, Chiu W-Y , Wu T-R . J Appl Polym sci; 1999, 74:229-237.
6. Ooi SK, Cook WD, Simon GP, Such C K. Polymer 2000 ;41:3639-49
7. Matsukwa k,Hasegawa k,Inoue h, Fukuda A, Arita y. J Polym Sci Polym Chem; 1992, 30:2045-48
8. Belot V,Corriu RJP,Leclercq D, Mutin Ph, Vioux A. J Polym Sci Polym Chem 1992;30:613-23.
9. Lin S T, Hung Sk. J Polym Sci Polym Chem, 1996;34:869-84.
10. Sung P H , Lin C Y. Eur Polym J1997;33:903-06
11. Lee SS, Kim SC, J Appl Polym Sci; 1998, 69:1291-1300 .
12. Agrawal JP, Venugopalan S, Athar J, Sobane J V, Muralidharan M. J Appl Polym Sci 1998;69:7-12
13. Zhang, H., Zhang , J ., Yang, Y., Macromol Theory Simul 1995, 4, 1001.

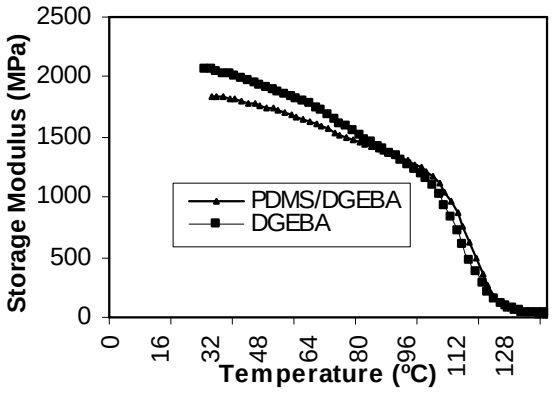

Fig.1 Storage modulus of DGEBA & PDMS/DGEBA

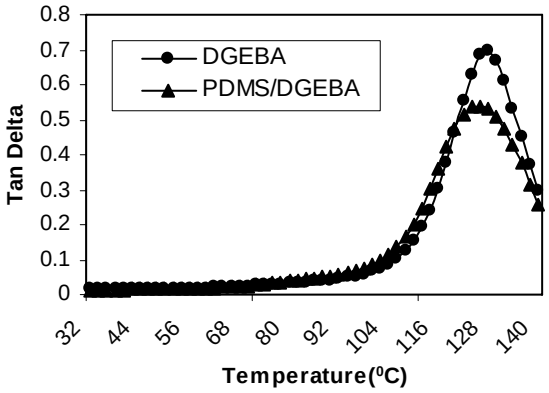

Fig.2 Tan δ relaxations of (a) DGEBA & PDMS/DGEBA

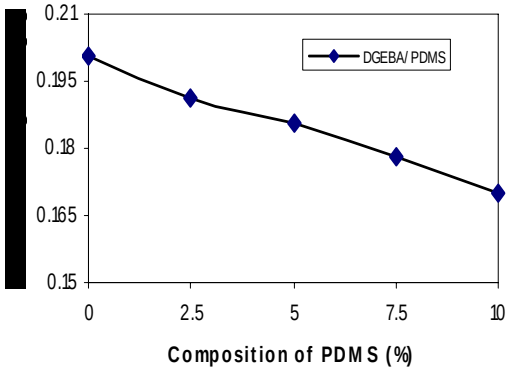

fig 3Water Absorption Vs composition of PDMS

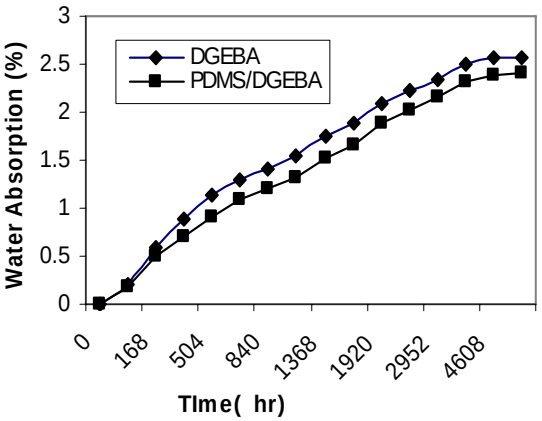

Fig 4 Water Absorption at maximum Uptake

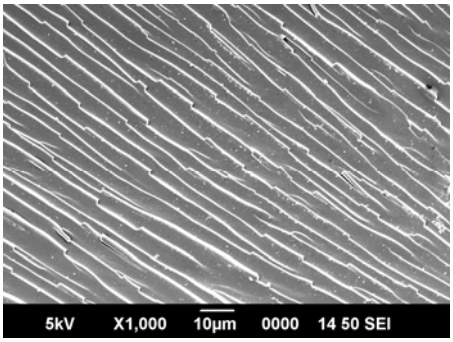

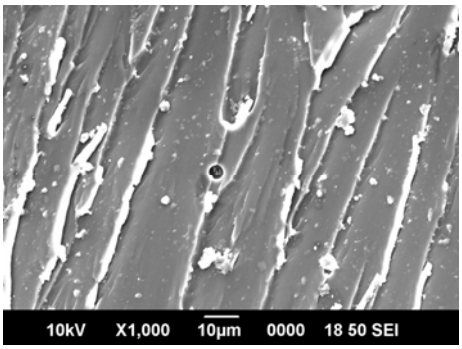

Fig.5.Scanning electron micrographs of (a) Neat DGEBA (b) PDMS / DGEBA

Miscibility and phase structure of the blends and copolymers of nylon 4,6/nylon 12

V. J. Jijo, T. Mathew, S.K. Menon and C. Ramesh

Division of Polymer Science and Engineering, National Chemical Laboratory,

Pune-411008, India.

Email: c.ramesh@ncl.res.in

Abstract:

The present study deals with the preparation nylon 4,6/ nylon 12 blend and copolymers. The blend was prepared by melt blending of the nylons in the presence and absence of Triphenyl phosphite (TPP). Thermal and crystallization behaviour of the blends indicate that the components crystallize individually and phase separate due to crystallization. However, it seems the presence of nylon 12 increases the crystallizability of nylon 4,6. In the case of nylon 12, the crystallization is inhibited by nylon 4,6 which is already in the solidified form. These results indicate partial miscibility of nylon 12 and nylon 46 in the melt state. The melting and crystallization behaviour of these blends in the presence of TPP, which can catalyze the amide exchange reaction between polyamides and form random copolymer, indicates that the wide difference in polyamide polarity of nylon 4,6 and nylon 12 makes the exchange reaction difficult to happen. On the other hand the copolymer prepared by condensation of monomer resulted in the formation of a random copolymer as evident from the single peak nature of the crystallization and melting thermograms as well as the depression of the melting and crystallization temperatures. The phase structure of the copolymers and blends were studied using WAXD and FT-IR.

Introduction:

Blends and copolymers in general provide opportunities for developing new materials with tailored properties. Copolyamides have been synthesized since the early 1940's[1]. Widely used copolymers are made up of nylon 6 units with nylon 6,6 monomers in various ratios. Copolyamides are of commercial interest because copolymerization allows tailoring of physical properties and the ability to process, mainly from decreased crystallinity compared to that with homopolyamides. However, even in copolymers with reduced crystallinity, all the amide linkages are fully hydrogen-bonded, leading to a material with good mechanical properties[1]. Comonomers may be entirely aliphatic or may incorporate some aromatic content. Polyamides are widely used as industrial products and information of their behavior in blends and copolymer is interesting. However, reports of investigations in this area are few. The work described here was undertaken to provide further information to understand the phase behavior of nylon 46/nylon 12 copolyamides, systematically over the whole range of composition.

Experimental Section:

Tetramethylenediamine, adipic acid and, 12-amino dodecanoic acid were obtained from Aldrich Chemical Company Inc., USA. The copolymers with different weight compositions were prepared by the melt polycondensation of mixture of nylon 46 salt and 12-amino dodecanoic acid. The inherent viscosities were measured using an Ubbelhode viscometer in the Schott AVS350

instrument. The WAXD experiments were performed using a Rigaku Dmax 2500 diffractometer equipped with a copper target and a diffracted beam monochromator with 2θ scan range of 5-30^{o} at room temperature. The thermal behavior of the samples was analyzed using TA Instruments DSC-Q100, under standard conditions. The room temperature infrared spectra of samples were taken using a Perkin-Elmer FTIR GX spectrometer.

Results and Discussion:

Melt mixing of polyamides results in transamidation reaction between the components. Such a reaction will result in the formation of block or random copolymer. Phosphite compounds are found to catalyze transamidation reaction in polyamides[2]. But it has been shown that in blends, a miscible nylon 46/12 copolymer is not formed, even in the presence of Triphenyl phosphite (TPP). Here, by melt polycondensation of the respective monomer all the homopolymers and copolymers were obtained in high yields, in the range 80% - 90%. The discolouration, which occurred during the synthesis of nylon 4,6 was considerably reduced by the incorporation of nylon 12 moiety in the nylon 4,6 backbone. The copolyamides exhibited inherent viscosities in the range of 0.36 to .9 g dL^{-1} .The inherent viscosity of the copolyamide is increased with increasing nylon 12 content. The copolymerization rate thus became greater with the incorporation of nylon 12 content, and resulted in higher molecular masses of copolyamides, which was reflected by greater inherent viscosity.

The DSC melting thermograms of the samples, as presented in the Figure 1 clearly shows the presence of a single melting peak, which suggests the formation of a random copolymer. The broad melting temperature in the intermediate region of copolymers suggests that crystallites formed during recrystallisation may have a broad distribution of thickness including small size crystals. The crystallization exotherms of the copolyamides on cooling from the melt is shown in Figure 2. The melting and crystallization temperatures of the copolyamides showed a eutectic behavior and the eutectic composition was 20/80. The typical eutectic behavior indicates that the cocrystallization is isodimorphic in nature and monomer units of one type are included in the crystal lattice of the other type.

Figure 3 shows the room temperature XRD patterns of nylon 46/12 copolymers. At room temperature nylon 46 crystallizes in the stable α-structure and nylon 12 crystallizes in the γ-structure[3]. It can be inferred from the diagram that up to 50 % of nylon 46 content XRD patterns shows the crystalline peaks corresponding to d-spacing 0.44 nm and 0.37 nm and crystallizes in the α-form. In the case of 35/65 composition the strong peak relating to d-spacing at 0.415 nm is due to the presence of γ-phase of nylon 12. While the peaks at 0.44 and 0.40 are due to the presence of α-phase of nylon 46. XRD studies shows considerable percentage of crystallinity in the 35/65 composition, while the reason for showing very broad peak over a large area in the DSC thermogram may be because of the coexistence of multiple phases. The 20/80, and 10/90 composition shows crystallizes predominantly in the γ-phase with a trace of material in the α phase of nylon 4,6.

FTIR spectra of nylon copolyamides and homo-polyamides confirm the XRD studies discussed before. The typical bands in infrared spectra of nylon 46, nylon 12 and their copolymers are shown in the Figure 4. In 35/65 compositions, two additional sharp peaks at 722 and 622cm^{-1} are appeared due to the presence of γ-phase while the intensity of peak at 690 and 580, 524 cm^{-1} has been reduced considerably. The different crystalline forms present in the nylon 46/12 copolymers are shown in the Table 1.

Conclusion:

The melting and crystallization behavior nylon 46/nylon12 blends in the presence of TPP indicates that the wide difference in polyamide polarity of nylon 46 and nylon 12 makes the exchange reaction difficult to happen. However, random copolymer may be prepared by the condensation of monomers. The melting and crystallization temperatures of the copolymer exhibit typical eutectic behavior; the eutectic composition is 20/80. This indicates that the nylon 46 component dominates and controls the crystallization behavior of the copolymer.

Reference:

1) Utraki, L.A, Polymer blends and alloys
2) Kristofic, M., Hricova, M., Ujhelyiova, A., Macromol Symp. 2001,170,291
3) Ramesh, C. Macromolecules 1999,32,3721

Figures and Tables:

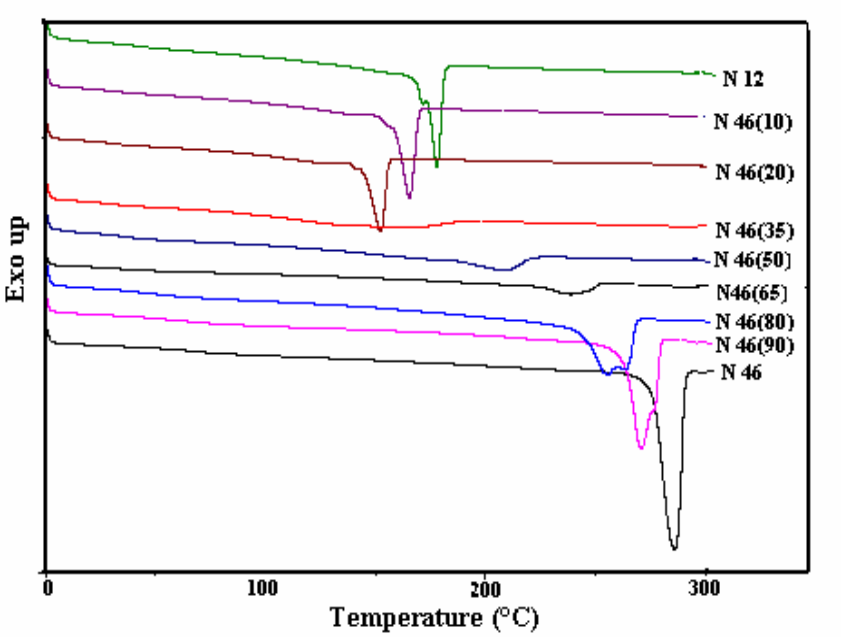

Fig 1. DSC Thermograms indicating melting point (T_m) of nylon 46/12 copolymers.

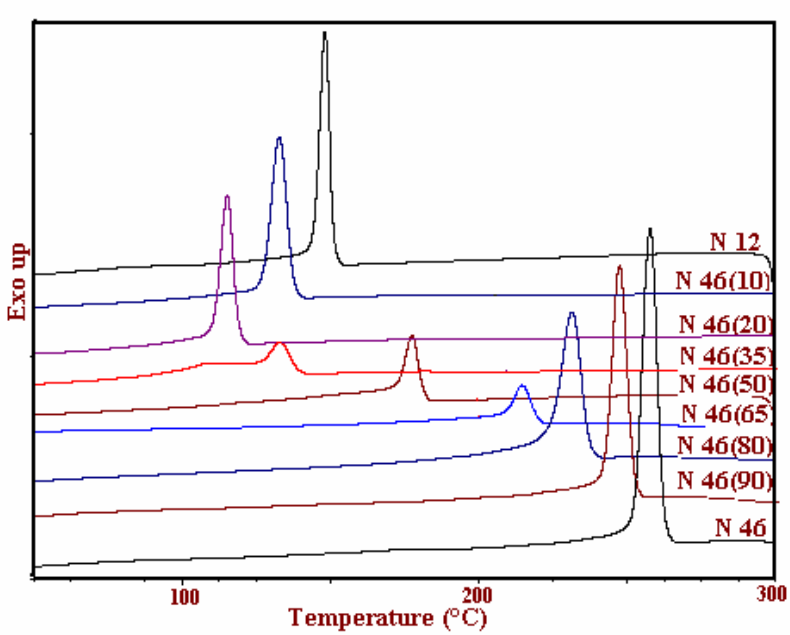

Fig 2. DSC Thermograms indicating crystallization temperature (T_c) of nylon 46/12 copolymers.

Fig 3. X-ray Diffractograms of nylon 46/12 copolymers

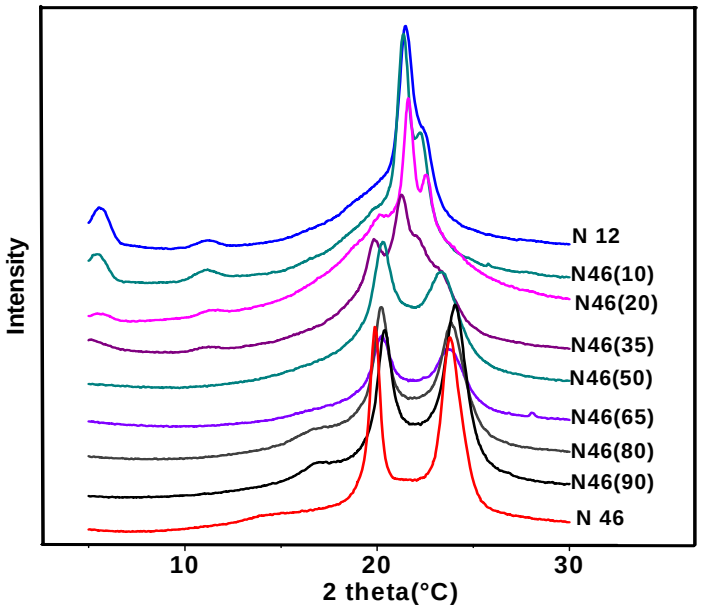

Fig 4. FT-IR spectra of nylon 46/12 from 400-1600 cm^{-1} copolymers

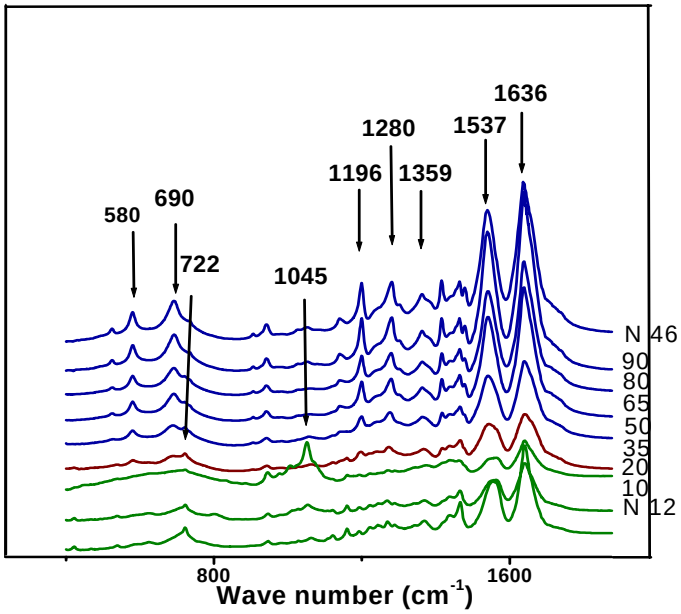

Table 1. IR bands and d-spacings of the nylon 46/12 copolymers.

Sample	IR bands (cm^{-1})		Inter-planar (d) spacings (nm)		Structures present
	Amide V band	Amide VI band			
N 46	690	580	0.445, 0.371		α
N 46(90)	690	580	0.439, 0.369		α
N 46(80)	690	580	0.439, 0.369		α
N 46(65)	690	580	0.439, 0.369		α
N 46(50)	690	580	0.436, 0.376		α
N 46(35)	690, 722	580, 630	0.441, 0.377	0.415, 0.4	γ, α
N 46(20)	722	630	0.441, 0.393	0.412	γ, α
N 46(10)	722	630	0.438, 0.398	0.414	γ, α
N 12	722	630	0.413	0.413	γ

Droplet orientation and its morphology in polymer dispersed ferroelectric liquid crystal composite films

K K Raina* and Shikha Kapila

Materials Research laboratory, School of Physics and Materials Science, Thapar University, Patiala 147 004 India
*Email: kkraina@gmail.com, kkraina@thapar.edu

Abstract

Multiwalled carbon Nanotubes (CNT) have been dispersed in a chiral smectic c liquid crystal mixture in the ration of 0.05% and 0.1% (wt/wt). Morphological investigations were carried out which shows uniform distribution of the CNT in the liquid crystal matrix. The transition temperature of the liquid crystal increases slightly after dispersing CNT in it. The dielectric constant (measured in the frequency range 50Hz to 1 MHz) increased by about ~ 27%.

1. Introduction

Composites based on liquid crystals (LCs) have attracted much attention in the recent past due to their modified properties with respect to dielectrics, morphological and electro- optic effects and then giving rise to novel display applications. Typical examples of these systems are polymer dispersed liquid crystals [1], suspensions of aerosils in LC matrices [2] and suspensions of nanotubes in ferroelectric LCs [3, 4]. The inclusions in known composite LC systems produce director distortions that extend over macroscopic scales. A new approach, by based on the idea of controlling the properties of the composites by adding a low concentration of nanotubes into a LC matrix, however, has been proposed recently [5]. The earliest attempts to employ the LC orientational order to align CNTs were all done using standard thermotropic nematic hosts [6-9].

Due to their exceptional mechanical, electronic and electromechanical properties, carbon nanotubes are very promising for a wide range of applications [10]. The nanotubes are so small that they do not disturb the LC orientation and thus macroscopically homogeneous structures are obtained. At the same time, the nanotubes are sufficiently large to maintain the intrinsic properties of the materials from which they are made and share these properties with the LC matrix due to anchoring with the LCs [11-14].

Carbon nanotubes (CNT) occur in two general morphologies, single-wall (SWCNT) and multiwall carbon nanotubes (MWCNT). The latter are chemically more resistant and their high aspect ratio together with their flexibility leads to physical entanglement, while attractive Vander Waals interactions between individual nanotubes invariably results in their association in bundles. The latter is also responsible for the generally poor solubility of nanotubes in most solvents.

The research efforts on chiral smectic c liquid crystals (also refered as ferroelectric smectic c liquid crystals) have shown exponential growth soon after their discovery by Meyer et al. in 1975. It is due to the fact that these materials are very interesting for understanding the soft condensed matter and also their practical applications suited for fast electro-optical displays [15, 16]. The dielectric spectra of multiwalled carbon nanotube dispersed ferroelectric liquid crystal gives useful information about the static and the dynamic properties of these compounds. The dielectric spectroscopy behavior of multiwalled carbon nanotube dispersed ferroelectricliquid crystals can also be described by two relaxation processes: the dominant Goldstone mode (GM) due to the phase fluctuations and the softmode (SM) due to the fluctuation in the amplitude of the tilt angle. It appears in the vicinity of SmC*-SmA phase transition temperature (T_{C*A}).

Here we report on the studies of the dielectric properties of a ferroelectric liquid crystal containing carbon nanotubes and the effect of frequency and temperature parameters on the dielectric spectra of material. We found that embedding the carbon nanotubes in LC material results in the change of the dielectric spectra of the matrix, caused by the strong interaction between LC and carbon nanotubes.

2. Experimental

2.1 Materials

The dispersing liquid crystal is an eutectic mixture of ferroelectric liquid crystal(ZLI-4237-100) obtained from E-Merck Darmstadt. Its phase sequence is given by

$$\text{Cryst} \xrightarrow{-20^0C} \text{SmC} \xrightarrow{61^0C} \text{SmA} \xrightarrow{73^0C} \text{N*} \xrightarrow{83^0C} \text{Isotropic}$$

Multi-wall carbon nanotubes (with dimensions 110-170 nm, length between 5-9 micron) used in the experiment was purchased from M/S ALDRICH with reported purity of 90+ %. All materials were used as received without further chemical treatment.

2.2 Methods

One of the most challenging tasks was to uniformly disperse the CNTs in the liquid crystal matrix due to their tendency for aggregate formation. These CNTs aggregates generally form micrometer scale agglomerates that can be seen under optical microscopy. To achieve a finer dispersion of CNTs, sonication at 42 kHz (60^0C) was applied to the CNT mixture. We employed mixing of CNTs in ferroelectric liquid crystal (FLC) at ambient temperature. To ensure proper and uniform dispersion of CNTs, few drops of chloroform were added and further sonificated at isotropic temperature.

The planer cell of 5μm thickness (obtained from M/S Linkam Instruments, UK) was filled with this mixture by capillary action at the isotropic temperature. It consists of two aligned, indium tin oxide (ITO) coated, glass substrates. The alignment was confirmed by viewing the cell through the polarizing microscope (OLYMPUS BX-51P) interfaced to LINKAM-TP94 and THMS600 temperature programmer coupled to hot stage at an accuracy of ±0.1° C. The dielectric measurements were carried out using a programmable automatic RCL meter (FLUKE PM 6306) in the frequency range 50Hz to 1MHz. The cell was calibrated using air and benzene as standard references. The frequency and bias dependence of the real and imaginary parts of the complex dielectric permittivity have been studied in detailed.

3. Results and discussions

3.1 Morphological studies of CNT dispersed FLC

Fig. 1(a) shows optical micrographs exhibiting large CNTs aggregates in the continuum of FLC prepared by simply shaking the compound. Optical micrograph shown in Fig. 1(b), exhibit CNT dispersed through sonification and suggestive of a finer dispersion. The concentration of the CNT-FLC mixtures was diluted by decreasing the concentration of CNTs and the diluted procedure was repeated to achieve very dilute solutions down to about 0.05%wt/wt.

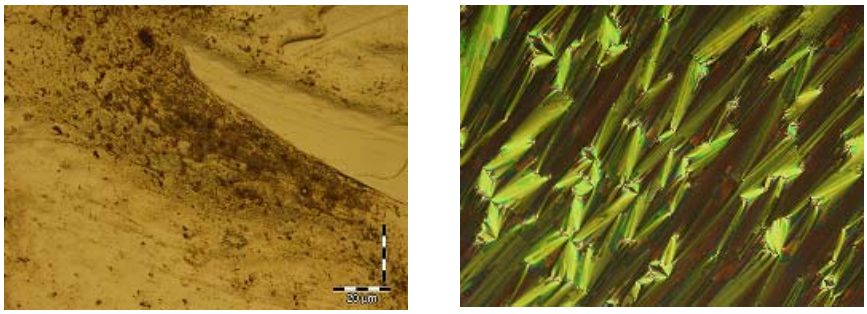

(a) (b)

Fig.1 Optical micrographs of 0.1% MWCNT in FLC (a) with shaking (b) after sonification at 10 X

Fig 2 shows micrographs of a 0.1% CNT concentration obtained under crossed polarizer at an above the smectic–isotropic transition temperature (T_{SI}). Fig 2(a) represents the isotropic state whereas birefringent domain structures appeared at 103^0 C

The structure continues to grow at the expense of the smaller domains (at 99^0C) and then evolves to larger chiral nematic domains exhibiting disclination line (at 95 ºC). The growing chiral nematic domains eventually coalesce at 78^0C and the interface disappears, exhibiting Smectic A phase at ambient temperature. Our textural study confirms that the Smectic A – Smectic C* transition temperature of the mixed CNT-FLC is about 68 ºC higher by about 7 ºC over the undispersed medium. This enhanced T_{NI} in the CNT-FLC mixture may be attributed to the preferred alignment of FLC induced by the CNT bundles [17].

A similar enhanced behavior of transition temperature from N* to isotropic phase can be seen in the 0.05% CNTs concentration. On decreasing to, 0.05%, the transition temperature of N* to isotropic is decreased to 90 ^{0}C. This transition eventually approaches to that of the FLC with further decrease of the nanotube concentration and then declines further to 83 ^{0}C at 0% CNT (FLCs).

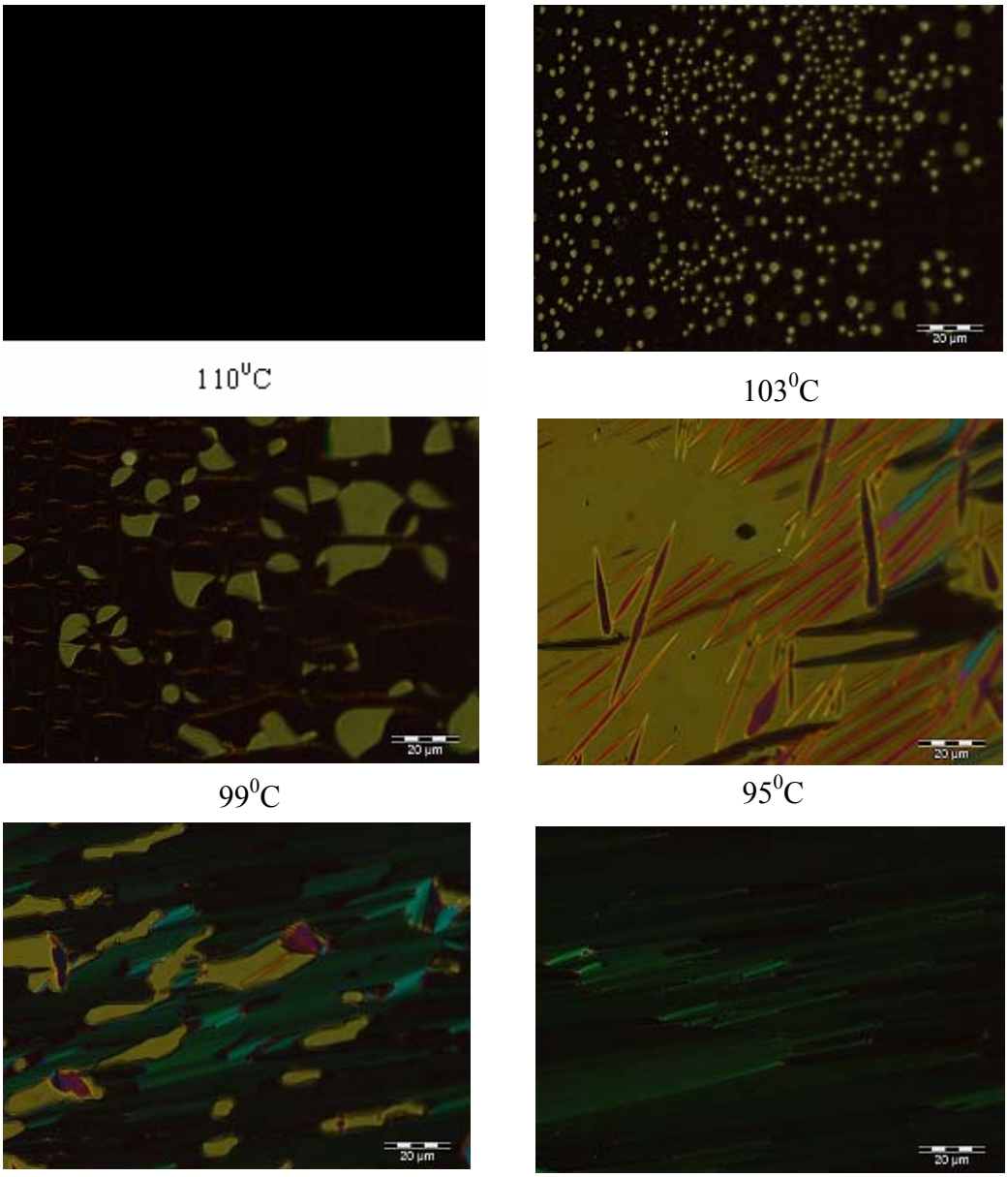

Fig.2. Micrographs showing structural evolution during cooling from the isotropic (110^{0}C) to 78^{0}C at 10X.

3.2 Dielectric spectroscopy constant

3.2.1 Temperature dependence of permittivity (ε')

Fig 3 shows that dielectric permittivity decreases with increasing temperature and then tends to attain saturation beyond 50 ^{0}C as shown in fig. 3. At high temperature, the thermal agitation became more dominant over intermolecular interactions which resulted in collisions between molecules and hence randomization of dipoles. This randomization results in decreased dielectric permittivity.

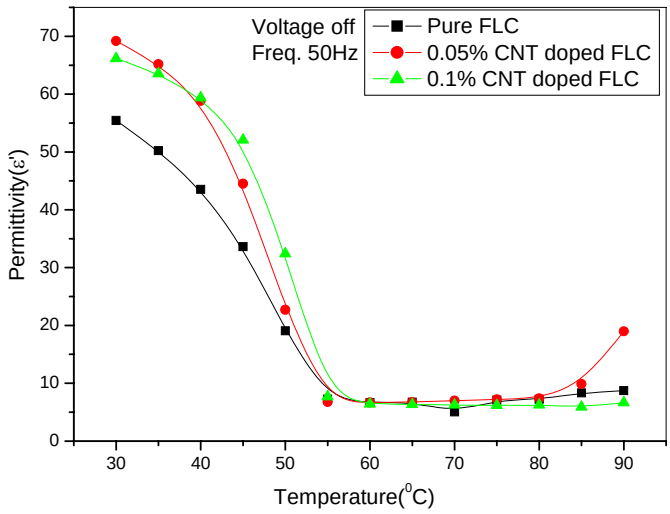

Fig. 3 Dielectric permittivity ε' as a function of temperatures for FLC and CNT dispersed FLC, at 50 Hz.

Fig. 3 shows the effect on the dielectric permittivity of MWNT in ferroelectric liquid crystals at zero biasing and frequency 50 Hz. It was observed that dielectric permittivity increased on dispersing CNT in ferroelectric liquid crystals at lower temperatures but at higher temperatures there was no significant variation in dielectric permittivity values. Such kind of behavior shown by CNT-FLCs composite might be due to the high conductivity and high anisotropic nature of CNT [18] and they had given alignment to liquid crystal molecules results in enhanced dielectric permittivity.

3.2.2 Frequency dependence of permittivity and dielectric loss

The permittivity decreased exponentially up to some frequency at all temperatures in the SmC* phase. At higher frequencies dipoles do not show simultaneous response to electric field and hence they do not align along the field direction. Thus dielectric permittivity was

decreased on increased frequency. Similar effects were seen at SmA phase except that the values were a smaller.

Fig 4 shows the effect on the dielectric permittivity of CNT dispersions in ferroelectric liquid crystals with out any bias voltage at room temperature. It was observed that dielectric permittivity increases on dispersing CNT in ferroelectric liquid crystals at lower frequencies but at higher frequency no significant variation in dielectric permittivity values was noticed

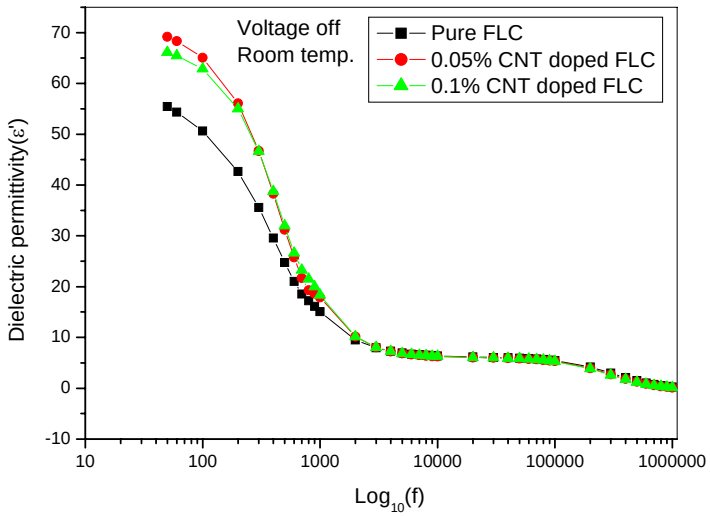

Fig 4 Dielectric permittivity ε' as a function of frequency for FLC and CNT dispersed FLC, at 30° C.

Fig 5 also shows the effect on the dielectric loss of CNT dispersions in ferroelectric liquid crystals at room temperature and zero bias voltage. It was observed that dielectric loss was increased on dispersing CNT in ferroelectric liquid crystals at lower frequencies but at higher frequencies there was no significant variation in dielectric loss. As CNT are conducting in nature, thus on adding the CNT in FLC there should be increased lattice vibration of molecules and hence there would be more dissipation loss. Fig. 5 shows the same behavior as defined in theory.

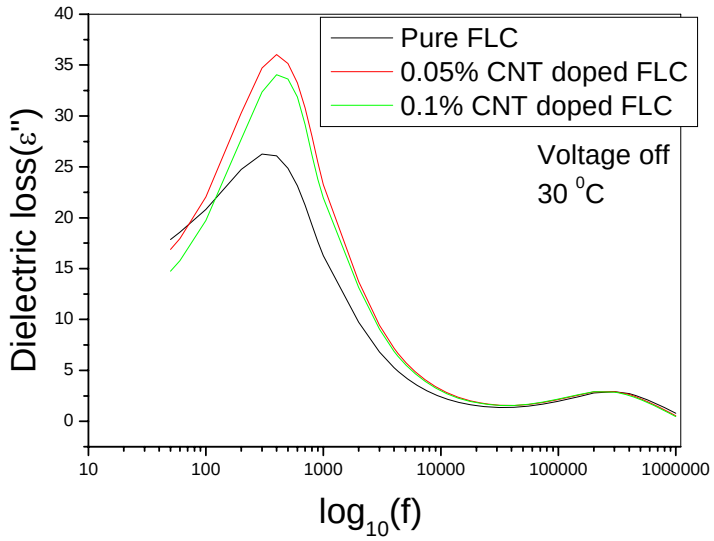

Fig 5 Dielectric loss ε" as a function of frequency for FLC and CNT dispersed FLC at 30 °C.

3.2.3 Relaxation spectra

This relaxation phenomena was also reflected in Cole- Cole plot as shown in Fig 6 The smaller semi- circle in this figure represents the relaxation due to the Soft Mode where as, bigger semi circle represents the contribution due to Goldstone Mode. In the vicinity of the $T_{c^*\text{-}A,}$ SM followed the Currie-Weiss law. The relaxation frequency (f_i) can be evaluated using an expression

$(v/u) = (\omega\tau)^{1-\alpha}$,

where

$v = [(\varepsilon_0\text{-}\varepsilon'(\omega))^2 + \varepsilon''(\omega)^2]^{1/2}$,

$u = [(\varepsilon'(\omega) - \varepsilon'(\infty))^2 + \varepsilon''(\omega)^2]^{1/2}$, $\varepsilon'(\omega)$ is dielectric permittivity at particular frequency.

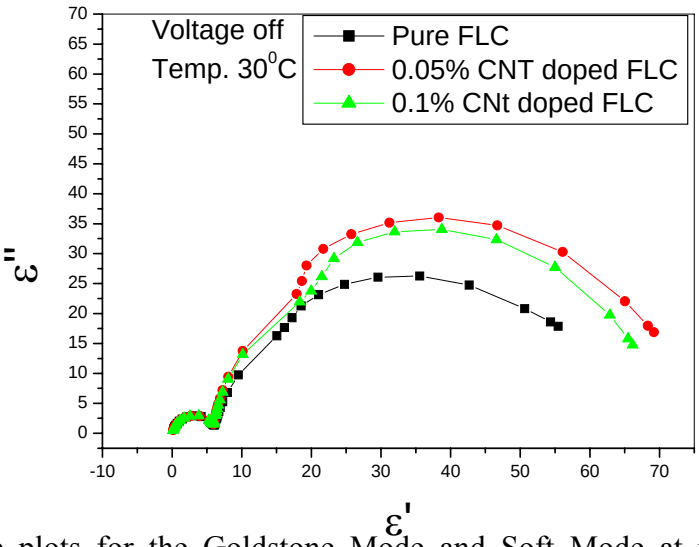

Fig 6 Cole-Cole plots for the Goldstone Mode and Soft Mode at room temperature for mixtures FLC and CNT dispersed FLC.

4.2.4 Effect of Bias voltage

The dielectric permittivity in SmC* phase was dominant due to the Goldstone mode contribution, so it became difficult to detect the other collective dielectric process. The Goldstone mode can be suppressed by applying a dc bias field, being strong enough to unwind the helicoidal structure. The effect of bias voltage on the Goldstone mode in the form of dispersion is shown in Fig. 7(a) and 7(b). We saw that the loss was highest without any bias (0V) voltage but decreased with bias voltage e.g. at 10V in the 0.1% CNTs dispersed FLCs. The Goldstone mode can be suppressed by applying a dc bias field, being strong enough to unwind the helicoidal structure.The voltage at which dielectric permittivity and losses become minimum, is called critical voltage. This voltage was sufficient to unwind the helical structure and suppress the Goldstone mode. The Goldstone mode can be suppressed by applying a dc bias field, being strong enough to unwind the helicoidal structure. But there was no significant variation in permittivity in FLCs. On adding the CNTs in FLCs, the molecules got aligned along CNT and were unable to follow the electric field and hence FLC lost their helical structure. Thus dielectric permittivity and dielectric losses got decreased on increasing dc bias field.

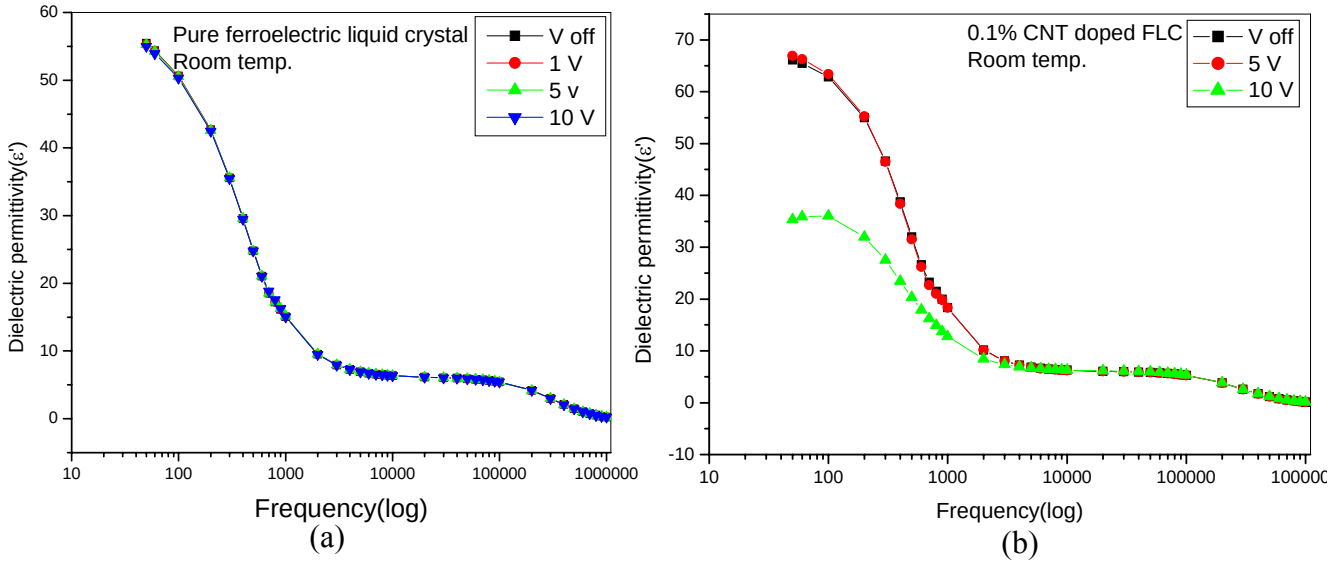

Fig.7 Dielectric permittivity as a function of frequency at different voltage for (a) FLC (b) 0.1% CNTs dispersed FLC

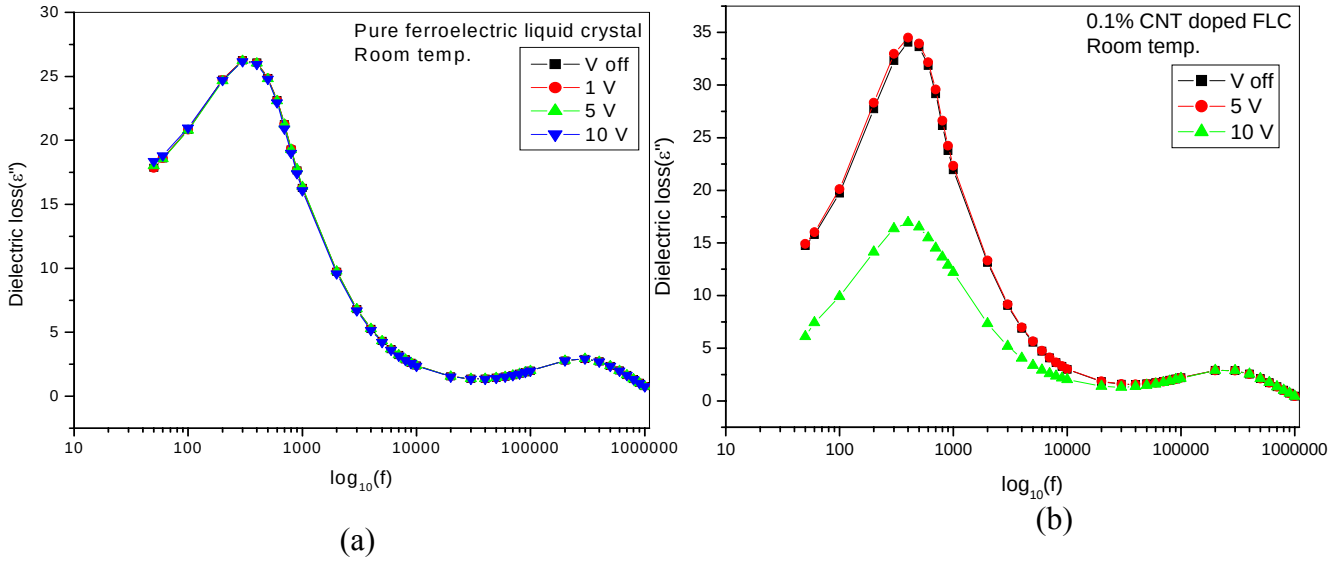

Fig 8 Dielectric loss as a function of frequency at different voltage for (a) FLC (b) 0.1% CNT dispersed FLC

Fig 8(a) shows the dielectric loss (ε") as a function of frequency at different voltages for pure FLC. It was observed that there was no effect of biasing on FLC. Fig 8(b) shows the dielectric

loss (ε”) as a function of frequency at different voltages for multiwalled carbon nanotube dispersed FLC. Two relaxation peaks at 500Hz and 500 kHz were observable. The first peak corresponds to a domain mode structure where as the second one corresponds to the soft mode. This was also reflected in the form of Cole-Cole plot.

5. Conclusions

- dispersed nanotubes in LC, enhanced the alignment of the LC molecules and thus macroscopically homogeneous structures was obtained. The inherent conductivity and spontaneous self- alignment properties of CNTs make them an attractive alternative as an alignment layer.
- transition temperature increased by 7% and 17% after addition of 0.05% and 0.1% wt/wt carbon nanotubes in FLC.
- dielectric permittivity got increased almost by 27% on dispersing CNT in ferroelectric liquid crystals at lower temperatures and frequencies values but at higher temperatures and frequency, there was no significant variation in dielectric permittivity values.
- relaxation peaks at 300Hz and 500 kHz were observable that corresponds to Goldstone mode and Soft mode respectively. This was also reflected in the form of Cole-Cole plot.

References

1. J. W. Doane., N. A., Wu, B. G. Vaz., And S. Zumer., Appl. Phys. Lett., **48**, 269 (1986), .
2. M. Kreuzer., T. Tschudi., And R. Eidenschink., Appl. Phys. Lett., **62,** 1712 (1993),.
3. F. Brochard , And P. G. De Gennes., J. Phys., **31**, 691(1970).
4. B. J. Liang., And S.H. Chen., Phys. Rev., **39**, 1441 (1989),.
5. Yu. Reznikov., O. Buchnev., O. Tereshchenko., V. Reshetnyak., A. Glushchenko., And J. West., Appl. Phys. Lett., **82**, 1917 (2003).
6. Jan P. F. Lagerwall and Giusy Scalia, J. Mater. Chem., **18**, 2890 (2008).
7. Dierking, G. Scalia and P. Morales, J. Appl. Phys., **97**, 044309 (2005).
8. I. Dierking, G. Scalia, P. Morales and D. Leclere, Adv. Mater., **16**, 865 (2004).
9. M. Lynch and D. Patrick, Nano Lett., **2**, 1197 (2002).
10. M. Endo, T. Hayashi, Y.A. Kim, H. Muramatsu. Jap. J. of Appl. Phys, **45**, 4883 (2006).
11. H.Y. Chen, N.A. Clark, W. Lee. Appl. Phys. Lett, **90**, 033510 (2007).
12. C.Y. Huang, H.C. Pan, C.T. Hsieh. Jpn J. Appl. Phys. Part 1, **45**, 6392 (2006).
13. S.Y. Jeon, S.H. Shin, S.J. Jeong, S.H. Lee, S.H. Jeong, Y.H. Lee, H.C. Choi, K.J. Kim. Appl. Phys. Lett, **90**, 121901 (2007).
14. I.S. Baik, S.Y. Jeon, S.J. Jeong, S.H. Lee. J. Appl. Phys, **100**, 074306 (2006).
15. A.M. Birader, S.S. Bawa, C.P. Sharma, Subhas Chandra, Ferroelectrics **122**,81(1991).
16. K. Kondo, T. Kitamura, M. Isogai, A. Mukoh, Ferroelectrics **132,** 99 (1988).
17. Giusy Scalia, Clemens von Bu¨hler, Constanze Ha¨gele, Siegmar Roth, Frank Giesselmann and Jan P. F. Lagerwall, Soft Matter, 4, 570,(2008).
18. CECILE ZAKRI, Liquid Crystals Today, **16**, 1, (2007).

Breathing in-breathing out approach to prepare nanosilver loaded hydrogels: highly efficient antibacterial nanocomposites

Varsha Thomas*[#1], Murali Mohan Yallapu[2], B. Sreedhar[3] and S. K. Bajpai[1]

[1] Polymer Research Laboratory, Department of Chemistry, Govt. Model Science College, Jabalpur (M.P.) – 482001, India.
[2] Department of Polymer Science & Technology, Sri Krishnadevaraya University, Anantapur, A.P-515003, India
[3] Inorganic and Physical Chemistry, Indian Institute of Chemical Technology Tarnaka , Hyderabad – 500007, (A.P) India

E. mail: annvarsha82@rediffmail.com

Abstract

The key objective of developing novel materials for hygienic living conditions is to lower the risk of transmitting diseases and bio-foul. Among inorganic antibacterial agents, silver has been identified as extensively studied material since ancient time to fight infections and control spoilage. With this aim**,** a number of silver-hydrogel nanocomposite systems are under development. In this study, we put forward a unique strategy to prepare silver nanoparticles loaded poly (acrylamide-*co*-*N*-vinyl-2-pyrollidone) hydrogel composites. The hydrogel networks provide excellent stability for silver nanoparticles and can be stored at room temperature and along with this hydrogels are highly biocompatible in nature. In order to load nanosilver particles into such non-ionic hydrogel, a novel **"Breathing in - Breathing out" (BI-BO)** approach was employed. As the number of BI-BO cycle increases the amount of silver nanoparticles loading into these hydrogels also increases. This behavior is obvious and confirmed by UV-vis spectral and thermal analysis. Further, the formed hydrogel-silver nanoparticle composites are confirmed by FT-IR spectral and transmission electron microscopy (TEM) studies. The antibacterial studies of these hydrogel silver nanocomposites showed excellent results on Escherichia coli (*E.coli*).

Introduction

Among inorganic antibacterial agents, silver has been identified as extensively studied material since ancient time to fight infections and control spoilage [1]. The antibacterial and antiviral actions of silver, silver ions and silver compounds have been thoroughly investigated [2-8]. Recently, polymer scientists have focused on the development of such polymeric-nanosilver materials that exhibit anti-microbial properties. The reason behind these continuous efforts is that such anti-microbial polymers, when coated on the surface of various medical devices like urinary catheters, cannulae,

surgical gloves, dressing material and so on, prevent bacterial infections [9-12]. A few trends based on hydrogel-silver nanocomposite systems revealed outstanding antibacterial properties. The three-dimensional networks of hydrogels provide enough space for nucleation as well as the growth of nanoparticles and are of bio-medical interest due to their compatibility with biological molecules, cells, tissues, etc [13 - 15]. Most recently, we reported a unique approach to incorporate nanosilver into poly (acrylamide-*co*-acrylic acid) hydrogel [16] and also investigated biocidal action of resulting material. This approach involved immersion of swollen hydrogel in $AgNO_3$ aqueous solution to induce ion-exchange between Ag^+ ions of the solution and H^+ ions present in the swollen hydrogel network, followed by citrate reduction. However, this approach cannot be applied to incorporate Ag^+ ions into a polymer networks composed of non-ionic monomers. Therefore, in order to prepare silver nanoparticles containing polymeric hydrogel having neutral monomers as repeat units, we hereby report a unique "Breathing in- Breathing out" (BI-BO) method for the synthesis of nano Ag-loaded poly(acrylamide-*co*-*N*-vinyl-2-pyrrolidone) hydrogels. When a shrunken gel is placed in aqueous solution of silver nanoparticles it undergoes appreciable swelling by absorbing surrounding aqueous medium. The absorption of aqueous medium by the gel may be considered as 'breathing in' process. Later on when the swollen gel is put in the acetone, the gel undergoes drastic deswelling by expelling water. The expulsion of water from the swollen gel network may be considered as 'breathing out' process. This swelling-shrinking behavior of gels has been exploited to introduce silver nanoparticles into the gels. Finally, the resulted nano Ag containing gels have also been investigated for antibacterial properties against *E.coli*.

Experimental

Silver nanoparticles were synthesized by reduction of silver nitrate by sodium citrate.The hydrogel discs were prepared by carrying out free-radical aqueous co-polymerization of AAm and NVP in the presence of MBA crosslinker using KPS as initiator. The silver nanoparticles were loaded into the swollen gel by using newly developed Breathing in - Breathing out (BI-BO) approach at 27 ± 0.2°C. The silver nanocomposites were characterized by TGA, XPS and TEM analysis. Microbial experimentation was done to see the effect of silver-hydrogel composite on Gram-negative bacteria *E.coli*. For this purpose approximately 10^8 colony forming unit (CFU) of *E.coli* were cultured on nutrient agar plates supplemented with a calculated amount of nanosilver loaded hydrogel particles (size = 211 μm). Plain hydrogels were used as control. The plates were incubated for 24 h at 37^oC and the number of colonies was counted.

Results and Discussion

In our work we have proposed a new BI-BO approach for the formation of silver nanocomposites. This involves swelling of gel in aqueous solution of silver nanoparticles followed by de-watering of gels in acetone. The overall mechanism of proposed BI-BO approach may be explained as follows. When swollen hydrogel sample is placed in acetone, there occurs a drastic volume change due to expulsion of water molecules. Then, the shrunken gel is transferred to aqueous solution of citrate-stabilized silver nanoparticles, where hydrogel re-swells due to simultaneous absorbtion of water molecules along with suspended silver nanoparticles. After equilibration of gels in aqueous solution of citrate-stabilized silver nanoparticles, it is placed again in acetone, which causes rapid de-swelling of gel network due to expulsion of water. However, the silver nanoparticles remain stuck inside the gel, probably due to (i) physical entanglement within macromolecular networks and (ii) hydrogen bonding interactions between the polymer chains and citrate surface of the nanoparticles.The increasing concentration of silver nanoparticles in the gel with 'Breathing in' cycles has been well illustrated in the Fig.1 (A), (B), (C) which correspond to plain hydrogel, hydrogel after first and second 'BI-BO' cycles respectively. It can be clearly seen that the gel, which underwent two 'breathing in' cycles, contains more nanosilver than the sample with one cycle.

Thermograms of hydrogel-silver nanocomposites obtained with different cycles and a plain hydrogel (HGA) are presented in Fig. 2. All hydrogels showed 3 major weight loss steps. Small weight loss below 100^{o}C, must be due to loss of water molecules. The second weight loss due to decomposition of the pendant groups of hydrogel macromolecular chains was found in the range of 300 to 450°C for all the hydrogels. However the third weight loss (i.e. final decomposition temperature) for samples processed with 0, 1, 2 and 3 BI-BO cycles was found in the range of 460 to 600, 500 to 650, 550 to 750 and 600 to 750°C respectively. The observed increase in the final decomposition temperature with number of BI-BO cycles may be attributed to the fact that as number of BI-BO cycles increases, silver content within the hydrogel networks also increases. As silver has high thermal stability, its presence within the gels enhances their thermal stability

Further, to confirm the amount of nanoparticles loading into gels with increase of number BI-BO cycles, UV-vis spectral study was employed. The hydrogel-silver nanoparticles, HGA, obtained by different number of BI-BO cycles were soaked for a week in distilled water. The released silver nanoparticles from the plain HGA hydrogels and HGA composites were monitored by absorbance in UV-vis spectra. Fig. 3. illustrates higher absorbance for gels with 3rd BI-BO cycles which directly represents for the presence of higher amounts of particles compared to the 1st and 2nd processed gels.

In order to demonstrate the presence of silver nanoparticles within the hydrogel network, TEM images were recorded. For this, finally grinded HGB hydrogel-nanocomposites were put in distilled water

for seven days, and then their suspension was sonicated. This allowed a few particles to come out of the swollen network. This may probably be attributed to the increased mesh sizes of the swollen network, relaxation of polymeric chains entanglements around the nanoparticles and finally the decrease in the extent of binding between stabilized Ag nanoparticles and N and O atoms present in the hydrated macromolecular chains. The TEM images, recorded, have been shown in the Fig, 4. A close look at these figures reveals not only the presence of released silver nanoparticles but also that of hydrogel-silver nanocomposites. From the size distribution graph, Fig.7.B., it can clearly seen that the average diameter of the silver nanoparticles in the hydrogel comes out to be ~ 12.573 nm.

Antibacterial property of silver hydrogel nanocomposites were studied by differing the number of BI-BO cycles, cross-link density of gel and concentration of silver nanoparticles in the gels. It was clearly seen that with the increase in the number of BI-BO cycles, more and more silver nanoparticles are loaded into the gels and hence extent of their biocidal action also increases. This can be clearly seen in Fig.5. Similarly it was also found out that the nanocomposites with higher crosslinking show lesser antibacterial property as compared to nanocomposites with lesser crosslinking. This may be expalined on the basis of their different swelling capacities. The hydrogel prepared with lesser MBA, had greater degree of swelling in silver nanoparticle solution during the ‘breathing in’ step thus allowing more silver nanoparticles to enter into the swollen networks. On the other hand, the other sample, with higher MBA, exhibits lower degree of swelling during the ‘breathing in’ step, thus permiting lesser number of silver nanoparticles into the network. Also the silver loaded in lesser cross-linked gels are released more easily than the silver loaded in highly crosslinked gels and therefore the silver loaded in hydrogel cross-linked with lesser MB shows more antibacterial activity.

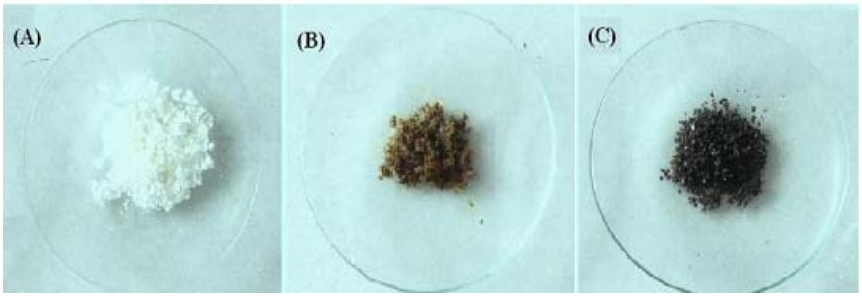

Fig.1. Photograph showing (A) Plain hydrogel and (B) silver nanocomposites formed after one (C) two BI-BO cycle.

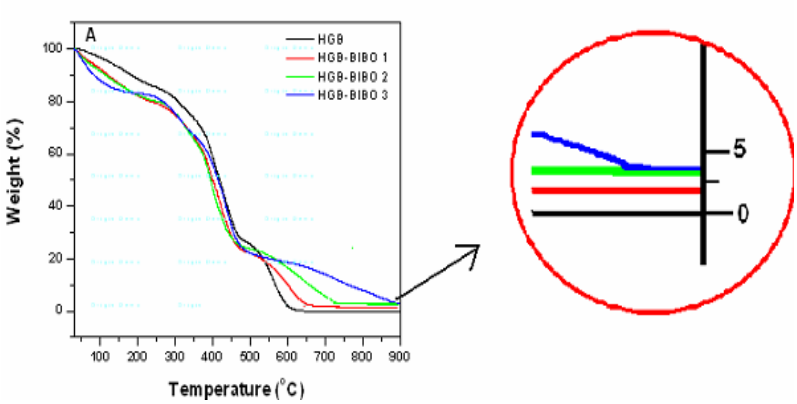

Fig.2. TGA of plain hydrogel sample HGA and silver loaded samples with one, two and three BI-BO cycles. (magnified area shows percent mass remained at 900°C).

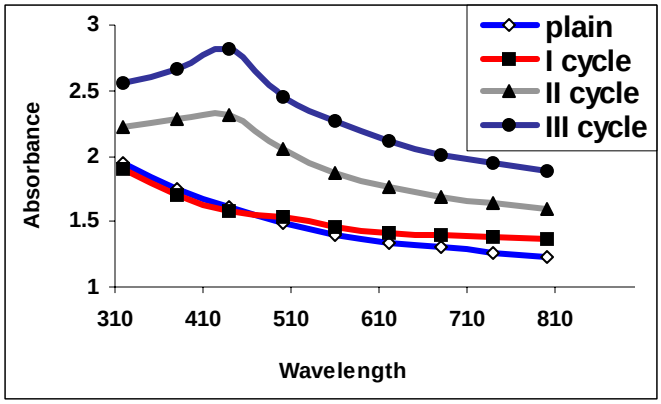

Fig.3. UV-vis spectra of plain HGA hydrogels and HGA silver nanocomposites undergone 1st, 2nd and 3rd BI-BO cycles

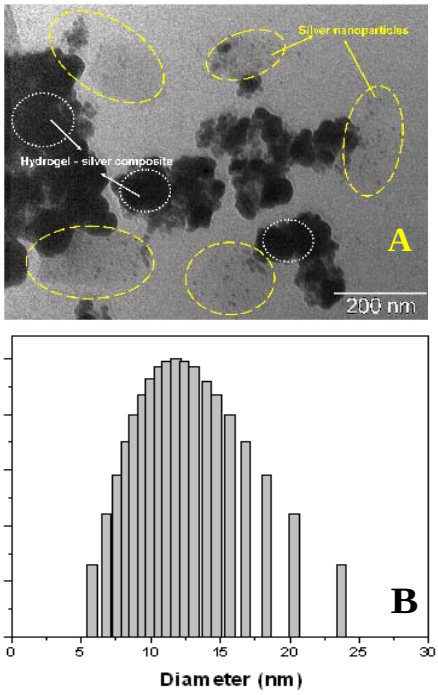

Fig. 4. A. TEM image of hydrogel-silver nanocomposite, HGB, prepared by completing two BI-BO cycles. B. Size distribution of silver nanoparticles within the hydrogel.

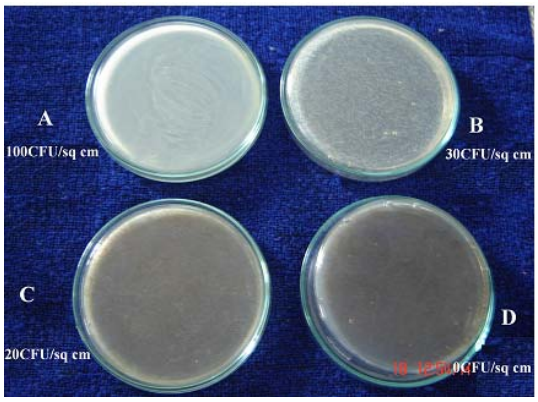

Fig.5 Photograph showing bacterial colonies in (A) control set and in hydrogel undergone (B) one (C) two (D) three BI-BO cycles.

Conclusion:

From the above study it can be concluded that non-ionic hydrogels, poly(acrylamide-co-N-vinyl-2-pyrrolidone)s are highly successful in loading the silver nanoparticles with our novel 'Breathing in - Breathing out' (BI-BO) approach. These novel nanosystems were extensively characterized by spectral, thermal and nanostructural aspect. These nanosilver loaded hydrogels express good antibacterial activity against *E. coli.* Their antibacterial action depends upon amount of silver nanoparticles within the hydrogel, which can be altered by the number of BI-BO cycles, amount of $AgNO_3$ in the solution and cross-linker in the hydrogels.

References:

1. Silver, S.; Phung, L.T. *Annu Rev Microbiol* 1996, **50**, 753.
2. Feng, Q. L.; Wu, J.; Chen, G. Q.; Cui, F. Z.; Kim, T. N.; Kim, J. Q. *J Biomed Mater Res* 2000, **52**, 662.
3. Catauro, M.; Raucci, M. G.; De Gaetano, F. D.; Marrotta, A. *J Mater Sci Mater Med* 2004, **15,** 831.
4. Sondi, I.; Salopek-Sondi, B. *J Colloid Interf Sci* 2004, **275,** 177.
5. Pal, S.; Tak, Y. K.; Song, J. M. *Apl Environ Microbiol* 2007, **73,** 1712.
6. Duran, N.; Marcato, P. D.; De Souza, G. I. H.; Alves, O. L.; Esposito, E. *J. Nanotechnol.* 2007, **3,** 1.
7. Baker, C.; Pradhan. A.; Pakstis, L.; Pochan, D. J.; Shah, S. I. *J Nanosci Nanotechnol* 2005, **5,** 244.
8. Li, P.; Li. J.; Wu, C.; Wu, Q.; Li, J. *Nanotechnology* 2005, **16,** 1912.
9. Furno, F.; Morley, K. S.; Wong, B.; Sharp, B. L.; Arnold, P. L.; Howdle, S. M.; Bayston, R.; Brown, P. D.; Winship, P. D.; Reid, H. J. *J Antimicrobial Chemother* 2004, **54,** 1019.
10. Lai, K. K.; Fontecchio, S. A. *Am J Infect Control* 2002, **30,** 221.
11. Li, Y.; Leung, P.; Yao, L.; Song, Q. W.; Newton, E. *J Hospital Infect.* 2006, **62,** 58.
12. Yu, H.; Yu, X.; Chen, X.; Lu, T.; Zhang, P.; Jing, X. *J Appl Polym Sci* 2007, **103**, 125.
13. Mohan, Y. M.; Premkumar, T.; Lee, K.; Geckeler, K. E. *Macromol Rapid Commun* 2006, **27,**1346.
14. Wang, C.; Flynn, N. T.; Langer, R. *Adv Mater* 2004, **16,** 1074.
15. Zhao, X.; Ding, X.; Deng, Z.; Zheng, Z.; Peng, Y.; Long, X. *Macromol Rapid Commun* 2005, **26,** 1784.
16. Thomas, V.; Yallapu, M. M.; Sreedhar, B.; Bajpai, S. K. *J Colloid Interf Sci* 2007, **315,** 389.

Guidelines for ORAL and POSTER presentations for the International Conference on Advances in Polymer Technology, APT'08.

***For ORAL presentations: ***

1) The presentation time for the various oral presentations are as follows:

a) Invited Lecture: 30(25+ 5) minutes;
b) Contributed Lecture: 15 (12+3) minutes.

2) All times include the time for set up. Every attempt will be made to maintain the published presentation times.

3) The standard audio-visual equipment will consist of an LCD projector, screen, pointer, and wireless microphone.

4) The projector will be connected to a PC running on Windows XP with the MS Office suite, Adobe Acrobat Reader, etc. However, presenters can use their own laptop too.

***For POSTER presentations: ***

1) The poster dimensions are 1 m width (max) and 1.3 m height. The posters may be displayed in the "Portrait" mode. Double stick tape will be provided for attaching the posters to the board.

2) Please print the Title and Authors Name/s in extra large characters (over 3 cm high) across the top of your display.

3) Each poster will be assigned a board.

Ultrasound-triggered release of Ibuprofen from a chitosan-mesoporous silica composite- a novel approach for controlled drug release

Dilip Depan*, Raj Pal Singh#
Division of Polymer Science and Engineering, National Chemical Laboratory, Dr. Homi Bhabha Road, Pune – 411 008
E-mail: *d.depan@ncl.res.in, #rp.singh@ncl.res.in

Abstract
In this work, an attempt was made to synthesize a novel Chitosan-Mesoporous silica (CS-MS) composite to design a drug delivery system based on ultrasound triggered stimuli-responsive smart release. The in-vitro drug release properties of both the Mesoporous Silica (MS) and Chitosan (CS) hybrids were investigated. Ibuprofen (Ibu) was used as a model drug. The results from powder X-Ray diffraction (XRD) patterns, and BET N_2 adsorption isotherms exhibited that MS can accommodate drug molecules into the lumen of the channels and pores, while CS acts as biopolymer matrix. Control of drug release through the porous network was performed by measuring the uptake and release of Ibu.

Introduction
Chitosan (CS), [poly-β(1, 4)-2-amino-2-deoxy-D-glucose], is the deacetylated product of chitin, a pH dependent cationic natural polymer found in the cell wall of fungi and microorganisms. Due to its biocompatibility, biodegradability and avirulence, CS has been used in many biomedical applications[1]. The ability of CS to form films may permit its extensive use in the formulation of film dosage forms or as a promising encapsulating agent in drug delivery systems. Ibuprofen (Ibu) is a non-steroidal anti-inflammatory (NSAID) drug used for the relief of rheumatoid arthritis. Due to frequent side effects, its use is often limited which are also consequences of high plasma levels following the administration of conventional formulations. These problems could be reduced by a formulation able to control the drug release. As matrices to prepare a controlled release formulation, we have taken into account the use of porous materials. The idea was to store the drug in the channels of a porous host and allow the drug release as a consequence of a de-intercalation or diffusion process. Recently, there has been increased concern in Mesoporous silica (MS) materials for use as carriers in controlled drug release, to necessitate the prolonged and better control of in-vitro and in-vivo drug administration.

Moreover, mesoporous silica have been found as a sustained release drug carrier agent because of their biocompatibility, non-toxic nature, adjustable pore diameter, and very high specific surface area with abundant Si-OH bonds on the pore surface. For a drug-delivery system, it is desirable that drug-delivery pattern is optimized to a pulsatile behavior in which the drug molecules are naturally released at the targeted site from the implant body. Particularly applicable on diabetic patients, the on/off or pulsatile control of drug release is especially important when higher doses of insulin are required after meals. Ultrasound is considered as the most potential technique of external trigger for pulsatile delivery in which the release rate of the incorporated bio-molecules/drugs can be repeatedly modulated by applying ultrasound irradiation from a position external to the delivery system. In the present work, we have reported the preparation of Ibu loaded Chitosan-Mesoporous silica (CS-MS) composites. Mesoporous silica (SBA-15) was used as a drug reservoir, while CS acts as an implantable body of the drug carrier.

Experimental

Preparation of Mesoporous silica (SBA-15)

SBA-15 was prepared by the method already reported by Stucky et al.

Preparation of Ibu loaded CS and CS-MS hybrid composites samples and Ultrasound triggered drug release procedure

To prepare Ibu loaded MS (MI-1); MS was dispersed in Ibu solution and stirred for 24 h. The drug-loaded powder was washed carefully with hexane to remove Ibu and finally dried at 60 °C.
For preparation of CS-MS composite (CMI-1), Ibu-loaded MS was mixed with an aqueous solution of CS. The drug-loaded MS powder was dispersed and stirred vigorously in the CS solution with the ratio of 1:10 (MS/CS). The final solution was poured on a glass Petri plate, and was vacuum dried at room temperature for 48 h and cured at 60 °C for 24 h.

Results and discussions

The small angle X-ray diffraction (SXRD) pattern of MS (SBA-15) and MI-1 is given in Figure 1. As predicted for MI-1, there is a remarkable decrease in the intensity of the peaks, as compared to pristine MS, corresponding to (100), (111) and (200) planes based on the hexagonal unidirectional structure. The peak positions were shifted to higher 2θ value because of the inclusion of drug molecules to the inter-pore region of MS. The d_{100} spacing and unit-cell size (a_0) for MI-1 measured to be 40.30 Å and 45.42 Å, respectively. As a_0 represents the repeated distance between two pore centers in the hexagonal array, the pore diameter can be calculated from a_0 by subtracting 10 Å, which is an approximate value of the pore-wall thickness. Therefore, a pore diameter of 35.42 Å is obtained which means that the pore size of MS is large enough to allow access to the large internal surface area to accommodate Ibu molecules.

The wide angle X-ray diffraction (WXRD) patterns of CMI-1 and CI-1 are given in the INSET of Figure 1. All the samples show a characteristic peak at around 21 °, which confirms the presence of crystalline CS in the composites. Figure 2 shows the FT-IR spectra of pristine Ibu and drug loaded MS samples. As compare to the pristine Ibu, the band corresponding to a free carboxylic acid (1718 cm^{-1}) in Ibu, has changed to a carboxylate one (1461 and 1634 cm^{-1}) in MI-1, which suggests the interactions between carboxylate group of Ibu and Si-OH group of the MS host. Typical υ (CH) stretching vibrations of Ibu are observed at 2958, 2927, and 2871 cm^{-1} for pure Ibu as well as that loaded on MS. The Si-OH vibration band at 965 cm^{-1} present in pristine MS, almost disappears after Ibu loading, it suggests that the –H bond has been formed between the –COOH group of Ibu and the Si-OH of the MS host.

Delivery procedure

Figure 5a shows the cumulative release profiles of Ibu from MI-1, CI-1, and CMI-1, and subsequent pulsatile release profile for CI-1 and CMI-1 samples under ultrasound irradiation. The release of Ibu stored in MS occurs only after the release medium has penetrated among the channels and subsequent dissolution of Ibu in the aqueous media. Remarkably, under silent conditions, MI-1 showed very fast release within first 100 min, while the subsequent release rate was quite low as compare to the initial rate. This behavior of drug release could be ascribed to favorable physical hosting of the drug

inside the inter-pore network of MS and ionic interactions of –Si-OH group of MS and –COOH group of Ibu molecules. As shown in Figure 5a, the initial drug release rate of CMI-1 was substantially reduced. The Ibu release profile of CMI-1 was quite similar to that of CI-1. Conceivably, this similar release rate could be attributed to a strong dipolar interaction and H bonding between the abundant Si-OH groups of MS, -NH_2 of CS and –COOH groups of Ibu. The release profile was found to be a two step. In the initial stage a small amount of drug was continuously released for about the first 250 minutes, which may be due to the release of excessive drug molecules which were weakly entrapped inside the pores or located at the external MS surface. The second stage shows extremely slow liberation of Ibu, which could be due to the physical blocking of the entrapped drug molecules inside the solvent filled channels of MS, along with CS chains. This demonstrates that the release of Ibu can be successfully controlled by the mixing of CS with MS. In order to understand the effect of ultrasound on the drug release profile of CI-1 and CMI-1, the samples were exposed to ultrasound to increases the release rates after 1100 minutes of release experiment. For this the samples were immersed in the release media, and kept in an US bath, maintained at a constant temperature.

During the course of ultrasonic irradiation, it was observed that Ibu was continuously released from both CI-1 and CMI-1, while US was found to have an apparent effect to enhance the drug release kinetics of both the systems. It can be ascribed to the enhancing effect of ultrasound irradiation which is capable of reversibly losing the rigid packing of the self-assembled hydrocarbon chains which results in increase the permeability of water and drug through the polymer film. These effects can generally be explained by an important phenomenon called cavitation which is generated by ultrasonic irradiation. To investigate the effect of ultrasound on the pulsatile release of the drug from CI-1 and CMI-1, the specimens were exposed to ultrasound for around 120 min. The results were shown in Figure 5b, where the release of Ibu was observed to start immediately for CMI-1, and sustained until the ultrasound irradiation was discontinued, while in the case of CI-1, the amount of released Ibu continuously decreased after a second irradiation. On the other hand, for CMI-1 regular pattern was displayed with repeated ultrasonic dose and the amount of Ibu released in each step was nearly the same each time, and was higher than that of CI-1 release profile. Since, the extent of Ibu loading for both the systems was same at around 15 mg g^{-1}, this difference does not originate from the amount of Ibu present in the matrix. It suggests that CMI-1 released the Ibu more effectively than CI-1, and it is believed that the hydrophilicity, high permeability, and subsequent high ultrasonic susceptibility of CMI-1, makes it possible for ultrasound to be transferred deep into the biopolymer matrix, hence promoting the regularity of the pulsatile release of the drug from the CMI-1 system. This may allow repeated operation for a continuously controlled release of a drug into a patient's body to maintain a therapeutically effective dose for a longer period of time to efficiently treat the disease. We have studied the stimuli-responsive investigation of the effect of temperature on the drug release of CS-MS system. The results are given in Figure 6a and it depicts that the range of temperature over which the transition takes place is quite broad (30-40 °C), which is due to the steric hindrance of CS chains with the silica host, and a transition is detected at 35 °C for CMI samples. At low temperature, the drug molecules are restrained in the porous MS channels, and along with CS molecular chains, Ibu molecules takes part in the formation of -H bonding between CS and Ibu molecules. CS has a high

water retention capacity, and it absorbs enormous amount of water. So, when the Ibu loaded CS-MS samples immersed in the aqueous release media, the films absorbs enough water, eventually taking the form of a hydrogel. However, at low temperature this water is in the form of a bound state, and as the temperature increases these bound-water molecules gains an enthalpy and changes from a bound state to a free state, with subsequent release of the incorporated drug molecules from the matrix. Moreover, MS is not a thermo-sensitive material, so we may predict that as the temperature increases, the biopolymer chains swells within the MS pore network resulting in the disruption of weak -H-bonds, accelerating the drug molecules from the pores.

The release profiles of Ibu loaded samples were determined in simulated gastric fluid (pH 1.4) and simulated body fluid (pH 7.4). It is evident from Figure 6b that the release profile of both the systems (MI-1 and CMI-1) are very similar in the medium of pH 1.4, where the amount of drug released from the two systems reaches >75 % in 50 h, under continues ultrasound irradiation. This behavior shows that both systems display sustained release, which is pH sensitive and the possible explanation is, in this low pH acidic media, protonation can occur at the $–NH_2$ groups of CS, leading to the dissociation of the H-bonds involving the CS amine groups with the -COOH groups of the Ibu molecules. Hence, we can say that at this low pH, CS matrix could not cap the openings of the MS channels. Therefore, the drug molecules can easily diffuse out from the MS pores into the release medium.

Conclusions:

In conclusion, we have demonstrated a concept to design a novel stimuli-responsive controlled drug-release system where ultrasonic irradiation was used as an external trigger for smart drug release to obtain optimal therapeutic effects. The overall system was composed of MS as a drug storage device and CS as an implantable body. This smart system is efficient for storage and release of drug, further controlled by temperature and pH at will. CS successfully suppressed the initial burst of Ibu from the MS. Besides; the ultrasound was effective to improve the release kinetics of CS-MS system in a nondestructive manner. The addition of MS into CS could increase the ultrasonic susceptibility and reliability of pulsatile drug release. We envision that this novel system, which combines the advantages of both high drug storage capacity and the property of stimuli-responsive controlled release, could play a significant role in the development of new generation, site specific, and smart drug release.

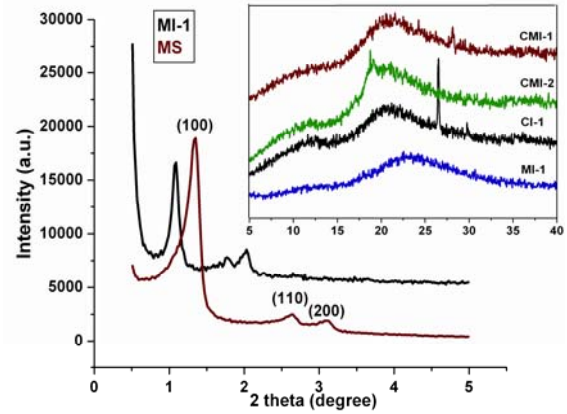

Fig.1 (a) WXRD patterns of the prepared composites.

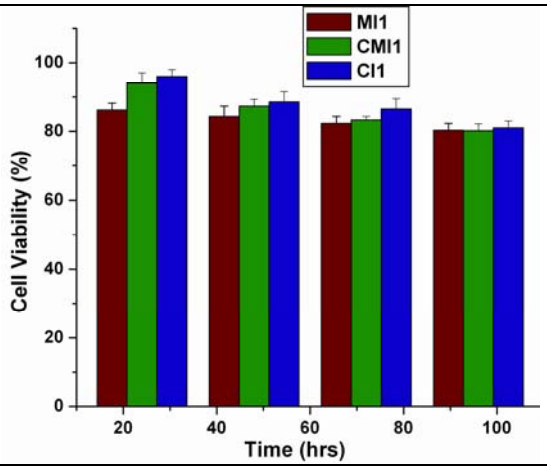

Fig. 1 (b) FT-IR patterns of composites.

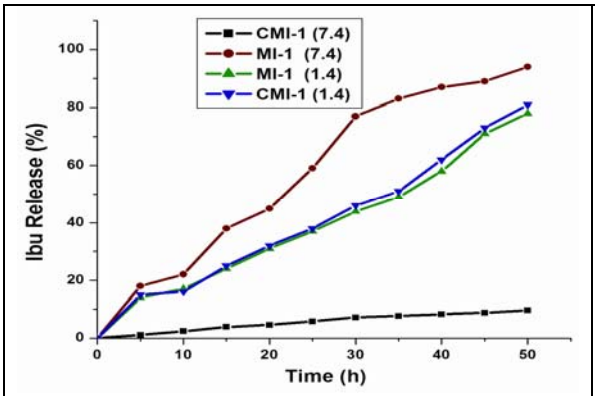

Fig. 2 (a) Effect of pH on drug release

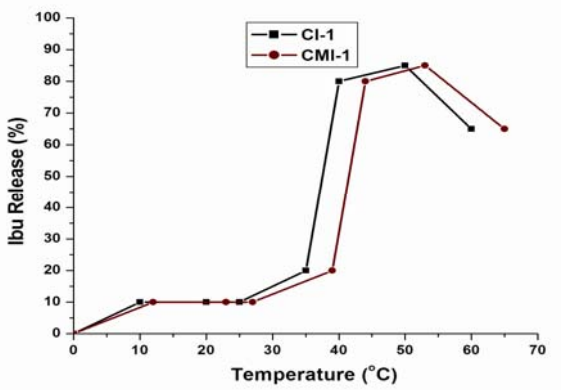

Fig. 2 (b) Effect of temperature

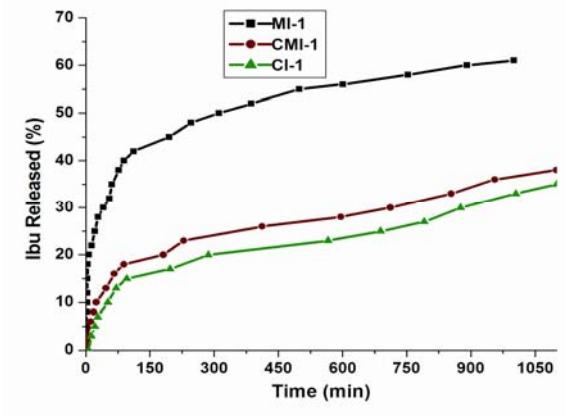

Fig. 3 (a) Ibu Release under silent conditions.

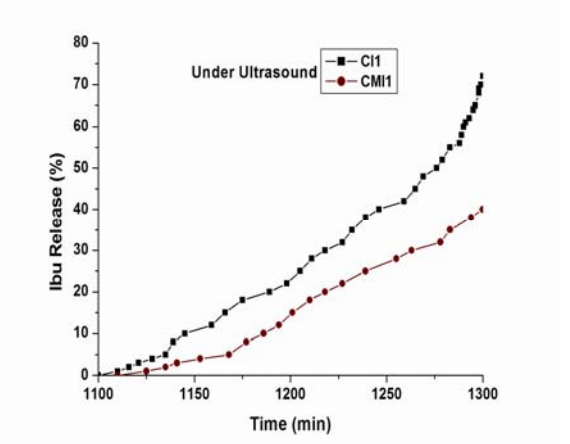

Fig. 3 (b) Effect of ultrasound on release.

Copper (II) ions and copper nanoparticles loaded chemically modified cotton cellulose fibres with fair antibacterial properties

Grace Mary[1]* [#], S. K. Bajpai[1] and Navin Chand[2]
[1] Polymer Research Laboratory, Department of Chemistry, Govt. Model Science College, Jabalpur (M.P.) – 482001, India.
[2]Polymer Composite Group, Advanced Materials and Process Research Institute, Regional Research Laboratory, Bhopal (M.P.), India.
Email: gracemary9@gmail.com

Abstract

This work describes release of copper(II) ions from cellulose fibers which have been chemically modified by periodate induced oxidation of cellulose, followed by covalent attachment of biopolymer chitosan. The release of copper(II) ions has been investigated in physiological fluid (PF) and protein solution (PS) both at 37ºC. Fibers have demonstrated excellent antibacterial activity against *E.coli*. Finally, their borohydride-induced reduction has yielded copper nanoparticles loaded fibers, with average diameter of particles, nearly 28.94nm. The formation of copper nanoparticles has been established by surface plasmon resonance. These fibers also show fair biocidal action against *E.coli*.

Introduction

Recently, there has been a growing interest to develop metal nanoparticles loaded fibers. Fibers, made from natural sources, especially polysaccharides, have been considered as the most promising materials due to their excellent biocompatibility, non-toxicity and potential bioactivity. These include alginates [1], chitosan [2], cellulose [3] etc. The antibacterial nature of chitosan and its capability to immobilize metal ions at its amine functionality are attractive features.

Therefore, in order to develop an ideal fiber with fair ion-binding and releasing properties, mechanical strength, easy processibility, excellent biocompatibilty and excellent commercially production feasibility, we hereby propose a novel cellulose-based fiber, obtained by periodate induced oxidation of cotton cellulose fibers to give dialdehyde cellulose, followed by covalent attachment of $-NH_2$ group of chitosan through coupling reaction. This novel chitosan bound cellulose (CBC) fiber has been used for immobilization

of Cu(II) ions and copper nanaoparticles to obtain fair antibacterial property against the model bacteria *E.coli*.

Copper, in its different forms, has been used by ancient civilization to treat people stricken with afflictions and to maintain hygiene [4]. Recently, Zhang et al [5] have introduced copper into medical polymer, polyethylene (PE) by means of copper plasma immersion ion implantation (CPIII) technique and investigated its antimicrobial properties. Copper nanoparticles embedded poly (vinyl methylketone) films have also been investigated for their biocidal action against growth eukaryote and prokaryote target microorganisms [6]. In a work by the same group of workers, copper-fluoropolymer (Cu-CFX) nanocomposite films have shown strong inhibitory action against growth of *E.coli* and Lysteria [7]. Apart from polymer-based antibacterial films, various synthetic and natural polymers, in the form of fibers, have also been developed with antibacterial properties.

Cu(II) is reported to play a key role in collagen crosslinking, thus aiding in the normal formation of bone matrix [8]. Since burn injuries are associated with reduced bone formation and resorption in both adult and children [9], the copper ions may be expected to play a dual role in healing of burn injuries, i.e. preventing the wound from infection and helping in formation of bone matrix.

Experimental

Chitosan was covalently attached to oxidized cellulose fibers and these fibers were placed in Cu(II) ion solution. This lead to the formation of copper bound chitosan attached cellulose. Along with these some copper nanoparticle loaded chitosan attached cellulose fibers were also formed. The FTIR, TEM analysis, mechanical strength analysis of the treated fibers were done. Cu(II) ions release studies of Cu(II) ions loaded fibers were done. Antibacterial studies of fibers loaded with ions as well as nanoparticles were done on gram-negative bacteria *E.coli*..

Results and Discussion

Cellulose, with a large amount of hydroxyl groups, has been widely employed as a substrate for graft-copolymerization of vinyl monomers [10-11], and for the immobilization of macromolecules such as enzymes [12]. In the present study the covalent attachment of chitosan to the cellulose has been carried out by periodic acid induced oxidation of cellulose to dialdehyde followed by coupling reaction between amino group of chitosan and aldehyde

group of oxidized cellulose. The chitosan attached cellulose (CAC) fibers, so produced, were used to immobilize Cu(II) at nitrogen atom present in amine groups of chitosan chains. However, the binding of Cu(II) at oxygen atom of –OH groups of cellulose chains is also to be taken into consideration. In a novel work, Lee et al [13] suggested that-OH groups present in cellulose network in cotton fabric act as binding sites for immobilization of silver ions. Therefore, their observation may equally hold good in the present study also.

The result of the TEM analysis, as shown in the Fig. 1(A) clearly indicates that particles are almost monodisperse in nature. The almost uniform sizes of copper nanoparticles may probably be attributed to the fact that nitrogen atoms of $–NH_2$ groups of chitosan and O atoms of hydroxyl groups of cellulose act as binding sites for immobilization of Cu(II) ions. Hence, on reduction of copper(II) loaded CAC fibers these functionalities act as active sites for formation of copper nanaoparticles. We also carried out particle size distribution analysis, selecting copper nanoparticles from different arbitrarily chosen areas of TEM image (see Fig. 1(B)). On the basis of distribution curve the average diameter of the copper nanoparticles was found to be 28.9 nm.

Further, to confirm the formation of copper nano particles NCLCAC fibers, we carried out UV-Visible absorption studies. In Fig. 2, a strong characteristic absorption peak around 567 nm is noted for the copper nano particles in NCLCAC fibers due to the surface plasmon resonance effect. However Cu(II) bound CAC fiber did not show any such Peak.

The results of the mechanical strength (i.e. tensile strength) analysis has been well depicted in the Fig.3 . The tensile strength of Chitosan-attached cellulose (CAC), copper bound cotton-attached cellulose (CBCAC) and nano copper loaded chitosan attached cellulose (NCLCAC) fibers was found to be approximately 30.58, 59.77, 38.88 MPa respectively. It is quite clear that CBCAC fibers possess more tensile strength than plain CAC fibers which is obviously due to presence of Cu(II) ions that bind firmly with the N atoms of amino group of chitosan chains in CBCAC fibers. Thus, there is almost two-fold increase in tensile strength due to binding of Cu(II) ions. However, after carrying out borohydred-induced reduction of Cu(II) ions, the tensile strength of resulting NCLCAC fibers decrease to 38.88 MPa which may be attributed to the fact that due to reduction of Cu(II) to Cu^0, their binding with chitosan chains and with –OH group of cellulose networks decrease, thus resulting in less mechanical strength.

Dynamic release of Cu(II) from Copper bound chitosan attached cellulose (CBCAC) composite fibers were studied. The results of the release experiments carried out with copper loaded cellulose fibers i.e. CLC (4) and copper bound chitosan- attached cellulose fibers i.e.

CBCAC (4) fibers in the physiological fluid have been shown in the Fig. 4. It is quite clear that CBCAC (4) fibers demonstrate higher release as compared to CLC (4) fibers. The major driving force for the observed release from CBCAC (4) fibers in the physiological fluid (PF) is perhaps the 'ion-exchange process' taking place between Cu(II) ions bound with amino residue of chitosan chains and external Ca(II) ions present in the PF.

It is well known that Cu(II) ions demonstrate strong antibacterial action, either alone or in the form of complexes. We tested biocidal action of fibers by preparing two fibers, namely CBCAC (2) and CBCAC (4) where the number in parenthesis denotes the percent concentration (w/v) of copper solutions used for loading copper ions into fibers. The results of the antibacterial test have been shown in the Fig.5. It can be seen in the Fig. 11 that petridish containing bunch of plain fibers as control (see Fig. 5 (A)) shows dense population of bacterial colonies while petridishes, supplemented with fibers CBCAC (2) and CBCAC (4), as shown in the Fig.5(B), and 5(C) respectively, show zones of inhibition around the bunch of the fibers. It is also be noted that radius of inhibition zone increase with the increase in the copper content of loading solutions. The observed findings may simply be attributed to the biocidal action of Cu(II) ions that are released from the CBCAC fibers. In fact, as the copper content in the loading solutions increases, the amount bound to fibers also increases and therefore , the antibacterial action of resulting fibers becomes more effective, thus resulting in formation of 'zone of inhibition' with greater area (or radius).

Finally we also studied the antibacterial action of nanocopper loaded fibers, namely NCLCAC (2) and NCLCAC (4) against *E.Coli*, taking plain fibers as control. The results, as depicted in the Fig. 13, clearly indicate that petridish with plain fibers (see Fig. 13(A)) show dense population of bacterial colonies while petridishes, supplemented with nanocopper loaded fibers, NCLCAC (2) and NCLCAC (4) (see Fig. 6 (B) and (C) respectively) show less growth of colonies as indicated by a clear 'zone of inhibition' around the bunch of amount of copper nanoparticles present in the fibers which, in turn, depends upon concentration of Cu(II) solution used for copper loading.

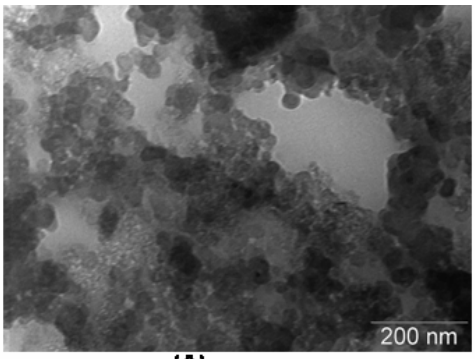

(A)

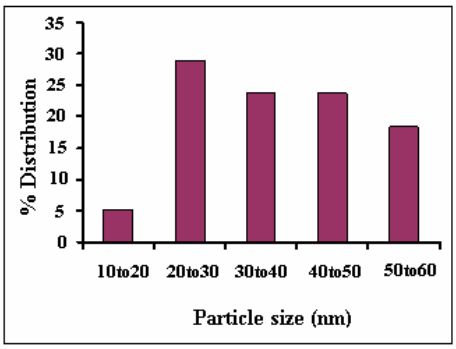

(B)

Fig1 (A) TEM image of copper nanoparticles (B) Size distribution graph of copper nanoparticles

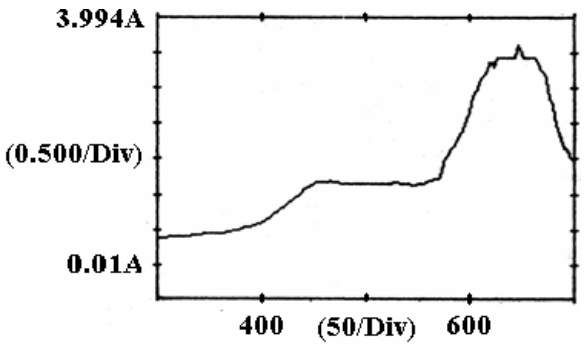

Fig.2. Surface plasmon resonance (SPR) of copper nanoparticles

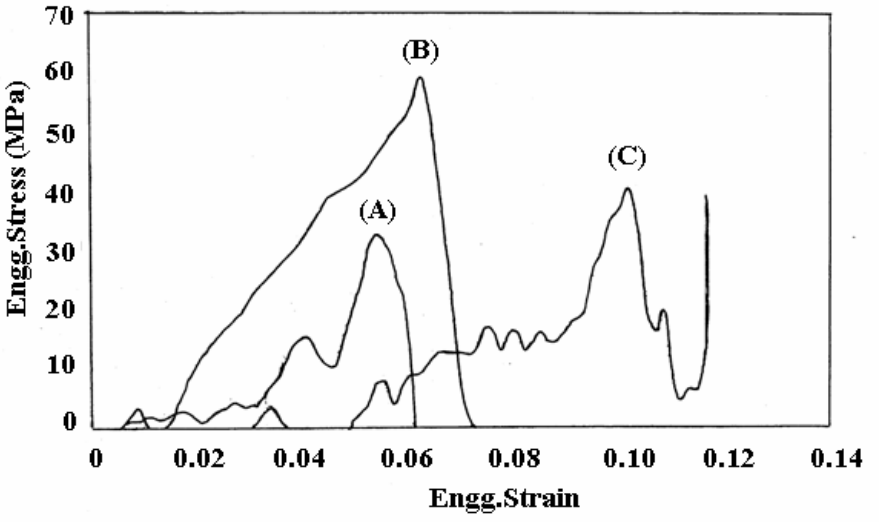

Fig.3. A comparative depiction of tensile strength of (A) chitosan attached cellulose (CAC) fibers, (B) copper bound chitosan attached cellulose (CBCAC) fibers, (C) nano copper loaded

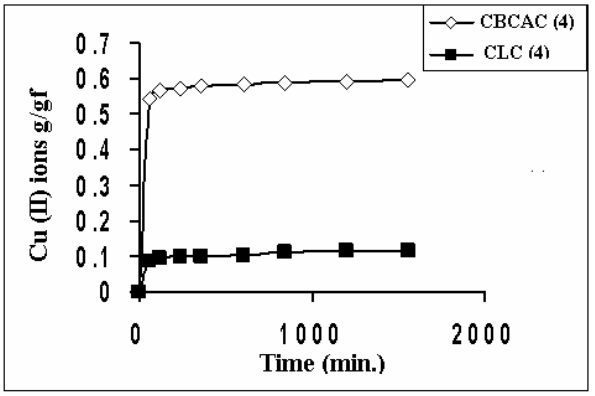

Fig.4. Dynamic release of Cu(II) ions from CBCAC (4) and CAC(4) fibers in physiological fluid at 37°C

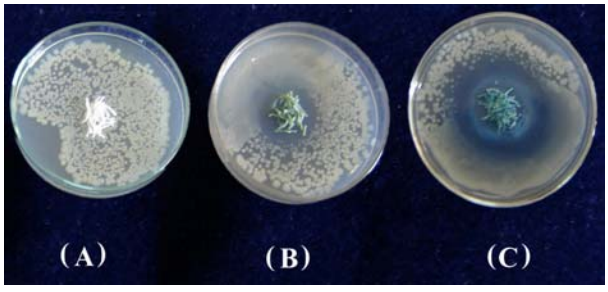

Fig.5. Biocidal action of (A) plain cellulose fibers (B) CBCAC (2), (C) CBCAC (4) fibers against E.coli as studied by zone inhibition

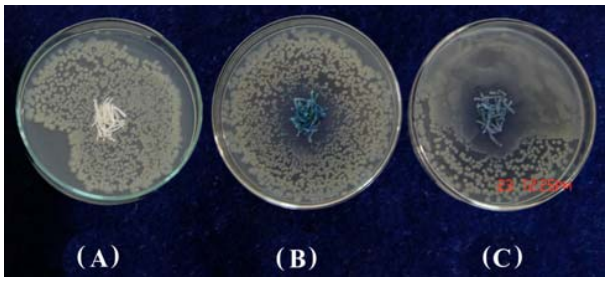

Fig.6. Bacterial growth in pertidishes supplemented with (A) plain fibers, (B) CBCAC (2) and (C) CBCAC (4).

Conclusion

From the above study it may be concluded that binding of copper(II) to chitosan-attached cellulose fibers results in formation of novel antibacterial fibers with fair Cu(II) releasing capacity and biocidal action. In addition, the borohydride-induced reduction of these fibers also yields copper nanoparticles-loaded fibers which also possess fair antibacterial property. These fibers have great potential to be used in burn/wound dressing and also in fabrication of antibacterial dressing.

References

1. Qin, Y. *Int Wound J* 2005, **2**,172.
2. Qin, Y.; Zhu, C.; Chen, J.; Liang, D.; Wo, G. *J Appl Polym Sci* 2007,**105**,527.
3. Hipler, U.; Elsner, P.; Fluhr, J. W. *J Biomed Mater Res Part B: Applied Biomaterials* 2005, **77B**,156.
4. Faundez, G.; Troncoso, M.; Navarrete, P.; Figueroa, G. *BMC Microbial* 2004, **4**, 19.
5. Zhang, W.; Zhang, Y.; Ji, J.; Yan, Q.; Huang, A.; Chu, P. K. *J Biomed Mater Res A* 2007,**83**,838.
6. Cioffi, N.; Ditaranto, N.; Torsi, L.; Picca, R. A.; Giglio, E. De.; Sabbatini, L.; Novello, L.; Tantillo, G.; Bleve-Zacheo, T.; Zambonin, P.G. *Anal Bioanal Chem* 2005,**382**,1912.
7. Cioffi, N.; Ditaranto, N.; Torsi, L.; Picca, R. A.; Giglio, E. De.; Sabbatini, L.; Novello, L.; Tantillo, G.; Bleve-Zacheo, T.; Zambonin, P.G. *Anal Bioanal Chem* 2005,**38**,607.
8. Tapeiro, H.; Townsend, D.M.; Tew, K. D. *Biomed Pharmacother* 2003, **57**,386.
9. Klein, G.L.; Herndon, D.N.; Longman, C.B.; Phillips, W.A.; Dikson, I.R . *Bone* 1995,**17**, 455.
10. Sabaa, M.W.; Makhtar, S.M. *Polymer Test* 2002, **21**,337.
11. Bajpai, S.K.; Bajpai, M.; Gupta, P.; ***J. Macromol. Sci., Pure & Appl. Chem.*** 2008, **45**,179.
12. Varavinit, S.; Chaokasem, N.; Shobsngob, S. *Science Asia* 2002, **289**, 247.
13. Lee, H.Y.; Park, H.K.; Lee, Y.M.; Kim, K.; Park, S.B. *Chem Commun* 2007,2959.

Gas permeability properties of metallocene polyolefin/ethylene vinyl acetate copolymer blends intended for medical applications

M. C. Sunny[1*], P. Ramesh[1] and K. E. George[2#]
[1]Sree Chitra Tirunal Institute for Medical Sciences and Technology
Biomedical Technology Wing, Poojapura, Thiruvananthapuram-695 012
[2] Department of Polymer Science and Rubber Technology,
Cochin University of Science and Technology, Kochi, Kerala- 682 022
Email: kegeorge@cusat.ac.in , mcsunny@sctimst.ac.in

Abstract:

The advances in metallocene catalysis technology have enabled the properties of polyolefins to meet specific end-use needs of some of the medical products such as blood/platelet bags, intravenous fluid containers and medical tubings. Because of its narrow molecular weight distribution, the processability of these types of polymers becomes difficult even though it gives the benefit of low extractable from the product while in use. In order to improve the processability and functional properties, these polymers are being used in blends with other conventional polyolefins. Blends of metallocene based ethylene-α-olefin copolymer (m-PO) with ethylene vinyl acetate copolymers (EVA) have been studied, with the purpose of exploring their properties and potential in medical film packaging applications. As gas permeability is one of the prime parameter of blood/platelet storage containers, an attempt has been made in this study, to understand the permeability properties of the blends. Melt-mixing of m-PO with EVA having different vinyl acetate content (12, 18 and 28%) were carried out in a torque rheometer and melt viscosities of the materials were evaluated from their respective torque values. The oxygen (O_2) and carbon dioxide (CO_2) permeability of the thin sheets of these blended materials having 0.3 mm thickness were studied at three different temperatures (10, 25 and 40^oC). The temperature dependence of the permeability of these gases was also evaluated. Gas permeability studies indicated that the permeability of both O_2 and CO_2 gases were less permeable through m-PO compared to its blends with EVA. It could be seen that an increasing trend in gas permeability with the increase of vinyl acetate content in the blend for both O_2 and CO_2 gases. It was further observed that the permeability of carbon dioxide was higher than that of oxygen in all the cases. The temperature dependence of the gas permeability was found to be in accordance with the Arrhenius expression.

1. Introduction

In modern blood banking system blood or blood components are collected and stored in plastic containers prior to patient transfusion [1]. Plasticised polyvinyl chloride (PVC) has been used in medical field since the 1950s for the collection and storage of blood and blood components. But, the use of PVC has been reduced considerably in recent years due to the growing public concern about the alleged toxicity of plasticizers and the emission of dioxin gas, an environmental pollutant, at the time of the post-use disposal by incineration [2]. Alternative materials such as thermoplastic polyurethane, silicone, ethylene vinyl acetate copolymer (EVA) and polyolefin were investigated in place of PVC [3]. Polyurethanes and silicones have their high cost against them while; EVA and polyolefin lack the performance properties of flexible PVC. With the advent of new generation single site catalyst –Metallocene- a new era in polymer synthesis has been initiated [4]. Since these catalysts have single site character, it can uniquely polymerize monomers to any given tacticity having fairly uniform and narrow distribution of chain lengths and uniform co-monomer content and branching [5]. Due to the narrow molecular weight distribution, the polyolefins produced using metallocene catalyst (m-POs), possess many features like improved hot tack, lower heat seal temperature, reduced leakage rates, improved packaging line speeds, improved toughness and puncture resistance, ability for down-gauging, higher stiffness, improved clarity and negligible quantity of extractables [6]. As metallocene polyolefins resemble plasticized PVC in many material properties and functions, they may have great potential as a prospective candidate for the replacement PVC in the medical field [7]. Since blending of polymers is an inexpensive route to the modification of polymer properties, blends have become a very important subject for

scientific investigation. In order to improve the processability and functional properties, metallocene polyolefins are being used in blends with other conventional polyolefins.

During storage, the blood components, by their metabolic activity, convert glucose, present in the anticoagulant, to lactic acid (anaerobic metabolism) and carbon dioxide (CO_2) (aerobic metabolism) [8]. The CO_2 thus produced lowers the pH, which in turn adversely affects the survival of the blood components. However, the presence of O_2 suppresses the conversion of glucose to lactic acid and CO_2. So, for the extended viability of the living blood components and for extended storage times the exchange of oxygen and carbon dioxide ie. the gas permeability is essential for the materials used for the blood component storage application purposes.

2. Experimental

2.1 Materials

Polyolefin copolymer containing 9.5wt% octane (Affinity Polyolefin Plastomer PL 1845) polymerized by metallocene single site constrained geometry catalyst was obtained from Dow Plastics, Dow Chemical Company, Midland. Three grades of EVA copolymer with different vinyl acetate content i.e., 12, 18 and 28wt% (EVA12, EVA18 and EVA28) were procured from National Organic Chemicals India Limited, Mumbai, India.

2.2mPO/EVA blends

Blends of m-PO with three grades EVA having different vinyl acetate contents (composition, grades and designations are as given in the table-1) were prepared by melt mixing in Brabender plastograph fitted with cam type rotors at 160^{o}C and 40rpm. The mixing was allowed for 6 minutes till the torque stabilized to a constant value. The compound obtained from the mixer was then passed through a laboratory two-roll mill set at 1.1mm-nip setting to get the material in the sheet form.

The apparent viscosity of the molten mass was calculated from the torque data generated from the mixer by the use of the following equations.

$$\eta = \left(\frac{2\Gamma}{\pi L \left(R_e + R_i\right)^2 \left(1 + g^{n+1}\right)\dot{\gamma}} \right) \quad \text{----------(1)}$$

Here, Γ is the torque on the rotors, L is the length of the rotor, Re is the effective radius (i.e. distance from the center of the rotor to the wall of the mixer), Ri is the radius of the rotor, g is the rotor ratio and $\dot{\gamma}$ is the shear rate. Since the rotors used in this study have the same rate, g = 1 and the $(1+g^{n+1})$ term in the above equation equals two and cancels the two in the numerator, leaving an expression based only on the geometry and physical parameters of the mixer. For a given rotor and mixer configuration, L, Re, and Ri are constants. Hence the equation-1 could be simplified to equation-2

$$\eta = \frac{\Gamma}{\dot{\gamma}} \quad \text{---------- (2)}$$

$\dot{\gamma}$ is equivalent to the rotor speed in rad s^{-1}.

2.3 Preparation of 0.3mm thick sheets

Sheets of 0.3mm thickness were prepared by compression moulding of the melt mixed samples in a stainless steel mould having the dimensions 120mm x 120mm x 0.3mm at 170^{o}C for 3 minutes at a pressure of 50 kg/cm^2 in an electrically heated press (Santhosh Industries, India).

2.4 Gas Permeability Studies

The gas permeability measurements were made using samples having 110 x 110 mm^2 size and 0.3 mm thickness. The samples were preconditioned according to ASTM D618-96(8). The gas permeability measurements were carried out using oxygen and carbon dioxide in a manometric gas permeability tester (Model L-100, 2402/1, Switzerland) at three different temperatures (10, 25 and 40^{o}C) as per ASTM D1434-98 (9).

3. Results and discussion

The mixing curves (torques vs. time) of m-PO, three grades of EVA and its blends are shown in figures 1 and 2. The curve displays an initial increase, which is due to the loading of the material, subsequent decrease and finally stabilization of the mixing torque. The high loading peak for m-PO may be due to the narrow molecular weight distribution. A stabilized level had been reached within 2 minutes of mixing in all cases and there was not much deviation from the stabilized level in the torque during the entire period of 6 minutes mixing. This indicates the stability of the material during mixing at 160^{o}C. The stabilized torque value for m-PO was found to be more or less similar to that of EVA12 and slightly less than that of its blend (AE1225). Similar trend was seen in the case of m-PO and its blend with EVA12. As the torque value indicates the energy demand for processing of the material, m-PO, EVA12 and its blend need higher energy for mixing than the other two grades EVA and their blends. Apparent viscosities of samples are tabulated in the Table 2. The viscosity values indicate that the melt viscosity of m-PO is slightly lower than that of EVA12. This indicates that the processibility of m-PO is comparatively similar to that of EVA12.

The results of oxygen and carbon dioxide permeabilities of m-PO, AE1225, AE1825 and AE2825, at three different temperatures (10, 25, 40^{o}C) are as shown in figure 3 and figure 4 respectively. The blending of m-PO with EVA found to increase the permeabilities of both gas. The increase was in the increasing order of vinyl acetate content in EVA (EVA12<EVA18<EVA28). Same trend was seen in all the three temperatures tested. Plots of ln P versus 1/T for O_2 and CO_2 permeabilities of the samples at 10, 25 and 40^{o}C are shown in figures (5 and 6), respectively. A linear relationship is obtained in the temperature range of 10-40^{o}C for m-PO and its blends with all three grades of EVA. This indicates that the Arrhenius expression governs the temperature dependence of permeability.

The ratios of carbon dioxide to oxygen permeabilities of the samples at three different temperatures are given in the table-3. The ratio of carbon dioxide to oxygen permeabilities found to be high in blends which indicated the preferential permeability of CO_2 in the blends. The ratio of carbon dioxide to oxygen permeabilities of the material used for blood or blood component storage application is an important factor. Higher value of this ratio indicates the high permeability of CO_2 which in turn avoid its dissolution and subsequent pH drop of the fluid stored in. An increased permeability of carbon dioxide is very much favoured for the improved viability and long storage life of the blood components. In the ratio of carbon dioxide to oxygen permeability point of view, the blend containing EVA 12 and EVA18 found to be more favourable candidates for blood/ blood component storage application purposes.

4. Conclusions

In this investigation, the mixing torque, melt viscosity and gas permeability of m-PO and its blends with three different grades of EVA were evaluated. The mixing torque and melt viscosity indicated that the energy requirement for processing AE1225 blend was slightly higher than that of the virgin m-PO and other two blends. Blending of m-PO with EVA (all the three grades) was found to increase the permeability of both carbon dioxide and oxygen gases and the increase was more prominent at higher temperatures. The temperature dependence of gas permeability was confirmed by the linear relationship of permeability and temperature in the Arrhenius expression. The carbon dioxide to oxygen permeability ratio indicated the favourable candidature of the blends, AE1225 and AE1825 as the materials for blood/blood component storage applications.

5. References

1. Hong KZ, Journal of Vinyl & Additive Technology, 1996, Vol.2, No.3, 193-197.
2. De Groot, Hendrik , Vervoort, Freddy Maria Armand United States Patent 6846535, 2005.
3. Shah T., Medical Device & Diagnostic Industry, Sept.2002, 24, 9: 62–68.
4. Thayer A.M., Chemical & Engineering News, September 11, 1995
5. Kaminsky, Macromol. Chem. Phys., 1996, 197, 3907-3945.
6. Mukhopadhyay D., Popular Plastics & Packaging, March 1998, 51.
7. Lipsitt B., Proce. Soci.of Plast. Eng. Annual Technical Conference, Toronto, May 1997, 2854.

8. Szabo E., Elcik R., Gelfand D., U. S. Patent US 2004/0146671A1.

Table 1 Percentage composition of blends

Blend designations	Volume percentage composition of			
	m-PO	EVA12	EVA18	EVA28
AE1225	75	25	-	-
AE1825	75	-	25	-
AE2825	75	-	-	25

Table 2 Mixing torque and melt viscosities of the samples

Sample	Mixing Torque at 5minutes	Melt viscosity (Nm.s/2π)
m-PO	8.96	2.14
AE1225	9.27	2.21
AE1825	7.31	1.75
AE2825	5.76	1.38

Table 3 Ratios of carbon dioxide to oxygen permeabilities of the samples at three different temperatures.

Blends	Ratio of CO_2/O_2		
	10°C	25°C	40°C
m-PO	2.78	3.45	3.23
AE1225	4.31	4.56	4.04
AE1825	4.12	4.11	4.02
AE2825	4.26	3.90	3.81

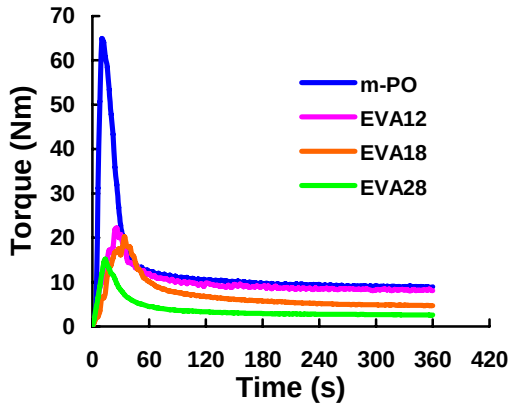

Figure1 Mixing torques of m-PO and three grades of EVA

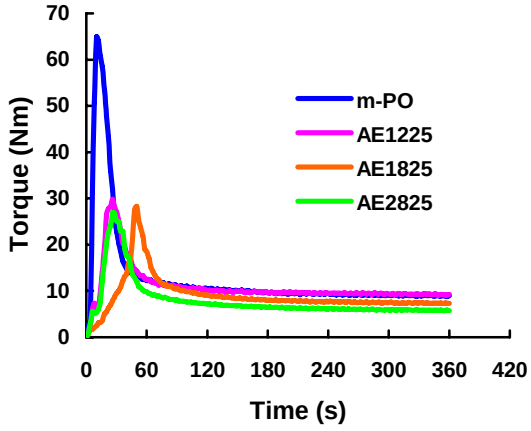

Figure 2 Mixing torques of m-PO and its blend with EVA

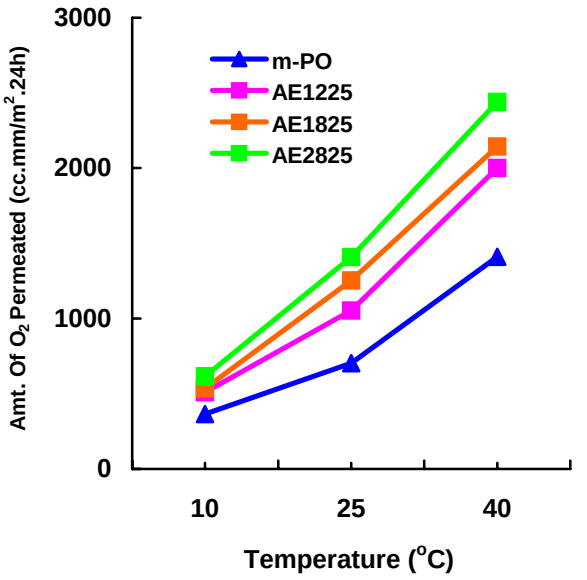

Figure 3 Amount of oxygen permeated through the samples at three different temperatures (10, 25, 40°C)

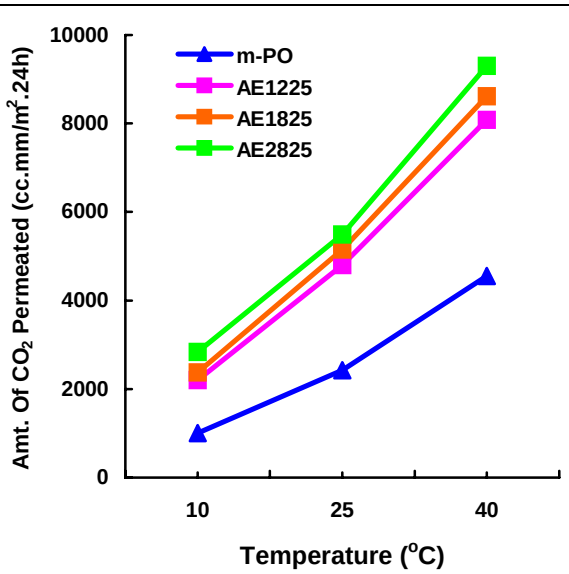

Figure 4 Amount of carbon dioxide permeated through the samples at three different temperatures (10, 25, 40°C)

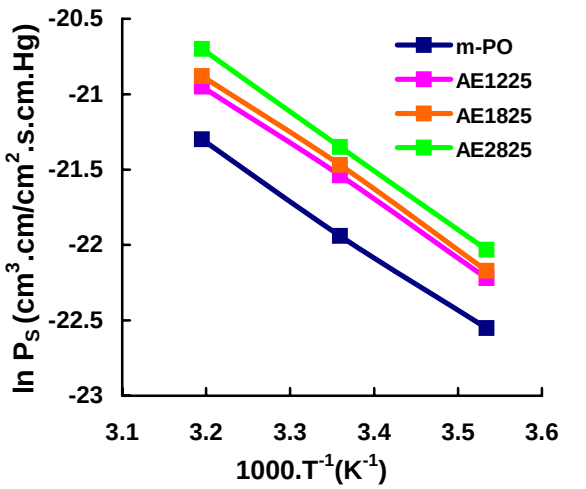

Figure 5 Temperature dependence of oxygen permeability of m-PO and blends at three different temperatures (10, 25, 40°C)

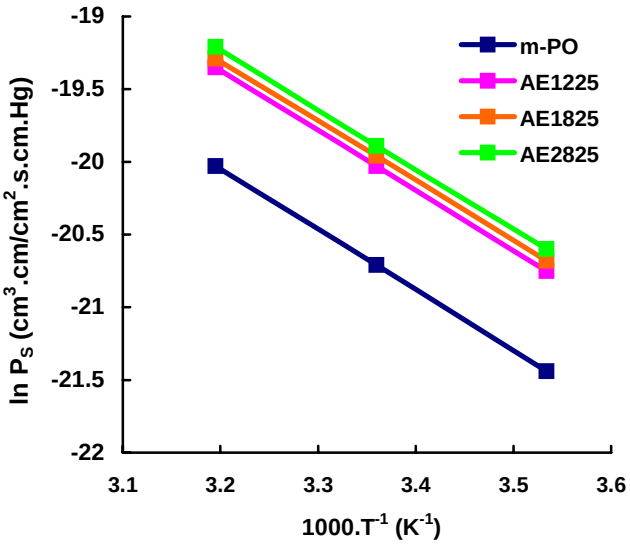

Figure 6 Temperature dependence of Carbon dioxide permeability of m-PO and blends at three different temperatures (10, 25, 40°C)

Effect of low temperature prevulcanisation on the colloidal and mechanical properties of natural rubber latex

*Devi.P.V[1], #Shiny Palaty[1],Honey John[2] and Rani Joseph[3]

1Department of Chemistry, Bharata Mata College, Thrikkakara, Kerala, India
2Department of Applied Sciences, Indian Institute of Space Science and Technology, ISRO, Thiruvananthapuram 695 022, India
3Department of Polymer Science and Rubber Technology, CUSAT, Kochi, Kerala, India

Email: shpalaty@gmail.com

Abstract*:* Sulphur prevulcanisation of Natural Rubber Latex(NRL) was conducted at low temperature(30^0C) using zinc butyl xanthate[$Zn(bxt)_2$]– zinc diethyl dithiocarbamate[ZDC] accelerator combination. $Zn(bxt)_2$ was prepared in the laboratory. The optimization of prevulcanisation time and the amount of accelerators used for prevulcanisation were done. Films were casted from this compounded latex and their crosslink density and tensile properties were determined. Effect of thermal ageing on mechanical properties of these latex films was investigated. After thermal ageing, tensile properties and cross link density of low temperature prevulcanised latex films were improved. The morphology of the tensile fracture surface of these latex films before and after thermal ageing was monitored using scanning electron microscopy (SEM). The low temperature prevulcanised latex was stored for 30 days and the colloidal properties were measured at different storage intervals. These colloidal properties were compared with that of high temperature prevulcanised latex using ZDC alone. The mechanical stability time (MST) was increased during storage. Both mechanical and colloidal properties were found to be superior for low temperature prevulcanised latex.

Keywords: Prevulcanisation, zinc butyl xanthate, swell index and colloidal properties.

Introduction

Prevulcanisation is an important process in latex goods manufacturing industry. It is the process of vulcanization in the latex stage. In prevulcanisation individual particles in the rubber latex were vulcanized without destroying the colloidal character of the latex as a stable hydrophobic sol.(1) It is the period for which the compounded latex is stored after mixing prior to use in the production line.(2) Prevulcanisation can be effected by the reaction with sulphur, sulphur donors, peroxides or radiation.(3) Prevulcanised latex eliminates the need for further compounding by the product manufacturer and requires less energy for drying.(1) Vulcanisation temperature is very important in determining the quality of the rubber products. Optimum properties are obtained when curing is done at the lowest possible temperature. Several studies were reported on the effect of temperature, vulcanization time and storage on sulphur prevulcanised NRL.(4) This paper reports the effect of low temperature vulcanization on the colloidal and mechanical properties of NRL.

Experimental

(1)Equipments used:-The equipments used in this study include a Universal Tensile Testing Machine Model 1445(M/s Instron , Buckingshire,UK), Scanning electron microscope JEOL JSM-840 model-6211(Oxford, England), Brookfield LVT Viscometer(Brookfield Engineering Laboratories, MA), Mechanical stability apparatus(Klaxon Signals, England).

(2) Materials used:- Commercial high ammonia centrifuged NRL conforming to the BIS 5430-1981 was used for prevulcanisation. The compounding ingredients were commercial grade. Chloroform and toluene were reagent grade and were used as supplied.

(3)Experimental procedure:- $Zn(bxt)_2$ was prepared in the laboratory.(5) 50% dispersions of the vulcanizing agents were prepared using a ball mill. NRL was deammoniated to 0.2% before compounding

to avoid ZnO thickening. NRL is compounded as per the formulations given in Table 1. After compounding, the latex mixes were allowed to mature at room temperature for 24 hours. Compound A was prevulcanised by heating to (55-60)^{0}C for three hours. Chloroform test of the compounded latices (A-D) were done at an interval of one day for 5 days and the chloroform numbers are reported in Figure 1. Latex films were then casted in glass cells according to ASTM D 1076-88 from these latex mixes at 30^{0}C.

Equilibrium swelling test, apparent cross link density, chemical crosslink density and tensile property measurements of the latex films were done at an interval of one day for 5 days to determine the time for prevulcanisation. The equilibrium swelling values were determined by immersing a thin film of rubber latex in toluene for 24 hours at room temperature and measuring the increase in weight. The equilibrium swell index was calculated as: - Swell index (Q) = $(W_2-W_1)/W_1$, where W_1 is the initial weight and W_2 is the swollen weight. The results are given in Figure 2. The total chemical crosslink density was also determined by equilibrium swelling method using Flory Rehner equation [6] and the results are given in Figure2. Dumb bell and crescent shaped tensile and tear specimens were punched out of the casted films. Stress-strain measurements were carried out at a crosshead speed of 500mm/min on a UTM. Tensile and tear strengths were measured according to ASTM D 412-87(method A) and ASTM D 624-86 respectively. The results are reported in Figures 5,9-12. Effect of thermal ageing at 70^{0}C for 24 hours on crosslink density and tensile properties of prevulcanised latex films were studied as per ASTM D 865-88 and are reported in Table 2. The colloidal properties of the prevulcanised latex were determined after 5 days, 10 days and 30 days of storage and the results are given in Table 3.

Result and Discussion

Figure 1 shows the variation of $CHCl_3$ number of the compounds A to D with prevulcanisation time. From the Figure 1 it is evident that prevulcanisation of NRL can be done at 30^{0}C using $Zn(bxt)_2$/ ZDC accelerator combination. Positive synergistic effect of xanthate /ZDC accelerator combination on the cure rate and mechanical properties of NBR compounds and carbon balck filled NR compounds has been already reported.[7,8] For compound B, the chloroform number becomes 3(moderately vulcanized) after 5 days. But for compounds C and D, the chloroform number becomes 4(fully vulcanized) after 5 days. So $CHCl_3$ number studies reveals that the optimum time needed for the prevulcanisation of NRL at 30^{0}C is 5 days. The increase in $CHCl_3$ number with time is due to the increase in crosslinking between the rubber chains (as evident from Figure 4). As temperature is lowered crosslinking occurs very slowly.[3] When 1.5phr ZDC/1.5 phr $Zn(bxt)_2$ accelerator concentration is used(compound C),optimum prevulcanisation time is 5 days. When the total accelerator concentration is increased to 4 phr (compound D), there is no change in the $CHCl_3$ number. So 1.5 phr ZDC/1.5 phr $Zn(bxt)_2$ is taken as the optimum accelerator dosage needed for prevulcanisation. Prevulcanisation of latex mix containing ZDC alone is done at (55-60)^{0}C by heating the latex compound for 3 hours. In this case, the $CHCl_3$ number becomes 3 after one day and the prevulcanisation is completed after 2 days as represented by the $CHCl_3$ number 4.

Figure 2 shows the variation of swell index with prevulcanisation time of different latex mixes. Swell index can be used as an indicator for the formation of crosslinks. The extends to which the sample swells, is an inverse measure of the degree of vulcanization. As prevulcanisation time increases swell index decreases due to increase in crosslinking of rubber molecules. For compound A, swell index reaches a minimum steady value after 2 days, indicating complete prevulcanisation. But for compounds B to D, swell index decreases with time and reaches a minimum value after 5 days. The reciprocal of swelling ratio, 1/Q, was reported as the apparent crosslink density in Figure 3. Apparent crosslink density increases with prevulcanisation time. Compound A attains maximum apparent crosslink density after 2 days. Compound C and D attain the same value after 5 days. Figure 4 shows the variation of total chemical crosslink density with prevulcanisation time for different latex mixes. As prevulcanisation time increases chemical crosslink density increases. After 5 days sample C shows maximum crosslink density. This is due to the lower degradation of rubber chains because of the non-application of temperature.

Figure 5 shows the variation of tensile strength with prevulcanisation time for the latex mixes A to D. From Figure 5, it is evident that as prevulcanisation time progresses, tensile strength increases because crosslinking increases with prevulcanisation. The time taken for attaining maximum

tensile strength is taken as the optimum cure time. Compound A attains maximum tensile strength after 2 days, indicating complete prevulcanisation. For compounds B to D, maximum tensile strength is obtained after 5 days and thereafter tensile strength of samples remains almost constant. So tensile studies also suggest that the prevulcanisation time of NRL at 30^0C is 5 days. When prevulcanisation is complete, tensile strength is maximum for compound C compared to B and D. This confirms that the optimum accelerator concentration required is 1.5 phr ZDC / 1.5 phr $Zn(bxt)_2$.

The tensile strength of prevulcanised latex is governed not only by the introduction of cross-links but also by the ability of particles to coalesce among themselves. The tensile strength of films prepared using room temperature prevulcanised latex is high compared to high temperature prevulcanised latex films. The increase in tensile strength may be a consequence of increasing ability of latex particles to coalesce and integrate when the film dries at lower temperatures.[1] The higher crosslink density of C compared to A is also due to the lower degradation of rubber at low temperatures. The stability of the accelerator is also high at low temperature. This is further confirmed by the SEM studies. Figure 6 to 8 are the SEM photographs of the tensile fracture surface of the films prepared using compounds A, C and commercially available prevulcanised latex respectively. Figure 6 shows the presence of microcoagulums formed in compound A during heating. This suggests that the colloidal stability of the latex is slightly disturbed during prevulcanisation at higher temperature. Figure 7 shows that there is more bonding interaction between rubber matrix and vulcanisating agents when prevulcanisation is done at 30^0C. It also shows that the vulcanization is uniform throughout the latex compared to high temperature prevulcanised latex (Figure 6) and commercially available prevulcanised latex (Figure 8).

Variation of modulus (100% & 300%), elongation at break (%) and tear strength values with prevulcanisation time are given in Figures 9,10,11and 12 respectively. From the above figures it is clear that as prevulcanisation time increases modulus and tear strength values increases and elongation at break values decrease for compounds B to D. When the rubber particles are lightly crosslinked, the coalescence of particles is better causing a higher elongation. Compound C attains minimum elongation at break, maximum modulus and maximum tensile strength after 5 days. From chloroform number test, swell index, chemical crosslink density values and tensile strength values, it is understood that optimum prevulcanisation time of NRL at 30^0C using $Zn(bxt)_2$/ZDC accelerator combination is 5 days. After 5 days, compound C attains more tear strength compared to Compound A. The tearing energy of NR latex film was found to decrease as the temperature of vulcanization was increased which might be attributed to lower concentration of polysulphidic type of crosslinks at high vulcanization temperature than that produced at low temperature vulcanization.

Table 2 shows the effect of thermal ageing at 70^0C for 24 hours on tensile properties of casted films from different latex mixes.In the case of vulcanisate A, tensile strength and tear strength decreases after ageing. This may be due to the degradation of rubber molecular chains at high temperature which results in decrease of crosslink density. Sulphur linkages, especially polysulphides, are dissociated by heating and these bring about a decrease of the crosslink density. But in the case of vulcanisates B to D, tensile strength increases after ageing. This may be due to the increase in crosslink density. The increased crosslinking after the thermal ageing can be explained with the formations of new crosslinks by free curative residues such as elemental sulphur, cure accelerator residues and zinc complexes remained in the vulcanisate. Especially, free sulphur remained in the vulcanisate reacts well with rubber chains and makes new crosslinks. A pendent sulfide group terminated by an accelerator residue reacts with another pendent group of the neighbouring rubber chains, so a new crosslink will be formed.[9] Sample C exhibits maximum tensile strength and tear strength after ageing. The SEM photograph of the tensile fracture surface of compound C after ageing shows the presence of more crosslinks compared to the same film before ageing(Figure 13). The roughness of tensile fracture surface may be considered as an indication of the energy consumed during fracture of the material.[10]

The physical and colloidal properties of the prevulcanised latex were evaluated at different storage intervals and these properties were compared with that of high ammonia centrifuged unvulcanised latex, high temperature prevulcanised latex(compound A) . The results were reported in Table 3. The properties of sulphur prevulcanised NRL may undergo changes during storage

of because of the presence of surface-active agents and residual vulcanizing ingredients.[4] The colloidal stability of prevulcanised latex depends on many factors such as the nature of the latex, amount of potassium hydroxide and carboxylate soap, dosage of vulcanizing ingredients and prevulcanisation conditions such as time and temperature. The colloidal stability is affected by two opposing factors. The presence of residual vulcanizing ingredients such as ZnO may reduce the stability of latex because of ZnO thickening. At the same time the addition of alkalies and carboxylate soaps can increase the stability by increasing the negative charge on the surface of the particles and by increasing surface adsorption.[4]

From Table 3 it is clear that DRC, TSC, non rubber solids and coagulum content of latex prevulcanised at 30^0C remains almost constant during storage for 30 days and is comparable to high temperature prevulcanised latex. VFA number and KOH number increase on storage but they do not exceed the acceptable limit for the concentrated latex industry. During storage, the bacterial degradation of latex constituents causes the formation of short chain fatty acids with the resultant decrease in the pH value of the latex and a corresponding increase in VFA number. Increase in KOH number indicates an increase in the concentration of acids which are present as ammonium salts. On storage ammonia present in the latex, alkali and potassium soap added during compounding slowly hydrolyze the proteins and phospholipids to fatty acid anions and other products. The liberated fatty acid anions are adsorbed at the particle interfaces and thus enhance the stability of latex due to a higher surface charge and therefore a higher repulsive energy between particles. This accounts for the increase in MST on storage.[11] The increase in Brookfield viscosity during storage is due to ZnO thickening of latex and also due to the slow liberation of Zn ions from the accelerator ZDC present.[1]

Conclusions

(1)$Zn(bxt)_2$-ZDC accelerator combination can bring about prevulcanisation of NRL at 30^0C and optimum prevulcanisation time is 5 days. (2)The amount of $Zn(bxt)_2$ and ZDC required for the prevulcanisation is optimized as 1.5 phr each of $Zn(bxt)_2$ and ZDC. (3)The tensile properties were found to be better for the low temperature prevulcanised latex compared with that of high temperature (55-60^0 C) prevulcanised latex using ZDC alone. (4)Tensile properties of films prepared from low temperature prevulcanised latex is improved after ageing but that of prevulcanised latex prepared by heating decreases. (5)On storage, MST of low temperature prevulcanised latex increases. These findings would be of significant technological importance to the rubber dipped goods manufacturing industry providing a means for effecting better product quality control and improvement.

Acknowledgment

The authors would like to acknowledge KSCSTE and the University Grants Commission for the financial support.

References

1. K.K.Sasidharan, Shiny Palaty, K.S. Gopalakrishnan, K.E. George, Rani Joseph, Room Temperature Prevulcanisation of Natural Rubber Latex Using Xanthate, Journal of Applied Polymer Science, (2004),Vol.94,1164-1174.

2. C.C.Ho and M.C.Khew, Surface Morphology of Prevulcanised Natural Rubber latex Films by Atomic Force Microscopy: New Insight into the Prevulcanisation Mechanism, Langmuir, (1999), 15, 6208-6219.

3. N.M.Claramma, N.M.Mathew, (1997), Effect of Temperature on Sulphur Prevulcanisation of Natural Rubber Latex, John Wiley & Sons,Inc .J.Appl Polym Sci, (1997), 65:1913-1920.

4. K.K.Sasidharan, Rani Joseph, Shiny Palaty, K.S. Gopalakrishnan, G.Rajammal, Effect of the vulcanization Time and Storage on the Stability and Physical Properties of Sulphur-Prevulcanised Natural Rubber Latex, Journal of Applied Polymer Science,(2005),Vol.97,5,1804-1811.

5. Rani Joseph, and Shiny Palaty, Xanthate Accelerators for Low Temperature Curing of Natural Rubber, Journal of Applied Polymer Science,(2000), Vol.78, 1769-1775.

6. P.J.Florey and J.Rehner, J.Chem.Phys., (1943), 11,512.

7. Shiny Palaty,Rani Joseph, Low Temperature Curing of NBR for Property Improvement, J. of Elastomers and Plastics, (2006), Vol.38, p.199-209.

8. Shiny Palaty and Rani Joseph, Synergism of Xanthate/Dithiocarbamate Accelerator in Carbon Black Filled NR Compounds, Iranian Polymer Journal, (2004), 13(2), 85-91.

9. Sung-Seen Choi,Sung-Ho Ha, and Chang-Su Woo, Thermal Ageing Behaviours of Rubber Vulcanisates Cured with Single and Binary Cure Systems,Bull.Korean Chem.Soc., (2006),Vol.27,No.3,429.

10.P.Thavamani and D.Khastgir, Physical, Mechanical and Thermal Degradation Properties of Ethylene Vinyl Acetate and Hydrogenated Nitrile Rubber Blends, Journal of Elastomers and Plastics, (1997), Vol.29,p.124-147.
10. N.M.Claramma,L.Varghese and N.M.Mathew, Influence of Storage on Properties of Natural Rubber Latex Concentrate and Vulcanizates, Indian Journal of Natural Rubber Research, (1995), 8(1),p.1-7.

Tables and Figures:

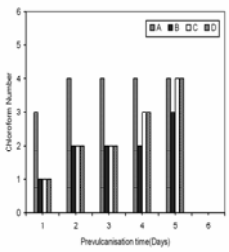

FIGURE 1: Variation of chloroform number with prevulcanisation time of different latex mixes.

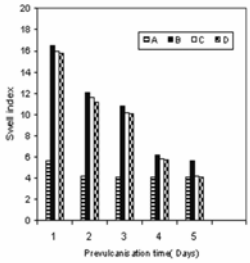

FIGURE 2: Variation of swell index with prevulcanisation time for different latex mixes

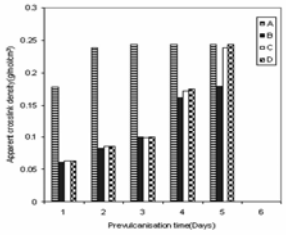

FIGURE 3. Variation of apparent cross link density with prevulcanisation time for different latex mixes

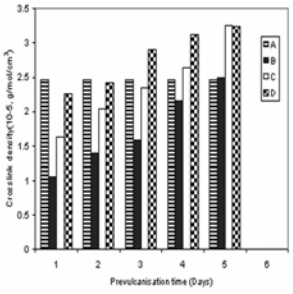

FIGURE 4: Variation of crosslink density with prevulcanisation time for different latex mixes

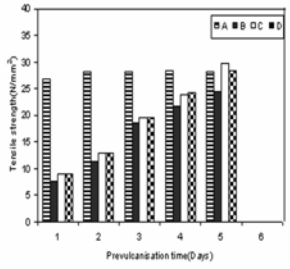

FIGURE 5: Variation of tensile strength with prevulcanisation time for different latex mixes.

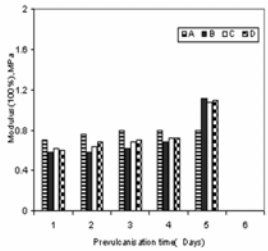

FIGURE 9: Variation of Modulus(100%) with prevulcanisation time for different latex mixes.

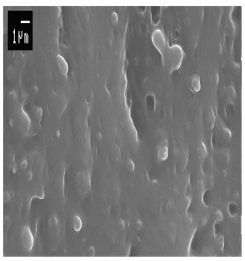

FIGURE 7: SEM photograph of tensile fracture surface of room temperature prevulcanised NR latex film containing Zn(but)$_2$-ZDC accelerator combination

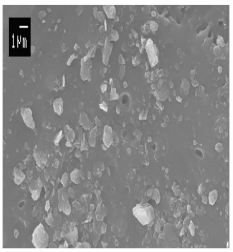

FIGURE 8: SEM photograph of tensile fracture surface of commercially available prevulcanised NR latex film

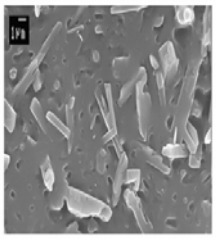

FIGURE 6 SEM photograph of tensile fracture surface of prevulcanised NR latex film containing ZDC alone.

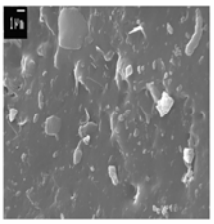

FIGURE 13: SEM photograph of tensile fracture surface of room temperature prevulcanised NR latex film containing Zn(but)$_2$-ZDC accelerator combination after thermal ageing at 70°C for 24 hours.

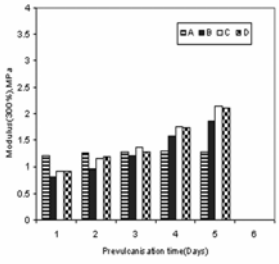

FIGURE 10: Variation of Modulus(300%) with prevulcanisation time for different latex mixes.

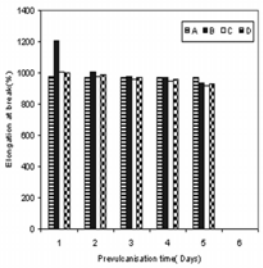

FIGURE 11: Variation of Elongation at break (%) with prevulcanisation time for different latex mixes.

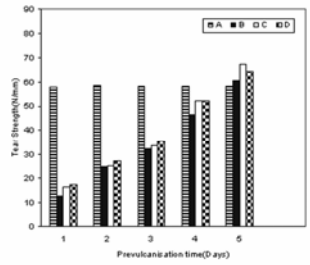

FIGURE 12: Variation of Tear Strength (N/mm) with prevulcanisation time for different latex mixes.

Table 1:.Formulation of latex mixes

Ingredients	Parts by weight(gms)			
	A	B	C	D
NR latex	167	167	167	167
10% KOH	1.5	1.5	1.5	1.5
10% potassium oleate	0.75	0.75	0.75	0.75
10%Vulcastabe VL	1.0	1.0	1.0	1.0
50% S	2.5	2.5	2.5	2.5
50% ZDC	1.5	1.0	1.5	2.0
50% ZnO	1.0	1.0	1.0	1.0
50% $Zn(bxt)_2$	-	1.0	1.5	2.0

Table 2: Effect of thermal ageing at 70^0C for 24 hours on tensile properties of casted films from different latex mixes.

Properties	A		B		C		D	
	Before ageing	After ageing	Before ageing	After ageing	Before ageing	After ageing	Before ageing	After ageing
Tensile strength(N/mm^2)	28.2	26.14	24.36	25.36	29.62	30.62	28.34	28.10
Modulus (100%), MPa	0.80	0.86	1.12	1.14	1.08	1.22	1.10	1.18
Modulus(300%), MPa	1.28	1.32	1.86	1.92	2.14	2.16	2.10	2.08
Elongation at break (%)	970	960	940	910	920	890	930	900
Tear strength (N/mm)	58.46	56.92	60.52	60.96	67.56	69.12	64.36	63.56
Cross link density (10^{-5}, $g/mol/cm^3$)	2.463	2.365	2.49	3.77	3.26	4.68	3.24	4.37

Table 3: Properties of centrifuged and prevulcanised latex

Properties	Centrifuged latex	Compound A	Compound C		
			After 5 days	After 10 days	After 1 month
Dry rubber content (mass %)	59	59.8	58.9	59.1	59.2
Total solid content (mass %)	60	60.8	60.1	60.3	60.1
Non rubber solids (mass %)	1.0	1.0	1.2	1.2	0.9
Ammonia content (mass %)	0.86	0.51	0.52	0..4	0.4
Potassium hydroxide number	0.35	0.35	0.375	0.386	0.392
Mechanical stability time(s)	990	586	820	865	870
Brookfield viscosity(cps)	90	50	83	83	85
Volatile fatty acid number	0.02	0.03	0.03	0.04	0.06
Coagulum content (mass %)	0.01	0.01	0.013	0.013	0.014
P^H	9.89	9.98	9.93	9.85	9.52

Modification of carbon black filled natural rubber using novolac resins

Bhuvaneswary. M .G* and Eby Thomas Thachil[#]

[#]Department of Polymer Science and Rubber Technology, Cochin University of Science and Technology, Kochi - 682022, Kerala, India.

*Department of Chemistry,S.N.M. College, Maliankara - 683516, Kerala, India

Email: ethachil@cusat.ac.in, bhuvana@cusat.ac.in

Abstract

This work investigates the effect of addition of novolac resins of varying phenol: formaldehyde ratios into carbon black filled NR compounds. The cure characteristics and mechanical properties of the compounds were studied. Results indicate that the cure time increases with increasing resin content. Similarly the maximum torque and viscous torque exhibit an increasing trend. Novolac resins, in general, are seen to improve the tensile modulus and tear strength of the rubber but the tensile strength and elongation at break decrease slightly. There is, in addition, an improvement in oil resistance and thermal ageing resistance of carbon black filled NR by the incorporation of novolac resins. The resins for the study were synthesized in the laboratory at various P/F ratios. Extraction studies prove that the resin is inextractable from the rubber. Summing up, the presence of the resin has addressed to a considerable extent the limitations of NR, namely poor age and oil resistance.

1. Introduction

Natural rubber (NR) is a low cost material with excellent physical properties such as good resilience, high tensile strength, superior resistance to tear and abrasion, excellent tack and self adhesion. However it has very poor resistance to ageing in the presence of air, ozone, fuels and oils[1]. These limitations restrict its use in high temperature applications and hydrocarbon environment. Rubbers are reinforced with fillers to improve mechanical properties. Carbon black and silica are the most important fillers in the rubber industry.

Properties of NR can also be modified by the addition of different polymeric resins[2-4]. Foremost among these are phenolics. Phenolic resins were the first polymeric resins produced commercially from simple low molecular weight compounds. They are mainly used for moulding, bonding, surface coating, adhesive and laminating applications[5]. British Resin Products Limited has developed a range of synthetic phenolic resins to reinforce both synthetic and natural rubbers[6]. Giller, Chow and Steiner reported that phenolic resin (novolac types) and hexamine, when incorporated into the rubber, cure in the normal way during vulcanization to increase the hardness of vulcanizates[7]. Addition of phenolic resin has also been found to provide superior resistance to abrasion and heat as well as improved tackiness for the gum compounds. The service life of sulfur cured vulcanizates at elevated temperature can be extended by using phenol-formaldehyde resins[8-10]. These resins can give very thermally stable crosslinks.

In this study, the effect of novolac resin on the cure characteristics and mechanical properties of carbon black filled natural rubber vulcanizate are examined.

2. Experimental

2.1 Raw materials

Phenol, formaldehyde, sodium hydroxide and oxalic acid (LR grade) were supplied by Loba Chemie, Mumbai, India. Hexamethylene tetramine was supplied by Laboratory and Industrial Chemicals, Cochin and was industrial grade. Natural rubber (ISNR5) was obtained from Rubber

Research Institute of India, Kottayam. Zinc oxide was obtained by M/s Meta Zinc Limited, Mumbai. Stearic acid was supplied by Godrej Soaps Pvt Ltd, Mumbai. HAF black was supplied by M/s Philips Carbon Black India Ltd Cochon, India. Mercapto benzo thiazol sulphenamide (MBTS) was supplied by Bayer Chemicals, Mumbai. Tetramethyl thiuram monosulphide (TMT) was obtained from Polyolefine Industries, Mumbai. Sulphur was supplied by Standard Chemicals Co. Pvt. Ltd. Chennai.

2.2 Preparation of novolacs

The novolacs were prepared by reacting phenol with formaldehyde in the molar ratio 1:0.5 in the presence of oxalic acid catalyst in a 3-necked flask fitted with a mechanical stirrer, water condenser and thermometer. The reaction mixture was heated to 100^{o}C and allowed to reflux for 2-3 hours. When the resin separated from the aqueous phase the reaction was stopped. The resin was neutralized with sodium hydroxide, filtered, washed with water and vacuum dried. Novolac resin containing phenol and formaldehyde in two other ratios viz 1:0.7 and 1:0.9 were also prepared.

2.3 Compounding and testing

NR, ZnO, stearic acid, novolac resin, HAF, MBTS, TMT and S were mixed on a two roll mill according to ASTM D 3184-89(2001). The resin content varied from 0 to 8%. The formulations of the mixes are given in Table 1.

Cure characteristics of the mixes were determined at 150^{o}C using Rubber Processing Analyser RPA. Vulcanization to optimum cure time was then carried out in an electrically heated hydraulic press at 150^{o}C **.**The moldings were cooled quickly in water at end of the curing cycle and stored in a cool dark place for 24 hours prior to physical testing.

Tensile properties (ASTM D 412) and tear strength (ASTM D 624) were measured using Shimadzu Universal Testing Machine (10 kN) with a grip separation of 40mm, at a crosshead speed of 500mm/min. The hardness of the sample (Shore A) was determined using Zwick 3114 hardness tester according to ASTM D-2240

3. Results and discussion

The effects of novolac resin on the cure characteristics and mechanical properties of HAF black filled NR vulcanizates are shown in Table 2. Fig.1 shows the variation of cure time with resin content. Cure time of the compounds increases with resin content. As the resin content increases, the curatives may get diluted by the resin and its effective concentration may decrease. Consequently, the time required for the optimum cure increases. Scorch time of the compound is found to decrease with resin content. This is due to the heat of mixing resulting in the premature curing of the compound. Variation of CRI with resin content is shown in Fig. 2. Cure rate index indicates that the reaction progresses slowly with increase in resin content. As the resin content increases the volume fraction of the rubber decreases. Hence, the rate of cure reaction, which depends on the concentration of the rubber phase, decreases with increase in resin content.

Fig.3 indicates the variation of maximum torque with resin content. Maximum torque value is found to increase with resin content. These values are a reflection of the resin polymer interaction which leads to stiffening of the rubber matrix.

Some mechanical properties of the vulcanizates improved after the addition of resin. Tear strength, modulus and hardness were increased with resin content. Some interpenetration between the rubber and phenolic resin may be the reason for this.

4. Conclusion

The cure characteristics such as cure time, minimum torque, and maximum torque increase with the addition of novolac resin, where as the scorch time decreases gradually. There is improvement in tear strength, modulus and hardness on addition of novolac resin.

Reference:

1. 1. Abhimanuo O. Patil, Thomas S. Coolbaugh : *Rubber Chemistry and* T*echnology*,2005, **78**, 525-526
2. A. R. R. Menon, C. K. S. Pillai and G. B. Nando : *J. Appl. Polym. Sci*, 1998, **68**, 1303-1311.
3. R. A. Rajapaske, W. A. S. Gunasena and K. B Wijekoon : *Polymer*, 1978, **20**, 887
4. S. D. Shinkle, patent No. US 2648613.
5. J. A. Brydson *: Plastic Materials*, 4th edn, 568;1982, Butterworth Scientific publishing.
6. *Cellobond Rubber Reinforcing Resins*, Technical Manual No. 11, 1959
7. V. Nigam, D.K. Setua, G.N. Mathur: J. Materials science, 2001, 36, 43-47.
8. J. C. Sarer : *Rubber Age*, 1947, **62**, 191.
9. R. P. Latimer, R, A. Kinsey and R. W. Layer : *Rubber Chem. Technol.* 1982, **62**, 107.
10. M. Morton *: Rubber Technology*, Chapman & Hall, 1995.

Table1. NR formulation for varying resin content

Ingredients	**Content (phr)**
NR	100
Zinc oxide	4
Stearic acid	2
HAF	30
MBTS	0.8
TMT	0.2
S	2.5
Resin	0 - 8

Table 2. Effects of resin on the cure characteristics and mechanical properties of filled NR vulcanizate

Properties		**Novolac 0.5**				**Novolac 0.7**				**Novolac 0.9**			
	0	**2**	**4**	**6**	**8**	**2**	**4**	**6**	**8**	**2**	**4**	**6**	**8**
Scorch time (min)	2.23	1.76	1.57	1.40	1.39	1.89	1.63	1.68	1.61	1.75	1.49	1.42	1.44
Cure time (min)	3.77	3.78	3.81	3.96	4.96	3.90	3.91	4.64	5.77	3.57	3.91	4.92	6.72
CRI	64.9	49.5	44.6	39.1	28.0	49.7	43.8	33.8	24.0	54.9	41.3	28.5	18.9
Max.Torque (dNm)	4.26	4.35	4.39	4.49	4.54	4.53	4.89	4.91	5.14	4.67	5.06	5.11	5.23
Tensile strength(MPa)	30.8	32.5	30.3	29.8	28.4	30.5	31.6	28.8	28.6	30.8	30.9	29.7	29.1
EB(%)	888	895	887	846	803	811	811	792	771	825	837	776	771
300%Modulus (MPa)	4.91	5.59	5.93	6.3	7.14	6.29	6.36	6.49	6.64	5.8	6.37	6.42	6.85
Tear strength(N/mm)	76.5	84.8	88.2	92.8	77.3	93.5	90.8	79.1	65.9	85.1	86.2	86.3	82.8
Hardness (ShoreA)	55	56	58	59	61	57	58	60	61	61	62	61	63

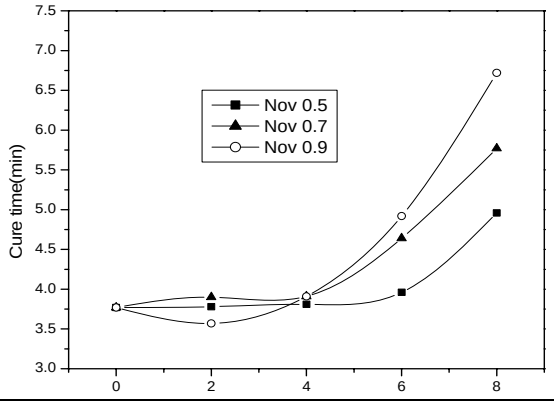

Fig.1 Variation of cure time with resin

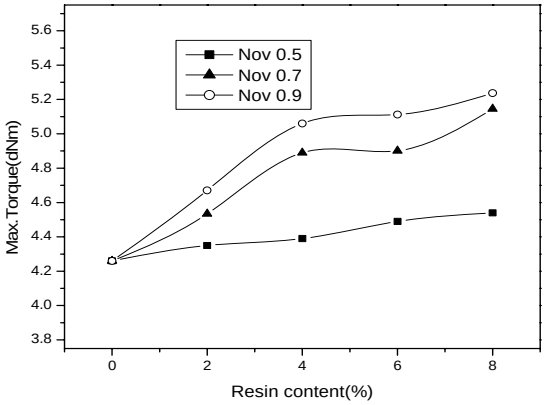

Fig.2 Variation of max.Torque

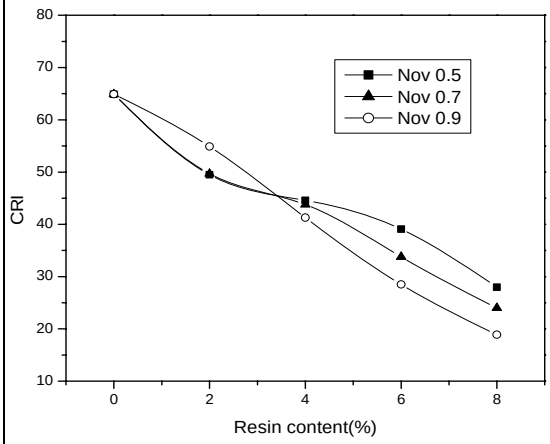

Fig.3 Variation of CRI with resin

Carbon Black Master Batch from Fresh Natural Rubber Latex

K. K. Sasidharan[a], Rosamma Alex[a] and Thomas Kurian[b]

[a] Rubber Research Institute of India., Kottayam-686009, India
[b] Department of Polymer Science and Rubber Technology, Cochin University of Science and Technology, Kochi-682 022, India

Email: rosammaalex2000@yahoo.com

ABSTRACT

A new process for production of carbon black master batches with enhanced mechanical properties has been developed. The unit operations in the process are the preparation of carbon black slurry, addition of the slurry to the fresh natural rubber latex under stirring, coagulation of the mixture by the addition of acid in presence of a suitable surfactant, dewatering of the coagulum, and drying. The competence of the new technique was established by comparing the coagulation behaviour of the mixture with the carbon black slurry–fresh natural rubber latex mixture containing no surfactant (control). Conventional compounds of the control and the surfactant incorporated master batches containing various loading of the filler were prepared and the mechanical properties of the vulcanizates were evaluated. The effect of ageing on the mechanical properties is also discussed. Carbon black filled mixes prepared by the new process show better cure characteristics as compared to the conventionally produced carbon black master batch (control). The mechanical properties like tensile strength, modulus, tear strength and hardness are superior for the vulcanizates prepared by the new method. Comparatively better ageing resistance was also recorded by these vulcanizates. The improvement shown by the vulcanizates prepared by the new process is attributed to better filler dispersion evident from the result of the scanning electron micrograph (SEM) studies.

INTRODUCTION

The level of dispersion of carbon black in a rubber matrix is an important issue in a large variety of rubber products(1). Filler dispersion is generally influenced by the point of incorporation of filler along with other factors like the nature of rubber, and presence of plasticizers (2). In the case of carbon black there are issues such as air pollution and higher energy consumption when incorporated in dry rubber. Production of rubber latex-carbon black master batch by the addition of carbon black as a slurry has been suggested as one of the methods to avoid some of these problems. Generally a high Mooney viscosity is recorded by carbon black master batches which

can be reduced by addition of chemical additives during the master batching process (3,4). The main drawback with this technique is the long mixing and coagulation time(5). There has been no systematic study on the production of carbon black master batches using fresh natural rubber latex. It has been reported that the coagulation time of latex is reduced by addition of suitable surfactants .When carbon black incorporated latex is coagulated quickly by addition of acids it is excepted that carbon black is uniformly distributed in rubber matrix as compared to conventional coagulation methods where the coagulation time is high.

EXPERIMENTAL

Fresh natural rubber latex used in the study was obtained from the Rubber Research Institute of India, Kottayam. Fluffy carbon black samples, high abrasion furnace black (N330) was obtained from M/s Phillips Carbon Black Limited Kochi, India. Other ingredients used were rubber grade chemicals. The surfactant used was based on alkali salts of fatty acid

Preparation of carbon black master batches by quick coagulation method.

A slurry of fluffy carbon black was prepared by finely dispersing carbon black in water mechanically in presence of a suitable surfactant. The slurry was added slowly in to fresh natural rubber latex under stirring and coagulated by addition of acid. The coagulaum was washed well to remove the acid and dried in an air oven. Carbon black was incorporated in latex so as to have levels of 5-40 parts per hundred parts of dry rubber(phr). The dried rubber was mixed as per formulation given Table1, and vulcanized by conventional methods. A control master batch with a loading of 30 phr carbon black without surfactants, was also prepared.

Vulcanization Characteristics, Mechanical Properties and SEM evaluation.

The cure behaviour was determined using moving die rheometer Monsanto(MDR2000) at 150ºC. The Mechanical properties were determined from relevant ASTM standards (Tensile Properties ASTM D412-92, Heat Build up ASTM D623-93, Abrasion Resistance ASTM D5963-96, Hardness ASTM D2240-95, Compression Set ASTM D395-89,Resilience ASTM D2632-92, Tear Strength ASTM D624-98) The ageing tests were carried out according to ASTM D573, after ageing at 100ºC 3 days.

Filler dispersion in rubber was assessed by using a Hitachi Scanning Electrone Microscope (model 2400). Tensile fracture surface of vulcanizates was coated with gold to carryout SEM study.

Results & Discussion

Coagulation Characteristics

Carbon black slurry-fresh latex mixture containing surfactant was coagulated immediately on addition of acid, while the control compound coagulated slowly in about one hour. On addition of fatty acid soaps to latex they cause displacement of protein and get strongly adsorbed on rubber particles. In this way the protein stabilized latex gets transformed into a soap stabilized system. On addition of acids to soap treated latex the adsorbed soap anions react with acid to form un-dissociated fatty acid, and deprive the latex particles of stabilizers. As a consequence, latex coagulates immediately (6,7,8)

Vulcanization Characteristics

The cure characteristics of the carbon black master batches prepared using surfactant (NR5, NR 10, NR20, NR 30, NR40) in comparison with carbon black master batch without surfactant (* NR30) are given in Table 2. The master batches from quick coagulation showed a higher levels of vulcanization and lower optimum cure times as compared to carbon black master batches prepared by conventional sheet preparation method. When surfactant (fatty acid soap) is added to latex it disperses uniformly in latex due to adsorption on rubber particles. During coagulation the surfactant gets converted into the corresponding fatty acid. This helps in better vulcanization characterists of rubber as fatty acids are activators of vulcanization(9)..

Mechanical Properties

The vulcanizates prepared from carbon black master batches by the new method showed higher tensile strength and a higher modulus, along with higher hardness resilience and tear strength. The compression set abrasion loss and heat build up were found to be lower (Table 3). The mechanical properties obtained after ageing the samples are given in Table 4 . The enhancement in mechanical properties and ageing behaviour is attributed due the better filler dispersion along with higher level of cross linking (10).

Scanning Electron Micrograph images studies.

Scanning Electron Microscopy is being widely used to characterize the filler distribution and dispersion characteristics (11,12,13). More information on filler dispersion is obtained from SEM images of tensile fracture surface, shown in fig. (1). The vulcanizates obtained using new method has more uniform surface, as compared to vulcanizates prepared by conventional methods. From SEM images it can be seen that carbon black master batches using new method exhibit better distribution. It is expected that fatty acid obtained from the surfactant act as plasticiser and help in better filler dispersion (14).

CONCLUSION

A uniformly mixed carbon black slurry and latex in presence of suitable surfactant coagulates quickly an addition of acids. The carbon black master batch prepared by this method shows enhanced cure characteristic, filler dispersion and superior mechanical properties as compared to conventionally prepared carbon black master batches.

Reference:

1. Brendan Rodgers. (2004) Rubber Compounding Chemistry and Application. Marcel Dekker, Inc. New York P 240-257.
2. Shukri Bion Abdul Wahab, KPNG. Kamarul Baharain BVibn Basir and WP Chang (1978) Natural Rubber Carbon Black Masterbatches from Field Latex, Proceedings of NR Technology Seminar, 4-5 December. P 29-41
3. MJ Wang, Billerica Massachusets (USA). (2005) New Development in Carbon black dispersion KGK P – 631
4. Zainul Abdin Bin Maidunny, Mohd Raffali Bin Mohd Nor,Sidek Bin Dulngali,Sharif Bin Othman and Wan Idris BinWanYaacob.(1984) J. Rubb. Res. Inst. Malaysia 32(2) P 103-118
5. Werner Hofmann (1989) Rubber Technologist's Hand Book Chapter 5, Hanser Publishers, New York. P 143
6. Van gils, G.E (1947) Transaction of Instution of Rubber Industries, 23, 74-76
7. Alex R,Premalatha,CK.Nair and Kurikose,B.(2003).Journal of Rubber Research,6(4): P 221-230.

8. Blackley DC,(1997),Polymer Latices, Science and Technology, Vol.2 Types of lattices Chapter 9 Chapman & Hall, UK, Second Edition.
9. Franta, I. (1989), Elastomers and Rubber Compounding Materials Manufacture Properties and Apploications. Elsiever Publications, Chapter 6.
10. A Wesley, Wampler, Tharas F Canson and William R Jones (2005). Carbon Black, Sid Richardson Carbon Company, Farthwark Texas, USA P 239
11. Yu-chun Ou, Zhang-Zhhen Yu, A Vidal and J.B. Donnet (1994), Rubber Chem.Technol., 67, 834
12. J.Wen and J.E. Mark (1994) Rubber Chem. Technol., 67, 806
13. A. Voet, Morawski and J.B.Donnet (1997), Rubber Chem Technol., 50, 342
14. John S. Dick (2001) Rubber Technbology, Hanser Publishers, Munich P. 310

Table No.1

Standard Formulation

Ingredient	*NR30	NR0	NR5	NR10	NR20	NR30	NR40
NR1	130	100	105	110	120	130	140
ZnO	5	5	5	5	5	5	5
Stearic Acid	2	2	2	2	2	2	2
A/o HS	1	1	1	1	1	1	1
CBS	0.75	0.75	0.75	0.75	0.75	0.75	0.75
Sulphur	2.5	2.5	2.5	2.5	2.5	2.5	2.5
*NR 30 : Natural rubber carbon black mix without surfactant, NR1: The weight of rubber includes the weight of carbon black (NR5-5 phr, NR10 -10 phr, NR20-20 phr, NR30 – 30 phr and NR 40-40phr)							

Table. 2

Cure characteristics of Carbon black Mixes

Parameters	*NR30	NR0	NR5	NR10	NR20	NR30	NR40
Torque Min, dNm	1.18	0.65	0.88	0.95	1.01	0.56	1.09
Torque Max,dNm	10.82	6.80	7.15	8.46	9.84	12.30	12.48
Optimum curetime t90(min)	10.05	6.23	8.29	7.22	8.14	9.5	10.23

Table No. 3

Mechanical Properties of Carbon black master batch Vulcanizates

Parameters	*NR30	NR0	NR5	NR10	NR20	NR30	NR40
Modulus 100%(Mpa)	1.54	0.95	1.15	1.22	1.34	1.63	1.50
Modulus 300%(MPa)	4.75	1.78	2.47	2.76	3.46	5.89	4.79
Elongation at break (%)	625	690	745	742	640	690	619
Tensile Strength (MPa)	26.42	21.80	24.30	26.07	26.28	28.08	25.53
Hardness (Shore A	50	40	44	46	47	56	52
Compression set (%)	38	12.5	30	32	33	35	38
Heat buildup (ºC)	24	7	12	16	17	20	24
Abrasion loss(mm^3/hr)	17	68	152	142	131	109	115
Resilience (%)	75	85	83	82	80	76	70
Tear strength kN/m	57.0	17.23	28.97	43.80	52.40	58.50	58

Table 4

Mechanical Properties of Carbon black master batch Vulcanizates (After ageing 100 ° C (3 days)

Parameters	*NR30	NR0	NR5	NR10	NR20	NR30	NR40
Modulus 100%(Mpa)	1.50	0.90	1.14	1.30	1.44	1.64	1.58
Modulus 300%(MPa)	4.45	1.68	2.58	2.80	3.46	4.75	6.79
Elongation at break (%)	600	685	730	700	630	620	607
Tensile strength (MPa)	25.35	20.8	23.49	24.80	25.53	25.91	23.43
Heat buildup (ºC)	7.0	4.0	5.0	5.0	4.0	7.0	12.00
Abrasion loss(mm^3/hr)	332	166	154	140	155	148.00	149.00

Fig. 1.

SEM IMAGES OF CARBON BLACK MASTERBATCH VULCUNIZATES

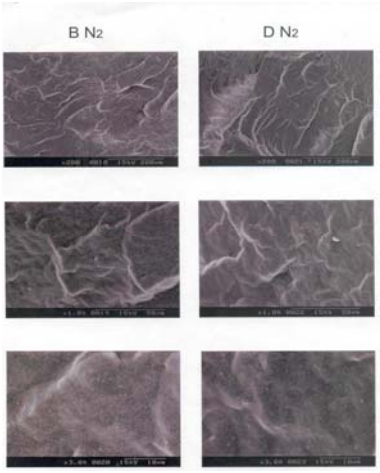

(BN_2 & DN_2 photomicrographs under three different magnifications of NR 30 & *NR30 samples)

Mechanical properties and transport behaviour of chitin whiskers (CW) reinforced carboxylated styrene butadiene rubber latex (XSBR) nanocomposites

Visakh. P .M[1], Anu Tresa Sunny[1], S. Thomas[1] and Aji. P. Mathew[2]

[1]School of Chemical Sciences, Mahatma Gandhi University, Kottayam, Kerala, India
[2]Division of Manufacturing and Design of Wood and Bionanocomposites,
Luleå University of Technology, SE-93187 Skellefteå, Sweden

Email: sabut@sancharnet.in, sabut552001@yahoo.com

Abstract

Nanocomposites were successfully prepared using a colloidal suspension of chitin whiskers (CW) as reinforcement in carboxylated styrene butadiene rubber latex (XSBR) by water evaporation method. The chitin whiskers were prepared from commercial crab shell chitin powder by acid hydrolysis. Atomic force microscopy (AFM) was carried out to see the size and structure of chitin nanowhiskers and scanning electron microscopy (SEM) and atomic force microscopy (AFM) were used to study the nanocomposite morphology. The mechanical properties of nanocomposites like tensile strength, tear strength, tensile modulus and elongation at break were measured. Transport parameters such as diffusion coefficient, sorption coefficient and permeation coefficient were also calculated from water diffusion studies and all of them showed a decrease with filler loading. The result indicates that there exist a strong interaction between chitin whiskers and XSBR latex by the hydrogen bonding. The properties of the nanocomposites were strongly affected by the concentration of chitin whiskers in the rubber matrix. This has been explained on basis of the network formation of chitin whisker in XSBR latex.

Keywords
Nanochitin whisker, nanocomposites, tensile properties, diffusion, morphology

e-mail: visagam143@yahoo.co.in, anutresa@gmail.com, sabut552001@yahoo.com, aji.mathew@ltu.se

*Corresponding author: Prof. (Dr.) Sabu Thomas, School of Chemical Sciences, Mahatma Gandhi University, Priyadarsini Hills P.O., Kottayam-686560, Kerala, India
Phone: +91-481-2730003, 2731036, Fax: +91-481-2731002
Email: sabut@sancharnet.in and sabut552001@yahoo.com

1. Introduction

Chitin is polymer that is present all around us, in plant and animal creature and can be found in anything from the shells of beetles to web of spiders. It is the second most abundant biopolymer in nature after cellulose [1]. Chitin and cellulose are molecular similar polysaccharide compounds, cellulose contains a hydroxyl group, and chitin contains acetamide group. It is glucose based branched polysaccharide. Chitin is highly crystalline and depending on its origin it occurs in three forms identified as α, β, and χ chitin. Chitin is natural, non-toxic, non-allergenic, anti-microbial and biodegradable it is insoluble in water and resistant to acid, alkalis, and many organic solvents [2]. Chitin has found applications in many areas other than food such as in biosensors [3]. Main development of chitin film and fiber is in medical and pharmaceutical applications as wound-dressing material [4,5] and controlled drug release [6,7]. Chitin has

versatile biological activity, excellent biocompatibility and complete biodegradability in combination with low toxicity α-chitin is by the most abundant than other [8]. Chitin is high molecular weight linear polysaccharide, specifically β-(1 to 4) (N-acetyl -D- glucosamine). Chitin has been known to form microfibrillar arrangements embedded in a protein matrix and these microfibrils have diameters ranging from 2.5 to 2.8 nm [9]. Crustacean cuticles possess chitin microfibrils with diameters as large as 25 nm [10,11]. The chitin- protein fibers are arranged in horizontal planes forming a typical twisted plywood structure or Bouligand pattern. Chitin can easily be isolated from crab shell, when it is found to be highly thixotropic and liquid crystalline [12,13]. Dufresne and coworkers has successfully isolated the crystalline regions of chitin named whiskers from the crab shells and squid pens by hydrochloric acid hydrolysis [14,15]. It was reported earlier that the reinforcing effect strongly depends on the aspect ratio of the chitin whiskers [14-18].

Whiskers are very promising reinforcing materials for the polymer composites and polymer nanocomposites because of their high stiffness and strength [19]. Owing to their small diameter, whiskers are nearly free of internal defects, thereby yielding strength close to the maximum. The reinforcing effect of the chitin whiskers strongly depended on their ability to form a rigid three-dimensional network, which result from strong interactions such as hydrogen bonds between the whiskers [14,15,17].

Biopolymer based nanocomposites are relatively a new class of nanomaterials and owns a unique place in nanocomposite research owing to the biodegradability, biocompatibility and the environmental friendliness of these materials [20,21]. Utilization of biobased nanoreinforcements was found to improve the water vapor permeability, mechanical properties and thermal stability without affecting the transparency of the biopolymers to a great extend. [14,15,22]

In these nanocomposites the reinforcement of the XSBR latex with chitin whiskers (CW) combines the elastic behavior of the XSBR rubber with the high strength and stiffness of the chitin whiskers. The processing, morphology, mechanical properties and transport behavior of these nanocomposites are presented in this paper.

2. Experimental section

Materials

α-Chitin powder was supplied by Marine Chemicals, Cochin, Kerala, India. Carboxylated styrene butadiene rubber latex (XSBR) was supplied by Apar Industries Ltd., Bombay, Maharashtra, India. The basic characteristics of latex are given in Table 1. Other materials are 3N hydrochloric acid (HCl), 5% potassium hydroxide (KOH) solution, sodium hypochlorite (NaClO2) solution for bleaching and 3N sodium acetate buffer were procured from local chemical suppliers.

Table 1. Characteristics of Carboxylated Styrene Butadiene Rubber latex

	Carboxylated Styrene Butadiene Rubber latex (XSBR)
Supplier	Apar Industries Ltd., Bombay, India.
Dry rubber content (DRC)%	47
Total solid content (TSC) %	50.66
Styrene content (%)	59
pH	8.60
Mechanical stability	Good

Deproteinisation of the Chitin

The chitin powder was first stirred and boiled with 5-wt % aqueous KOH solution for 6 h. Then, the specimens were rinsed with distilled water and filtered. Recently Domard et al [23] have reported that concentration of sodium hydroxide concentration depended on the nanostructure of chitin whiskers. Following this treatment, chitin samples were bleached with 17 g of $NaClO_2$ in 1 L of distilled water mixed with 27 g of NaOH in 75 ml of acetic acid completed with 925 ml of distilled water. The suspension was heated at 80 °C for 2 h under stirring; this procedure was repeated three times.

Preparation of Nanochitin whiskers

The chitin whisker suspensions were prepared by hydrolyzing the purified chitin sample with 3 N HCl at the boil under stirring for 1.5 h. After acid hydrolysis the suspensions were dialyzed for 2 h in distilled water and then overnight in running water. An additional dialysis by dialysis bag for 12 h by changing the distilled water every 2 h was performed until a pH = 6 was reached. The dispersion of whiskers was completed by three successive Ultrasonic treatments [24] for 2 min each for every 40 ml. The concentration of the chitin whisker suspension was 2.88g

Preparation of Nanocomposites

The XSBR latex was used as matrix and the chitin suspension was introduced in to the latex and stirred for 2 hours, casted in Petri dishes .The solid nanocomposite films were obtained by evaporating the water by drying in an oven at 40 ^{0}C. In all these concentration, volume fraction of the XSBR latex was kept constant. Composites were prepared by changing the volume fraction of chitin whiskers suspension from 10 to 90 vol% which corresponded to 0.72 to 6.48 wt%. The weight percentage and volume percentage of the XSBR and chitin whiskers are given in the Table 2. The compositions of the nanocomposites are referred to in terms of volume percentages, throughout the text, for convenience. The pure XSBR matrix is also prepared and used as the control.

Table 2. Composition of chitin whisker and XSBR latex for the preparation of chitin.whisker/ XSBR latex nanocomposites

Amount of XSBR latex (V %) (ml)	Chitin content (V %) (ml)	Chitin content (Wt %) (g)
100	10	0.72
100	20	1.44
100	30	2.16
100	40	2.88
100	50	3.6
100	60	4.32
100	70	5.04
100	80	5.76
100	90	6.48

3. Characterization

Microscopy

The fractured surfaces of the nanocomposite films were studied in JEOL, JSM-5200 Scanning Electron Microscope (SEM). The films were fractured under liquid nitrogen and sputter-coated with gold. The films were observed in the SEM at an acceleration voltage of 25kV. 30% CW, 50% CW, 70% CW were used for this analysis.

The chitin whiskers, as well as the nanocomposites, were characterized using a Veeco MultiMode scanning probe microscope with a Nanoscope V controller. For the analysis of chitin, a droplet of the aqueous whisker suspension (0.5% by weight) was dried on a mica surface prior to AFM examination. The nanocomposite films were microtomed using a diamond knife after embedding in epoxy resin and were analyzed directly. The images for the whiskers and the nanocomposites were collected using a tapping mode etched silicon tip, with a nominal spring constant of 5 N/m and a nominal frequency of 270 kHz.

Mechanical property measurements.

The tensile strength and tear strength were performed with Universal Testing Machine (UTM) (Cochin University of Science and Technology (CUSAT) Kerala, India) using dumb bell-shaped samples obtained by the evaporation of chitin whisker and carboxylated styrene butadiene rubber latex nanocomposites. The measurements were conducted at a crosshead speed of 500 mm/min with 4 cm intergrip distance. More than five samples were tested and average values were reported. The mechanical behaviour of the chitin whisker/XSBR nanocomposites films was analyzed at room temperature. 40% CW, 60% CW, 80% CW were used for the mechanical studies.

Diffusion experiments

Circular samples of 2 cm diameter were cut from polymer sheets by means of a standard die. The thickness and initial weight of the samples were taken. The thickness of the samples was in the range 1.5–2 mm. The experimental procedure was continued until the equilibrium swelling was attained. The samples were removed at specific intervals (t) and weighed (W_t) up to an equilibrium value (W_∞). The swelling rates of the samples were calculated by dividing the gain in weight (W_t-W_0) by the initial weight (W_0) 30% CW, 50% CW, 70% CW were used for the diffusion experiments.

Solvent uptake at equilibrium $Q_t(\%) = (W_t - W_0)/ W_0 \times 100$

W_t - Weight of sample at time (1h, 2h...)

W_0 - Weight of sample at zero time

W_ω . - Weight of sample at infinite time.

4 Result and discussion.

Biobased whiskers are very promising reinforcing materials for developing polymer nanocomposites because of their high stiffness and strength [19]. The fiber-fiber interaction through hydrogen bonding generates a stiff fiber net work in the matrix phase during the process of evaporation. In the chitin whiskers reinforced XSBR latex nanocomposites the elastic behavior of the XSBR rubber is combined with the high strength and stiffness of the chitin whiskers. High reinforcing effect and diffusion improvement of the chitin whisker (CW)/XSBR latex nanocomposites are expected due to the formation of a rigid network of chitin whiskers with in the XSBR matrix through hydrogen bonding. It is also expected that the uniform dispersion of the high modulus reinforcing phase restricts the molecular mobility of the polymer leading to increased mechanical properties and reduced transport properties.

4.1. Structure and Morphology

Chitin whiskers used for the processing of nanocomposites were prepared from commercially available crab shell chitin powder. The scanning electron microscopy (SEM) images of starting material and the atomic force microscopy (AFM) image of the prepared chitin whiskers are

shown in Figure 1. The starting material is microsized chitin flakes having an average particle size of 300-600 μm (Figure 1a). The structure and size distribution of the prepared suspension of CWs are analyzed by AFM and showed the presence of well isolated and nanosized needle shaped whiskers obtained after the acid hydrolysis (Figure 1b). These fragments have a broad distribution in length (*L*) ranging from 100 to 500 nm and diameter (*D*) ranging from 10 to 80 nm. The average of length and diameter were estimated to be 500±50 nm and 50±10 nm, respectively. Therefore, the average aspect ratio, *L*/*D*, is 10±5, which is very close to dimensions of commercial crab chitin (16) [14] and squid pen (15) [25] but much lower than chitin from Riftia tubes (120) [15]. The size of whiskers measurements based on AFM images are not accurate as some broadening effects may occur based on the tip geometry during scanning [26].
The morphology of the pure matrix and the chitin whisker (CW)/ XSBR nanocomposites were examined with the help of SEM and compared to verify the presence of any microscaled aggregates in the system. Figure 2 shows the SEM images the matrix and the nanocomposites with 30, 50 and 70 vol% nanowhiskers. It is not possible to see any microsized agglomerates or bundles of whiskers in the cross-section of the nanocomposites. The AFM image of 50 vol% whiskers nanocomposites are given as the representative sample to show the detailed nanostructured view of the system. (Figure 3) The phase image of the 50 vol% nanocomposite shows two phased system and clearly shows the needle shaped chitin whiskers embedded uniformly through out the matrix.

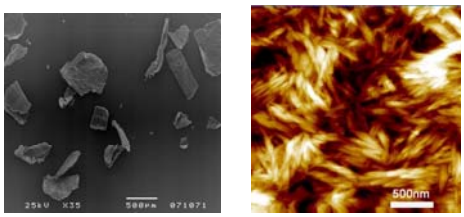

(a) (b)

Figure 1. (a) SEM image of crab shell chitin powder (b) AFM imaging of a dilute suspension of nanochitin whiskers.

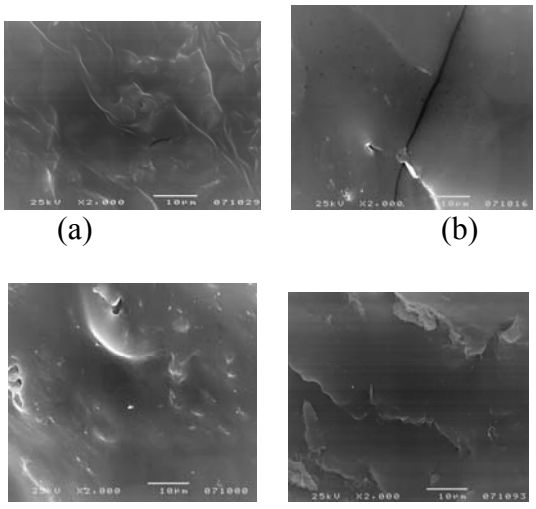

(a) (b)

(c) (d)

Figure 2. SEM image of a) XSBR matrix and XSBR-chitin whiskers nnaoocmposites with b) 30% c) 50% and d) 70% chitin whiskers

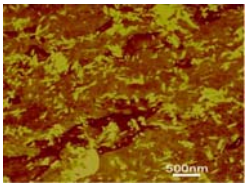

Figure 3. AFM imaging of 50% chitin whisker nanocomposites

4.2 Tensile tests

Typical stress vs strain curves for the chitin whiskers (CW) / XSBR latex nanocomposites are shown in Figure 4. For each measurement, it was observed that the strain was macroscopically homogeneous and uniform along the sample until its break. The stress continuously increases with the strain; the tensile strength of resulting nanocomposites was increases with increase in chitin whisker content. In Figure 5 neat XSBR film the tensile strength is 5 MPa. For 40%, 60% and 80% chitin whisker / XSBR nanocomposites the tensile strength is 32MPa, 44MPa, 72 MPa respectively. The tensile modulus of the nanocomposites also increases with increase the chitin whisker content shown in Figure 6. Elongation at break of chitin whisker (CW) / XSBR latex nanocomposites as a function of chitin whiskers content is plotted in Figure 7. For the neat XSBR film percentage of elongation is 368 but in 80 % chitin whisker content nanocomposites the value is 68 %. This indicates that addition of chitin whisker in XSBR matrix, results in strong interactions between whiskers and between whisker and matrix.

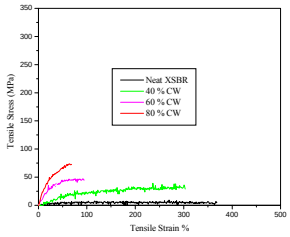

Figure 4. Stress vs. Strain curve for chitin whisker (CW) / XSBR nanocomposites

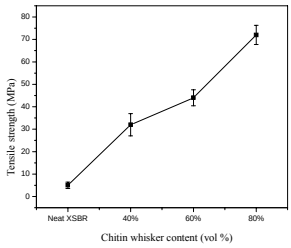

Figure 5. Effect of chitin whisker (CW) content on tensile strength

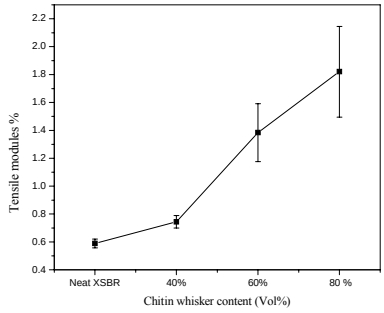

Figure 6. Effect of chitin whisker (CW) content on tensile modules (100% elongation)

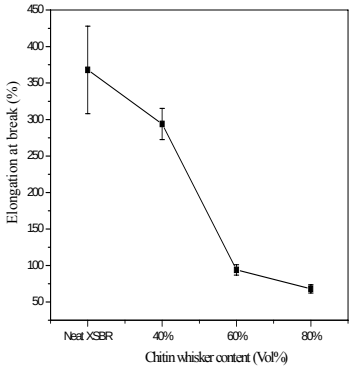

Figure 7. Effect of chitin whisker (CW) content on elongation at break.

4.3. Tear strength

In the Figure 8 it can be seen that the tear strength neat XSBR is 5.58 MPa and resulting nanocomposites increases from 11.56 MPa to 16.18 MPa by the increase of chitin whisker content from 40% to 80%. The increase in tear strength of the nanocomposites films with increase in α-chitin whisker (CW) content could be due to the uniform dispersion of whiskers and the favourable interaction between XSBR latex and α- chitin whiskers.

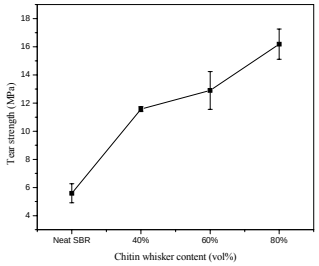

Figure 8. Effect of chitin whisker (CW) content on tear strength

4.4. Water resistance

Water resistance of the nanocomposites is related to the capacity of the cross-linked polymer in the diffused medium. The mass and the dimensions of the polymer system may be changed due to

the penetration of the solvents in to swollen specimens. The diffusion in water is strongly influenced by the microstructure of the nanocomposites [27,28]. Water absorption of XSBR film and chitin whisker (CW) / XSBR nanocomposites is plotted as a function of the square root of time in Figure 9. Two well-separated zone were observed at shorter time (zone I: $t^{1/2}<20$) and longer times (zone II $t^{1/2}>20$). In zone I, a rapid increase in water up take occurs whereas in zone II, percentage of absorption of water stabilizes.

The results of the sorption experiments are presented as the mol uptake Qt of the water by neat XSBR latex film and different volume percent of chitin whisker as a function of square root of time and are given in Figure 9

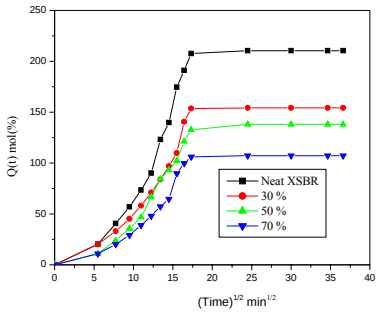

Figure 9. Effect of square root of time on water up take percentage of nanocomposites samples

4.4.1. Diffusion coefficient (D)

The diffusion process is a kinetic parameter depending on the free volume within the material, segmental mobility of polymer chains and the size of the penetrant molecule [28]. The diffusion coefficient of a polymeric sample immersed in an infinite amount of solvent can be calculated using the equation [29].

$$Q_t/Q_\omega = 1-(8/\pi^2) \sum_{n=0}^{n=\omega} [\, 1/(2_{n+1})^2 \exp [-D\,(2_{n+1})^2\, \pi^2\ \ t/h^2]]$$

Where t is the time, h the initial thickness of the sample, D the diffusion coefficient and n is an integer. From this equation, it is understood that a plot of Q_t versus $t^{½}$ is linear at short time and D can be calculated from the initial slope. The equation for short time limiting is,

$$Q_t/Q_\omega = 4/h\ (D/\pi)^{1/2}\ t^{½}$$

By rearranging this equation, the diffusion coefficient can be calculated using the equation,

$$D = \pi\ (h\dot{\theta}/ 4\ W_\omega)^2$$

D - Water diffusion coefficient

h - Thickness of each sample

$\dot{\theta}$ - Slop of the linear portion of the curve

W_ω - Weight of each sample at infinity

From the slope h of the initial linear portion of the sorption curves the diffusion coefficient (D) was calculated using the equation [31]. Thus when the concentration of nanoparticles increases, the diffusion coefficient values decrease. Diffusivity is a kinetic parameter, which depends on the polymer segmental mobility and the mobility of the polymer chain depends on the amount of free volume in the matrix [30]. A penetrant molecule may exist in a hole of sufficient size and can jump into a neighboring hole once it acquires sufficient energy. The water diffusion coefficients

(D) of the neat XSBR latex film and the chitin whisker/XSBR latex nanocomposites shown in Table 3. The neat XSBR film shows the highest water diffusion coefficient of about 5.62 x 10^{-10} cm^2 s^{-1}. However, with an increase of chitin whisker content in the XSBR matrix, the water diffusion coefficient of the nanocomposites decreases from 4.69 x $10^{-10}$$cm^2$ s^{-1} to 3.46 x $10^{-10}$$cm^2$ s^{-1}, which can be ascribed to chitin whisker networks and strong interactions between whiskers and XSBR chains.

4.4.2. Sorption coefficient

The sorption coefficient, which is the maximum saturation sorption value, is calculated using the equation

$$S = W_\omega / W_0$$

S - Sorption coefficient

W_ω - Weight of polymer sample at infinity

W_0 - Initial weight of polymer sample.

In Table 3 it can be seen that the weight percentage of chitin whisker increases sorption coefficient decreases in the nanocomposites. The sorption coefficient (S) value is maximum for neat XSBR latex film and minimum for the 70 % chitin whisker content. This indicates that the water molecules are best accommodated in this system. This is because of the amorphous nature of the neat rubber sample. The chitin whisker / XSBR latex nanocomposites show a decreased value of sorption coefficient and as the amount of chitin whisker in XSBR latex matrix. This is because the nanocomposites have varying proportions of chitin whisker which is crystalline and offers resistance to solvent uptake.

4.4.3. Permeability coefficient

The permeation of a penetrant into a polymer membrane depends on the diffusivity as well as the solubility or sorptivity of the penetrant. The permeability coefficient P can be calculated from the equation,

$$P = DS$$

P - Permeability coefficient

D - Diffusion coefficient

S - Sorption coefficient

The permeability coefficients of neat XSBR latex film and different compositions of chitin whisker/XSBR latex nanocomposites shown in Table 3. Permeability coefficient is higher value for neat XSBR latex film lower for the 70% chitin whisker content. The 'P' value decreases with increase in weight percentage of chitin whiskers in the resulting nanocomposites. The permeability coefficients 17.46 x 10^{10} (m^2s^{-1}) for Neat XSBR film and 11.92 x 10^{10} (m^2s^{-1}), 10.40 x 10^{10} (m^2s^{-1}) and 7.16 x 10^{10} (m^2s^{-1}) for 30 %, 50%, 70%, chitin whisker nanocomposites respectively. This is because the presence of chitin whisker hinders the movement of water molecules between the polymer chains. Since the permeability coefficient is the net effect of D and S, the P value decreases with increase in chitin whisker content in the nanocomposites given in Table 3.

Table 3. Values of D, S and P for chitin whisker/XSBR latex nanocomposites at room temperature

	D x 10^{10} (m^2s^{-1})				S gg^{-1}				P x 10^{10} (m^2s^{-1})			
Water	XSBR	30%	50%	70%	XSBR	30%	50%	70%	XSBR	30%	50%	70%
	5.62	4.69	4.37	3.46	3.10	2.54	2.38	2.07	17.46	11.92	10.40	7.16

4.4.4. Diameter variation

$$\text{Diameter Variation (\%)} = (d - d_0)/ d_0$$

d_0 - Diameter before swelling

d - Diameter after 24 h,

Diameter variation of the neat XSBR film and different weight percentage of chitin whisker content in nanocomposites were measured before and after swelling in water [14]. The diameter variations of nanocomposites are shown in Table 4 the diameter of the nanocomposites decreases with increasing amount of chitin whisker content

Table 4. Diameter variation of the CW/XSBR nanocomposites

Water (d0-20mm)		
	Diameter after 24h (d) (mm)	Diameter Variation (%)
Neat XSBR	22.5	12.5
30% CW	21.5	7.5
50%CW	21.0	5
70%CW	20.4	2

4.4.5. Relative weight loss (RWL)

Thin discs of neat XSBR film and different weight percentage of chitin whisker content nanocomposite samples were first weighed (W_0) and then immersed in water for 48 h they were subsequently dried for 12 h at 45-50 °C and weighed again (W_0'). Relative weight loss (RWL) $[W_0 - W_0']/W_0 \times 100$) were determined, [14] the results are reported in Table 5. The relative weight loss (RWL) of the neat XSBR is 8.34 but in 70% chitin whisker content nanocomposites is 3.87, in all case the relative weight loss (RWL) decreases with increasing the chitin whisker content in XSBR matrix. This is the formation of a hydrogen-bonded with inside the chitin whiskers. The results of relative weight loss (RWL) shown that the strong interaction between chitin whisker and XSBR matrix. The "sol" fraction of the neat XSBR film and different weight of chitin whiskers nanocomposites were also determined by this equation (W_0'/W_0), the results are reported in Table 5, and this is also related to relative weight loss (RWL) that is (1-RWL). The sol fraction of the neat XSBR is 91.66and 70% chitin whisker content nanocomposites is 96.13, the sol fraction increases with increasing chitin whisker content in XSBR matrix.

Table 5. Relative weight loss (RWL) and Sol fraction of nanocomposites in water

water		
	RWL	Sol fraction
Neat XSBR	8.34	91.66
30% CW	7.32	92.68
50% CW	5.05	94.95
70% CW	3.87	96.13

5. Conclusions

NanoChitin whiskers were prepared from macro chitin powder by chemical treatment. The resulting nanochitin whiskers were incorporated in to the Carboxylated styrene butadiene rubber latex (XSBR) matrix by the water evaporation method. Various mechanical properties viz. tensile strength, tear strength, tensile modulus and elongation at break were measured. All the results lead to the conclusion that the chitin whisker content plays a major role in the properties of final composites developed. The stress continuously increases with the strain, the tensile strength of

nanocomposites increases with increasing chitin content and modulus of elasticity and tear strength are also increases with increase in chitin whisker content, whereas the elongation at break of the nanocomposites decrease the reinforcing effect of the chitin whiskers strongly depend on their ability to form a rigid three-dimensional network, resulting from strong interactions such as hydrogen bonding between the whisker. The increase in tensile strength with increase in chitin content gives clear evidence for the presence of a three-dimensional chitin network with in the nanocomposites. The diffusion in water is strongly influenced by the microstructure of the nanocomposites. This is due to the formation of a rigid chitin network resulting from three-dimensional hydrogen bonding between chitin whiskers and XSBR latex. AFM shows that nanosized chitin whiskers content in the XSBR matrix and SEM observations conformed that the chitin whisker were uniformly distributed with in the XSBR latex matrix and there providing good mechanical properties.

6. Reference

[1] Li, J.; Revol, J. F.; Marchessault, R. H. *Appl. Polym. Sci.* **1997**, 65, 373.
[2] Yamaguchi, Y.; Nge, T. T.; Takemura, A.; Hori, N.; Ono, H. *Biomacromolecules* **2005**, 6, 1941-1947.
[3] Krajewska, B. *Enzyme Microbiol Technol.* **2004,** 35, 126–39.
[4] Yusof, N. L.; Wee, A.; Lim, L. Y.; Khor, E. *J. Biomed Mater Res A.* **2003,** 66A, 224–32.
[5] Hudson SM. Applications of chitin and chitosan as fiber and textile chemicals. In: Domard A, Roberts GAF, Va˚ rum KM, editors. Advances in chitin science, vol. 2. Lyon (France): Jacques Andre´ Publ.; **1998**. p. 590–9;
[6] Kanke, M.; Katayama, H.; Tsuzuki, S.; Kuramoto, H. *Cheam Pharm Bull.* **1989,** 37,523–5.
[7] Kato, Y.; Onishi, H.; Machida, Y. *Curr Pharm Biotechnol.* **2003**, 4, 303–9.
[8] Marguerite, R. *Prog. Polym. Sci*. **2006**, 31, 603–632.
[9] Li, R. J.; Marchessault, J. F. *Biomacromolecules* **1993**, 15, 329.
[10] R. A. Muzzarelli, Chitin microfibrils. In chitin; Pergamon Press: New York, **1977**, pp 51-55.
[11] C. J. Brine and P. R. Austin. Renatured chitin fibrils, films and filaments. In Marine Chemistry in the Costal Environment; Church, T.D., Ed.; ACS Symposium series 18; American Chemical Society: Washington, DC, **1975**; pp 505-518.
[12] Murry, S. B.; Neville, A. C. *Int. Boil Macromol* **1997**, 20, 123-130.
[13] Murry, S. B.; Neville, A. C. *Int J Boil Macromol* **1998**, 22, 137-144.
[14] Gopalan Nair, K.; Dufresene, A. *Biomacromolecules* **2003**, 4(3), 657-665
[15] Morin, A.; Dufresne, A. *Macromolecules* **2002**, 35, 2190-2199.
[16] Gopalan Nair, K.; Dufresene, A. *Biomacromolecules* **2003**, 4(3), 666-674.
[17] Gopalan Nair, K.; Dufresene, A. *Biomacromolecules* **2003**, 4(6), 1835-1842
[18] Gopalan Nair, K.; Dufresene, A. *Macromolecules* **2004**, 37, 1386-1393.
[19] Yongshang, L.;Weng, L.; Zhang, L. *Biomacromolecules* **2004**, 5, 1046-1052.
[20] Grunert, M.; Winter, W. T. *Journal of Polymers and the Environment* **2002**, 10. 1-2.
[21] Oksman, K.; Mathew, A. P.; Bondeson, D.; Kvien, I. *Composites Science and technology* **2006**, 66, 2776-2784.
[22] Bondeson, D.; Syre, P.; Oksman, K. *Journal of Biobased Materials and Bioenergy* **2007**, 1, 1-5.
[24] Domard, A.;. Lamarque, G.; Chaussard, G. *Biomacromolecules* **2007**, 8, 1942-1950

[25] Campana-Filho, S. P.; Signini, R.; Cardoso, M. B. *International Journal of Polymeric Materials* **2002**, 51, 695 ± 700,
[26] Paillet, M.; Dufresne, A. *Macromolecules* **2001**, 34, 6527-6530.
[27] Kvien, I.; Tanem, B. S.; Oksman, K. *Biomacromolecules* **2005**, 6, 3160-31655.
[28] Yongshang, L.; Weng, L.; Zhang. L. *Biomacromolecules* **2004**, 5, 1046-1051
[29] Y. Saito. *Macromolecules* **1997**, 30, 3867-3873
[30] Smith, M.T.; Peppas, N. A. *Polymer* **1985**, 26, 569.
[31] Crank, J. The Mathematics of Diffusion, second ed., Clarendon Press, Oxford, **1975**.
[32] C. J. Brine and P. R. Austin. Renatured chitin fibrils, films and filaments. In Marine Chemistry in the Costal Environment; Church, T.D., Ed.; ACS Symposium series 18; American Chemical Society: Washington, DC, **1975**; pp 505-518.

Effect of nanosilica on the mechanical properties of HDPE-nylon fibre composite

Sinto Jacob, Suma K.K., Jude Martin Mendaz and K.E.George
Dept. of Polymer Science & Rubber Technology, Cochin University of Science and Technology, Kochi-22
E-mail- kegeorge@cusat.ac.in

Introduction

Fibre reinforced polymers offer a combination of strength and modulus that are either comparable to or better than many traditional metallic materials. Because of their low density, the strength–weight ratios and modulus–weight ratios of these composite materials are markedly superior to those of metallic materials. In addition, fatigue strength as well as fatigue damage tolerance of many composite materials are excellent. For these reasons, fiber reinforced polymers have emerged as a major class of structural materials and are either used or being considered for use as substitution for metals in many weight-critical components in aerospace, automotive, and other industries[1-3].

High particle loadings result in products with much higher weight than that of the pure polymers. Hence a composite with improved properties at low filler loading is always the optimum choice. Nanostructured materials often exhibit superior physical and mechanical properties compared to conventional materials. But the dispersion of the nanoparticles is the main difficulty in the development of nanocomposites.

Micro and nano fillers are widely used for modifying thermoplastics[4,5]. Development of polyethylene based composites for improving the mechanical properties is the topic of this study. The reinforcing and toughening effects of nano fillers on HDPE-nylon fibre composite is also proposed to be studied at different loading levels of nylon fibre and nanosilica powder.

Experimental

Materials

The high density polyethylene (HDPE) used was LGG104, MFI 18g/10 min, supplied by LG Plastics. Nylon fiber (N6) was obtained from SRF Ltd., Chennai, India, The continuous nylon fibers were cut into staples, so that the fibers used as reinforcement had an average length of

8±2mm. Nanosilica was synthesized by acid hydrolysis of sodium silicate using dilute hydrochloric acid as suggested by Reddy and Das[6].

Composite Preparation

HDPE granules, nylon fibre and silica nanoparticles were dried by keeping them in an oven at 100^{o}C for four hours. Nylon fibre reinforced polyethylene (HDPE/nylon fiber) composites were prepared by adding nylon fibre to the polyethylene melt in a Thermo Haake Rheocord 600 mixing chamber with a volumetric capacity of 69cm^{3} and fitted with roller type rotors. HDPE was added directly to the chamber and after it had melted and homogenized, nylon fibre was added. Silica nanoparticles/nylon fibre hybrid HDPE composites were prepared by adding nylon fibre and nanosilica into HDPE melt. The temperature was kept at 170^{o}C to ensure proper melting of HDPE. In the first series of experiments, 10, 20 and 30 weight percentage of nylon fibre reinforced polypropylene composites were prepared. In the second series, 10, 20 and 30 weight percentage of nylon fibre were added together with 1&2 weight percentage of nanosilica powder to HDPE melt to get nanosilica modified HDPE-nylon fibre composites. A mixing time of 9 minutes was used at a rotor speed of 50 rpm. In all cases the torque stabilized to a constant torque in this time.

The hot mix from the mixing chamber was immediately passed through a two-roll mill and the test specimens were prepared using a semi-automatic plunger type injection-moulding machine, with a barrel temperature of 190^{o}C.

Mechanical Testing

The tensile properties and flexural properties of the composites were studied using a Shimadzu Universal Testing Machine (model-AG1) with a load cell of 50kN capacity. The tensile properties were determined at a crosshead speed of 50mm/min according to ASTM-D-638 standard. The flexural properties were determined at a crosshead speed of 5mm/min according to ASTM-D-790 standard. Impact strength of the samples was determined using Resil impactor junior (Ceast) (ASTM-D256). Five samples were tested for each case.

Results and Discussion

Mechanical Properties

Tensile tests were performed on dumbbell shaped samples prepared using semiautomatic plunger type injection mould. The effect of nanosilica on the tensile properties HDPE-nylon fibre

composite is shown in Figure 1 and the effect of nanosilica on the flexural properties HDPE-nylon fibre composite is illustrated in Figure 2.

From the figures it may be observed that the mechanical properties of HDPE-nylon fibre composite increases with increasing fibre loading. The HDPE-nylon fibre composite modified with nanosilica shows better properties. 1% of silica loading results in higher tensile strength, tensile modulus, flexural strength and flexural modulus for HDPE-nylon fibre composite compared to 2% silica loading. These results demonstrate that a small amount of nanosilica substantially enhances the mechanical strength of the polymer composite. This may be attributed to better wetting of the fiber in the matrix by nanosilica.

The effect of nanosilica on the impact performance of HDPE-nylon fibre composite is shown in Figure 3. The impact resistance of HDPE-nylon fibre composite increases up to 20% fibre loading and then decreases. The HDPE-nylon fibre composite modified with 1% nanosilica showes better impact resistance but the composite modified with 2% nanosilica does not show that improvement as in the case of the tensile/flexural properties. There may be agglomeration of nanoparticles in the matrix at high filler loading this may decrease the impact resistance of the composite.

Conclusions

The maximum reinforcement for HDPE-nylon fibre composite is found to be at a fibre loading of 30%. The incorporation of nanosilica powder enhanced the mechanical properties of HDPE-nylon fibre composites. Addition of 1% nanosilica with HDPE-10wt% nylon fibre composite showed higher mechanical properties than HDPE-30wt% nylon fibre.

References

1. P.K. Mallick, “Fiberreinforced composites materials, manufacturing, And design”, Taylor & Francis group, Boca Raton London
2. S.N.Maiti and K.K.Sharma, *J.Mater.Sci.*,27 (1992) 4605-4613
3. P.Mareri, S.Bastide, N.Binda and A.Crespy, *Compos.Sci.Technol.*,58 (1998) 747-7452
4. R.Varatharajan, S.K.Malhothra, L.Vijayaraghavan and M.Krishnamurthy, *Materials Science and Engineering:B*, 132 (2006) 134-137
5. Min Zhi Rong, Ming Qiu Zhang, Yong Xiang Zheng, Han Min Zeng and K.Friedrich, *Polymer,* 42(2001) 3301-3304
6. C.S.Reddy, C.K.Das, *Compos Interfaces*, 11(2005) 687

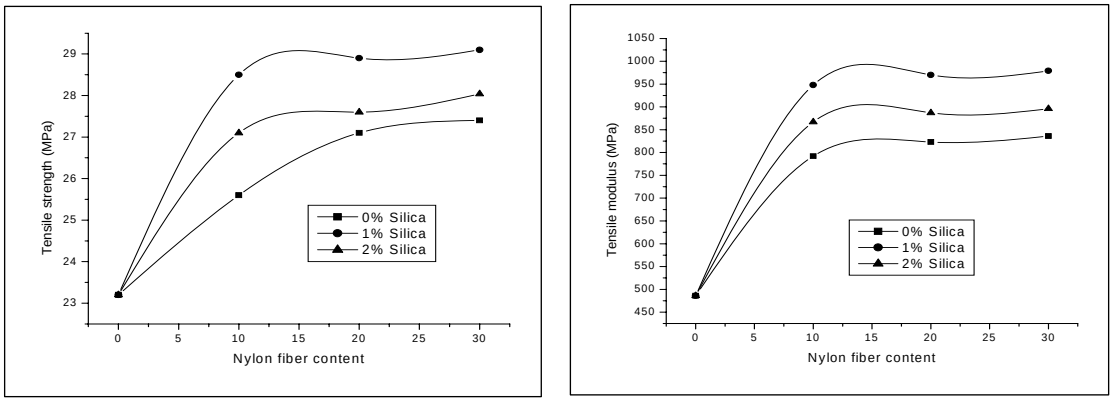

Figure 1. Variation of tensile strength and tensile modulus of HDPE-nylon fibre composite with nanosilica

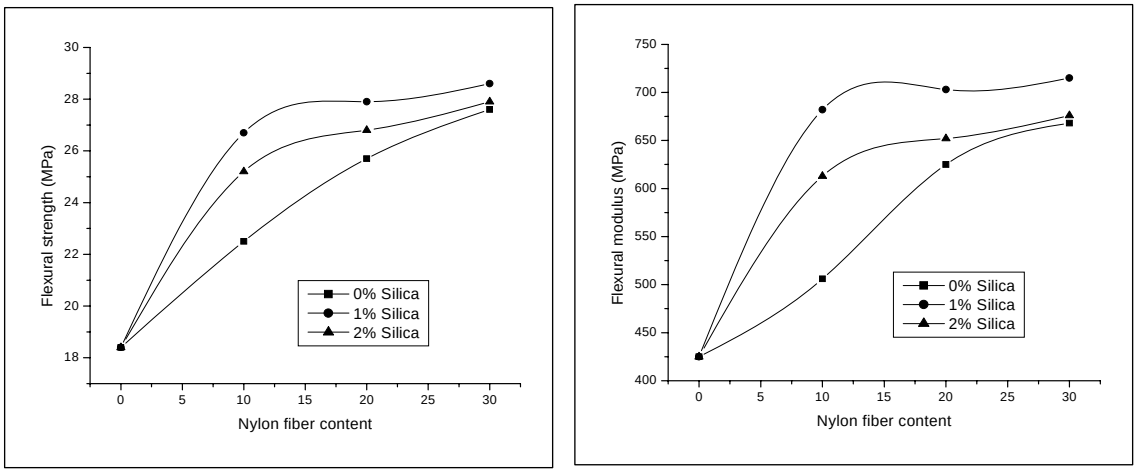

Figure 2. Variation of flexural strength and flexural modulus of HDPE-nylon fibre composite with nanosilica

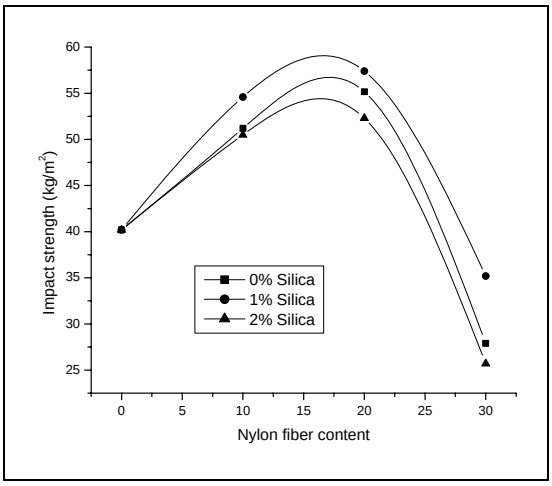

Figure 3. Variation of impact strength of HDPE-nylon fibre composite with nanosilica

Nanosilica based nylon-6 short fibre-natural rubber composites

Leny Mathew[1, 2], Sunil K. Narayanankutty[1]*

[1]Department of Polymer Science and Rubber Technology,
Cochin University of Science and Technology, Kochi- 682 022, Kerala, India.
[2]Mahatma Gandhi University College of Engineering,
Thodupuzha- 685 587, Kerala, India.

Email: sunil@cusat.ac.in

ABSTRACT

Nanosilica was synthesized by acid hydrolysis of sodium silicate using dilute hydrochloric acid under controlled conditions. The average size of the silica particle was 13 nm, as determined by XRD studies. This synthetic nanosilica was used in place of hydrated silica in HRH (hexamethylenetetramine, resorcinol and silica) bonding system for Natural rubber/nylon-6 short fiber composite. Nanosilica was also used as reinforcing filler in Natural rubber/nylon-6 short fiber hybrid composite. Cure characteristic and mechanical properties of the hybrid composites were evaluated. The minimum torque, maximum torque and cure time of the hybrid composites increased with silica loading. Scorch time decreased with fiber loading and increased with silica content. The thermal stability and tensile strength, modulus and tear strength were better than the conventional silica composites.

INTRODUCTION

Composite materials play a key role in aerospace industry, automobile industry and in other engineering applications as they exhibit outstanding strength-to-weight and modulus-to-weight ratios. Short-fiber-reinforced rubber composites have attracted much attention because of better processability, improved physical and mechanical properties and economic advantage. Short-fiber-reinforced rubber composites have been successfully used in the production of V-belts, hoses, tire treads, seals and complex- shaped mechanical goods. In these composites, a dry bonding system based on hexamethylenetetramine, resorcinol and hydrated silica (HRH) is used to improve fiber-matrix interfacial adhesion which is very critical for efficient transfer of load to the reinforcing member of the composites [1-5]. Rajeev et al [1], Sreeja et al [4], and Derringer [6], have described the various aspects of short fiber adhesion to rubber in the presence of the dry bonding system. In all these studies they have used conventional precipitated silica with particle size in microns. [1, 6-8]. In this work we report the effect of nanosilica based tri-component dry bonding system on short Nylon fiber – natural rubber composite. The nanosilica filler is used both

as a component of HRH dry bonding system and as a filler. The cure characteristics and mechanical properties of nanosilica/Nylon-6 short fiber/natural rubber hybrid composites are also presented.

EXPERIMENT

Nanosilica was synthesized from sodium silicate in aqueous medium by acid hydrolysis method using dilute HCl. NR-Nylon-6 short fiber-silica hybrid composites were prepared using the newly prepared nanosilica. Natural rubber used in this study was ISNR-20. Nylon fiber (N6) was chopped to approximately 6mm length. Fiber loading was varied from 0 to 30 phr and silica loading was varied from 0 to 9 phr. Hexa:Resorcinol:Silica(HRH) ratio was maintained as 2:2:1. HRH loading was adjusted as 16% of the fiber loading. Natural rubber-100 phr, Zinc oxide-5 phr, Stearic acid-2 phr, N-(1, 3- dimethylbutyl) N'-phenyl-p-phenylenediamine) -1 phr, CBS-0.6 phr, TMTD- 0.2 phr and sulphur-2.5 phr were common to all mixes. The mixing was done as per ASTM D-3184 (1989) on a two roll mill. Cure characteristics of the mixes were determined as per ASTM D 2084-1995 using Rubber Process Analyzer, RPA 2000® Alpha Technologies. The thin sheet obtained was cut in the required dimension and stacked one above the other to the desired volume and vulcanized to optimum cure time. Test specimens were punched out with fibers oriented along the milling direction (longitudinal-L) and the tensile properties were determined according to relevant ASTM standards.

Sample identification

The A, B, C, D and E series represent the Mixes containing 0 phr, 3 phr, 6 phr and 9 phr nanosilica and 6 phr commercial silica, respectively. The subscripts 0, 10, 20, 30 indicate fiber content in the mixes.

RESULTS AND DISCUSSION

Cure Characteristics

Variations of minimum torque with fiber loading at various silica contents are shown in figure1. The minimum torque increases with silica loading for all the mixes. Mix series B, C and D show higher viscosity than the E series. The higher viscosity of the nanosilica composites may be due to the better interaction between silica and the rubber matrix. Lower particle size silica has higher surface area and hence can have improved interactions. Figure 2 gives the variations of scorch time with silica content and fiber loading. Scorch time decreases with fiber loading for all the mixes. This indicates that nylon fiber has an accelerating effect on cure reaction. The variation of cure time with filler loading is shown in figure 3. Cure time increases with silica loading for all the mixes up to 20 phr fiber loading and then remains more or less constant. This may be

attributed to the slight acidic nature of silica. Generally acids retard the cure reaction. For higher fiber loading the accelerating effect of the nylon fiber was compensates for the retarding effect of the silica. The differential torque i.e., the difference between the minimum and maximum torques developed during cure is marginally increased with fiber loading and silica content and it is higher for nanosilica composite (Fig.4). The differential torque is a measure of the extent of the cross link formation and the filler–matrix interaction. The higher values for the nanosilica compounds indicate that the matrix is more restrained.

Mechanical Properties

The tensile strength increases with fiber content with an initial minor drop at 10 phr (Fig.5). This drop may be due to the dilution effect of the fibers at lower loadings. At higher fiber loadings, however, the reinforcing effect takes over; resulting in an improved ultimate strength. Series A-D represent the mixes containing 0-9 phr of nanosilica in addition to varying levels of short fibers. It can be seen that Series D gives the highest tensile strength. The improvement in tensile strength for 30 phr fiber loaded composites is 34% in the presence of 9 phr nanosilica. At 10 phr fiber loading, the improvement is about 10%. This may be attributed to better chances of interaction between the fiber and the matrix through silica surface. Mix E shows tensile strength values almost equal to the mixes without silica (Mix A). This implies that the nanosilica has better interaction with the matrix and hence improves wettability of the short fibers, resulting in higher tensile strength

The variation of tear strength with fiber loading is shown in figure 6. The tear strength registers a significant increase in the presence of short fibers. For 30 phr fiber loaded sample the tear strength is improved from 106 to118 N/mm in the presence of 6 phr of nanosilica. The tear strength obtained by using commercial silica is only 108 N/mm.

There is a very good improvement in modulus values with silica content (Fig. 7). By the addition of 9 phr nanosilica, the modulus values increase by 55%, 33% and 28% respectively for 10 phr, 20 phr and 30 phr fiber loaded samples. It indicates that the silica filler has a significant role in the modulus value of the hybrid composite. The Mixes A_0, B_0, C_0 and D_0 show very low modulus values. The silica improves the modulus only in the presence of fibers. Commercial silica mixes show modulus values lower than that of the mixes containing 3 phr nanosilica.

CONCLUSIONS

Nanosilica could be successfully prepared by acid hydrolysis method. The synthesized silica could be used in rubber composites based on natural rubber and Nylon-6 fibers. The efficiency of HRH dry bonding system is improved in the presence of nanosilica. The minimum torque,

maximum torque and cure time of the hybrid composites increase with silica loading. Scorch time decrease with fiber loading and silica content. Nanosilica improves the tensile strength, modulus and tear strength of rubber composites better than the conventional silica. Thermal stability of NR-Nylon-6 composite is also improved by the use of the nanosilica.

REFERENCES

1. Rajeev, R. S.; Bhowmick, A. K.; De, S. K.; Bandyopadhyay, S., J. Appl. Polym. Sci., 2003, 90, 544.
2. Suhara, F.; Kutty, S. K. N. ; Nando, G. B., Polym. Plast. Technol. Eng., 1998, 37, 241.
3. Yu. Yang, Chunxiang.; Lu.Xiaolei,; Su Xinkui Wang, J. Mater. Sci., 2007, 42, 6347.
4. Sreeja, T. D.; Kutty, S. K. N., Polym. Plast. Technol. Eng., 2002, 41, 77.
5. Seema, A.; Kutty, S. K. N., Polym. Plast. Technol. Eng., 2005, 44, 1139.
6. Derringer, G. C., J. Elastoplast, 1999, 3, 230.
7. Ismail, M. N.; Ghoneim, A. M., Polym. Plast. Technol. Eng. 1999, 38, 78.
8. Geethamma, V. G.; Mathew, K. T.; Lakshminarayanan, R; Sabu Thomas, Polymer, 1998, 39, 1483.

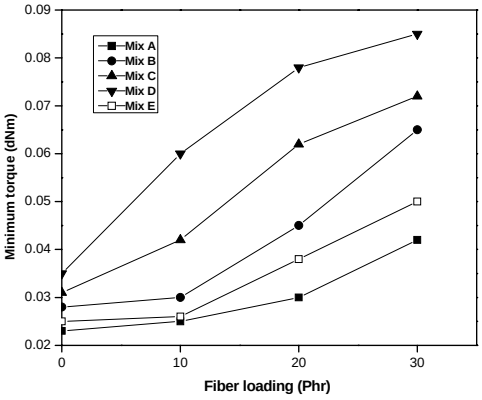

Fig. 1 Variation of minimum torque with fiber loading

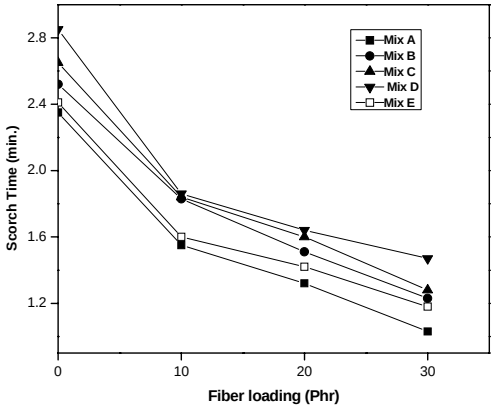

Fig. 2 Variation of scorch time with fiber loading

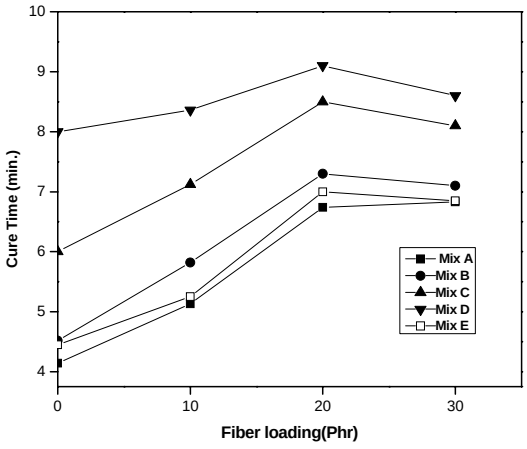

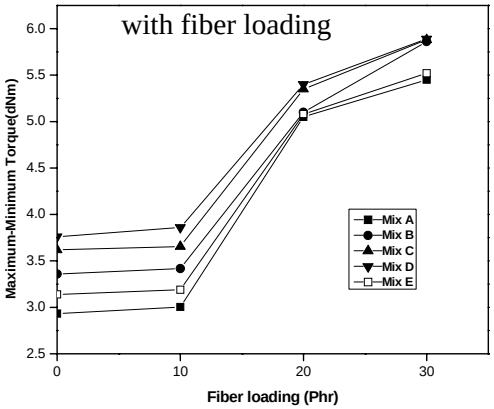

Fig. 3 Variation of cure time with fiber loading

Fig. 4 Variation of differential torque with fiber loading

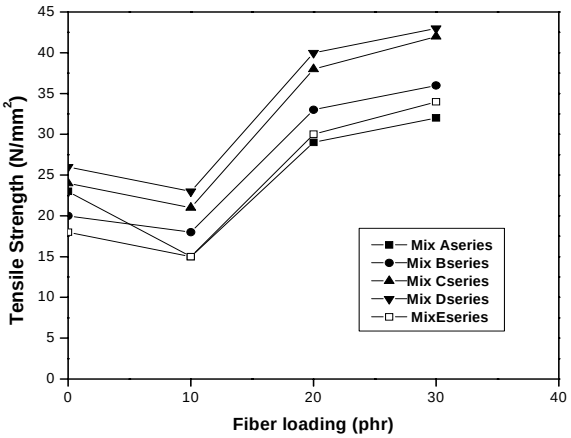

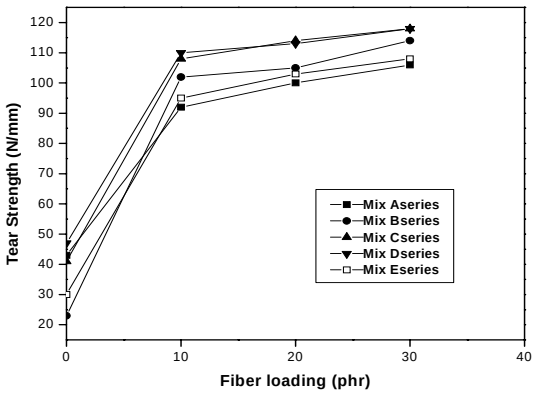

Fig.5 Variation of tensile strength with fiber loading

Fig.6 Variation of tear strength with fiber loading

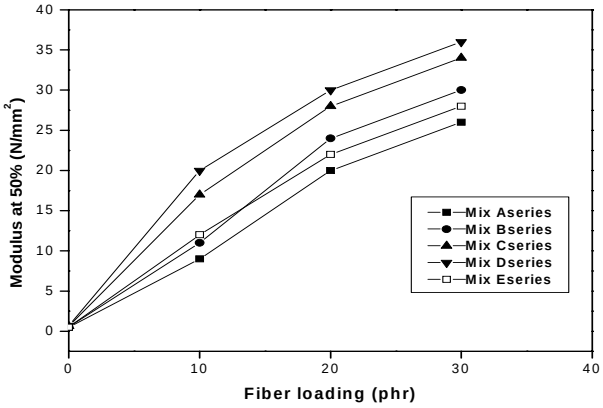

Fig.7 Variation of modulus with fiber loading

Surface modification of carbon nanofibres by high energy electron and gamma radiations

Jinu Jacob George*# and Anil K. Bhowmick

Rubber Technology Centre, Indian Institute of Technology,

Kharagpur-721302, India

Email: jinujac@gmail.com

Abstract

Carbon nanofibers (CNFs) were surface treated with high energy electron beam and gamma radiations at varying doses. The neat and the modified CNFs were examined by Scanning electron microscopy (SEM), X-ray photoelectron spectroscopy (XPS), Raman spectroscopy, TGA and X-ray diffraction (XRD) to characterize the changes caused by modifications. After high energy irradiation, surface defects were introduced and fiber surface became rougher as evident from the SEM analysis. The generation of surface polar groups after high energy irradiations was investigated by XPS. Raman spectra revealed that there was an increase in degree of disorderness and a decrease in crystallite size after high energy treatments. The results are corroborated from the XRD results. However, there was no significant change in d-spacing on high energy treatments.

1. Introduction

Properties of carbon fiber-reinforced polymer composites depend mainly on individual fiber properties and fiber matrix adhesion. It is very well accepted that adhesion can be improved by surface treatment of the fibers and hence various approaches have been developed, such as oxidation, coating, and grafting. Surface treatments that have proven useful for nonpolar carbon fiber surfaces include oxidation by various plasmas [1-7], high energy radiation [8] and chemical methods [9-12]. Most of the above mentioned studies were carried out on micrometer sized conventional carbon fibers, while comparable studies are still absent in the case of carbon nanofibers (CNFs). The effect of chemical treatments and high energy irradiations on CNFs has not been studied extensively. The surface of CNF consists of short graphitic planes parallel to the fiber axis, which allow for the attachment of chemically active groups.

2. Experimental techniques

CNF (Pyrograf III, PR-24 AG grade) was supplied by Applied Sciences Inc., United States. From the SEM micrograph, the average diameter was found to be 120 nm.

2.1 Surface treatment with high energy radiations

The CNFs were irradiated by electron beam accelerator (model ILU-6) at Bhabha Atomic Research Centre (BARC), Mumbai, India. Irradiation doses used were 50, 200 and 800 kGy at room temperature (dose per pass was fixed at 10 kGy). The CNFs were irradiated with gamma rays at three different doses 1, 5 and 10 kGy using Gamma Chamber 5000 (Source: Co-60) at a dose rate of 3.2 kGy/h.

2.2 Characterization methods

Morphological studies of different CNF samples were performed using a SEM model JSM800 manufactured by JEOL at 20 kV acceleration voltage at room temperature. TGA of the neat and the functionalized CNFs was performed using DUPONT TGA instrument [Model: 2000] from ambient temperature to 800°C at a programmed heating rate of 10°C/min in oxygen atmosphere. XPS measurements were obtained on a KRATOS-AXIS165 instrument equipped with dual aluminium–magnesium anodes using MgKα radiation. The peak positions were based on calibration with respect to the C1s peak at 284.6 eV. The excitation wavelength was 514.5 nm from an Ar-ion laser with a laser power of about 8 mW at the sample surface. The equipment was calibrated by the first order Raman band of silicon at 520 cm^{-1} prior to sample runs. The XRD

was done using a Rigaku CN 2005 X-ray diffractometer, model: Miniflex (30 kV, 10 mA) with a Cu target (CuK_α radiation with λ= 0.154 nm) in the range of 2θ =10° to 60°.

3. Results and discussion

Figure 1a-d shows the SEM microphotographs of electron beam irradiated fibers at three different doses of 50, 200 and 800 kGy (abbreviated henceforth as $CNF_{EB\text{-}50kGy}$, $CNF_{EB\text{-}200kGy}$ and $CNF_{EB\text{-}800kGy}$ respectively) along with that of the unmodified CNF, taken at very high magnification. The neat CNF displays a smooth surface (**Figure 1a**). It can be observed from the other three pictures that some blister like features are generated on fiber surface up on electron beam irradiation. As a result, the fibers have lost their surface smoothness to some extent. There is an increase in blister formation with higher electron beam doses of 200 and 800 kGy. Shown in **Figure 2a-d** are the SEM images of neat as well as the gamma irradiated CNF samples with different irradiation doses (abbreviated henceforth as $CNF_{\gamma\text{-}1kGy}$, $CNF_{\gamma\text{-}5kGy}$ and $CNF_{\gamma\text{-}10kGy}$). It can be observed from the photographs that the fiber surface exhibits the generation of similar kind of blisters upon gamma irradiation adding to the total roughness and surface area. With doses higher than 1 kGy irradiation (5 and 10 kGy), there is no significant change in blister formation. Even after various high energy modifications, the fiber diameter does not change. The average diameter of the modified CNFs is 120 nm.

The thermal degradation plots of the electron beam irradiated samples are depicted in **Figure 3a**. The sample irradiated with 50 kGy dose exhibits early T_{max} (the temperature at which maximum degradation occurs) by approximately 15°C. The increase in dose (800 kGy) does not have any further change in degradation temperature, T_{max}. Also, the irradiated fibers degrade at a slightly faster rate. This behaviour indicates that during high energy irradiations the CNFs undergo some amount of degradation. **Figure 3b** depicts the thermal degradation plots of gamma irradiated (1 and 10 kGy) fiber samples along with that of the neat fibers. The **γ-**irradiated fibers exhibit a slightly higher rate of degradation similar to that shown by electron beam modified ones. With increased dose of irradiation i.e. 10 kGy, the degradation temperature is further lowered to 567°C. This may be due to formation of defects and chemical changes that the fibers undergo during high energy irradiation.

The surface composition of untreated and irradiated CNFs was determined and the results are given in **Tables 1-2**. Figure 6a is the fit of the C1s peak of untreated CNF sample. The deconvoluted data show the presence of four peaks corresponding to graphitic carbon (C-C) at 284.6, and the carbons attached to hydroxyl group (C-OH) at 286.1, carbonyl group (C=O) at 288.4 and O-C=O at 290.6 (**Figure 4a**).

All the data on the modified fibers are also deconvoluted in a similar way. **Figure 4(b-c)** shows the deconvoluted C1s and O1s XPS spectra of the treated CNF samples along with those of the untreated one. The O1s peaks are assigned to the oxygen present with the functional groups C-OH at 532.8, C=O at 531.3 and O-C=O at 535.9. The relative concentration of oxygen, attached to C=O group increases by 5.5 % from 28.9 % (untreated) to 30.5 % after electron beam irradiation and increases by 13.1 % from 28.9 % to 32.7 % after gamma irradiation (**Table 2**). These observations suggest that after irradiating with high energy radiations of electron beam as well as gamma, the CNFs undergo surface oxidation. It is interesting to note that the amount of oxygen present as –OH shows a decrease after electron beam (3.0 %) and gamma irradiations (6.8 %). This should not be confusing, as C-OH is converted to C=O. The amount of oxygen bonded as O-C=O, which is 2.3 % in the untreated CNF surface, shows similar amount of increment after various modifications (**Table 2**).

The individual concentrations of carbon, oxygen, nitrogen and silicon on various CNFs are reported in **Table 3**. $CNF_{EB\text{-}800kGy}$ shows a lowering of surface carbon concentration, whereas $CNF_{\gamma\text{-}1kGy}$ exhibits a slight increment. The O/C ratio is a measure of the extent of oxidation occurred on the fiber surface. Electron beam irradiation causes the ratio to increase considerably, indicating oxidation. The O/C ratio, on the other hand, shows a decrement after gamma irradiation.

The ratio of the integrated intensity (I) of D peak to G peak, denoted by $R = I_D/I_G$, gives the information about the generation of surface defects due to functionalization. The value of R increases after electron beam as well as gamma irradiations (**Figure 5a-b and Table 4**). An increase in I_D/I_G after high energy treatment of CNF, therefore, indicates an increment in the number of defect sites on the CNFs.

Tuinstra & Koenig and Knight & White [13-14], have shown that the peak intensity ratio R depends on the in-plane apparent graphitic crystallite size L_a

$$L_a(nm) = \frac{4.4}{R} \qquad \text{..... (1)}$$

Using this equation, L_a was estimated. The calculated crystallite size values are reported in Table 4. The results indicate marked decrease of L_a after various modifications of CNF.

The d-spacing of CNF graphene layers is calculated to be 0.34 nm. Modified CNFs do not exhibit any shift in peak position or generation of new peaks implying that the carbon structure in the bulk of the CNF does not change significantly after various treatments. However, due to high energy irradiations, the peaks corresponding to the (100) and (004) planes undergo small increment in intensity (**Figure 6a-b**). This increment is observed for both electron beam and gamma irradiated CNFs. These changes can be attributed to the generation of surface defects and also to the marginal change in the crystalline nature of the CNFs after various modifications. The average crystallite size, calculated using Debye-Scherrer equation, for all fiber samples is reported in **Table 4**.

4. Conclusions

Electron beam and gamma irradiations generate surface roughness on the fibers resulting in increased surface areas. These results have been well supported by the SEM, TGA, Raman spectroscopy and XRD studies. XPS studies suggest oxidation of fiber surface after irradiations. XRD analyses reveal that the crystallite size reduces after various modifications.

References

[1] Alexander B, Emin KM, Jurgen S. J Colloid and Interface Sci1999; 210: 60-72
[2] Paredes JI, Martınez AA, Tascon JMD. Carbon 2002; 40 (7):1101-8
[3] Loh IH, Cohen RE, Baddour RF. J Mater Sci 1987; 22: 2937-47
[4] Brandl W, Marginean G. Thin Solid Films 2004; 447- 448: 181–6
[5] Heintze M, Bruser V, Brandl W, Marginean G, Bubert H, Haiber S. Surf Coat Technol 2003; 174: 831-4
[6] Bruser V, Heintze M, Brandl W, Marginean G , Bubertc H. Diam Relat Mater 2004;13:1177-81
[7] Yong G, Peng H, Jie L, Mark JS, Jiang Z, Wei W. J Appl Polym Sci 2007; 103:3792-7
[8] Li J, Huang y, Xu Z, Wang Z. Mater Chem and Phys 2005; 94: 315-21
[9] Figueiredo JL, Serp P, Nysten B, Issi JP. Carbon 1999; 37:1809-16
[10] Asif R, Jane YH, Mark DD, Phillip FB. Carbon 2007; 45: 1072-80
[11] Serp PH, Figueiredo JL, Bertrand P, Issi JP. Carbon 1998; 36(12):1791-9
[12] Febo S, Leonardo F, Mario P, Luca P. Carbon 2002; 40; 735-41
[13] Tuinstra F, Koenig JL. J Chem Phys 1970; 53:1126–30
[14] Knight DS, White WB. J Mater Res 1989; 4; 385–93

Figures and Tables

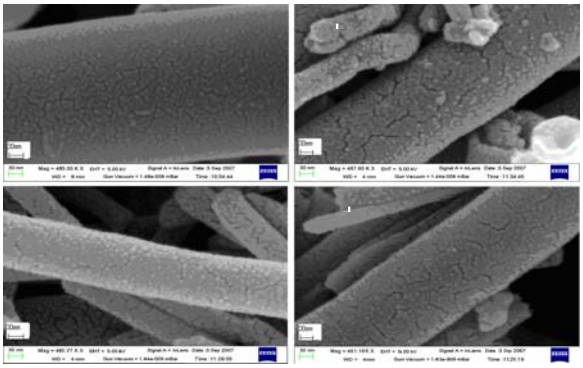

Figure 1: SEM micrographs of (a)CNF, (b) $CNF_{EB\text{-}50kGy}$,(c)$CNF_{EB\text{-}200kGy}$ and (d)$CNF_{EB\text{-}800kGy}$

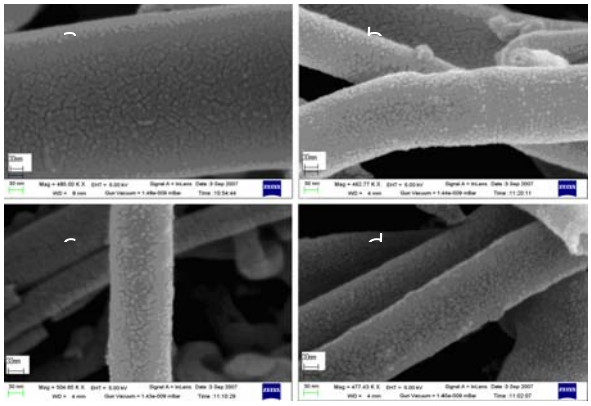

Figure 2: SEM micrographs of (a) CNF, (b) $CNF_{\gamma\text{-}1kGy}$, (c) $CNF_{\gamma\text{-}5kGy}$ and (d) $CNF_{\gamma\text{-}10kGy}$

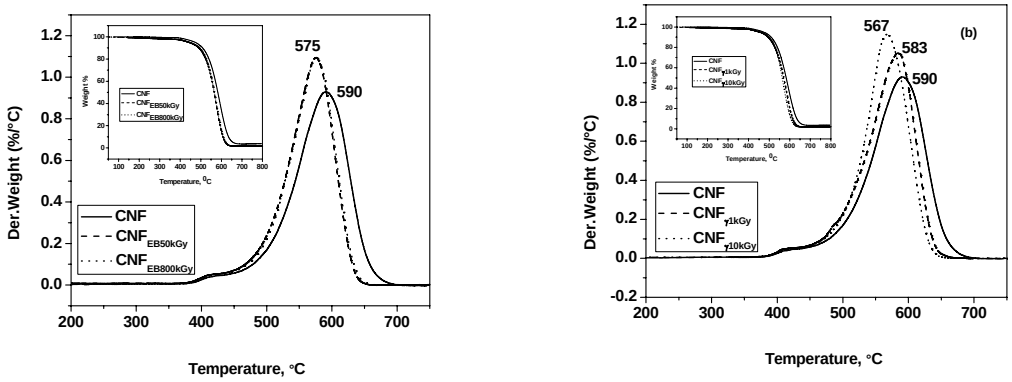

Figure 3(a-b). Comparison of the DTG and TGA (inset) curves of (a)CNF, $CNF_{EB\text{-}50kGy}$ and $CNF_{EB\text{-}800kGy}$, (b) CNF, $CNF_{\gamma\text{-}1kGy}$ and $CNF_{\gamma\text{-}10kGy}$

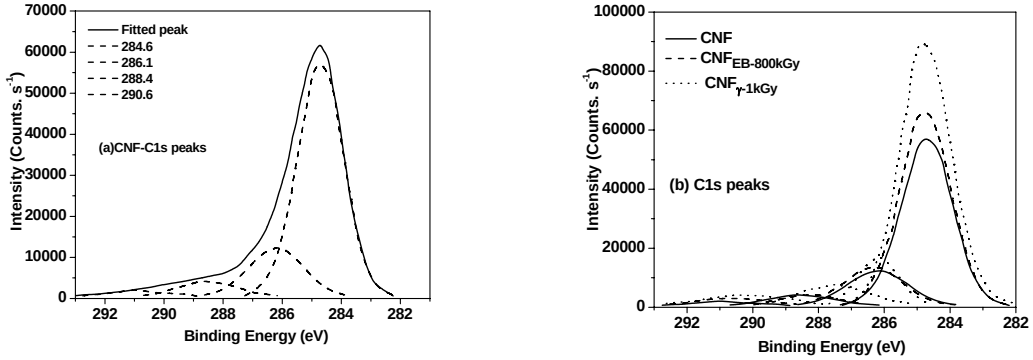

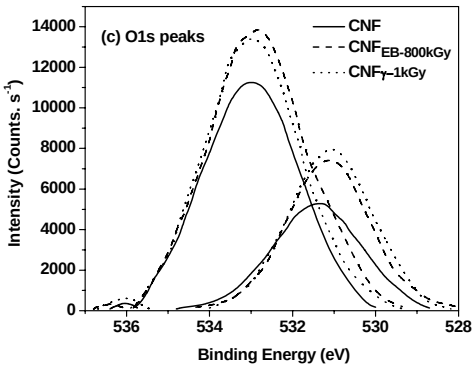

Figure 4(a-c). XPS spectra of representative CNFs

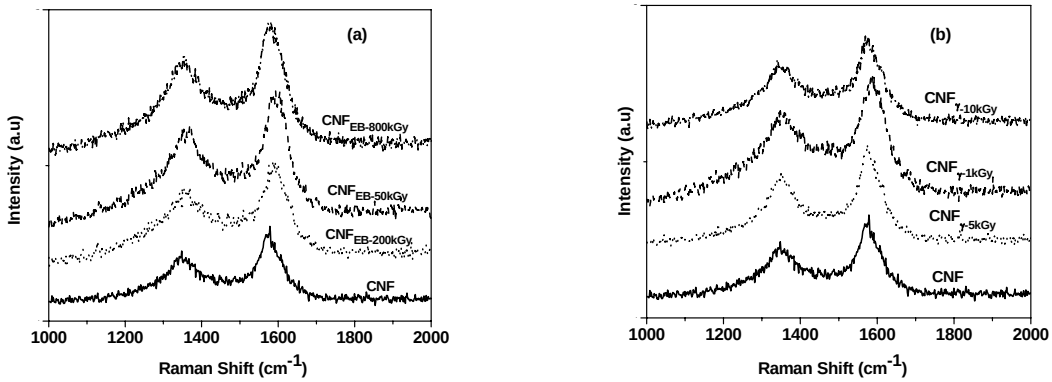

Figure 5. Raman spectra of (a) EB irradiated and (b) γ irradiated CNFs

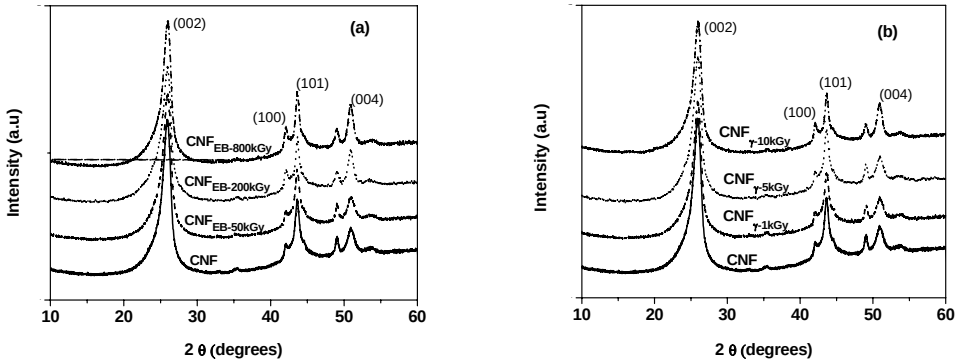

Figure 6. XRD spectra of (a) EB irradiated and (b) γ irradiated CNFs

Table 1. Surface functional components obtained from the deconvolution of C1s peak of CNFs

Sample	Peak assignment			
	C-C (%)	C-OH (%)	C=O (%)	O-C=O (%)
CNF	71.0	18.7	7.1	3.2
$CNF_{EB\text{-}800kGy}$	72.3	17.3	5.5	4.9
$CNF_{\gamma\text{-}1kGy}$	74.0	11.3	8.5	6.1

Table 2. Surface functional components obtained from the deconvolution of O1s peak of CNFs

Sample	Peak assignment		
	C-OH (%)	C=O (%)	O-C=O (%)
CNF	68.8	28.9	2.3
$CNF_{EB\text{-}800kGy}$	66.7	30.5	2.8
$CNF_{\gamma\text{-}1kGy}$	64.1	32.7	3.2

Table 3. Elemental composition on various CNF surfaces

Sample	C (%)	O (%)	O/C Ratio
CNF	87.6	12.4	0.14
$CNF_{EB\text{-}800kGy}$	86.5	13.5	0.15
$CNF_{\gamma\text{-}1kGy}$	89.2	10.8	0.12

Table 4. Disorder to order intensity ratios and crystallite sizes of various CNFs

Sample	$R=I_D/I_G$	Crystallite size (from Raman spectra), L_a =4.4/R, nm	Crystallite size (from XRD), nm
CNF	0.64	6.9	6.4
$CNF_{EB\text{-}50kGy}$	0.78	5.6	5.8
$CNF_{EB\text{-}200kGy}$	0.78	5.6	5.6
$CNF_{EB\text{-}800kGy}$	0.77	5.7	5.6
$CNF_{\gamma\text{-}1kGy}$	0.78	5.6	6.0
$CNF_{\gamma\text{-}5kGy}$	0.77	5.7	5.8
$CNF_{\gamma\text{-}10kGy}$	0.78	5.6	5.8

Barrier properties of maleated natural rubber / clay nanocomposites developed by masterbatch technique

Vijayalekshmi V. [1]*, George K.E. [1#], Pavithran C. [2]

[1] Department of Polymer Science & Rubber Technology, Cochin University of Science & Technology, Kochi- 682 022, Kerala, India
[2] National Institute for Interdisciplinary Science and Technology, (NIIST, CSIR) Thiruvananthapuram-695 019, Kerala, India

Email: kegeorge@cusat.ac.in

Abstract

10% Maleated natural rubber masterbatch was used for preparing natural rubber based nanocomposites.The nanoclay loading was taken up to 7 weight %.The swelling resistance and ozone resistance seems to be good by the addition of nanoclay.Air permeability shows a decrease in clay filled nanocomposites.

Introduction

Polymer/clay nanocomposites have attracted significant interest in the last decade, since they show extraordinary advantages in the mechanical, thermal, optical, barrier, swelling resistance, flame retardant and physicochemical properties when compared to the pure polymer.[1-2] In rubber, clay behaves as an effective reinforcing agent showing a stronger reinforcing effect than the carbon black while retaining the elasticity of the elastomer. In recent years, organic-inorganic nanocomposites have attracted great interest because they frequently exhibit unexpected hybrid properties synergistically from the two components[3,4].Polymer nanocomposites are a class of reinforced polymers with low quantities of nanometric-sized fillers which give them improved properties[5, 6]. Being highly unsaturated, natural rubber is easily attacked by heat, oxygen, ozone and chemicals leading to degradation of polymer chains and deterioration of properties. In this study the ability of clay layers to improve the swelling, oil and ozone resistance, and the air permeabily of MA-g-NR masterbatch is examined as a function of clay content.[3]

Materials and Methods

ISNR -5 grade natural rubber [Mooney viscosity (1+4) at 100˚C =85.5] was supplied by the Rubber Research Institute of India, Kottayam.The organically treated nanoclay (Cloisite 30B,d_{001} spacing =18.4 A˚) from Southern clay products, Texas was used as the nanofiller for composite preparation.

At first maleated natural rubber (MANR) nanoclay masterbatch was prepared and rubber compounds were prepared in a torque rheometer according to the ASTM standards. The properties were measured at different clay content (1, 3, 5, and 7). The compounds were vulcanized up to their optimum cure times at a temperature of 150˚C and at a pressure of 200 $kgcm^{-2}$ in a hydraulic press and the cure characteristics of the mixes were determined as per ASTM D2084-1995 using a Rubber Process analyzer (RPA 2000-Alpha Technologies). Swelling studies were carried out by immersing vulcanized samples of 2cm diameter and 1mm thickness in airtight test bottles containing about 20ml of solvent and automobile oil maintained at constant temperature. The mass of the swelled sample was determined periodically until no further increase in solvent uptake was detected. The air permeability of the samples were tested by

conducting the Manometric gas Permeability Testing in a Lyssy Manometric Gas Permeability Tester, L100-2402. Vulcanised sheets of ≈ 2mm were used for the study. Ozone resistance of the samples were tested in a ozone test chamber (MAST,USA).The composites after exposure to ozone for 24 hours and the time for the crack intiation of various samples on ozone ageing was noticed.

Results

Swelling studies

Swelling in toluene

The mol percent uptake of the sample is calculated from the diffusion data.

Q_t = (Wt of the solvent sorbed at a given time)/(Molwt of solvent)
(Initial wt of the rubber specimen X 100)

Sorption curves of the composites which are obtained by plotting Q_t (mole% uptake/100g of the solvent) against time as shown in Figure 1.

It can be seen that, upon the addition of nanofiller, with in the matrix to a particular level, the swelling rate decreases and there after any considerable change is not noticed .The decrease in swelling can be ascribed in terms of the tortuosity of the path and the reduced area of transport in presence of nanofillers.

Swelling in oils

The swelling resistance of the nanoclay filled composites in different oils was studied by swelling a cut sample in oil for constant weight. The swelling index is shown in figure 2.

In the case of transformer oil, hydraulic oil and engine oil the swelling index is reduced from 65 to 53.09%, 72.81 to 64.98 and 54.76 to53.56 respectively.

The air permeability values of the composites are given below in table .1

The air permeability decereases substantially by the incorporation of 5 % filler loading.

The reduction in air permeability is due to the improved polymer filler interaction. As the inter layer distance increases permeation resistance also increases.

The ozone samples after subjected to ozone radiation for 8 hours and 3.5 hours are shown in figures 3a and 3b.

Fig .3a and 3b shows the ozone resistance of nanocomposites

A crack is intiated in gum sample after 3.5 hours while in the case of 5% nanoclay filled sample the crack initiated only after 8 hours.

Conclusions

The preparation of natural rubber-clay nanocomposites using 10% maleated rubber and using a masterbatch seems to be a promising one.The sample shows good swelling resistance, oil resistance and ozone resistance.The air permeability is also reduced by adding the nanoclay.

References

1. Mark,J.E; Ceramic reinforced Polymers and Polymer-modified Ceramics, Polymer Eng.Sci. 1996, 36, 2905.

2. Calcagno,C.I.W.; Mariani, C.M; Teixeira, S.R.; Mauler, R.S. Polymer (2007), 48, 966.

3. Schmidt, H. In Polymer based Molecular Composites; Schaefer D. W.; Mark, J. E. Eds.; Material Research Society: Pittsburgh, 1990, P.3.

4. Beecroft, L. L.; Ober, C.K. chem. Mater 1997, 9,1302

5. Jang, L.; Kim,E.; Jin –san yoon , H.S . JAPS, (2005), 98,1229.

6. Chiu, F.C.; MouLa, S.; Chen,Y.L.; Lee, T.H. polymer. 2005, 1160.

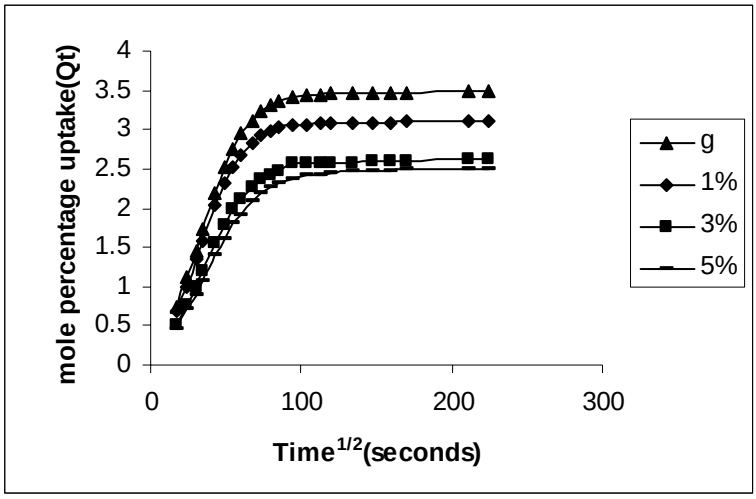

Fig. 1 Q_t (mol%) vs $t^{1/2}$ for MANR-NR /clay composites at 30^0C in toluene

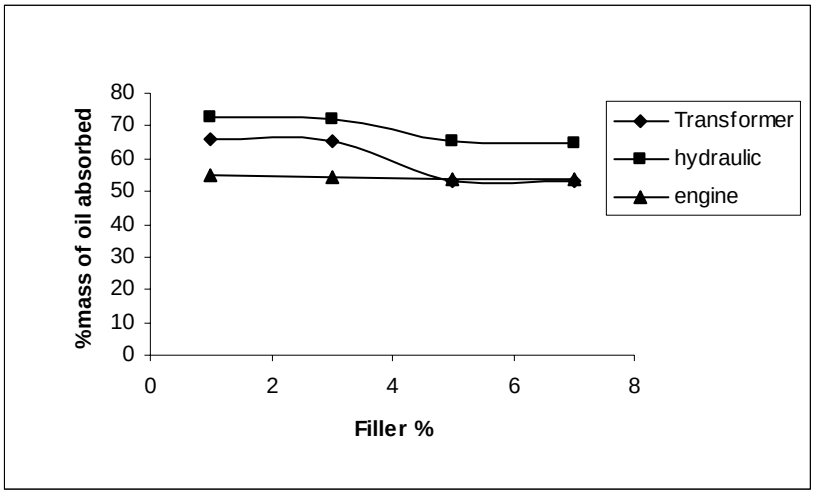

Fig.2 percentage mass of oil absorbed Vs Filler %

Sample	Permeability (mL/m^2x day)
Gum (NR)	321.23±17
1% filler	220.77±20
3% filler	210.77±21
5% filler	164.56±29
7% filler	169.26±14

Table .1 Variationof filler loading Vs air permeability of nanocomposites

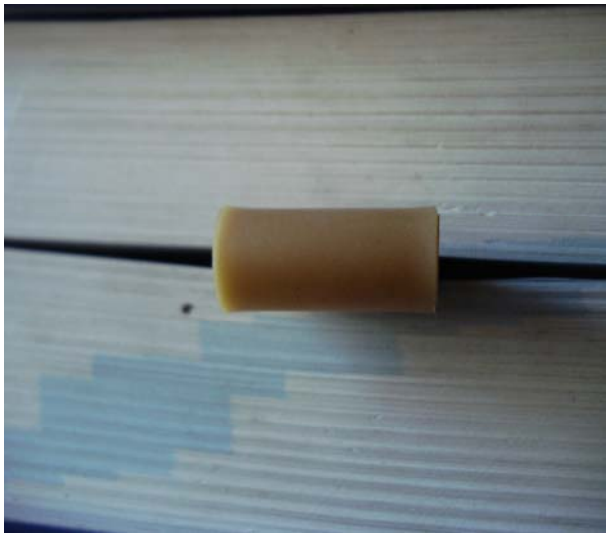

Fig.3a 5%nanoclay loading after 8 hours

Fig 3b NR gum after 3.5hours

Pine apple leaf fibre (PALF) reinforced polypropylene nanocomposites

M. Biswal[1], S. Mohanty [2] and S.K. Nayak [2*]
Laboratory for Advanced Research in Polymeric Materials
[1]Central Institute of Plastic Engineering and Technology, Bhubaneswar-751024, India.
[2]Central Institute of Plastic Engineering and Technology, Chennai-600032, India.
Email: drsknayak@gmail.com

Abstract
Polypropylene nanocomposites reinforced with Pine Apple Leaf Fibre (PALF) were compounded using Haake Rheocord 9000. Variation in mechanical properties, crystallisation behaviour, water absorption and thermal stability with the addition of nanoclay in Polypropylene/PALF composites were investigated. It was observed that the tensile, flexural and impact properties of Polypropylene increases with the increase in fiber loading from 10-30 wt%. Composites prepared using 30wt% PALF and 5wt% MAPP exhibited optimum mechanical performance with an increase in Tensile strength to 31%, Flexural strength to 45% as compared with virgin PP. Further, incorporation of organically modified nancolay additionally increases the mechanical performance in the composites. An increase of 20% in Tensile, 24.3% in Flexural strength was observed in case of PP/PALF/MAPP composites which is probably due to intercalated morphology. However, addition of nanoclay decreased the impact strength of MAPP treated PP/PALF composites to about 7.5%. Dynamic Mechanical Analysis (DMA) data showed an increase in Storage Modulus (E') and damping factor (tanδ), presenting a strong influence between the fibre/nanoclay and coupling agent. DSC, TGA/DTG thermogram also displayed improved thermal properties as compared with virgin Polypropylene. Morphological studies evaluated from SEM revealed improved interfacial adhesion between the fibres/nanoclay and PP matrix. WAXD studies indicate an increase in d-spacing from 22.4 A^0 in Cloisite 20A to 40.1 A^0 in PP/PALF nanocomposite due to improved intercalated morphology.
Keywords- PP, Nanocomposites, SEM, TEM, XRD

Introduction
Pine apple leaf fiber (PALF) is a multi-cellular and lignocellulosic material extracted from the leaves of plant *Ananas cosomus* belonging to the *Bromeliaceae* family by retting. PALF has a ribbon-like structure and is cemented together by lignin, pentosan-like materials, which contribute to the strength of the fiber. The excellent mechanical properties of PALF associated with high cellulose content and low microfibrillar angle have been taken into consideration for enhancing strength and performance characteristics in the polymer matrix [1,2]. However relatively few efforts have been taken in studying the reinforcing potential of PALF fibers in developing thermoplastic and thermoset composites using different processing techniques [3,4]. The effects of organoclays on the mechanical and physical characteristics of a natural fiber polymer composite have not been yet reported. There exist some hypotheses that indicate that the introduction of nanoclays in the fiber/polymer system can be satisfactory for enhancing the mechanical properties. The hydrophilic nature of both the natural fibres and the silicates suggest a good compatibility of these two materials to each other. In the present investigation, an effort has been made to evaluate the performance characteristics of PP/PALF fiber reinforced composites filled with organically modified nanoclays. Maleic anhydride grafted PP (MA-g-PP) has been used as the coupling agent to improve the interfacial bonding between the fibers and PP matrix. Variation in mechanical properties of PP/PALF composites as a function of nanoclay loading has been evaluated. The composites samples are also subjected to DMA measurements to evaluate the glass transition temperature (Tg), stiffness, and damping properties under specific periodic stress. The fractured surface and interfacial adhesion morphology of composites were also observed using scanning electron microscopy (SEM) and transmission electron microscopy (TEM). Thermal stability of samples has been studied employing DSC and TGA thermograms. Water absorption and aging behavior were also investigated to evaluate the extent of mechanical degradation in the composites with ageing.

#Corresponding Author:- drsknayak@gmail.com, Fax-191-44-22254787

Experimental

Materials

Isotactic PP (H110MA), MFI:11g/10min and density: 0.91g/cc, obtained from M/s Reliance Industries Ltd. India, has been used as the base polymer matrix. Cloisite 20A (C20A), having CEC of 95meq/100g clay, procured from M/s Southern clay products, Inc. (Gonzales, Texas) has been used as nanoclay. Epolene® G-3003 having density 0.91g/cc and acid number 8 with Mw 26,000 procured from M/s Eastman Chemicals Germany was used as compatibilizer. Pineapple leaf fiber (PALF, pinus sp.) of 50μm diameter, was procured from SITRA, Coimatore (India), was used as a reinforcing agent.

Preparation of PP/PALF/clay Nanocomposites

The fibers were detergent washed and dried in vacuum oven at 70^0C for 24 hrs and cut to 6 mm length prior to composite preparation. Compounding was carried out using a melt mixer (Haake Rheomix 9000 in two stages: Initially, PP/PALF composites containing different weight percentage of PALF fibers (10%, 20%,30%, 40%) with and without MA-g-PP were prepared at a temperature of 180^0C, mixing speed of 40rpm for a duration of 10 mins. In the second stage, MA-g-PP clay master batch was prepared at a screw speed of 50 rpm for 10 mins at 200^0C and the masterbatch was subsequently compounded with PP/PALF 30% composites Finally, these premixes were brought to room temperature and compression molded using Delta Malikson Pressman 100T(India) compression molding machine at 190^0C temperature to produce sheets of 3 ± 0.1 mm thickness.

Mechanical Properties

Tensile and Flexural properties were measured as per ASTM-D 638 and 790 using Universal Testing Machine (LR 100KLLoyds Instruments Ltd. UK). Notched izod impact strength of the specimens was evaluated using an Impactometer (Ceast, Italy) as per ASTM-D-256 with a notch depth of 2.54 mm and notch angle of 45^0. Tests for determination of mechanical properties were carried out in a standard temperature 23 ± 2^0c and 50 ± 2% RH.

Thermal Characterization

The melting, crystallization and thermal stability of have been studied using Differential Scanning Calorimetry (Perkin-Elmer Diamond DSC, USA) and Thermogravimetric analysis (Perkin –Elmer Pyris-7 TGA, USA), respectively.

Wide angle X-Ray diffraction (XRD)

WAXD analysis was carried out using Philips X'Pert MPD (Japan), which had a graphite monochromator and a Cu Kα radiation source operated at 40kv and 30 mA.

Scanning Electron Microscopy

The SEM of tensile fractured composite specimens was carried out using JEOL-JSM T330A (Germany). The samples were sputtered with platinum and were dried for half an hour at 70^0C in vaccum, prior to study.

Dynamic mechanical properties

The dynamic mechanical behavior of the samples was studied using Dynamic Mechanical Thermal Analyzer (NETZSCH DMA 242).

Results and Discussion

Mechanical Properties

The mechanical properties of PP/PALF composites at variable weight percentage of PALF fibers and nanoclay are represented in table 1. It is evident that with an increase in the PALF fiber content from 10-30% there is a linear increase in the mechanical properties of the composites. Nearly 31% increase in the tensile strength, 45% in flexural strength was observed with the incorporation of fiber. A similar increase in tensile and flexural modulus was also observed. However, incorporation of PALF fibers resulted in the decrease in the impact strength of the composites from 23.25 J/m to 19.11 J/m respectively, which may be due to non-uniform dispersion of fiber in the matrix. Further, addition of MA-g-PP resulted in significant increase in the mechanical properties of PP/PALF composites [4-5]. The composites prepared at 30% PALF loading and 5 wt% of MA-g-PP exhibited optimum

mechanical strengthwith an increase in tensile strength to 44%, flexural and impact strength to 36 and 67% respectively as compared with PP/PALF composites without MA-g-PP. As observed from table 2, with incorporation of nanoclay from 1-3 wt%, the tensile and flexural strength of PP/PALF composites also increases to 20 and 24.3% between 1 to 3 wt% of clay loading. Similarly the tensile and flexural modulus showed a linear increase with the increase clay content. However addition of nanoclay decreased the impact strength of MA-g-PP treated PP/PALF composites to about 7.5%. Presence of 5 wt% of MA-g-PP resulted in further improvement in mechanical properties as compared with PP/PALF nanocomposites without MA-g-PP. This indicates that the multistage process used in the fabrication of nanocomposites i.e. melt blending of MA-g-PP with nanoclay followed by addition of PP/PALF composites resulted in exfoliation of clay galleries.

Thermal Characterization

Figure 1 and 2 shows the heating and cooling curves of DSC analysis of virgin PP, 5 wt% MA-g-PP compatibilised; PP/PALF composites along with PP/PALF/C20A nanocomposites. Comparing the DSC cooling thermogram of pure PP with respect to PP/PALF composites, it is observed that the T_c of virgin PP was about 104.43 ^{0}C, with a degree of crystallinity Xc of 51.1%. Incorporation of 5 wt % MA-g-PP in PP/PALF composite matrix results in an increase in Tc to 110.74^{0}C which may be attributed to the presence of PALF fibers that restricts the chain mobility of the matrix chains. However, the degree of crystallinity X_c decreased to 40.6%, suggesting that presence of MA-g-PP reduced the perfection of PP crystals. Nevertheless, addition of MA-g-PP to PP/PALF/C20A system, increased the crystallization rate suggesting that exfoliated clay and PALF with aid of MA-g-PP acts as nucleating agent and lowers PP crystal perfection. The DSC melting temperature of the matrix polymer in PP/PALF composites however decreased due to the lower melt viscosity as compared to virgin PP. Further, incorporation of nanoclay additionally reduced the melting point of the composite matrix while increasing its crystallinity level which clearly indicates that the nanoclay acts as a nucleating agent promoting nucleation sites. The TGA thermograms of virgin PP, PP/PALF composites, PP/PALF/C20A nanocomposite with MA-g-PP is represented in figure 3. It is evident that, the thermal degradation of virgin PP started at 246.2^{0}C and 100% degradation was noticed at 426^{0}C. Incase of PALF fiber, dehydration and degradation of lignin occurred around 40-275^{0}C and maximum percentage of cellulose was found to decompose at a temperature of 380^{0}C from literature. This decomposition temperature range was comparatively less than that of virgin PP. PP/PALF composites with MA-g-PP exhibited an initial decomposition peak between 249^0 and 342.3^{0}C with a maximum of 312.6^{0}C corresponding to a weight loss of about 20%. At 426^{0}C, PP got completely decomposed while in the composites a charred residue of carbonaceous product of 2.1% was left. However, with the incorporation of nanoclays there was substantial enhancement in the thermal stability of PP/PALF composites with an initial degradation decomposition peak at 252.6^{0}C and final decomposition peak at 451^{0}C.

Wide angle X-Ray Diffraction (WAXD)

Figure 4 displays the Wide-angle X-ray diffraction patterns of Cloisite 20A, PP/C20A and PP/PALF/20A nanocomposites. The XRD pattern of modified clay C20A reveals a reflection peak at $2\theta = 4^0$ with a d-spacing of 24.2A^0. PP/C20A nanocomposites displayed a shift of diffraction peak to $2\theta = 3.15^0$, with d-spacing of 28A^0 thus indication of intercalated structure. Further the incorporation of nanoclay to PP/PALF composites resulted in further shifting of the diffraction peak to lower angles at $2\theta=2.2^0$ with d-spacing of 40.1A^0. This increase in interlayer distance of C20A with the incorporation of PALF is probably due to strong shearing forces that resulted during processing of PP/PALF/C20A nanocomposites. Further, the XRD patterns of MA-g-PP compatibilized PP/PALF/C20A nanocomposites revealed absence of diffraction peak within the experimental range, thus indicating exfoliation of the clay galleries.

Scanning Electron Microscopy (SEM)

The morphology of the tensile fractured surfaces of PP/PALF composites without MA-g-PP and PP/PALF/C20A nanocomposites without MA-g-PP is depicted in figure 5 and 6 respectively. Figure 5, reveals extensive fiber pullouts and wide gaps between the fiber and PP matrix in case of PP/PALF composites without MA-g-PP, whereas in presence of MA-g-PP compatibilizer, the fibers were well coated and embedded within the PP matrix shown in figure 6. Incase of PP/PALF/C20A (figure 6) nanocomposites samples; addition of nanoclay to PP/PALF composites in presence of MA-g-PP

exhibited improved dispersion of PALF fibers within the PP matrix with considerable reduction in the gaps between the fiber and the matrix. However SEM micrographs of the PP/PALF composites and PP/PALF/C20A nanocomposites with MA-g-PP could hardly show any phenomenal morphological distinction.

Dynamic Mechanical Analysis

The variation of storage modulus as a function of temperature for different samples is graphically represented in figure 8. It is evident that with the addition of PALF fibers, the modulus of the virgin matrix increased. This behaviour is primarily attributed to the reinforcing effect imparted by the fibers that allowed a greater degree of stress transfer at the interface. A comparative higher magnitude of E' was observed with the PP/PALF fiber reinforced nanocomposites over the entire range of temperature, thus showing improved dispersion of the nanoclays within the matrix. In all the samples the storage modulus decreased with the increase in temperature and exhibits a significant fall between –20 to 10^0C, which probably due to glass transition region of the matrix. In case of virgin PP the storage modulus drops steeply on increasing the temperature due to increased segmental mobility of the polymer chains. However incorporation of PP/PALF fibers and nanoclay reduces the rate of fall of the matrix modulus with temperature thus indicating higher stability of PP in the fiber reinforced nanocomposite system.

Conclusion

The mechanical, thermal, dynamic mechanical and morphological properties of the PP/PALF nanocomposites has been investigated. It was observed that the composites prepared at 30 wt% of fiber loading with 5% MA-g-PP showed optimum mechanical performance. Incorporation of 3 wt% of cloisite 20A additionally increases the mechanical and thermal properties of PP matrix. Based on the observations from the experimental findings, it can be concluded that PALF reinforced PP matrix along with nanoclay shows the ability for high performance applications.

References

1. J. George, S.S. Bhagawan, Sabu Thomas, " Mechanical properties of pine apple leaf fiber reinforced polyester composites » J. Appl Polym Sci. Pp 64,1997.
2. L.U. Devi, Kuruvila joseph, K.C. Manikanada Nair and Sabu Thomas, Ageing studies of pineapple leaf fiber reinforced polyester composites », J. Appl. Polym Sci ., pp 94,2,503,2004.
3. Wong, S.; Shanks, R. A.; Hodzic, H. Macromol Mater Eng2004, 289, 447.
4. A.N. Shah and S.C. Lakkad, Fiber Sci Technol.15,pp 41-46,1981.
5. J. George, S.S. Bhagawan, Sabu Thomas, " Mechanical properties of pine apple leaf fiber reinforced polyester composites » J. Appl Polym Sci. Pp 64,1997.

Table 1 : Mechanical Properties of PP anf PP/PALF Nanocomposites

Sample	Tensile strength (Mpa)	Tensile Modulus (MPa)	Flexural strength (Mpa)	Flexural Modulus (MPa)	Impact Strength (J/m)
Virgin PP	17.92 (.03)	2143.88(.14)	29.40(.65)	2770(.04)	23.25(.21)
PP/PALF (90:10%)	20.14 (.05)	2437.18(.24)	31.04(.72)	2814(.07)	22.84(.34)
PP/PALF (80:20%)	23.68 (.04)	2619.00(.36)	35.94(.54)	2921(.08)	20.06(.36)
PP/PALF (70:30%)	25.97 (.06)	3812.00(.23)	38.51(.38)	3033(.02)	19.11(.23)
PP/PALF (60:40%)	23.62 (.08)	3143.78(.16)	37.02(.61)	2817(.06)	18.92(.18)
PP/PALF/MA-g-PP (69:30:1%)	28.03 (.02)	3916.14(.34)	40.12(.85)	3097(.05)	24.28(.37)
PP/PALF/MA-g-PP (67:30:3%)	30.14 (.03)	4201.32(.31)	46.82(.52)	3110(.03)	28.37(.31)
PP/PALF/MA-g-PP (65:30:5%)	37.62 (.05)	4428.59(.19)	52.37(.54)	3217(.04)	31.91(.17)
PP/PALF/MA-g-PP/Clay (64:30:5:1%)	39.02 (.07)	5253.96(.21)	60.28(.66)	3820(.07)	30.12(.21)
PP/PALF/MA-g-PP/Clay (63:30:5:2%)	42.67 (.03)	5723.28(.24)	63.44(.78)	4196(.06)	30.54(.24)
PP/PALF/MA-g-PP/Clay (62:30:5:3%)	45.14 (.04)	6448.12(.23)	65.01(.84)	4458(.03)	29.52(.29)

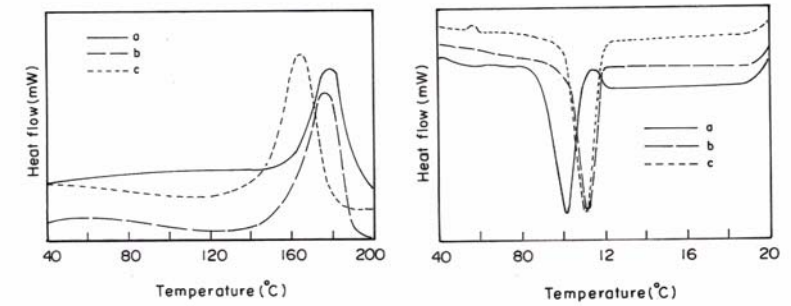

Figure 1 & 2: DSC Heating curve of a. PP (V), b. PP/PALF/MA-g-PP c. PP/PALF/MA-g-PP/C20A

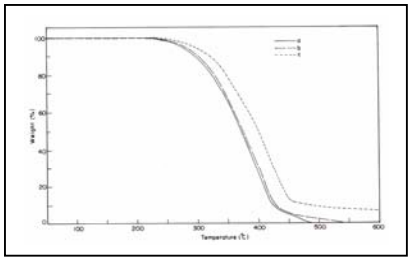

Figure 3: TGA of a. PP (V), b. PP/PALF/MA-g-PP c. PP/PALF/MA-g-PP/C20A

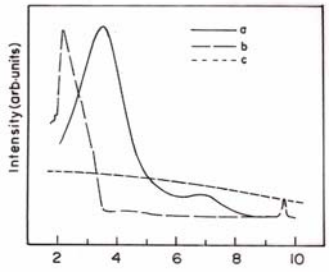

Figure 4: WAXD of a)C20A b)PP/PALF/C20A c)PP/PALF/MA-G-PP/C20A

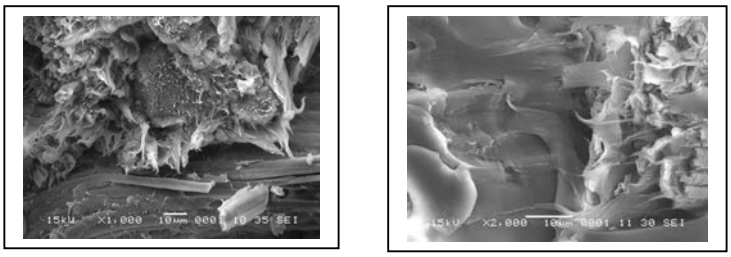

Figure 5 & 6: SEM Micrographs of a) PP/PALF composites without MAPP b)PP/PALF/MA-g-PP/C20A

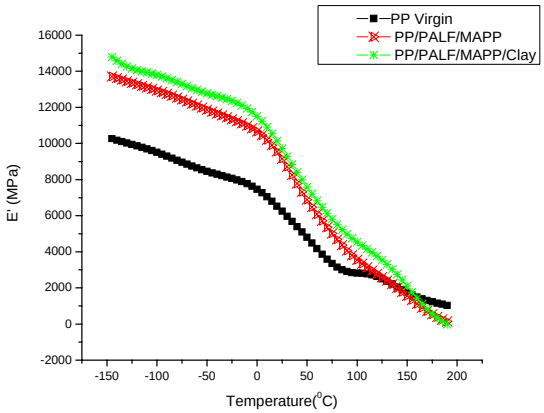

Figure 7: Variation of Storage Modulus with Temperature

Short nylon fiber – natural rubber composite prepared by latex masterbatching: cure characteristics and mechanical properties

***Bipinbal P.K and Sunil K. N. Kutty#**
Department of Polymer Science and Rubber Technology, Cochin University of Science and Technology, Kochi-22, Kerala, India.

Email: sunil@cusat.ac.in

Abstract

Short nylon fiber -natural rubber composites was developed by, a novel method in which short fibers chopped to approximately 6 mm were incorporated in the latex stage and processed into sheet form. By this method mixing cycle time was reduced without compromising the fiber dispersion. Fiber breakage during mixing was reduced. Cure characteristics and mechanical properties of the new composites, when compounded with a dry bonding system based on hexamethylenetetramine, resorcinol and hydrated silica (HRH) were evaluated. Out of the mechanical properties studied modulus, tensile strength and abrasion resistance showed improvement compared to conventional composites. Tear strength, resilience and compression set were similar to the conventional composites.

Introduction

Short fibers have been used as reinforcing fillers in many rubber compounds to get products with improved properties [1-10]. It became very popular due to the possibility of obtaining anisotropic properties, ease of processing and economy [1-3]. In rubber compounding fillers are incorporated on a two roll mixing mill or in an internal mixer. Fillers being the major volume component, it takes more time to disperse uniformly. Consequently it takes up about 60 – 70% of the total energy input of the mixing operation. Any reduction in the energy requirement, even to the extent of 10-20% can give reduced mixing time and hence improved production volume. This calls for developing less energy intensive and less time consuming processes for incorporation and distribution of fibers in the rubber matrix. One method developed by us is to incorporate fibers in the latex stage and then to process into sheet rubber. The composite can then be compounded on two–roll mill or internal mixer. In this study the cure characteristics and mechanical properties of the short nylon fiber- natural rubber composites, prepared by this novel route and comparison of these properties with those of the conventional composites are presented.

Experimental

Materials Used

Single clone (RRII-105) natural rubber field latex was procured locally. Crumb rubber (ISNR-5) was obtained from the Rubber Research Institute of India, Kottayam. Nylon fibers manufactured by SRF Ltd., Chennai, were chopped to approximately 6mm length. Zinc oxide, stearic acid, HS (1,2-dihydro2,2,4-trimethylquinoline), MBTS (mercptobenzthiazylsulfenamide), TMTD (tetramethyl thiuram disulfide), sulfur, hexa (hexamethylenetetramine), resorcinol and hydrated silica used were of commercial grade.

Processing

The field latex was diluted to 12.5 dry rubber content (DRC). A sandwich of alternating layers of latex and short fibers cut to 6 mm length was made and the latex coagulated using dilute formic acid. The coagulum obtained was squeezed between rollers to remove water. The sheet obtained was dried in an air oven at 40°C for three days. Fiber loading was adjusted to get 10, 20

and 30 phr fiber in the final composites. The composites were then processed like conventional sheet rubber.

Formulation of the mixes is given in table 1. The mixes were prepared according to ASTM D 3182 on a laboratory size two-roll mixing mill. Fibers were extracted by dissolving out the matrix in a solvent. The lengths of fibers were determined by viewing fibers through a optical stereo microscope and taking photographs. The length distribution of fibers was determined.

The energy for mixing was determined by mixing in a Thermo Haake Rheomix. The mixing cycle was limited to 5.5 minutes at 80°C with a fill factor of 0.75. The fibers were incorporated at 1.5 minute and the torque was continuously measured for the remaining time of 4 minutes. Rotor speed was kept constant at 30 rpm during initial loading time of 1.5 minute and then at 60 rpm for the remaining running time of 4 minutes. The integrated energy input for the free mixing cycle was noted.

Cure characteristics were determined by using Rubber Process Analyser model RPA 2000 at 150°C. Fibers were oriented in the mill direction by passing through the tight nip in the mill at the end of the mixing process. The thin sheets obtained were cut in the required dimensions and stacked one above the other to the desired volume. The sheets were vulcanized at 150^0C under a pressure of 180 kg/cm2 in an electrically heated hydraulic press to their respective cure times. The samples obtained were tested for mechanical properties according to relevant ASTM standards.

Results and Discussions

Fig 1 shows the integrated energy input during the mixing process in the Rheocord mixer. For the latex stage composite energy input at any time is greater than the dry rubber composite. The higher energy for mixing is due to more restrained matrix resulting from better dispersion of fibers. As higher energy can be input in shorter time the total mixing time reduced without compromising the filler dispersion.

Fig 2 compares the fiber breakage during milling process. The figure shows that the average fiber length after mixing is larger in the case of latex stage compounding compared to the dry rubber compounding. This may be attributed to the reduced time of mixing in the case of latex stage compounds.

Cure characteristics

Cure characteristics of the compounds are given in Table 2.

Minimum torque

The minimum torque measured in RPA at 150ºC, which is a measure of minimum viscosity of the compounds, increases with fiber loading. The relatively higher viscosity of the latex stage composite may be attributed to higher average fiber length and low level of molecular breakdown due to shorter shear history.

Differential torque

Differential torque ie. maximum torque minus the minimum torque, increases with the fiber loading. This shows an increasingly restrained matrix with fiber loading. For the same fiber loading latex master batch and dry rubber compound show comparable differential torque.

Cure time & Scorch time

Cure time increases with fiber loading. Dry rubber composites show marginally higher cure time at all fiber loadings. Scorch time initially decreases and then remains almost constant with fiber loading. The cure and scorch behaviours show that at higher loadings of fiber there is retardation of cure rate. This may be due to the adsorption of curatives by the fibers making them unavailable for cross linking.

Mechanical properties

Tensile strength

Tensile strength in longitudinal direction initially decreases and then increases with the fiber content. Initial reduction is due to the interruption of stress crystallization of natural rubber by the short fibers. At higher fiber loadings the increased reinforcement will offset the reduction in stress crystallization. The latex stage composites show higher values than dry rubber composites. This is due to lower breakdown of fiber and matrix as a result of lower mixing cycle.

Modulus

The composites show an increase in modulus with fiber content. Latex master batch composites show better values than the dry rubber composites especially for 20 and 30 phr loadings. This is attributed to the reduced fiber breakage and lower molecular breakdown of matrix.

Tear strength

In the longitudinal direction the fibers are oriented perpendicular to the crack propagation. When the fiber content increases there will be more and more hindrance to the crack propagation as is evident from the increase in tear strength of the composites. For the same fiber loading, the values are comparable between latex and dry stage composites.

Elongation at break

Elongation at break decreases with fiber content. The reinforcing fibers progressively restrict the matrix resulting in a decrease in elongation at break. A sharp reduction in elongation is observed even at 10 phr of fiber loading.

Rebound resilience

Rebound resilience decreases with the increase in fiber content. The values are similar for both latex stage and dry stage composites.

Compression set

Compression set increases marginally with fiber content and then remains almost constant. In all compositions except 10 phr fiber loading, the latex masterbatch shows lower set values than dry rubber composites.

Abrsion resistance

Abrasion resistance is improved with the introduction of fibers. There is remarkable increase for latex masterbatch compounds compared to dry rubber, especially for 20 and 30 phr.

Conclusions

From the study following conclusions are drawn.

The natural rubber-short fiber composites prepared by latex stage master batching requires less mixing time for proper dispersion of fibers compared to the conventional composites. The fiber breakage during milling is reduced in the case of new method. . The composites prepared by the new technique show similar cure characteristics as of the conventional composites. Of the mechanical properties tested, modulus, tensile strength and abrasion resistance show better values indicating better reinforcement. Elongation at break is reduced. Tear strength, resilience and compression set show more or less similar values. The new method for the composite preparation is an efficient one to reduce the mixing time and hence to increase the production volume without compromising, and in most cases enhancing, the vulcanizate properties.

References

1. Chakraborty, S.K.; Setua, D.K.; De, S.K. Rubber Chem. Technol. 1982, 55, 1286
2. O' Connor J.E., Rubber. Chem. Technol., 1977, 50, 945.
3. Rajesh, C.; Unnikrishnan, G.; Purushothaman, E.; Sabu Thomas, J. Appl. Polym. Sci., 2004,92, 1023

4. Rajeev, R. S.; Anil K. Bhoumick, De, S. K.; Bandyopadhyay, S. J. Appl. Polym. Sci. 2003, 90(2), 544.
5. Coran, A.Y.; Hamed, P.; Goettler, L.A. Rubber Chem. Technol., 1976, 49, 1167.
6. Derringer,G.C.(1971).Short fibre elastomer composites.J.Elastoplast.3 , 230 –248.

6. Boustany, K.; Arnold, R.L. J. Elastoplast. 1976, 8, 160.
7. Coran, A.Y.; Boustany, K.; Hamed, P. Rubber Chem. Technol. 1974, 47, 396.
8. De S.K., White J.R (1996) Short fiber-polymer composites, Woodhead Publishing Ltd.
9. Seema A.; Kutty S. K. N J. Appl. Polym. Sci. 2006, 99, 532-539
10. Sreeja,T.D.;Kutty,S.K.N.(2003) Cure characteristics and mechanical properties of short nylon fiber reinforced natural rubber –reclaimed rubber blends.Polym. Plast.Technol.Eng., 42 (2),239 –252.

Table 1: Formulation of the Composites

Ingredients	A	B	C	D
NR*	100	100	100	100
ZnO	4	4	4	4
Stearic acid	2	2	2	2
HS	1	1	1	1
Fiber	-	10	20	30
Silica	1.6	1.6	1.6	1.6
Resorcinol	2.5	2.5	2.5	2.5
Hexa	1.6	1.6	1.6	1.6
MBTS	0.6	0.6	0.6	0.6
TMTD	0.2	0.2	0.2	0.2
Sulphur	2.5	2.5	2.5	2.5

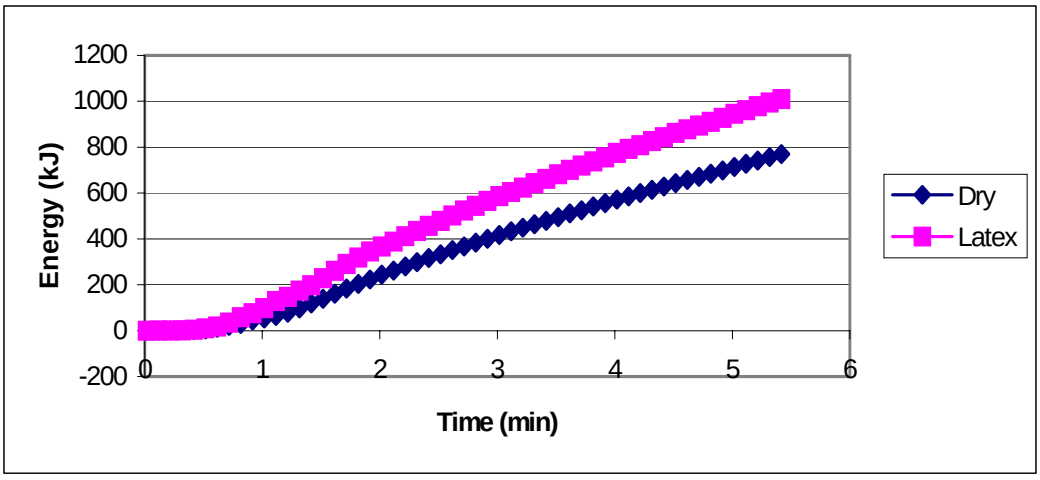
1200
1000
800
600
400
200
0
-200
Energy (kJ)
0
1
2
3
4
5
6
Time (min)
Dry
Latex

Fig 1

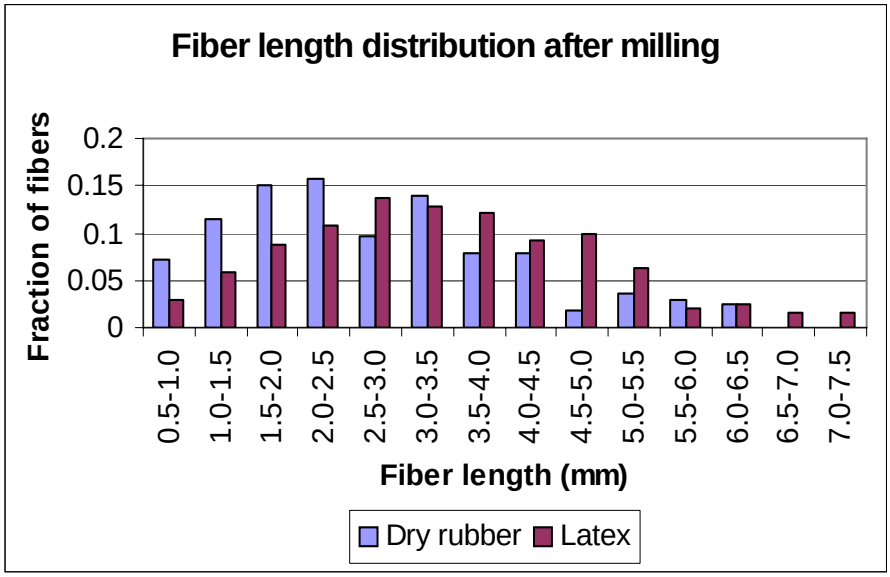
Fiber length distribution after milling
Fraction of fibers
0.2
0.15
0.1
0.05
0
0.5-1.0
1.0-1.5
1.5-2.0
2.0-2.5
2.5-3.0
3.0-3.5
3.5-4.0
4.0-4.5
4.5-5.0
5.0-5.5
5.5-6.0
6.0-6.5
6.5-7.0
7.0-7.5
Fiber length (mm)
Dry rubber
Latex

Fig 2

Table 2: Cure Charecteristics

	Minimum torque (dNm)		Differential torque(dNm)		Cure time (min)		Scorch time (min)	
Fiber (Phr)	Dry rubber	Latex	Dry rubber	Latex	Dry rubber	Latex	Dry rubber	Latex
0	0.025	0.029	3.515	3.693	5.77	4.99	1.36	0.9
10	0.02	0.035	4.494	4.662	5.79	5.51	1.01	0.86
20	0.045	0.049	5.979	5.426	6.08	5.75	1.00	0.97
30	0.069	0.094	7.198	6.849	6.39	6.16	0.98	0.92

Table 3: Mechanical Properties

	Tensile strength (N/mm^2)		Tear strength (Nm)		Elongation at Break (%)		Resilience (%)		Compression set (%)		Abrasion loss (cc)	
Fiber (Phr)	Dry rubber	Latex	Dry rubber	Latex	Dry rubber	Latex	Dry rubber	Latex	Dry rubber	Latex	Dry rubber	Latex
0	28.0	28.4	50.0	52.5	1084	1011	67	67	7.71	7.72	3.026	2.999
10	10.6	16.3	71.6	72.4	124	137	57	58	6.97	11.14	2.863	2.863
20	17.5	18.9	95.0	91.5	67	66	53	51	8.19	10.13	2.808	2.508
30	24.5	25.2	110.8	100.2	66	63	49	48	9.36	11.55	2.617	1.990

Preparation, properties and characterization of epoxidised natural rubber layered silicates nanocomposites

K.N.Madhusoodanan, Siby Varghese and K.T.Thomas
Rubber Research Institute of India, Kottayam - 686 009, Kerala, India

Email: madhuskn@gmail.com

Abstract

Polymer/layered silicate nanocomposites exhibit remarkable improvement in mechanical and barrier properties compared with the virgin polymers or their microcomposites. Nanoclay being organophilic are highly compatible with polymers especially with polar ones. Natural rubber (NR) being a non polar rubber has incompatibility problem. Epoxidised Natural Rubber (ENR), a polar form of rubber is expected to show high affinity and better performance with nanomaterials.

Epoxidised natural rubber nanocomposites were prepared by melt compounding of ENR having an epoxy content of 50 mole % at ambient temperature. Two grades of organically modified montmorillonite having layer distances of 2.1 nm and 1.85nm were used in this study. Accelerated sulphur curing system was used for the vulcanization of the nanocomposites. For comparison, commercial clay was included in this study and the filler loading was kept at 10 phr in all mixes. The cure characteristics and mechanical properties were evaluated. The dispersion of the silicate in the matrix was studied by and transmission electron microscopy (TEM). The addition of modified montmorillonite to the ENR reduced its cure time and scorch time. The maximum torque was higher for these composites. The montmorillonite filled composites showed better mechanical properties when compared to the reference material.The enhancement in properties was believed to be due to the partial exfoliation/ intercalation of the layered silicates in ENR. Among the two types of nanocomposites, the nanocomposite with montmorillonite having higher inter layer distance showed better mechanical properties.

Introduction

Nanocomposites are a new class of materials, which exhibit excellent barrier, mechanical, thermal, optical and physico-chemical properties, compared to the corresponding microcomposites. Nanocomposites can be categorized into three depending on how many dimensions of the dispersed particles are in the nanometer range. When all the diamensions are in the order of nanometers such as silica nanoparticles, they are called isodiamentional nanoparticles (1-3). Nanotubes or whiskers (4-6) are included in the second category where two dimensions are in the nanometer scale. The third type, characterized by only one dimension in the nanometer range are layered silicates nanocomposites. These materials are obtained by the intercalation of the polymers inside the galleries of layered silicates.

Several reports are available regarding the processing and properties of natural rubber/ organically modified layered silicate nanocomposites (7,8). However, NR being a non polar rubber is less compatible with organo silicates and their nanocomposites are inferior in some of the engineering properties. ENR, a polar form of rubber is expected to have high

affinity and better performance with nanomaterials. Hence, the objective of the present work is to evaluate the properties of ENR nanocomposites based on organically modified silicates.

Experimental

ENR used in the study was ENR-50 having an epoxidation level of 50 mol %. The organoclays used were octadecylammine modified (MMT-ODA)and methyl tallow *bis*-2-hydroxyehtyl quarternary ammonium (MMT-TMDA). The layer distance of MMT-ODA and MMT-TMDA were 2.10 and 1.85 nm respectively. For a comparision commercial clay was used. All the other ingredients were supplied by Bayer (India) Ltd.

The rubber compounds were prepared in a laboratory model two-roll mixing mill (David Bridge, England) of size 15 x 30 cm having a friction ratio 1:1.25, as per the formulation given in Table 1. The mixes were cured at 150^{o}C in an electrically heated hydraulic press to their respective cure time (t_{90}). The cure characteristics were measured using a moving die rheometer, Rheotech MD+. Alpha Technologies, USA. Tensile and tear properties were determined according to ASTM standards D 412 and D 624 on a Zwick 1474 universal testing machine at a crosshead speed of 500 mm/min. Hardness, resilience and compression set were tested as per the relevant ASTM standards and abrasion resistance was measured as per the DIN standards. Ageing studies were carried out as per the at 100 ^{0}C for 72 hours.

The dispersion of the silicates was studied by transmission electron microscope (TEM) TEM.Scanning were conducted using a LEO 912 Omega transmission electron microscope with an acceleration voltage of 120 keV. The specimens were prepared using an Ultracut E uiltramicrotome. The sections of about of 100 nm were cut with a diamond knife at -120 ^{o}C.

Results and Discussion

Cure characteristics of the compounds

Table 2. shows the cure characteristics of the compounds. Addition of modified silicates (MMT-ODA and MMT-TMDA) accelerated the vulcanization. This may be due to the action of modifiers used in the silicates (9-11). This could lead to a reduction in cure time. Consequently the scorch time is also low for modified silicate incorporated compounds. The M_H-M_L value which is a measure of the modulus is comparatively high for the modified silicates filled composites.

Dispersion of the silicates

Figure 1 shows the TEM micrographs obtained for the ENR composites containing MMT-ODA and MMT-TMDA and commercial clay. MMT-ODA showed a exfoliated structure in the photographs than the MMT-TMDA.

Mechanical properties

Mechanical properties of the different silicate filled composites are given in Table 3. Tensile strength follows the order MMT-ODA > MMT-TMDA > commercial clay > Gum. Due to the initial high interlayer distance of MMT-ODA intercalation between the galleries is rather easy and the degree of exfoliation is high than MMT-TMDA nanocomposites. This exfoliation causes significant increase in surface area. Hence the MMT-ODA incorporated composites

recorded high tensile strength. MMT-ODA also showed maximum modulus for 100% and 300% elongation.

The hardness values of the MMT-ODA incorporated composites showed higher values because of finely exfoliated silicate layers. Hardness and modulus of the commercial clay filled composite showed lower values than the modified silicate. This may be due to the larger particle size and low level of dispersion of commercial clay in ENR.

MMT-ODA filled composites showed the lowest elongation at break whereas the gum sample, commercial clay and MMT-TMDA composites showed comparatively high elongation at break. The values of tear strength, a useful tool for characterizing nanocomposites, were highest for MMT-ODA and MMT-TMDA filled composites. It can be seen that commercial clay has little effect on tear strength. Din abrasion loss is less in the case of MMT-ODA and MMT-TMDA filled composites than the control and commercial clay. This improved abrasion resistance in the modified silicate filled composites is due to the improved rubber-filler interaction generated via intercalation/exfoliation. The intercalation and exfoliation of the modified silicate increased the surface area of the filler leading to more interaction between the filler and the matrix.

Compression set values of the MMT-ODA and MMT-TMDA filled composites are found to be lower than that of commercial clay filled composite. The lower compression set values indicate a more restrained matrix. The higher compression set values of commercial clay filled composites may be due to the reduced elasticity of the matrix. Rebound resilience also showed the same trend as in the case of elongation. The resilience values are in the order gum >commercial clay > MMT-TMDA > MMT-ODA. Heat generation under dynamic condition is higher in MMT-ODA filled composites. This may be due the increased polymer filler interaction. Heat build up shows the reverse trend. The organoclay filled composites showed high heat build up values.

Ageing properties of the composites are given in Table 4. The MMT-ODA filled composites showed superior ageing resistance compared to the MMT-TMDA and commercial clay filled composites.

Conclusions

The addition of MMT-ODA and MMT-TMDA to ENR decreased the cure time and scorch time of the compounds whereas in the case of commercial clay there is not much change compared to the gum compound. Mechanical properties such as tensile strength, modulus, hardness, abrasion resistance, tear strength etc. of ENR improved by the addition of modified layered silicate. The improvement in the mechanical properties of the modified silicates is due to the exfoliation of the silicates which causes several fold increase in surface area. The TEM studies showed that modified layered silicates are partially exfoliated, partially intercalated and partially confined in the composites.The ageing resistance of ENR is also found to be improved by the addition of MMT-ODA.

Referebces

1. Mark, J. E., Polym Eng Sci 1996, 36, 2905.
2. Reynaud, E., Gauthier, C., Perez, J., Metall/ Cah.Inf Tech 1999, 96, 169.
3. von Werne, T., Patten, T.E., J Am Chem Soc 1999, 121, 7409.

4. Calvert, P., Carbon nanotubes, 1997, 277.
5. Favier, V., Canova, G.R., Shrivastava, S.C., Cavaille, J. Y., Polym Eng Sci 1997, 37, 1732.
6. Chazeau, L., Caville, J.Y., Canova, G.R., Dendievel, R., Boutherin, B., J Appl Polym Sci 1999, 71, 1797.
7. Wilson jr., O.C., Olorunyolemi, T., Jaworski, A., Borum, L., Young, D., Siriwat, A., Dickens, E., Oriakhi, C., Lerner, M.M., Apply Clay Sci 1999, 15, 265.
8. Oriakhi, C.O., farr, I.V., Lerner, M.M., Clays and Clay Minerals, 1997, 45, 194.
9. Varghese, S., Karger-Kocsis, J., J Apply Polm Sci 2004, 91, 813.
10. Varghese, S., Karger-Kocsis, J., Gatos, K.G., J Apply Polm Sci 2004, 91, 813.
11. Mousa, A., Karger-Kocsis, J., J Macromol Mater Eng 2001, 286, 260.

Table 1.Formulation of the mixes

Ingredients	phr
ENR-50	100
Zinc oxide	5
Stearic acid	2
Sodium carbonate	0.3
Antioxidant HS (2,2,4-trymethy 1,2-dihydroquinoline)	1
CBS (*N* –cyclohexyl benzothiozole- 2 –sulphenamide)	1.5
Sulphur	1.5
*Filler	10

* Commercial clay (CC), MMT-ODA, MMT-TMDA

Table 2. Cure characteristics of the compounds

Parameters	Gum	CC	MMT-TMDA	MMT-ODA
Maximum torque,M_H (dNm)	7.0	7.9	8.30	8.52
Minimum torque, $M_{L,}$ (dNm)	0.33	0.30	0.47	0.41
Optimum cure time, t_{90} (min)	8.01	6.7	3.37	3.01
Scorch time, t_{s2} (min)	3.42	3.44	2.23	2.11
M_H - M_L	6.69	7.6	7.83	8.11

Table 3. Mechanical properties of the ENR composites

Parameters	Gum	CC	MMT-TMDA	MMT-ODA
Tensile strength, MPa	20.6	20.8	22.3	24.7
Modulus, 100%	0.9	1.2	1.6	1.8
Modulus, 300%	1.7	2	3.8	4.5
EB, %	658	656	656	646
Tensile strength, N/mm	29.8	31.0	35.2	38.9
Hardness, Shore A	42	46	54	56
DIN abrasion loss, mm^3	162	160	110	103
Compression set, %	21	26	22	22
Resilience, %	78.3	75.7	68.8	67.3
Heat build up, $\Delta T\ ^oC$	6	12	16	16

Table 4. Retension (%) of mechanical properties after ageing at 100 ^{o}C for 72 h.

Parameters	Gum	CC	MMT-TMDA	MMT-ODA
Tensile strength	20	10	30	41
Modulus, 100 %	-	31.4	40.0	46.2
Modulus, 300 %	-	-	-	45.1
EB	37	37	41	52

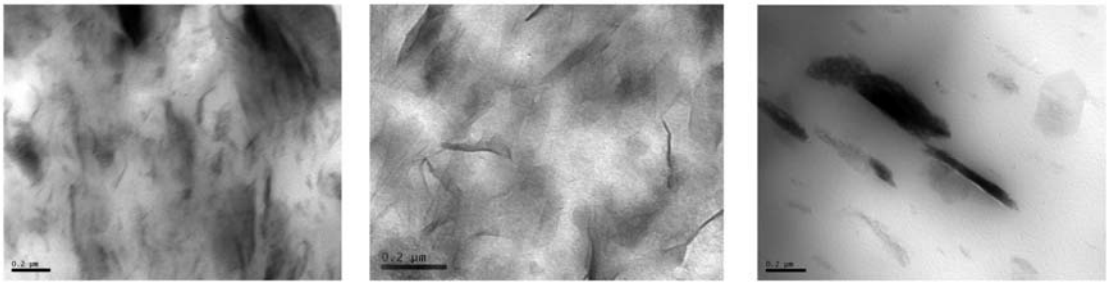

MMT-TMDA **MMT-ODA** **CC**

Figure 1. TEM pictures of the composites

Conducting short fibre/elastomer composites

Saritha Chandran A* and Sunil K. Narayanankutty[#]

Department of Polymer Science and Rubber Technology,
Cochin University of Science and Technology, Kochi – 682022, Kerala, India
E-mail: sunil@cusat.ac.in

Abstract

Natural rubber/polyaniline (PANI)/polyaniline coated short Nylon fiber (PANI-N) conducting polymer composites (CPCs) were prepared by mechanical mixing and its cure characteristics, mechanical properties, conductivity and thermal stability were evaluated. The amount of fiber was varied from 40 to 120 phr and the amount of PANI used was in the range 40-140 phr. PANI and PANI-N increased the rate of cure reaction. The PANI-N CPCs showed higher tensile strength, tear strength and modulus values and lower elongation at break. The DC electrical conductivity and the thermal stability of the CPCs increased with PANI and PANI-N concentration. The highest conductivity obtained was 1.99×10^{-6} S/cm.

Introduction

Polyaniline (PANI) is a very important conducting additive and is also considered as a potential candidate for the development of conducting blends because of its high conductivity, stability, ease of synthesis and low-cost reagents. Even though PANI/elastomer composites exhibit excellent conducting and shielding properties, the main concern with them is the lack of good mechanical properties. In order to couple these two properties, special materials have to be developed. The electrical and mechanical properties of the elastomer composites depend on the aspect ratio of the filler. Fibers are characterized by high aspect ratios. It is well established that the mechanical properties of rubber composites can be greatly improved by adding short fibers [1]. Generally, short fiber reinforced rubber composites are popular in industrial fields because of their processing advantages, low cost and their greatly improved technical properties such as strength, stiffness, modulus and damping [2-3]. These composites combine the elastic behavior of rubber with the strength and stiffness of fiber. Hence, the drawback of poor mechanical properties of the PANI/rubber conducting composites can be overcome by using short fibers grafted/coated with PANI. This will impart the elastomer, the high conductivity of PANI and good reinforcement of short fibers.

Works on PANI composites based on many synthetic rubbers have been reported, however, reports on natural rubber in this field are quite rare [4]. This work describes the preparation of conducting polymer composites (CPCs) of NR, PANI and PANI coated short Nylon fiber. PANI coated short Nylon fiber is expected to enhance the mechanical properties, simultaneously providing sufficient conductivity. The cure characteristics and mechanical properties of the composites are described. The DC electrical conductivity and thermal analysis of the composites are also presented.

Experimental

Materials

Natural rubber was obtained from Rubber Research Institute of India, Kottayam, Kerala, India. The sample had a Mooney viscosity ML1+4 (@100 $^{\circ}$C) of 85.3. Dicumyl peroxide (DCP) was supplied by S. D. Fine Chemicals Ltd., Mumbai, India. Rest of the chemicals used were of commercial grade.

Preparation and characterization of conducting polymer composites

PANI was prepared by the chemical oxidative polymerization of aniline in presence of hydrochloric acid. PANI coated Nylon fiber was prepared after giving an etching treatment to the fibers as described elsewhere [5]. The PANI coated etched fiber thus obtained is hereafter referred to as PANI-N. The formulation for the preparation of the CPCs is given in table 1. Two series of CPCs were prepared- first series with varying amounts of PANI (P series) and the second with 90 phr PANI and varying amounts of PANI-N (F series). The CPCs were prepared in a laboratory size two-roll mill as per ASTM D 3184 (1980). The compounds were compression molded at 150 $^{\circ}$C in an electrically heated hydraulic press using standard mould and cured to their respective optimum cure times. The processing characteristics of the vulcanizates were monitored using a Rubber Process Analyzer (RPA 2000, Alpha Technologies). The mechanical properties of the CPCs were determined using a Shimadzu Universal Testing Machine (model AG1) with a load cell of 10 kN capacity at a cross-head speed of 500 mm/min at a gauge length of 40 mm. The measurements were carried out as per ASTM D 412-98a (2002). Tear strength of the samples were measured as per ASTM D 624-2000 using standard test specimens. The DC electrical conductivity of the CPCs (rectangular strips of dimensions 4 × 2 × 2 mm) was measured by a standard two-probe electrode configuration using a Keithley Nanovoltmeter (model 2182) in dry air at ambient temperature. Thermogravimetric analysis of the CPCs were performed on a TGA Q-50, TA

Instruments thermogravimetric analyzer (TGA) with a programmed heating of 20 °C/min from ambient to 800 °C.

Results and Discussion

Table 2 presents the cure characteristics of the P series and F series CPCs. For the P series, cure time; T_{90}, reduces with loading up to 90 phr, which then shows an increase. This means that PANI accelerates the cure reaction up to 90 phr loading. Addition of PANI-N to the CPC with 90 phr PANI (NP_2) further reduces the cure time. This indicates that the PANI-N can accelerate the peroxide cure reaction of the natural rubber matrix. Scorch time; T_{10}, shows an increasing trend with loading for P series indicating better processing safety. For the F series, it increases on PANI-N loading, stabilizes and then decreases drastically at higher loadings. Such a decrease at higher PANI-N content is attributable to the premature cure that might happen due to the high heat generated during mill mixing of highly fiber-loaded samples.

PANI has an intrinsic acid content and increasing the mass fraction of PANI in the composite induces degradation processes of the crosslinking agent by heterolytic decomposition, inhibiting the formation of the free radicals necessary for the vulcanization reaction [6, 7]. Thus, PANI inhibits the crosslinking process of the elastomer; hence we expect a decrease in the maximum torque (D_{max}) values. But this effect can be partially counterbalanced by using a higher concentration of the crosslinking agent [8]. Introduction of PANI causes a slight decrease in the D_{max} value initially, after which, there is a steady increase. The F series CPCs show a steady increase in the maximum torque values with PANI-N loading, as expected. This means that with the addition of PANI and PANI-N, some sort of interaction between them and the matrix develops. This effect is higher for the PANI-N-loaded samples. The minimum torque; D_{min}, is found to increase with filler loading for both the series. In the case of polymer composites filled with various particulate fillers [9], the minimum torque in rheographs is considered to be a direct measure of the filler content. D_{min} can be considered as a measure of stiffness of the unvulcanized compound. The increase in viscosity with the addition of filler suggests a reduced mobility of the rubber chains caused by the incorporation of these fillers.

The variation of tensile strength of the CPCs with loading is shown in fig. 1, and fig. 2 presents the variation of tear strength with loading. The tensile strength shows a sharp decrease (55 % reduction) on addition of 40 phr of PANI. Further additions do not have much effect on the tensile strength. PANI is not effective in improving the tensile strength due to dilution effect at these high loading levels. Generally, PANI is known as a very rigid material and the tensile strength of most PANI blends or composites has a decreasing tendency as the

concentration of PANI increases [10, 11]. The tensile strength of F series increases with loading due to the reinforcement effect of the fiber. The presence of fiber in the matrix along the longitudinal direction of the application of force requires that greater force be applied to pull out the fiber from the fiber/rubber interface. On incorporation of 120 phr PANI-N, the tensile strength of the CPC with 90 phr PANI (NP_2) increases by ~ 100 %. The decrease in tensile strength of the composites due to PANI incorporation is thus counter-balanced by the addition of PANI-N.

In the case of CPCs of the P series, tear strength decreases slightly on 40 phr PANI loading (NP_1), beyond which it shows a slight increase. For the F series, it sharply increases with PANI-N loading and reaches saturation at 80 phr PANI-N loading (NF_2). PANI-N oriented perpendicular to the direction of propagation of crack front deviates or arrests the crack more effectively. Hence the PANI-N CPCs show higher tear strength than the PANI CPCs.

Figs. 3 and 4 present the elongation at break and modulus at 25 % elongation of the CPCs, respectively. Both the series give an initial sharp decrease in elongation at break. The decrease in elongation at break with filler loading is due to the lower molecular mobility arising from the formation of physical bonds between the filler particles and the polymer chains, apart from the dilution effect. P series does not show any variation in the modulus whereas F series shows a sharp increase with increasing loading. This effect is assigned to the reinforcing nature of the PANI-N, changing the viscoelastic behavior of the rubber to a rigid material. The increase is less pronounced for the P series. This is assigned to the low viscosity of these composites. As the fibers restrain the rubber matrix more effectively, the modulus of the PANI-N composites is higher.

The variation of DC electrical conductivity of the composites with loading is given in fig. 5. Even a concentration of 40 phr PANI could not exert much influence on the conductivity of the composite. This might be due to the lesser interaction between the components in the composite, which causes agglomeration of the PANI particles in the matrix, resulting in a non-uniform distribution and hence poor conductivity. It was established by Zilberman *et al.* that the blend morphology and the level of interaction between components of the blends strongly affect the electrical conductivity of the blend [12, 13]. High fracturing level of the PANI particles occurs due to their high interaction with a compatible matrix. Interaction of the matrix polymer with the conducting polymer effects dispersion of the conducting phase in the matrix, and higher PANI fracturing is observed for matrices interacting more strongly with PANI due to better interphase shear stress transfer [12, 14]. Smaller PANI particles thus formed, lead to an increase in the conductivity by dispersing themselves uniformly in the matrix. The dispersed PANI particles partially reaggregate during processing and molding

due to PANI incompatibility with the matrix polymer. The poor conductivity exhibited by the 40 phr PANI-loaded CPC can be attributed to the lesser interaction of the conducting polymer with the NR matrix and its higher extent of agglomeration. Higher concentrations of PANI increase the conductivity. Percolation is observed at 90 phr PANI loading. Introduction of 40 phr PANI-N decreases the conductivity, but higher loadings give conductivity higher than that of the P series. A conductivity of ~ 2×10^{-6} S/cm is obtained for 120 phr PANI-N loading (CPC NF_3).

The thermal characteristics as estimated by TGA are presented in table 3. Pure NR (NP_0) gives a single degradation between 296 and 491 °C and peak maximum at 388.2 °C. The NR-PANI CPC, NP_1 shows an additional degradation starting at 225 °C. This degradation is seen for all NR-PANI composites and its intensity increases with PANI concentration. This can be assigned to the evolution of PANI dopant. Pure PANI gives a weight loss between 153 °C and 295 °C. In the composites, this weight loss occurs at a slightly higher temperature range, 201-320 °C. The onset of degradation slightly shifts to lower temperature with increasing PANI concentration, but the temperature of maximum degradation remains unaffected. With increasing PANI concentration, another degradation starting at ~ 415 °C and ending at 581 °C can be discerned overlapping with the NR degradation. NR degrades completely by around 491 °C. Hence, this weight loss is not connected with NR degradation. This process can be assigned to the dedoped PANI degradation. Pure PANI gives this degradation at 342-689 °C. As can be understood from table 3, the thermal stability increases with PANI concentration.

The thermal characteristics of the F series CPCs are given in table 4. As in the case of P series, three degradations are seen in F series also. The onset temperature of the first degradation due to the PANI dopant evolution increases on increasing the PANI-N concentration. There is no change in the degradation pattern on increasing the PANI-N concentration. The peak degradation temperature and the weight loss remain almost constant because of the fixed concentration of PANI in these composites. The second degradation is much more complex than in the case of P series due to the additional PANI-N degradation, overlapping in the same temperature range. The PANI-N degrades in the temperature range 293-523 °C. The second degradation of the CPCs starts at around 315 °C. The maximum temperature of this degradation shifts slightly to higher temperatures with increasing PANI-N content but the intensity of this degradation is unaltered. To conclude, the thermal stability of the composites increases with PANI-N concentration.

Conclusions

Conducting natural rubber/polyaniline/polyaniline coated short Nylon fiber composites (NR/PANI/PANI-N CPCs) with sufficient mechanical properties can be prepared by mechanical mixing. Addition of pristine PANI to NR improves its cure characteristics. Thermal stability and electrical conductivity increases with PANI concentration. The tensile strength decreases drastically with increase in PANI concentration. The tensile strength of the NR/PANI system can be improved by adding PANI coated short Nylon fibers. The addition of PANI coated short Nylon fiber not only brings about a significant improvement in the mechanical properties, but increases the cure rate, shear modulus, viscosity and thermal stability as well. The DC electrical conductivity of the composites decreases on addition of polyaniline coated short Nylon fiber. Higher conductivity values are obtained at higher loadings. A conductivity of ~ 2×10^{-6} S/cm is obtained for 120 phr PANI-coated short Nylon fiber loaded composite.

References

1. Goettler LA, Shen KS. Rubber Chem Technol 1983;56:620
2. Setue DK, De SK. J Mater Sci 1984;19:983.
3. Fitzer E, Gkogkids A, Heine M. High Temp High Pressure 1984;16:363.
4. Sreeja R, Pradeep P, Rossamma Alex. In: Proceedings of the15th Kerala Science Congress, India, 2003.
5. Saritha C. A., Kutty S. K. N. 17th Annual General Meeting of Materials Research Society of India- AGM-MRSI, February 13-15, 2006, University of Lucknow, India.
6. Van Drumpt JP. Rubber World 1988;197:33.
7. Keller RC. Rubber Chem Technol 1988;61:238-254.
8. Faez R, Gazotti WA, De Paoli M-A. Polymer 1999;40:5497-5503.
9. Mathew G, Kuriakose B, Thomas S. J Elastomers Plast 1997;29:163.
10. Chipara M, Hui D, Notingher PV, Chipara MD, Lau KT, Sankar J, Panaitescu D. Composites Part B 2003;34:637.
11. Choda´kI. Omastova´ M, Pionteck J. J Appl Polym Sci 2001;82:1903.
12. Zilberman M, Siegmann A, Narkis M. J Macromol Sci Phys 1998;B37(3):301-318.
13. Zilberman M, Siegmann A, Narkis M. J Macromol Sci Phys 2000;B39(3):333-337.
14. Narkis M, Zilberman M, Siegmann A. Polym Adv Technol 1997;8(8):525-528.

Table 1 Formulation for the preparation of CPCs

Ingredients (phr*)	P series				F series		
	NP_0	NP_1	NP_2	NP_3	NF_1	NF_2	NF_3
NR	100	100	100	100	100	100	100
PANI	0	40	90	140	90	90	90
PANI-N#	0	0	0	0	40	80	120

* parts per hundred rubber
# PANI coated etched fiber
All the mixes contain Stearic acid- 1 phr and DCP- 3 phr

Table 2 Cure parameters of the CPCs

CPC	T_{90} (dNm)	T_{10} (dNm)	D_{max} (dNm)	D_{min} (dNm)
NP_0	23.4	2.0	2.7	0.05
NP_1	21.8	2.6	1.7	0.06
NP_2	15.7	1.7	2.2	0.28
NP_3	19.1	2.7	3.5	0.13
NF_1	12.8	2.2	3.9	0.64
NF_2	15.2	2.2	5.0	0.57
NF_3	7.9	0.4	7.9	1.5

Table 3 Thermal characteristics of P series CPCs

	Degradation	NP_0	NP_1	NP_2	NP_3
Onset temperature (°C)	First	-	225.9	201.7	216.9
	Second	296.5	315.7	319.7	335.9
Peak degradation temperature (°C)	First	-	297.9	297.0	298.5
	Second	388.2	385.1	387.2	385.3
Weight loss (%)	First	-	5.58	11.03	14.88
	Second	50.8	58.1	60.3	62.1
Temperature at 50 % weight loss (°C)		388.7	392.1	400.6	406.9

Table 4 Thermal degradation data of F series CPCs

	Degradation	NP_2	NF_1	NF_2	NF_3
Onset temperature	First	201.7	212.8	216.9	220.8
(°C)	Second	319.7	315.7	321.9	316.8
Peak degradation	First	297.0	297.3	299.6	298.8
temperature (°C)	Second	387.2	388.4	393.7	392.3
Weight loss (%)	First	11.0	7.8	7.6	6.9
	Second	65.6	67.9	68.1	69.6
Temperature at 50 % weight loss (°C)		400.6	403.3	409.0	412.9

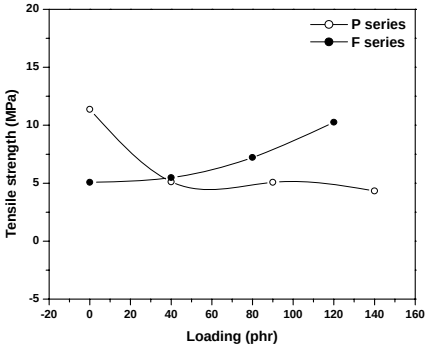

Fig. 1 Variation of tensile strength with loading

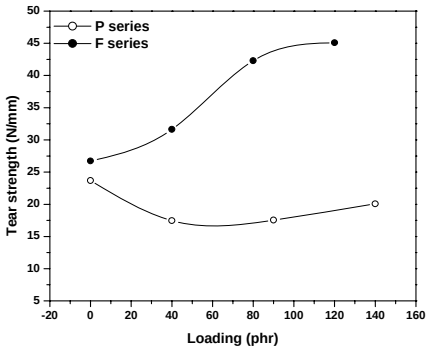

Fig. 2 Variation of tear strength with loading

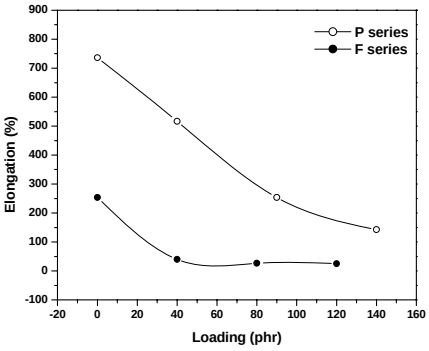

Fig. 3 Effect of loading on elongation at break of the CPCs

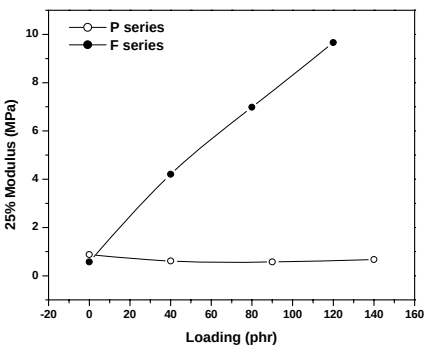

Fig. 4 Effect of loading on modulus of the CPCs

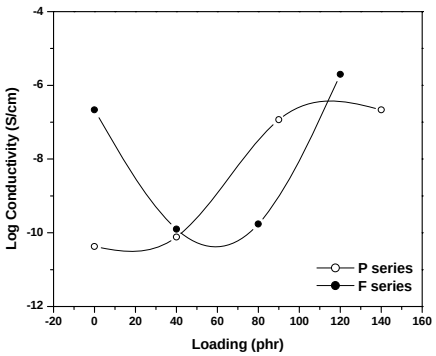

Fig. 3.5 DC electrical conductivity of the CPCs

Studies on the conductivity and tensile properties of polyaniline blended natural rubber latex

[*]Saisy.K.Esthappan[1], [#]Shiny Palaty[1], Honey John[2] and Rani Joseph[3]

[1]Department of Chemistry, Bharata Mata College, Thrikkakara, Kerala, India
[2]Department of Applied Sciences, Indian Institute of Space Science and Technology, ISRO, Thiruvananthapuram - 695 022, India
[3]Department of Polymer Science and Rubber Technology, CUSAT, Kochi, Kerala, India

Email : shpalaty@gmail.com

Abstract: In an effort to study tensile strength and conductivity of polyaniline (PANI) blended natural rubber latex (NRL) system, different films were prepared under different conditions. Perchloric acid ($HClO_4$) doped PANI was prepared at low temperature in the laboratory. PANI dispersions in water and in vulcastab-VL were made. Using both the PANI dispersions NRL was compounded. In each case incorporation of PANI dispersion in to the latex was done by two ways- before prevulcanisation and after prevulcanisation. The films were casted and dried at room temperature and in oven at 70^0C for different times. D.C conductivity, swell index, cross link density and tensile strength of these films were measured. Sem photographs of the uncompounded NRL and PANI incorporated NRL was taken. Conductivity was found to be in the order of 10^{-9} s/m. Incorporation of PANI dispersions to the latex mixes before prevulcanisation gave films of higher tensile strength than that after prevulcanisation. Conductivity and tensile strength is found to be higher for the film which is casted from PANI dispersion prepared in vulcastab-VL and cured in oven for sixty minutes.

Keywords
Polyaniline, perchloric acid, prevulcanisation, swell index, crosslink density, d.c conductivity.

Introduction

Polyaniline (PANI) is one of the most promising, intrinsically conducting polymers among the many types of conducting polymers due to its straight forward polymerization and environmental stability and high conductivity. The latest progress on the fabrication of PANI and its blends has attracted enormous industrial interests[1]. Several studies have reported that conducting poly blends prepared with PANI and a classical polymer (polystyrene, poly methyl methacrylate (PMMA), polyimide etc) in organic solvents which exhibit good mechanical properties associated with interesting electrical properties[2]. These blends are designed to combine the desired properties of both components. Synthesis of colloidal PANI particles[3] and their application in polymer/ PANI blends have been of great interest. Two main approaches in the preparation of PANI containing colloidal blends can be distinguished. Blends have been prepared by polymerizing aniline in the presence of the matrix polymer latex[4] or by simple mechanical mixing of a colloidal PANI dispersion with matrix polymer latex[5,6].

In this work perchloricacid ($HClO_4$) doped PANI was prepared at low temperature and this conducting emaraldine form of PANI was incorporated in to the NRL. Here PANI dispersions were made both in water and in vulcastab-VL. The films were casted in two ways (before prevulcanization and after prevulcanisation of NRL). The films were dried at different conditions (room temperature and in oven). Tensile strength, swell index, crosslink density and d.c conductivities of these films were measured. The aim of this work is to prepare the PANI incorporated latex films with good mechanical properties and electrical conductivity.

Experimental

(1)Equipments used

The equipments used in this study include a Universal Tensile Testing Machine Model 1445(M/s Instron , Buckingshire UK) , Scanning electron microscope JEOL JSM-840 model-6211(Oxford, England), 3 digit electronic balance(KERN& Sohn Gmblt.D.72336.Balingen,Germany), digital pH meter MKVI (Systronics Naroda, Ahemedabad), Hot air oven(ROTEK company, RHO-98-HFSS,W.Vengola, Kerala, India), Kiethely nanovoltmeter sourcemeter-2400, Ball mill (30-50 rpm), Magnetic Stirrer (Model No.KMS-350, 1 phase, 230V, 50 H_z), Distillation apparatus.

(2) Materials used

High ammonia centrifuged NRL conforming to the BIS 5430-1981 was purchased from Njavallil Rubber Latex, Eloor and was used for prevulcanisation. The compounding ingredients zinc diethyldithiocarbamate (ZDC), zinc oxide (ZnO), sulphur (S), oleic acid, dispersol F, n-butyl alcohol, potassium hydroxide (KOH), zinc chloride ($ZnCl_2$) and carbon disulphide (CS_2) were commercial grade was used. Toluene used for swelling studies and perchloric acid ($HClO_4$) were reagent grade and were used as supplied. Aniline used for the preparation after distillation.

(3) Experimental procedure

Conducting emeraldine form of PANI was prepared at low temperature using $HClO_4$ as dopant as reported earlier[7]. 50% dispersions of the vulcanizing agents were prepared using a ball mill. PANI dispersions in both water and in10% vulcastab-VL were prepared. NRL was compounded as per the formulations given in Table 1. In the case of A and B PANI dispersion was added at the time of compounding. But in the case of C and D, PANI dispersion was added after 5 days of maturation time. Latex films were then casted in glass cells according to ASTM D 1076-88 from these latex mixes. In the case of A and B the films were cured at different temperatures-room temperature and at 70^0C in oven for different times, 45 minutes, 60 minutes and 75 minutes. These samples are designated as A_R, B_R, A_{45}, B_{45}, A_{60}, B_{60}, A_{75} and B_{75}. Using C and D films were casted and the films were dried at different temperatures-room temperature and oven drying at 70^0C for different times of 20, 30 and 40 minutes. These samples are designated as C_R, D_R, C_{20}, D_{20}, C_{30}, D_{30}, C_{40} and D_{40} minutes. In A and C are PANI dispersions added were made in vulcastab-VL and B and D are in water.

The equilibrium swelling values were determined by immersing a thin film in toluene for 24 hours at room temperature and calculated using the equation,Swell index(Q) $=W_2 - W_1 / W_1$. The total chemical crosslink density was also determined by equilibrium swelling method using Flory Rehner equation[8].Dumb bell shaped tensile specimens were punched out of the casted films. Tensile strengths measurement was carried out at a crosshead speed of 500mm/min on a Universal Testing Machine, model 1445 according to ASTM D 412-87(method A). The results were given in Figure 3. The d.c. conductivities of these films were measured using a Kiethely nanovoltmeter sourcemeter-2400 and the values were reported in Table 2.SEM photographs of the film casted from uncompounded NR latex film and A_{60} were taken and given in Figure 4 and Figure 5.

Result and Discussion

Figure 1 shows the swell index values of PANI incorporated NRL films at different conditions. From Figure 1, it was clear that in the case of A, minimum swell index was shown by sample A_{60}. Maximum crosslinking occurs when film was cured at 70^0C for 60 minutes. By increasing the curing time to 75 minutes, swell index increases which indicate the over vulcanisation which leads to cross link shortening and crosslink decomposition[9]. As the curing time increases cross links and pendent groups undergo a variety of further reactions which take place at the same time as does crosslinking during overcure. In the case of B, maximum crosslinking occurs for sample B_{45} i.e., 45 minutes oven curing at 70^0C. As the curing time increases swell index also increases steadily indicating the chain breaking of rubber molecules. In the case of C and D, 30 minutes oven dried samples (C_{30} and D_{30}) have minimum swell index. Increasing drying time thereafter increases the swell index.

Figure 2 and 3 shows crosslink density and tensile strength values of PANI incorporated NRL films at different conditions. From figures it is clear that crosslink density and tensile strength

values are higher for A_{60} and when the time for oven curing increases tensile strength was found to be decreases. This may be due to, as the time increases the degradation of rubber chain start to takeplace. By considering room temperature cured films A_R,B_R,C_R,D_R it is clear that films casted before prevulcanisation show higher tensile properties than that of after prevlcanisation. It was already reported that prevulcanisation of NRL can be done at room temperature using zinc butyl xanthate dithiocarbamate ($Zn(bxt)_2$ /ZDC) accelerator combination and the prevulcanisation is completed by five days using this system[10]. So here PANI dispersion added before and after prevulcanisation of latex (after 5 days). Additon of PANI to the NRL decreases the tensile strength values of NRL films. The tensile strength of prevulcanised latex is governed not only by the introduction of cross-links but also by the ability of particles to coalesce among themselves. Since the latex is prevulcanised, the rubber particles are internally crosslinked and by the addition of PANI, the coalescence of rubber particles becomes more difficult resulting in a lower tensile strength[11]. PANI prepared using acid dopant affect the stability of latex and thus decreases the tensile strength values compared to the latex films in which PANI was not incorporated. From figures it is also clear that oven cured films show higher tensile strength than that of room temperature cured films.

Table 2 shows the d.c conductivities of the PANI incorporated NRL films at different conditions. From Table 2 it was found that the films show the conductivity of the order of 10^{-9} s/m. In the case of A, A_{60} shows the maximum conductivity. When the time for oven curing increases thereafter, the conductivity is found to be decreases. This may be due to the degradation of dopant molecules from the PANI chain. In the case of B samples conductivity obtained higher for B_{45} and in the case of C, C_{30} and in D, D_{30} shows higher conductivity. In each case tensile strength was also found to be higher for these films .

Figure 4 and 5 show the SEM photographs of uncompounded NRL film surface and $HClO_4$ doped PANI incorporated NRL film surface respectively. From figure 4 and 5 it was clear that PANI particles were uniformly distributed throughout the NRL after the incorporation of the PANI to the NRL. From the SEM surface of PANI incorporated latex it was clear that the sample is homogeneous. Conducting polymers are very sensitive to the temperature. Due to the interaction between electron and sample, considerable amount of heat is generated which causes the development of small cracks during SEM recording[12].

Conclusions

The tensile properties of the films casted before prevulcanisation show higher tensile strength than that after prevulcanisation .When the time for oven cure increases after a particular time the conductivity and tensile strength were found to be decreases. The SEM photographs of the uncompounded and film prepared from PANI added NRL mixes was explained. Conductivity and tensile values obtained is greater for the film prepared from vulcastab-VL dispersed PANI added NRL mixes before prevulcanisation which is cured in oven at 70^0C for sixty minutes. It is hopeful that this film can be used for antistatic applications.

Acknowledgement

The authors would like to acknowledge KSCSTE for the financial support.

References

1. Shi-Jian Su, Noriyuki Kuramoto, Yamagata university, Synthetic metals 108(2000)121-126.
2. E.Segal, Y.Haba, M.Narkis, A.Siegmann, Department of Chemical Engineering, and Department of Materials Engineering, Technion, IIT,Haifa 32000,Israel ,Journal of applied polymer science , Vol. 79,760-766(2001) .
3. Haba, Y.;Segal, E.;Narkis , M.; Titelman, G.I.; Siegmann,A.Synth Metals 1999,106,59.
4. Xia,H.Q.; Ma,Y.M.; Guo, J.S.Polymer 1998,40,261.
5. Gospodinova, N.; Mokreva, P.; Tsanov, T.; Terlemezyan,L.; Polymer 1997,38,743.
6. Haba, Y. ; Segal, E. ; Narkis, M. ; Titelman, G.I.;Siegmann, A.Synth Metals 2000,110,189.
7. Honey Jhon ; S.Bijukumar, K.T. Mathew , Rani Joseph; Journal of Applied Polymer Science; Vol.83, 2008-2012(2002)

8. P.J.Florey and J.Rehner, (1943), J.Chem.Phys., 11,512.
9. A.V. Chapman and M. Porter, in Natural Rubber Science and Technology, A.D Roberts, Ed.Oxford University press, Oxford Univrsity Press, Oxford,1988,Chap.12
10. Shiny Palaty, Devi P.V, Honey John, Rani Joseph, Saisy.K.Esthappan ; to appear
11.P.Pradeep and, R.Sreeja, Maciej Mazur, P.D Sharma, Journal of Elastomers and Plastics Vol.38-October 2006.
12.S.C. Raghavendra,Syed Khasim, M.Revanasiddappa, M.V.N. Ambika Prasad and A.B.Kulkarni, Bull.Mater.2003, pp.733-739. ci., Vol.26, No.7, December 2.

Figures and Tables

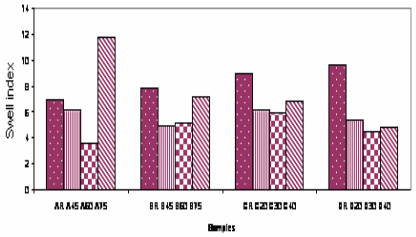

Figure 1: Variation of swell index values of PANI Incorporated NRL films at different conditions.

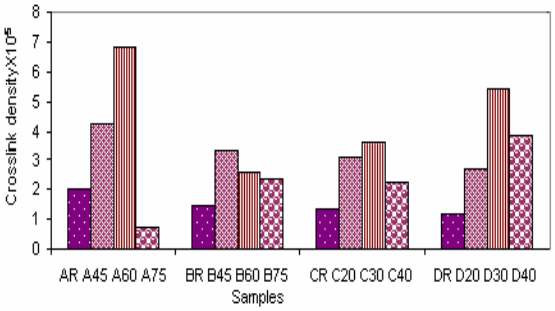

Figure 2: Variation of cross link density values of PANI films at different conditions.

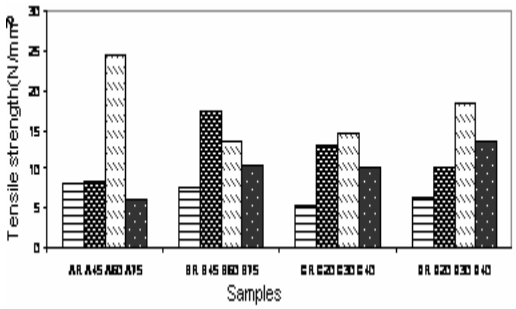

Figure 3: Variation of tensile strength of incorporated NRL PANI incorporated NRL films at different Conditions.

Ingredients		Parts byweight(gms)			
		A	B	C	D
NR latex		167	167	167	167
10% KOH		2.5	2.5	2.5	2.5
10% Potassium oleate		1.0	1.0	1.0	1.0
10% Vulcastab-VL		1.0	1.0	1.0	1.0
50% sulphur		2.5	2.5	2.5	2.5
50%ZDC		1.0	1.0	1.0	1.0
50% ZnO		0.75	0.75	0.75	0.75
50% $Zn(bxt)_2$		1.0	1.0	1.0	1.0
PANI	H_2O	-	5	-	5
	Vulcastab-VL	5	-	5	-
		Before prevulcanisation		After prevulcanisation	

Table 1:Formulation of NRL

Samples	Conductivity (S/cm)
A_R	$1.82x10^{-9}$
A_{45}	$2.4x10^{-9}$
A_{60}	$4.46x10^{-9}$
A_{75}	$1.01\ x10^{-9}$
B_R	$2.3\ x10^{-9}$
B_{45}	$2.6\ x10^{-9}$
B_{60}	$1.69\ x10^{-9}$
B_{75}	$1.62\ x10^{-9}$
C_R	$2.02\ x10^{-9}$
C_{20}	$3.38\ x10^{-9}$
C_{30}	$4.34x10^{-9}$
C_{40}	$1.69\ x10^{-9}$
D_R	$1.35\ x10^{-9}$
D_{20}	$1.69\ x10^{-9}$
D_{30}	$3.04\ x10^{-9}$
D_{40}	$1.35x10^{-9}$

Table 2: d.c conductivities of PANI incorporated NRL films

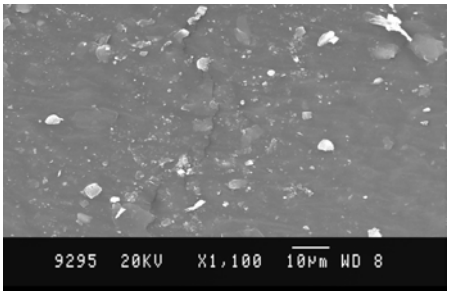

Figure 4: SEM photograph of uncompounded NRL film surface

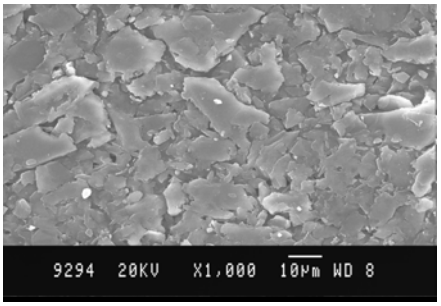

Figure5: SEM photograph of $HClO_4$ doped PANI incorporated NRL film surface

Effect of sealing on the diffraction efficiency of an acrylamide based photopolymer

[1 *]K.P. Nimmi, [2]V. Pramitha, [3]K.Sreekumar, [2]C.Sudha Kartha, [1#]Rani Joseph

[1]Department of Polymer Science & Rubber Technology, Cochin University of Science & Technology, Kochi - 682 022, Kerala, India
[2]Department of Physics, Cochin University of Science & Technology, Kochi - 682 022, Kerala, India
[3]Department of Applied Chemistry, Cochin University of Science & Technology, Kochi - 682 022, Kerala, India

Email: rani@cusat.ac.in

Abstract

Photopolymer media has gained much importance in the field of holography, because of its high sensitivity, low cost, versatility, and ease of processing. In this paper, we report the use of PVA based photopolymer as holographic recording medium. The maximum diffraction efficiency of ~75% was obtained for the recorded grating with exposure energy of 60mJ/cm^2 at an angle of 60 ^{o} using a He-Ne laser beam. Even though good diffraction efficiency was obtained, it was found to be decreasing on storage and also some cracking was observed on the surface of the film. This may be due to the variations in humidity and in order to avoid these problems, the film was sandwiched between two glass plates using an epoxy sealant. The sealed sample showed a maximum diffraction efficiency of 67% with the same recording parameters. Even though it showed an initial decrease in diffraction efficiency, it remained constant for a long time and no cracking was observed on these sealed films on storage.

Introduction

Holography is a method of storing optical information by means of photochemical and or photophysical processes. Holographic data storage is considered as the one of the next generation information storage technologies because of its potential in high storage capacity (10^{12}bits/sec) and fast readout speed (10^{11}bits/sec). Development of holographic material is important because many applications have been proposed in different areas like optical memories, holographic displays, scanners, optical disk system etc.

Silver halide photographic emulsions, dichromated gelatin, thermoplastics and photopolymers are generally used as holographic recording media, in which Photopolymeric materials are especially interesting because of their large refractive index contrast, high photosensitivity, low energetic exposures, good optical properties, and low cost [1-4].

Among the photopolymers for holographic recording, acrylamide based photopolymer is studied widely [4]. Photopolymeric system consists of poly (vinyl alcohol) as the binder, acrylamide as monomer, methylene blue as sensitizer and triethanol amine as the electron donor. The hologram formation in this photopolymer medium can be explained by the polymerization of the monomer and its diffusion [5]. This causes refractive index modulation of the medium and this modulation is related to the diffraction efficiency of the hologram recorded. The chemical process can be represented as;

$$\text{Dye} + h\upsilon \longrightarrow {}^1\text{Dye}^* \longrightarrow {}^3\text{Dye}^*$$

$${}^3\text{Dye}^* + \text{TEA} \longrightarrow \text{L Dye} + \text{TEA}^{\bullet}$$

$TEA^{\bullet} + M \longrightarrow P^{\bullet}$

$P^{\bullet} + M \longrightarrow P$

One draw back of the photopolymer film is that it is greatly affected by humidity [6] and as a result, cracking was observed on the surface of the film and thus the optical clarity of the film is lost. In this work, the effect of sealing on the diffraction efficiency of the film was studied.

Experimental

Poly(vinyl alcohol) [PVA], with molecular weight 1,25000 (CDH), methylene blue [MB] (SD Fine), acrylamide [AA] (Merck), triethanol amine, [TEA] (Merck) were used for film preparation. A 10% by weight solution of PVA in distilled water was prepared and used as binder. To this, AA, TEA, MB were added and this mixture was stirred well to get a homogenous solution. The film was prepared by gravity settling method under ambient conditions (relative humidity- 70%, tempearature-30^{o} C). 48 hours of drying was required for the film and after drying, the film was sandwiched between two clean plates using epoxy sealant. The absorption spectrum of the film was recorded by Jasco-V-570 spectrophotometer. Diffraction grating was recorded using a He-Ne laser (632.8nm) by double beam method [7].

Results and Discussions

A. Comparison of diffraction efficiency of sealed and unsealed films

Fig (1) shows the initial diffraction efficiencies of sealed and unsealed films (recorded using He-Ne laser, exposure energy 60mJ/cm^2, angle of recording 60^{o}, reconstruction power 1μW). From this it is clear that diffraction efficiency (DE) is higher for the film without sealant (75%). For the sealed film, there is a reduction in the initial DE (67%). The reason for this can be explained by the absorption spectrum of both films before exposure. Fig(2). In the case of sealed film, the abs_{max} in the red region of the spectrum is decreased slightly and this may be because of reduction of the dye molecule to the leuco form due to the presence of amine curing agent. This in turn decreases DE of the recorded grating, because DE depends on the concentration of dye molecules. Here the dye molecules were converted to leuco form and therefore not available for the chemical process for grating formation.

B Diffraction efficiency on storage of the sealed film

The initial DE of the recorded grating of the sealed film shows a decrease compared to the film without sealant (67%), it remained as such for two months and then decreased slightly to 53% and after one year, remained as 48%.Fig (3).

Conclusion

The diffraction efficiency of the sealed film was found to be slightly lower than the unsealed film, but it remained as 50%after one year and no cracking was observed for the film kept under sealed condition. So without much affecting the film properties, we can use epoxy sealant for protecting the film.

Acknowledgement

The authors gratefully acknowledge IRDE-DRDO for financial support through a research project.

References

1. Heanue.J.F, Bashaw.M.C, Heselink.L., Volume holographic storage and retrieval of digital data, *Science*, 1994; 265; *749*

2. Blaya.S, Carretero.L, Fimia.A, et al., Optimal composition of an acrylamide and N,N'-methylenebisacrylamide holographic recording material, *J.Mod.Opt*. 1998**;** 45; 2573

3. Martin.S, Feely.C.A, Toal.V, Holographic recording characteristics of an acrylamide based photopolymer, *Appl. Opt*. 1997; 36; 5757

4. Blaya.S, Carretero.L, Madrigal.R.F, et al., Study of effect of bifunctional crosslinking agent in polyvinyl alcohol- based photopolymerizaion holographic recording material using angular responds, *Jpn.J.Appl.Phys*. 2002; 41; 3730

5. Weiss.V, Millul.E, *Appl.Surface Sci*. 1996; 106; 293

6. Neill.F.T, Lawrence.J.R, Sheridan.J.T, Improvement of holographic recording material using aerosol sealant, *J.Opt.A, Pure Appl.Opt*. 2001; 3; 20

7. Ushamani.M, Sreekumar.K, Sudha Kartha.C, Rani Joseph, *Appl.Opt.* 2004; 43; 3697

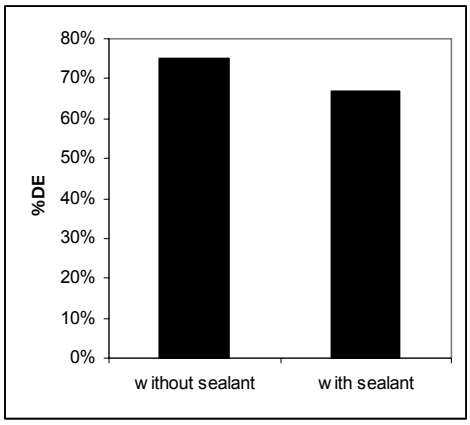

Fig (1) Comparison of %DE of sealed and unsealed films

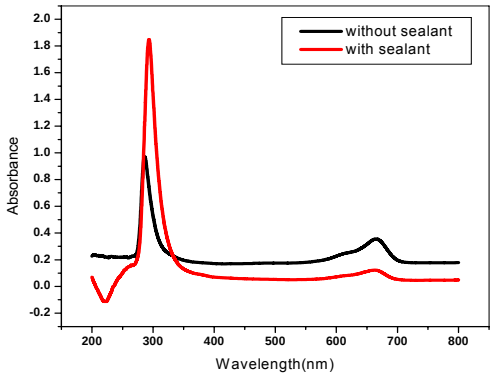

Fig (2).Absorption spectra of sealed and unsealed films before exposure

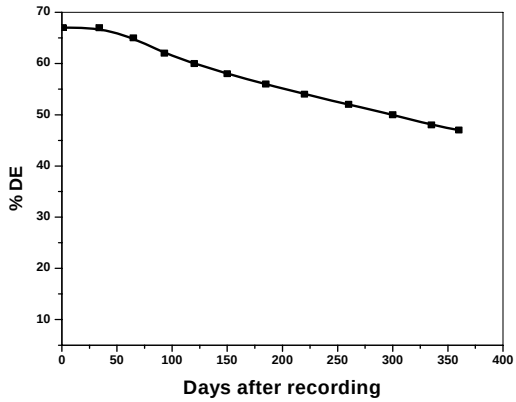

Fig (3) DE on storage of the sealed film

Functionalized MWNTs in natural rubber matrix: mechanical properties and electrical conductivity

Neena George*and Rani Joseph#

Department of Polymer Science and Rubber Technology, Cochin University of Science and Technology, Kochi – 682022, India.

Email: rani@cusat.ac.in

Abstract

Multiwalled carbon nanotube surface has been functionalized by acid treatment to get carboxylated multiwalled carbon nanotubes (MWNT-COOH). Better solubility (600 mg/L) of MWNT-COOH in water provided visual indication for the functionalization of carbon nanotubes. FTIR confirmed the presence of carboxyl moiety on the CNTs. Significant mass loss in TGA of MWNT-COOH compared to pristine MWNT indicated significant functionalization. The influence of MWNT-COOH on the mechanical properties and conductivity of natural rubber vulcanizates is investigated. Compared with pure NR tensile strength, tensile modulus and tear strength of the composites filled with 0.1 phr MWNT-COOH enhanced 66%, 54% and 58% respectively which could be attributed to improved interfacial bonding between the carboxylated nanotubes and the rubber matrix. Conductivity of the order of 10^{-8} Scm^{-1} at 1.0 phr concentration also indicates that exfoliated carbon nanotubes are well dispersed in the NR matrix.

Introduction

Carbon nanotubes have attracted a great deal of interest since their discovery in 1991 [1] because of their tremendous strength, extreme aspect ratio and excellent mechanical, thermal and electrical properties. Although polymer composites based on carbon nanotubes (CNTs) show an increase in tensile strength and young's modulus, the change is not remarkable due to poor adhesion and weak vander Waals forces, which give rise to lower stress transfer ability in the composites. In order to achieve high stress transfer [2,3], strong bonding between CNTs and polymer chains is necessary. It has been reported that an acid treatment of CNT could improve the processability and performance of composites by introducing carboxylic acid groups on the surface of CNT, which leads to stabilization in polar solvents and helps to covalently link polymers [4].

Carbon nanotubes can be oxidized by means of two methods, which are gas phase and liquid phase oxidation. The liquid phase oxidation is most commonly being performed by boiling nanotubes in a mixture of sulphuric and nitric acids. This oxidation procedure results in: – purification of the nanotube soot via etching away the less stable carbon impurities (amorphous carbon etc.), – it leads to local damage which can result in cutting (shortening) of the tubes and might destroy the tube caps (opening), – sidewall functionalisation on the nanotubes via formation of hydroxyl groups (–OH), carboxyl groups (–COOH) etc. Well separated and shortened nanotubes should be easier to uniformly distribute in the matrix and are expected not to show strong tendency to reagglomerate during processing.

In the present work, MWNT surface has been functionalized by acid treatment to get carboxylated multiwalled carbon nanotubes (MWNT-COOH) and it has been characterized using Fourier Transform Infrared Spectroscopy (FTIR) and Thermogravimetric analysis (TGA). Natural

rubber based nanocomposites have been prepared with these modified MWNTs and their influence on the mechanical properties and electrical conductivity of natural rubber is investigated.

Experimental

Multi walled carbon nanotubes (MWNTs) used in this study were supplied by Shenzhen Nano-Technologies Port Co., Ltd., China, synthesised by the Chemical-vapour deposition (CVD) method. AR grade H_2SO_4 and HNO_3 were procured from standard local suppliers. Natural rubber latex of dry rubber content (DRC) 60% was purchased from Njavalli latex, Kochi, India.

100mg of MWNTs were mixed with 3:1 conc.H_2SO_4/HNO_3 in a round bottom flask and the mixture were ultrasonicated (42 kHz) in a bath for 1hr, and then stirred at 100^oC for 30 min under reflux. The mixture was cooled and diluted with distilled water 1:5 by volume, allowed to stand overnight for precipitation and filtered through PTFE membrane filter (0.2 μm pore size), and washed with excess of water until no residual acid was present. The solid was dried under vacuum for 12hrs at 70^oC and labeled as **MWNT-COOH**. The yield of the oxidized samples was ~ 50%.

The as prepared carboxylated carbon nanotubes were dispersed in water and the stability and solubitlity of these aqueous dispersions were investigated. FT-IR characterization (FTIR Spectroscope, BRUKER) of pure and functionalized CNTs was done in the frequency range of 4000–500 cm^{-1}. Thermal studies were done using Thermo gravimetric analyser (TGA Q-50, TA Instruments) in the temperature range of 30-800 ^oC at a heating rate of 20 ^oC /min under nitrogen atmosphere.

MWNT-COOH dispersions have been prepared using a mechanical probe sonicator (13 mm, VibraCell Processor VC 750, operating at 40 % of the maximum power 750 W by sonicating aqueous suspension of modified nanotubes.

Natural rubber latex was compounded as per the formulation given in table 1.The nanotube dispersions have been mixed with the compounded latex at various compositions so as to result MWNT-COOH concentrations of 0.05, 0.1, 0.3, 0.5 and 1.0 phr in NR, and sonicated again for 30 minutes using a bath sonicator operating at 70 W power and 42 kHz frequency so as to achieve uniformity. The samples were then cast onto flat glass trays to get films. They were kept overnight to remove excess water and then cured at 100 ºC for 1 h in an oven.

Dumbbell shaped tensile and angle tear specimens were punched out from the vulcanized sheets and the mechanical properties were studied using a Shimadzu Universal testing machine (UTM, model- AG1) with a load cell of 10 kN capacity. The gauge length between the jaws at the start of each test was adjusted to 15 mm for tensile specimens and 40 mm for tear specimens and the measurements were carried out at a cross-head speed of 500 mm/min. Average of at least six sample measurements represents each data point.

The D.C. electrical conductivity of the samples was measured using a Keithley Nanovoltmeter using a standard four-probe electrode configuration to evaluate the effectiveness of MWNTs in imparting electrical conductivity to the NR matrix.

Results and discussion

Scheme 1 shows the reaction procedure where carbon nanotubes are carboxylated after acidic treatment with 3:1 conc.H_2SO_4/HNO_3. This carboxylation of CNTs causes them to disperse in water. Figure 1 shows the photographs of vials (taken after 4 months of preparation) containing dispersions of pristine MWNTs, and carboxylated MWNTs.

From the figure it is clear that only the carboxylated CNTs will disperse and pristine MWNT will agglomerate and settle at the bottom in pure water. Solubility of modified CNTs in water was

determined by first sonicating them in water followed by filtering through a tightly wadded glass wool plug to remove any insoluble particulate (The solution had no visible particulate and was stable for over two weeks) and measuring the weight of nanotubes in known volumes of solvent. Solubility determined by this method was found to be 600 mg/L.

According to the results of the FTIR (Figure 3) analysis some functional groups such as hydroxyl (–OH), carboxyl (–COOH), and carbonyl (>C=O) are formed on the CNTs surfaces after acid treatment. In the infrared spectroscopy, there exist evident peak of carbonyl functional group corresponding to wave number 1740 cm−1. The peaks at 1365 and 1216 cm−1 correspond to C-OH in plane band and –C-O stretching respectively. There is a broad band near 3000 cm-1 corresponding to O-H stretching.

These functional groups improve the water-affinity of CNTs and thus are beneficial for the preparation of the CNTs–NR latex suspension. Moreover, the functional groups loaded on the surfaces of CNTs are favorable for improving the interfacial bonding between CNTs and the rubber matrix, and correspondingly, the improved mechanical properties of the composites.

From TGA weight loss at 600^{o}C for pristine and functionalized MWNT was found to be 0.1% and 36.5 % respectively. This significant mass loss gives a rough indication of oxidation of MWNTs.

Mechanical properties of NR-MWNT nanocomposites prepared through latex stage mixing are shown in figure 3, 4 and 5. It is evident from the results, that carboxylated MWNTs significantly increase the strength and modulus of natural rubber vulcanizate. For example, the tensile strength of NR increases by around 66 % with a nanotube concentration as low as 0.1 phr. The tensile modulus of the NR/MWNT-COOH nanocomposite at this concentration is roughly 54 % higher as compared to that of pure rubber vulcanizate. Tear strength is also higher by around 58 % as compared with pure rubber at nanotube fractions as low as 0.1 phr.

The results are in agreement with those reported by Ji Liang et al [5] who investigated a significant improvement in mechanical properties of SBR-CNT composites. H. Daniel Wagner [6] et al studied silicone based elastomers mixed with SWNTs and reported enhancement of the initial modulus of the resulting specimens as a function of filler load. M.A Atieh et al and Sung Hun Ryu et al [7,8] reported similar increase in tensile strength and modulus.

The improved reinforcement observed in NR/MWNT-COOH nanocomposites is due to the interaction between carboxylated MWNTs and the rubber matrix. An essential condition for this interaction is the uniform distribution of the nanotubes in the matrix, which is accomplished through sonication. But though a significant increase in mechanical properties is obtained with 0.1 phr MWNT-COOH, the properties level off there after .It may be due to the tendency of the CNTs to agglomerate once incorporated in to the latex. Because the chance for sedimentation of nanotubes is more during the evaporation of water from the latex. Or it may be due to the increased retarding tendency of carboxylic groups on MWNTs towards curing of samples resulting in poor cross linking in polymer matrix.

The room temperature electrical conductivity results of NR/MWNT-COOH nanocomposites are given in figure 6. Conductivity increases with nanotube loading. With 1.0 phr CNTs the conductivity increased by 10^4 times. It is a clear evidence for better dispersion of MWNTs in the rubber matrix.

Liliane Bokobza et al [9] have reported the same value of conductivity for NR/MWNTs composites with 3.8 % MWNTs. Compared to this gain of similar conductivity at 1.0 phr shows very good dispersion of carboxylated MWNTs in the NR matrix.

Conclusion

In summary, MWNTs were functionalized with carboxyl moieties by the reaction with H_2SO_4/HNO_3 mixture. The solubility of the resulting samples in water provided visual indication for the functionalization of the carbon nanotubes. Strong evidence for the functionalization is observed in the IR spectrum. Natural rubber nanocomposites prepared with these modified carbon nanotubes exhibit excellent mechanical properties and electrical conductivity. All composites showed a decline in mechanical properties above 0.1 phr loading. This may be due to aggregation or sedimentation of carbon nanotubes after that concentration. Or it may be due to the increased retarding tendency of carboxylic acid groups on MWNTs towards curing of samples resulting in poor cross linking in polymer matrix.

References

1. Iijima S. Helical microtubules of graphitic carbon. Nature1991; 354:56–8.
2. Job AE, Oliveira FA, Alves N, Giacometti JA, Mattoso LHC. Conductive composites of natural rubber and carbon black for pressure sensors. Synth Met 2003; 135:99–100.
3. Xiao KQ, Zhang LC. The stress transfer efficiency of a single-walled carbon nanotube in epoxy matrix. J Mater Sci 2004; 39:4481–6.
4. Hill DE, Lin Y, Rao AM, Allard LF, Sun YP. Functionalization of carbon nanotubes with polystyrene. Macromolecules 2002; 35: 9466–71.
5. Xiangwen Zhou, Yuefeng Zhu, Qianming Gong, Ji Liang, Materials Letters2006; 60:3769–3775
6. Frogley MD, Ravich D, Wagner HD. Mechanical properties of carbon nanoparticle-reinforced elastomers. Compos Sci Technol 2003; 63:1647–54
7. A. Fakhru'l-Razi, M.A. Atieh, N. Girun, T.G. Chuah, M. El-Sadig, D.R.A. Biak, Composite Structures 2006; 75: 496–500
8. A.M. Shanmugharaj, J.H. Bae, Kwang Yong Lee, Woo Hyun Noh, Se Hyoung Lee, Sung Hun Ryu, Composites Science and Technology 2007; 67:1813–1822
9. Liliane Bokobza and Me´ lanie Kolodziej, Polym Int 2006;55:1090–1098

Table 1. Compounding formulation for NR latex

Ingredients	Amount (g)
Centrifuged latex (60 % DRC)	167.0
10 % KOH solution	1.0
10 % Potassium oleate solution	1.0
20 % Vulcastab VL* solution	1.0
50 % ZnO dispersion	1.0
50 % ZDC dispersion	2.0
50 % Sulphur dispersion	3.0

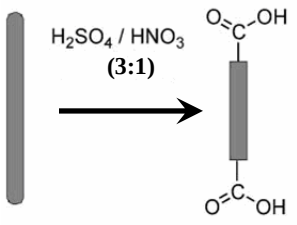

Scheme 1.Carboxylation of carbon nanotubes

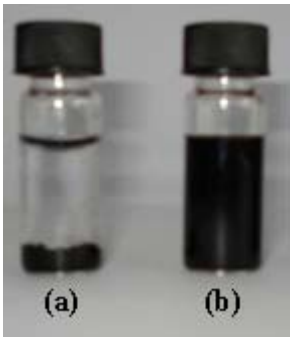

Fig. 1 Dispersions in water of (a) pristine MWNTs (b) MWNT-COOH

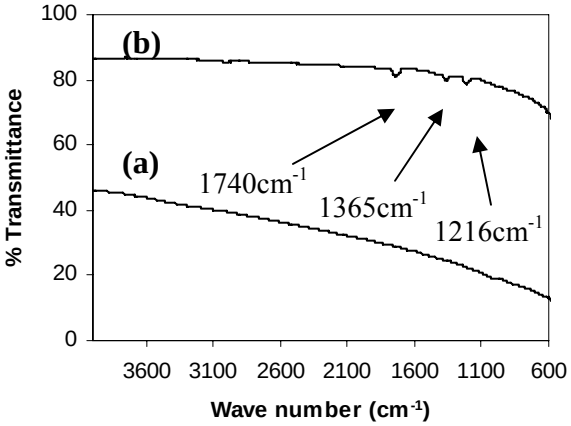

Fig.2 FT-IR spectra of pristine and chemically functionalized MWNTs :-(a) MWNT (b) MWNT-COOH

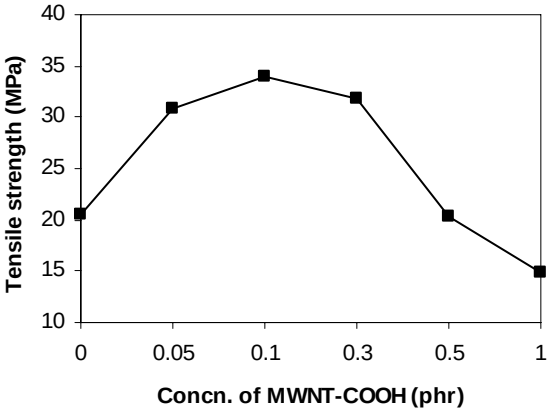

Fig. 3 Variation of tensile strength with concentration of MWNT-COOH

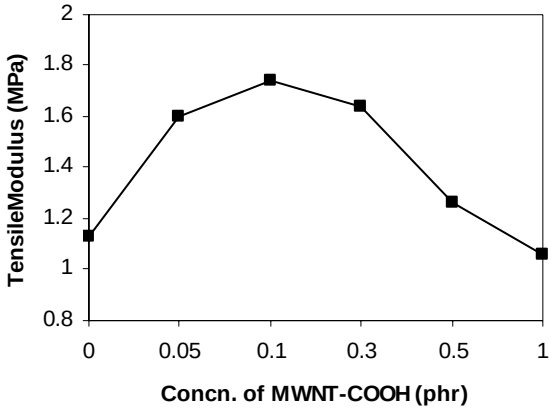

Fig. 4 Variation of tensile modulus with concentration of MWNT-COOH

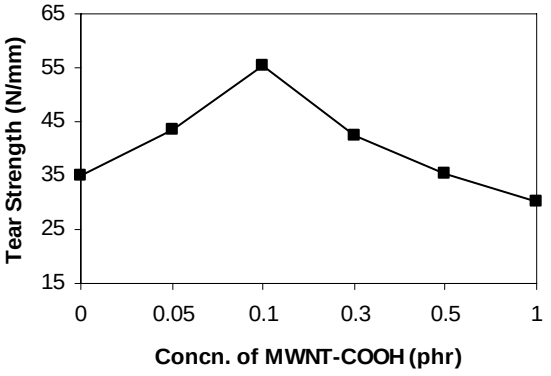

Fig. 5 Variation of tear strength with concentration of MWNT-COOH

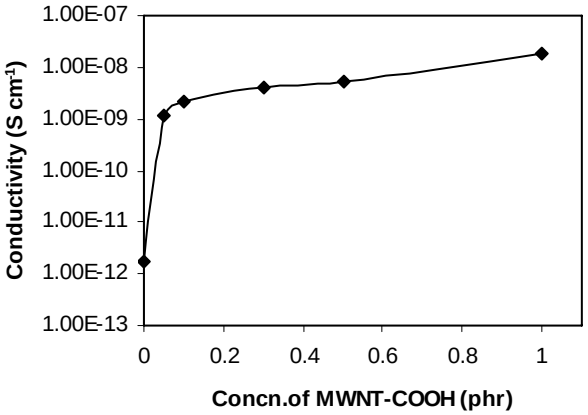

Fig. 6 Variation of conductivity with concentration of MWNT-COOH

Biodegradable polymers

R.Akila and K.Sangeetha

Amrita Vishwa Vidyapeetham, Amrita School of Engineering,
Ettimadai, Coimbatore, India

Email: akilaram1989@gmail.com

ABSTRACT:

A Rebirth of Plastic

Plastics are being used all over the world. From drinking cups and disposable silverware to parts for automobiles and motorcycles, plastics are continuing to rise. Plastics have been an environmental trepidation because of the lack of degradation. Plastics make up about 20% by volume waste per year. There are over 21,000 different types of plastics facilities in us.Plastics are extremely important to the job market as well as packaging throughout the world.Since plastics are vital to people's everyday lives, production of biodegradable plastics to make plastics more compatible with the environment is necessary. So biodegradable polymers are known as "REBIRTH OF PLASTIC". The two main reasons for using biodegradable materials, "the growing problem of waste resulting in the shortage of landfill availability and the need for the environmentally responsible use of resources". Biodegradable plastics began being sparking interest during the oil crisis in the 1970's. as oil prices increased, so did the planning and creating of biodegradable Materials. The 1980's brought items such as biodegradable films, sheets, and moldforming materials. Green materials (or Plant-based) have become increasingly more popular. This is due impart to the fact that they are a renewable resource that is much more economical then they were in the past.

This paper reviews biodegradable plastics focusing on their potential on starch based plastics,soy based plastics,bacteria based plastics,purpose and needs of biodegradable plastics,properties of biodegradable plastics,advantages and disadvantages of biodegradable plastics.

INTRODUCTION:

Biodegradable plastics are plastics that will decompose in the natural environment. Biodegradation of plastics can be achieved by enabling microorganisms in the environment to metabolize the molecular structure of plastic films to produce an inert humus-like material that is less harmful to the environment. They may be composed of either bioplastics, which are plastics whose components are derived from

renewable raw materials, or petroleum-based plastics. The use of bio-active compounds compounded with swelling agents ensures that, when combined with heat and moisture, they expand the plastic's molecular structure and allow the bio-active compounds to metabolise and neutralize the plastic.

BIODEGRADABLE PLASTICS:

Plastics are manufactured from numerous non-renewable resources like natural gas, coal, and oil. Biodegradable plastics are made with plant-based materials and result in 15% less carbon emission. Biodegradable plastic is expensive when compared to traditional plastics made from petroleum. However, when a chassis made out of biodegradable plastic gets disposed off, it decomposes in a few months whereas traditional plastic takes decades.

THE MANUFACTURING PROCESS:

Starch is a natural polymer. Cereal plants and tubers often contain a large quantity of starch, which can be processed into a ‘bioplastic’. Bioplastic is soluble in water; items made from starch can swell and get damaged when exposed to moisture. This can be overcome by modifying the starch into a different polymer. When the starch is harvested from corn, potatoes or wheat, a micro organism transforms it into lactic acid. It is then chemically treated to cause the molecules of lactic acid to link up into long chains or polymers, which bond together to form a plastic called polylactide (PLA).

PRODUCTS MANUFACTURED USING BIODEGRADABLE TECHNOLOGY:

Fujitsu Limited and Fujitsu Laboratories Limited use biodegradable plant based material as a substitute of polystyrene for the manufacture of embossed carrier tape used for packing large-scale

integrated circuit chips (LSIs) when shipping them on reels. The features of biodegradable plant-based embossed carrier tape are protection against electrostatic discharge, durability, its ability to maintain accurate dimensions, eco-friendly and it does not produce toxic emissions when incinerated.

PLASTICS CAN BE PRODUCED BY BACTERIA:

Another way of making biodegradable polymers involves getting bacteria to produce granules of a plastic called polyhydroxyalkanoate (PHA) inside their cells. Bacteria are simply grown in culture, and the plastic is then harvested. Going one step further, scientists have taken genes from this kind of bacteria and stitched them into corn plants, which then manufacture the plastic in their own cells

OTHER ECO-FRIENDLY PRODUCTS:

MicroPro, a company based in Dublin, Ireland produces eco-friendly computers, keyboards, mice and flat-panel monitors. The computers are updatable, upgradeable, reusable, recyclable and require less energy to manufacture. Users can remove individual parts and reuse them or replace them with more modern parts. Expected life span of iamco products (a range of eco-friendly computers from MicroPro) is 7-10 years, up to three times the lifespan of an average computer. Wood based frames and waste product of the pulp industry in Europe are used to manufacture biodegradable keyboards, mice and monitors.

ADVANTAGES AND DISADVANTAGES:

Under proper conditions biodegradable plastics can degrade to the point where microorganisms can metabolise them. This reduces problems with litter and reduces harmful effects on wildlife. However degradation of biodegradable plastic occurs very slowly, if at all, in a sealed landfill. Proper composting methods are required to efficiently degrade the plastic, which may actually contribute to carbon dioxide emissions.

Degradation of oil-based biodegradable plastics may contribute to global warming through the release of previously stored carbon as carbon dioxide. Starch-based bioplastics produced from sustainable farming methods can be almost carbon neutral.

Biodegradable plastics cannot be mixed with other plastics when sent for recycling; this damages the recycled plastic and reduces its value.

CONCLUSION:

Biodegradable plastics are one of the most innovative materials being developed in the packaging industry. Companies cannot work fast enough to produce this highly valuable technology. How widespread biodegradable plastics will be used all depends on how strongly society embraces and believes in environmental preservation. There certainly are an abundant amount of materials and resources to create and fund more uses for biodegradable plastics. The advancement of biodegradable technology has skyrocketed in recent years and there are growing signs that the public shows a high amount of curiosity in the product. With the variety of biodegradable plastics available in the near future, there will be a place for them current Age of Plastics.

Investigations on the physico chemical and thermal properties of Njavara rice variety

Chandroth Kalyad Simi *, Tholath Emilia Abraham #

Chemical Sciences and Technology Division
National Institute for Interdisciplinary Science and Technology (NIIST)
Thiruvananthapuram, India.

E- mail: emiliatea@yahoo.com

Abstract

The study on morphological, physicochemical, and thermal properties of Njavara rice starch confirms its unique position in Ayurveda. The starch granule size is bigger (5 – 6 μm) than the Chamba variety rice (1-2 μm). Thermogravimetric analysis reveals the exceptional thermal stability of this starch. The temperature dependent properties such as swelling power, solubility and water absorption capacity and enthalpy of gelatinization was also found to be very high. The gelatinization temperature of 85°C, Freeze thaw stability, gel strength, peak viscosity (957 cP), break down viscosity (324 cP) and set back values (421 cP) were higher than the chemba rice starch. Frequency sweep test showed that njavara starch gel was stronger than chemba rice starch against shear stress. Njavara starch gel texture also had high springiness. This inherent high thermal and pasting properties, makes njavara rice suitable as poultice for the body massage in the panchakarma treatment.

Key words: Njavara; physico-chemical properties; rheology; thermal analysis.

Introduction

Rice is one of the most important cereals and more than two thousand varieties of rice are grown commercially throughout the world. It is the main food item in Asia. Njavara is the unique rice, short duration cultivar grown only in certain pockets in Kerala state, south India[1] and belongs to the family Oryza. This is the only cultivar traditionally used effectively in the Ayurvedic system of medicine in certain specific treatments like Panchakarma. It is interesting to note that this treatment is now getting more and more popular, not only in this region of the

country but also in other parts of the nation and even in other countries. Njavara as a special cereal, reported to have properties to rectify the basic ills affecting the circulatory, respiratory as well as the digestive system. Black glumed Njavara has been used in Ayurveda treatment from the age of Charaka-ie, BC.600. Njvara rice endosperm has around 73 % of starch.

Starches exhibit difference in various properties in accordance with the source and genotype. The properties mainly depend on physical and chemical characteristics such as granule size, amylose amylopectin ratio etc. the shape and size of starch granules which is characteristics of their botanical origin[2]. The rheological properties of different starches vary to a large extent as a function of granule structure and physico chemical composition. Several rheological changes occur in starch, when starch–water systems are heated above the gelatinization temperature, the starch granules loose their crystallinity, absorb large amounts of water, and leach out amylose, thereby forming a paste composed of swollen starch granules dispersed in an amylose matrix[3]. Here we are reporting the unique physico chemical, thermal, rheological and textural characteristics of njavara starch compared to the native chamba rice starch.

Experimental section

Njavara (Black glumed) and chamba (Jaya) rice. All chemicals used were of reagent grade purchased from Central Drug House, Mumbai, India.

Starch was isolated from rice by a conventional method. Studied the amylase content according to the procedure of Sowbhagya and Bhattacharya [4]

Morphological characteristics of the starch grains were studied using scanning electron microscope (JEOL make, model JSM 5600 LV, Japan).

The percentage transmittance of this gelatinized starch was determined at 640 nm using a spectrophotometer (UV 2100, Shimadzu,Japan). The gel clarity was studied with time duration (2h, 4h, 6h, 24h, 48h, 72h).

Solubility and swelling power at various temperatures such as 60°C, 70°C, 80°C, 85°C and 90°C were determined [5]. Percentage solubility and swelling power were calculated using the formula

$$\% \text{ solubility} = \frac{\text{dry weight at } 120°C}{\text{Sample weight}} \times 200$$

$$\text{Swelling Power} = \frac{\text{weight of swollen granule}}{\text{Sample weight (100- \% solubility)}} \times 100$$

50 ml of 6% (w/v) starch solution was heated to 95°C and was held at this temperature for 15 minutes and gel was cooled down to room temperature. The gel was frozen at < 0°C over night and thawed to room temperature and then centrifuged at 604 x g for 15 minutes and measurements was taken for water separation (syneresis) from the starch gels and the process was repeated for 5 cycles.

Differential scanning calorimeter (Perkin Elmer, USA) was employed to measure the thermal analysis of rice starches.

The thermal properties of the starches were measured with a simultaneous DTA-TG apparatus (DTG –60, Shimadzu, Japan) at a heating rate of 20 ^{O}C/ minute in nitrogen atmosphere.

Pasting characteristics of the starches were determined with a rapid visco analyzer (RVA-4, Newport Scientific Warriewood, Australia) at a fixed starch concentration of 10%(w/V) and a constant speed 160g using the standard profile.

The digestability of starches was studied using the enzyme alpha amylase from *Bacillus amyloliquifaciens*.

Rheological measurements were made with a rheometer (Anton Paar rheometer TA Instruments Inc., New Castle, DE, USA). A cone and plate measuring geometry was used with a gap width of 0.5 mm. studied the temperature dependence and frequency dependence of starch sample

Textural properties of 10% starch gels were evaluated on a Food texture Analyser (model TADH stable microsystem, Godalming, Surrey, UK).

X-ray diffraction patterns of njavara starch, and native rice starch was analyzed using an X-ray diffractometer (XPERT, Philips, Eindhoven, The Netherlands) with Nickel filtered Cu K radiation (λ = 0.154 nm) at a voltage of 40 kV and current of 30 mA. The Degree of crystallinity of samples was quantitatively estimated

All the experiments were done in triplicate and the average values are given

Results and discussion

The rice starch granules are found to be hexagonal in shape, which is typical of a cereal starch. SEM shows that the njvara starch granule has diameter in the range of 5 – 6 µm. but in native rice starch size is small.The variation in starch granule morphology may be due to the biological origin and physiology of the plant and the biochemistry of the amyloplast.

Amylose content in njavara rice starch was found to be 20±2 %. The amylose content in rice varieties are in the range of 20-22% [1]

In the case of njavara starch, the swelling power increases steeply over the range of temperature studied. In the case of native rice starch, swelling pattern is less steep and shows a constant increase in swelling power.

Njavara rice starch transmittance value (87.45%) is less at the initial stage compared to native rice (95.30%). Rice starches generally show high transmittance value than the other cereal starches. In the case of njavara starch gel, the decrease in transmittance was sharp up to 6 h then it remained almost constant. However the native rice starch lost its clarity after 2 h significantly. The higher swelling power and solubility only at a higher temperature makes this starch unique and provides application for panchakarma in Ayurveda.

Njavara starch had low synerisis compared to the native rice starch. Freeze thaw stability of both the starches shows same pattern. The % synerisis is inversely related to the stability of the gel. Njavara rice starch separate less water at the first cycle than native rice starch.

Gelatinization endotherm of native rice starch was broader than njavara. A wide melting range might imply a large amount of crystals of varying stability, whereas a narrow range could suggest crystals of a more homogeneous quality and similar stability. Njavara rice had high gelatinization temperature (85°C) than the native starch (70.93°C). Njavara starch required more energy to gelatinize since its enthalpy of gelatinization was very high (ΔH=366.165j/g). The enthalpy of gelatinization of native rice starch was lower and is 61.8155j/g. The retrogradation properties of njavara and native rice starches were studied after storage of gelatinized starches at 4 °C for 7 days. Retrogradation peak of njavara and native starches were found to be shifted in the higher temperature regions. (87.2°C for njavara and 72.73°C for native rice starch). The percentage of retrogradation (%R) was less for njavara starch (85%) as compared to native rice starch (90.56%).

Njavara and native starch was subjected to thermal degradation. In the case of njavara starch, degradation starts at a temperature of 275 °C. But for native starch the degradation temperature starts at a lower temperature of 225 °C. This showed that njavara starch was thermally more stable than native rice starch.

Pasting profile of both rice starches are similar. Njavara starch showed higher peak viscosity, final viscosity, and higher break down value than native starch. The setback value of njavara is higher due to high peak viscosity and amylose content.

Njavara and native starch showed same rate of hydrolysis by bacterial alpha amylase. 14% of starch was hydrolysed at 30 minutes of incubation.

Both starches shows same pattern of shear modulus against temperature. Up to a certain temperature both moduli (storage [G’] and loss [G”]) were same after this storage modulus shows a sharp increase reaches a maximum then decreases. Njavara rice gelatinizes at higher

temperature 68°C and gelatinization starts at 59°C. But in native starch gelatinization temperature was found to be 58°C and gelatinization starts at a lower temperature 48°C. Higher value of G' compared to G" indicates the formation of gel.

Both rice variety show the same pattern of modulii. But the difference between the G' and G" value is more in njavara starch compared to the native rice. This indicates the gel rigidity is higher in the case of njvara starch gel.

Texture studies showed that njavara starch showed higher value of springiness, chewiness. Both the starch gel did not have much difference in cohesiveness and gumminess. Njavara starch gel has less hardness than native starch gel.

The XRD pattern of both rice starches are almost similar but differ in crystallinity as Njavara starch was more crystalline.

Conclusion

Physico chemical properties of njavara starch was studied and compared with properties of native chamba rice starch. The njavara starch has high gelatinization temperature, water absorption capacity, solubility and swelling power. It degrades at higher temperature than the native starch. Its enthalpy of gelatinization was very high. Pasting properties showed that it has higher peak viscosity, break down viscosity and set back values.

Acknowledgement

Ms.Simi grateful to Council of Scientific and Industrial Research (CSIR, India) for the financial support as SRF. The authors are grateful to Mr. Shanavas for rheology analysis, Mr. Sajeevan for textural analysis, and Mr. Chandran for SEM analysis.

References

1. Deepa, G.; Vasudeva Singh; Akhilender Naidu, K. Food Chemistry, 2008, 106, 65-171.
2. Madsen, M.H.; Christensen, D.H. Starch, 1996, 48, 245-249.
3. Ring, S.G. Starch/Stärke, 1985, 37, 80–83.
4. Sowbhagya, C.M.; Bhattacharya, K.R. Starke, 1971, 23, 53 – 55.

5. Methods in carbohydrate chemistry volume IV, (1964). Academic press, New York and London. 106 -10

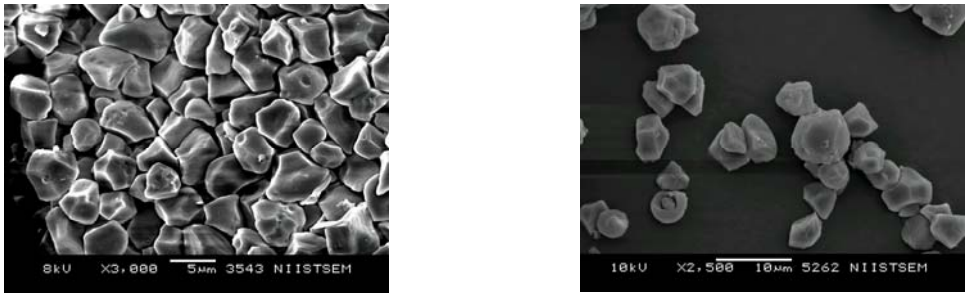

a) **(b)**

Figure 1 SEM micrograph of Njavara rice starch (a) and native chamba rice starch (b)

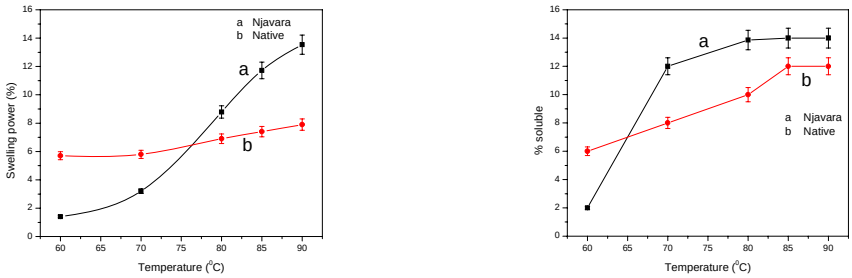

(a)

Figure 2 Swelling power (a) and solubility (b) of njavara and native rice starch

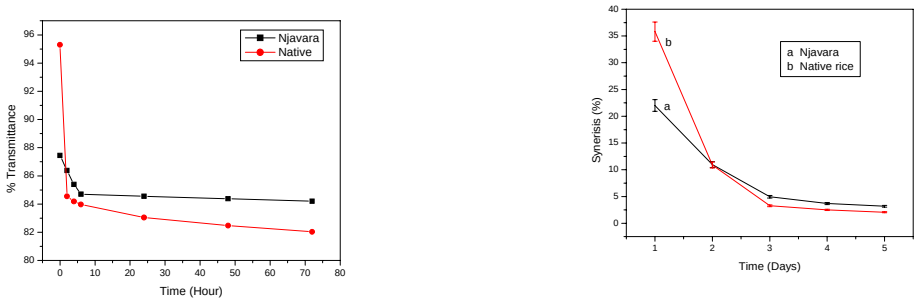

(a) **(b)**

Figure 3 Gel clarity (a) Freeze- thaw stability (b) of njavara and native rice starch

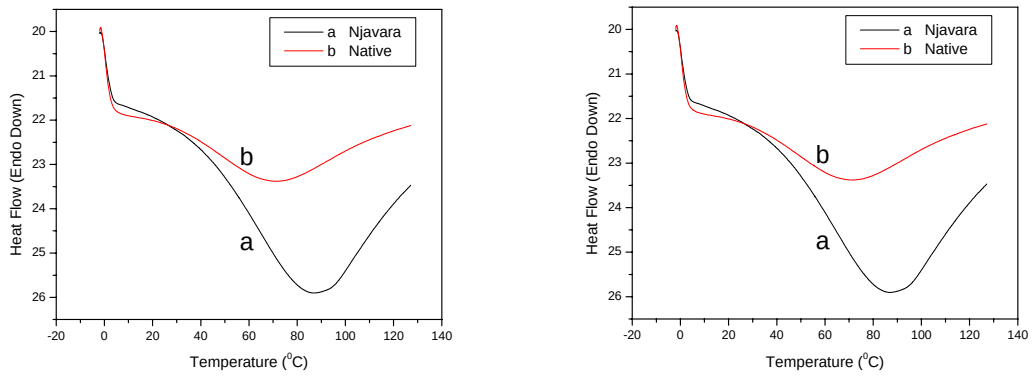

(a) **(b)**

Figure 4 Differential scanning calorimetry of original (a) and retrograded (b) njavara and native rice starch

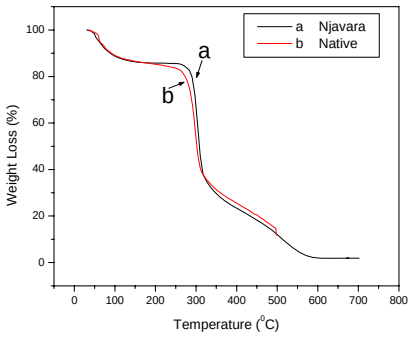

Figure 5 Thermogravimetric analysis of njavara and native rice starch

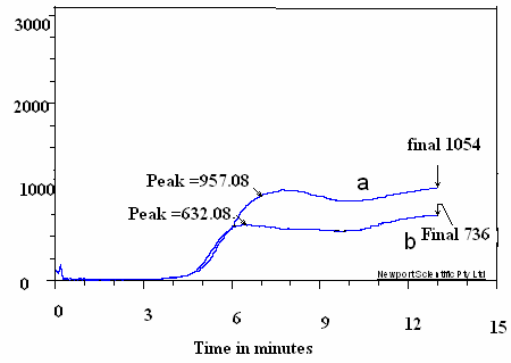

Figure 6 Pasting profile of (a) njavara and (b) native rice starch

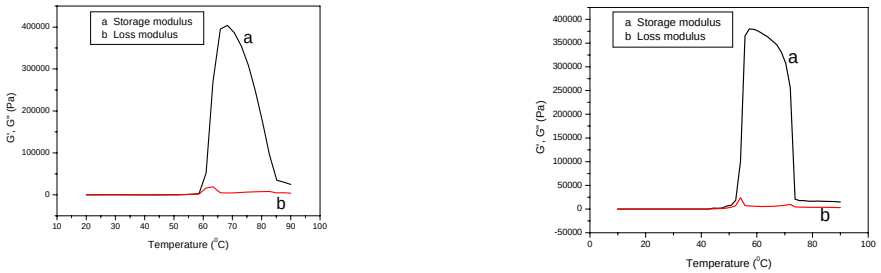

(a) (b)

Figure 7 Temperature dependence of (a) Njavara and (b) native rice starches

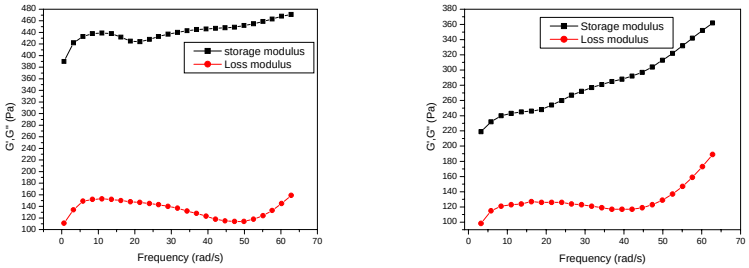

(a) **(b)**

Figure 8 Frequency dependence of (a) Njavara and (b) native rice starches

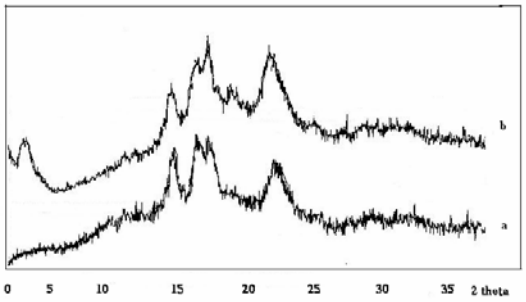

Figure 12 XRD of (a) njavara (b) native rice starches

Miscibility studies of HPMC/PEG blends in water by viscosity, density, refractive index and ultrasonic velocity method

Sudhir Ramswamy Illiger[1]; Chandralekha Fadnis[1]; T. Demappa[1]*; J. Jayaraju[2] and J. Keshavayya[2]

[1] Department of Post-Graduate Studies and Research in Polymer Science, University of Mysore, Sir M.V.PG .Center, Tubinakere, Mandya, 571402, Karnataka, INDIA
[2] Department of Chemistry, School of Chemical Sciences, Jnana Sahyadri, Kuvempu University, Shankaraghatta-577 451, Shimoga, Karnataka, India
Email: tdemappa2003@yahoo.co.in

ABSTRACT:

Hydroxy propyl methyl cellulose (HPMC) / Polyethylene glycol (PEG) blends are edible polymer films used for food packing and directly in foodstuffs. However they are water-soluble in ordinary temperature and have good mechanical properties. The miscibility of HPMC/PEG blend in water was studied by viscosity, ultrasonic velocity, density and refractive index techniques at 30 and 50º C. Using viscosity data, the interaction parameters μ and α were calculated. These values revealed that HPMC/PEG blend is miscible when the HPMC content is more than 60 wt-% in the blend at 30 and 50º C, below which is immiscible. Further the result was also confirmed by ultrasonic velocity, density, refractive index measurements, which also revealed that the change in temperature has no significant effect on the miscibility of HPMC/PEG polymer blend.

Keywords: **b**lend, density, hydroxy propyl methylcellulose, miscibility, poly(ethylene glycol), refractive index, ultrasonic velocity, viscosity.

1. Introduction

The importance of polymer blending has been increased in recent years, because of the preparation of polymeric materials with desired properties, low basic cost and improved process ability. Polymer blends are physical mixtures of structurally different polymers or co-polymers, which interact through secondary forces with no covalent bonding (Krause, 1978) and are miscible at molecular level. The basis of polymer-polymer miscibility may arise from any specific interactions, such as hydrogen bonding, dipole-dipole forces and charge transfer complexes for homopolymer mixtures (Varnell & Coleman, 1981; Varenell, Rant, Cdeman, 1983; Woo, Barlow & Paul, 1986). There have been various techniques of studying the miscibility of the polymer blends (Crispim, Rubira, Muniz, 1999; Patel, 2004; Ping, 1997; Jiang, Han, 1998; Cabanclas, Serrano & Baselga, 2005). Some of these techniques are complicated, costly and time consuming. Hence it is desirable to identify simple, low cost and rapid techniques to study the miscibility of polymer blends. Chee and Sun et al (Chee, 1990; Sun, 1992) have suggested a viscometric method for the study of polymer-polymer miscibility in solution. Singh and Singh (Singh, 1984; Singh, 1983) have suggested the use of ultrasonic velocity and viscosity measurements for investigating the polymer miscibility in solution. Paladhi and Singh (Palladi, 1994 a; Palladi and Singh, 1994 b) have shown that the variation of ultrasonic velocity and viscosity with blend composition is linear for miscible blends and non-linear for immiscible blends. Recently, Varada Rajulu et al (Varada Rajulu, Reddy, Ranga

Reddy, 1998) have used ultrasonic and refractometric technique to study the miscibility of polymer blend.

As part of our research work, we have studied the miscibility of HPMC/PEG blend in water at different temperatures by viscosity, ultrasonic velocity, density, and refractive index techniques (Demappa et al., 2006; 2007). We selected these polymers, because they have many pharmaceutical and biomedical applications (Zeng, Fang, 2004; Jumel, Harding, 1996). Hydroxy propyl methyl cellulose (HPMC) is a polysaccharide prepared from cellulose. It contains both methyl and hydroxy propyl substitutes. Poly (ethylene glycol) (PEG) is a synthetic water-soluble polymer with good film forming property, which offers good tensile strength (TS), flexibility and barrier properties to oxygen and aroma (Schellekens & Bastiansen, 1991). Poly (ethylene glycol) (PEG) is used in all applications of aqueous phase partitioning. For biochemical separations on the laboratory scale, the most commonly used aqueous phase system is composed of Dextron and PEG (Albertson, P.A., New York,1986) The structures of both HPMC and PEG are shown in scheme 1 and scheme 2 respectively.

2. Experimental

HPMC (E 15 LV premium; LOBA CHEMIE PVT LTD) and PEG ($\overline{M}_w = 200$; AR grade, Merck India Ltd., India) were used for this work. A dilute polymer solution of 1% w/v was prepared for viscometric studies. Stock solutions of homopolymers and the blends of HPMC/PEG of different compositions, 10/90, 20/80, 30/70, 40/60, 50/50, 60/40, 70/30, 80/20 and 90/10, were prepared in water. Viscosity measurements at 30 and 50 ºC were made using an Ubbelohde suspended level viscometer with the flow time of 98 s for distilled water. The total weight of the two components in the solution was always maintained at 1 g/dL. And the different temperatures were maintained in a thermostat bath, with a thermal stability of ± 0.05ºC. The ultrasonic velocity measurements were performed by an ultrasonic interferometric technique (Varada Rajulu, 1996). The temperatures were maintained at 30 and 50º C by circulating water from a thermostat, with a thermal stability of ± 0.05ºC, through the double–walled jacket of the ultrasonic experimental cell. The experimental frequency was 2-MHz, and the velocity measurements were accurate to better than ±0.5%. The densities of the solutions were measured at 30 and 50º C by specific gravity bottle. The refractive indices of the HPMC/PEG blend solutions were measured using an Abbe's refractometer, with a thermostat water-circulation system (Varada Rajulu, Mabusab, 1998) at 30 and 50 ºC (Singh, & Singh, 1984). The accuracy of the refractive index measurements is ± 0.02%.

3. Results and Discussion

HPMC, however, is known to be a flexible nonionic polymer, which obeys the classical Huggin's equation. The Huggin's plots for the pure components (HPMC and PEG) and their blends at 30 and 50º C are shown in figure 1, 2 & table 1, 2 respectively. The figure indicates the considerable higher slope variation for 80/20 and 60/40 HPMC/PEG blend compositions. This may be attributed to the mutual attraction of macromolecules in solution, because of the increase of hydrodynamic and thermodynamic interaction. Hence HPMC/PEG blend is found to be miscible, only when the HPMC content is more than 60 % in the blend. Below this critical concentration, a sharp decrease in the slope is observed in the Huggin's plot because of the phase separation.

To quantify the miscibility of the polymer blends Chee (Chee, 1990) suggested that the general expression for interaction parameter when polymers are mixed in weight fractions w_1 and w_2 is as follows:

$$\Delta B = \frac{b - \bar{b}}{2w_1 w_2} \qquad (1)$$

Where $\bar{b} = w_1 b_{11} + w_2 b_{22}$ in which, b_{11} *and* b_{12} are the slopes of the viscosity curves for the pure components. The coefficient b is related to the Huggin's coefficient K_H as

$$b = K_H [\eta]^2 \qquad (2)$$

for ternary systems, the coefficient b is also given by

$$b = w_1^2 b_{11} + w_2^2 b_{22} + 2w_1 w_2 b_{12} \qquad (3)$$

where b_{12} is the slope for the blend solution. Using these values, Chee (Chee, 1990) defined a more effective parameter as follows:

$$\mu = \frac{\Delta B}{\{[\eta]_2 - [\eta]_1\}^2} \qquad (4)$$

where $[\eta]_1$ and $[\eta]_2$ are the intrinsic viscosities for the pure component solutions. The blend is miscible when $\mu \geq 0$ and immiscible when $\mu < 0$ (Chee, 1990). The values of μ, calculated with the aforementioned expression at 30 and 50º C are represented in Table 3.

Recently, Sun et al (Sun, 1992) have suggested a new formula for the determination of polymer miscibility as follows:

$$\alpha = K_m - \frac{K_1 [\eta]_1^2 w_1^2 + K_2 [\eta]_2^2 w_2^2 + 2\sqrt{K_1 K_2}\,[\eta_1][\eta_2] w_1 w_2}{\{[\eta]_1 w_1 + [\eta]_2 w_2\}^2} \qquad (5)$$

where K_1, K_2 and K_m are the Huggin's constants for individual components 1, 2 and the blend, respectively. The long-range hydrodynamic interactions are considered while deriving this equation. Sun et al (Sun, 1992) have suggested that a blend will be miscible when $\alpha \geq 0$ and immiscible when $\alpha < 0$.The computed values of μ and α are found to be negative when the HPMC content is up to 50% and then positive beyond this value at 30 and 50º C, respectively and the data are given in Table 3 and Figure 3 shows the miscibility windows of the HPMC/PEG blend in water. As the long-range hydrodynamic interactions are considered in the equation for α, eq (5) is more accurate than eq (4). A similar observation was made by Varada Rajulu et al and Jayaraju et al (Varada Rajulu, 1998; Jayaraju, 2006) in case of polyvinyl pyrrolidone/ polystyrene and Chitosan/Hydroxypropyl methyl cellulose blends, where μ was found to be negative and α was found to be positive. They confirmed the miscibility of such blends by other methods. To confirm this further, we have measured the ultrasonic velocity (ν), density (ρ) and refractive index (n) of the blend under consideration at various compositions, at 30 and 50ºC. These values are presented in Table 3. The variation of the ultrasonic velocity in figure 4, density and refractive index with the blend composition is shown in fig 5 respectively. The adiabatic compressibility β_{ad} (Varada Rajulu, 1990) of different blend compositions was evaluated by using the equation.

$$\beta_{ad} = \frac{1}{v^2 \rho} \qquad (6)$$

Where v is the velocity of sound and ρ is the density of blend solutions, and the values are given in Table 3. The variation of adiabatic compressibility at 30 and 50 º C is shown in Figure 5. The graphs show both linear and nonlinear regions. It was already established (Cabanclas et al and

Sun et al) that the variation is linear for miscible blend and non-linear for immiscible blend. In the present case, the variation is found to be linear when the HPMC content is more than 60 % at 30 and 50º C respectively. This observation is in confirmation with μ and α value. So the present study indicates the existence of miscibility windows when the HPMC content is more than 60 % in the blend. This is because, the specific interaction between the polymer segments is more when the HPMC content is more than 60%, there by, leading to miscibility of the blend. And below this composition there will not be much interaction between the polymer segments, which leads to immiscibility of the polymer blend. Here, the miscibility of the blend may be due to some specific interaction like H-bonding between HPMC/PEG.

4. Conclusion

Using viscosity, Ultrasonic velocity, density and refractive index methods, it is concluded that the polymer blend of HPMC/PEG is found to be miscible, when the HPMC content is more than 60 % in the blend at 30 and 50º C respectively. Below this HPMC concentration, the blends were found to be immiscible. It is also observed that temperature has no significant effect on the miscibility of these blends even though the reduced viscosity, density, refractive index and adiabatic compressibility decreases and the ultrasonic velocity increases as the temperature increases. Thus afore mentioned techniques are simple, low cost, rapid and efficient methods in exploring the miscibility windows of HPMC/PEG blend in solution.

References

Albertson, P.A.-Partition of cell particles and macromolecules, 3rd ed; Wiley: New york, 1986.

Crispim, E.G; Rubira, A.F; Muniz, E.C. (1990).Solvent effect on the miscibility of poly(methyl methacrylate) /poly(vinyl acetae) blends : using differential scanning calorimetry and viscometry technique.*polymer 1999; 40,5129*.

Cabanclas, J.C; Serrano, B; Baselga.J (2005). Development of continous morphologies in initially heterogeneous thermosets blended with poly (methyl methacrylate). *Journal of Macromolecules, 38,961.*

Chee, K.K. Determination of polymer–polymer miscibility by viscometry. (1990). *European Polymer Journal, 26, 423.*

Demappa, T., Basavaraju, K.C and Rai, S.K. (2006). Preparation of chitosan and its miscibility studies with gelatin using viscosity, ultrasonic and refractive index. *Carbohydrate Polymers, 66,357.*

Demappa, T., Basavaraju, K.C, and Rai, S.K. (2007), Miscibility studies of Polysaccharide Xanthan gum and PEO (Polyethylene Oxide) in dilute solution. *Carbohydrate Polymers, 69,462.*

Jiang , W.H; Han, S.(1998). An improved criterion of polymer –polymer miscibility determined by viscometry. *European Polymer Journal,,34,1579.*

Jumel,K; Harding,S.E; Hayter.I. (1996).Molar mass and viscometric charecterization of hydroxy Propyl methylcellulose. *Carbohydrate Polymer, 29,105.*

Jayaraju, J., Raviprakash, S.D., Keshavayya, J., and Rai, S.K.(2006). Miscibility Studies on Chitosan/Hydroxy propyl methyl Cellulose Blend in Solution by Viscosity, Ultrasonic Velocity, Density, and Refractive Index Methods. *Journal of Applied Polymer Science,102, 2738.*

Krause, S. In Polymer–Polymer Compatibility in Polymer Blends; Paul,D.R., and

Seymour, N., Eds.; Academic Press: NewYork, 1978; Vol. 1.
Patel,M.(2004).viscoelastic properties of polystyrene using dynamic rheometry. Polymer Test, 23,107.
Ping, Z.(1997).A new criterion of polymer –polymer miscibility detected by viscometry. *European Polymer Journal, 33,411.*
Palladhi, R., Singh, R.P. (1994a). Miscibility and interaction studies on some aqueous polymer blend solution by ultrasonic and rheological techniques. *Journal of Applied Polymer Science, 51, 1559*
Palladhi, R., Singh, R.P.(1994b). Ultrasonic and rheological investigation on interacting blend solutions of poly (acrylic acid) with poly (vinyl pyrrolidone) of poly (vinyl alcohol). *European Polymer Journal, 30,251.*
Schellekens, R., Bastiansen, C.J. (1991). A drawing behaviour of polyvinyl alcohol fibers. *Journal of Applied Polymer Science, 43, 2311.*
Sun, Z., Wang, W., Fung, Z.(1992) Criterion of polymer-polymer miscibility determined by viscometry. *European Polymer Journal, 28,1259.*
Singh, Y.P., Singh, R.P.(1984)Compatibility studies on polyblends of PVC with chlororubber-20 and its graft polyblends by ultrasonic. *European Polymer Journal, 20,535*
Singh, Y.P.,Singh, R.P.(1983). Miscibility studies on polymer blends by viscometric and ultrasonic techniques. *European Polymer Journal, 19, 535*
Varnell,D.F, Coleman, M.M. (1981).FTIR, Studies of polymer blends,pt5: Further observations on polyester-poly (vinyl chloride) blends. *Polymer, 22,1324*
Varenell, D.F, Runt, J.P, Coleman, M.M.(1983), Fourier Transform infrared studies of polymer blends, further observations on the poly (bisphenol -A. carbonate) –poly (e-caprolactone) system. *Polymer, 24,37*
Varada Rajulu,A; Reddy,R.L; Ranga Reddy,R.N.V.(1998).Ultrasonic and viscometric investigation of cellulose acetate /poly (methyl methacrylate) blends in solution *Acoustica ,84,577.*
Vararda Rajulu, A., Mabusab, P.(1996). Ultrasonic studies of water/poly (ethylene glycol) mixtures. *European Polymer Journal, 32,267.*
Varada Rajulu,A;Mabusab,P.(1998). Refractometric studies in water /polethylene glycol-300 mixtures. *European Polymer Journal, 34,31*
Varada Rajulu,A; Siddaramaiah; Reddy,R.L. (1998). Ultrasonic,refractometric and viscosity studies of some polymer blends in solution. *Journal of Applied Polymer Science, 70,1823.*
Varada Rajulu, A; Rao,K.C; Naidu,S.V.(1990). Miscibility studies on chitosan/ hydroxypropyl cellulose .... *Journal of pure Applied Ultrason.. 12,115.*
Woo, E.M , Barlow, J. W.Paul, D.R. (1986). Phase behaviour of blends of aliphatic polyesters with a vinylidine chloride copolymer. *Journal of Applied Polymer Science, 32,3889.*
Zeng, M; Fang.Z;Xu,C. (2004).Novel method of preparing microporous membrane by selective dissolution of chitosan/polyethylene glycol blend membrane. *Journal of Applied Polymer Science,,91,2840.*

Table 1: The reduced viscosity data for HPMC/PEG and their blends in water at 30 °C

Concentration (g/dL)	η_{sp}/C (dL/g) at 30 °C										
			HPMC/PEG Blend composition								
	HPMC	PEG	90/10	80/20	70/30	60/40	50/50	40/60	30/70	20/80	10/90
0.1	1.40	0.09	1.22	1.16	1.11	0.90	0.69	0.58	0.38	0.33	0.21
0.2	1.54	0.12	1.38	1.25	1.42	0.96	0.72	0.64	0.42	0.33	0.22
0.3	1.67	0.12	1.39	1.32	1.20	0.99	0.79	0.64	0.42	0.36	0.25
0.4	1.79	0.15	1.51	1.37	1.25	1.05	0.82	0.68	0.45	0.41	0.23
0.5	1.93	0.17	1.58	1.42	1.27	1.07	0.83	0.72	0.52	0.42	0.25
0.6	2.07	0.18	1.65	1.50	1.31	1.19	0.86	0.73	0.55	0.43	0.29
0.7	2.21	0.20	1.78	1.61	1.38	1.21	0.95	0.76	0.57	0.42	0.28
0.8	2.33	0.20	1.98	1.64	1.46	1.26	0.95	0.80	0.58	0.42	0.29
0.9	2.46	0.23	1.99	1.74	1.49	1.30	0.99	0.85	0.62	0.47	0.29

Table 2: The reduced viscosity data for HPMC/PEG and their blends in water at 50 °C

Concentration (g/dL)	η_{sp}/C (dL/g) at 50 °C										
			HPMC/PEG Blend composition								
	HPMC	PEG	90/10	80/20	70/30	60/40	50/50	40/60	30/70	20/80	10/90
0.1	1.25	0.08	1.06	1.04	0.79	0.77	0.57	0.42	0.28	0.33	0.29
0.2	1.32	0.08	1.13	1.08	0.79	0.78	0.60	0.46	0.30	0.35	0.29
0.3	1.40	0.08	1.18	1.11	0.83	0.81	0.63	0.48	0.34	0.38	0.28
0.4	1.45	0.10	1.26	1.12	0.89	0.86	0.71	0.54	0.40	0.43	0.29
0.5	1.56	0.11	1.36	1.11	0.98	0.90	0.72	0.59	0.44	0.46	0.33
0.6	1.62	0.12	1.43	1.28	1.05	0.95	0.75	0.59	0.46	0.48	0.33
0.7	1.66	0.14	1.50	1.29	1.04	1.00	0.75	0.67	0.50	0.53	0.32
0.8	1.74	0.16	1.53	1.32	1.06	1.04	0.83	0.70	0.53	0.57	0.34
0.9	1.84	0.17	1.58	1.39	1.13	1.10	0.90	0.75	0.58	0.60	0.36

Table 3 : Interaction parameters, density, refractive index, ultrasonic velocity and adiabatic compressibility of HPMC/PEG blend at 30 and 50˚ C

Composition HPMC/PEG	Interaction Parameter				Ultrasonic velocity		Density		Refractive Index		Adiabatic Compressibi	
	μ	α	μ	α	(m/s)		(g/cm^3)		(n)		(Kg^{-1} ms^2) 1	
	30 °C		50 °C		30 °C	50 °C	30 °C	50 °C	30 °C	50 °C	30 °C	50
10/90	-0.3736	-4.3120	-0.1275	-2.6998	9950	13990	1.0337	1.0312	1.341	1.339	0.9990	0.4
20/80	-0.4942	-2.7278	-0.0140	-1.3419	11803	12923	1.0379	1.0305	1.342	1.347	0.6650	0.5
30/70	-1.3249	-2.7632	-0.0162	-3.1464	11956	11876	1.0349	1.0313	1.340	1.338	0.6760	0.6
40/60	-0.3138	-2.5312	-0.0205	-0.1469	8336	15987	1.0348	1.0290	1.341	1.339	1.3906	0.3
50/50	-0.3095	-1.4488	0.0233	-0.0660	11940	12818	1.0364	1.0308	1.340	1.337	0.6777	0.5
60/40	-0.1652	1.6743	0.0879	0.1948	9918	11886	1.0353	1.0300	1.341	1.339	0.9699	0.6
70/30	-0.0368	0.7001	0.0616	0.0715	9831	11920	1.0355	1.0305	1.341	1.339	0.9990	0.6
80/20	0.0320	0.4302	0.1105	0.3506	9865	11875	1.0359	1.0311	1.341	1.339	0.9920	0.6
90/10	0.0781	0.3880	0.1372	0.1691	9870	11899	1.0361	1.0316	1.341	1.339	0.9890	0.6

Scheme 1: structure of HPMC

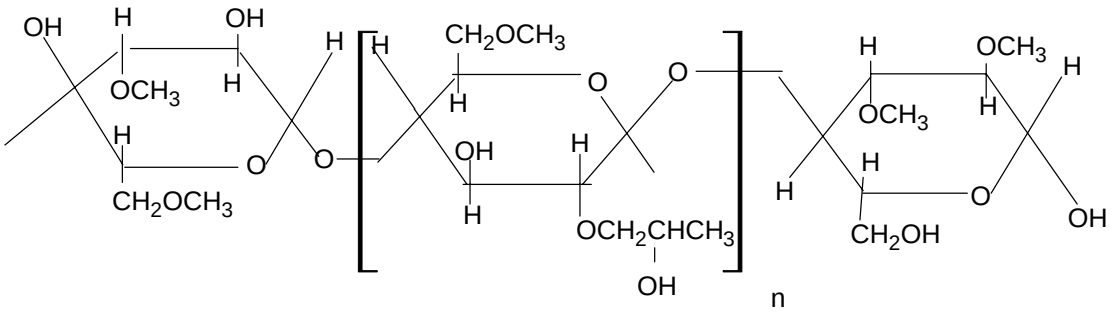

$C_8H_{16}O_8$ $(C_{10}H_{18}O_8)_n$ $C_8H_{16}O$

Scheme 2: structure of PEG

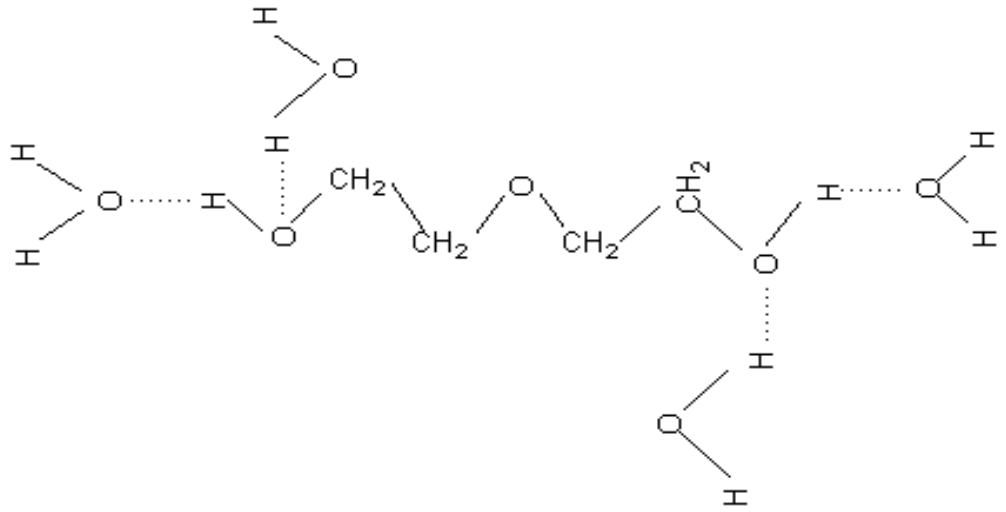

Polyethylene glycol

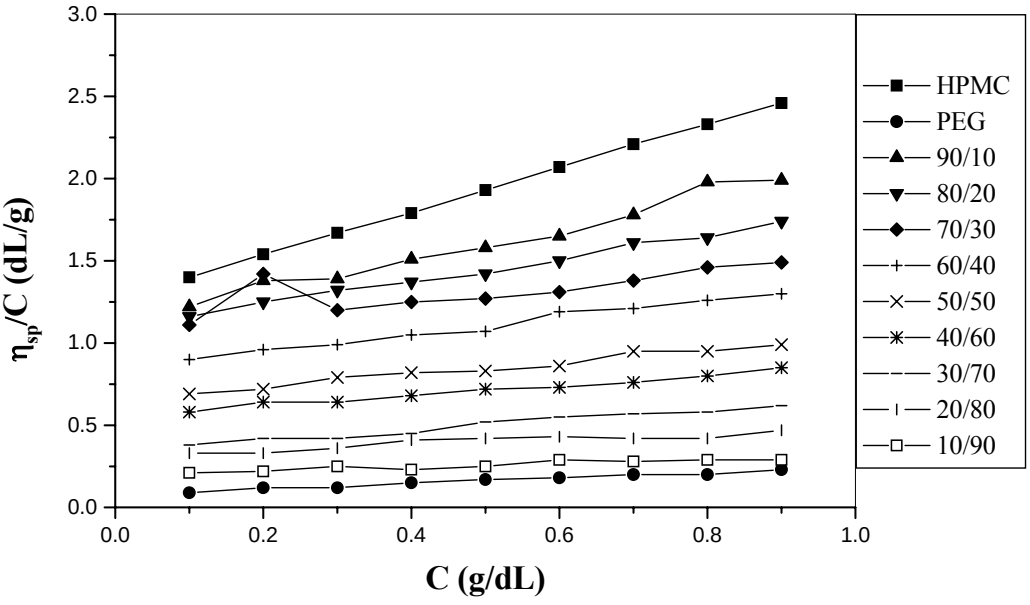

Figure 1. Huggin's plots for 1% w/v HPMC/PEG blend in water at 30ºC

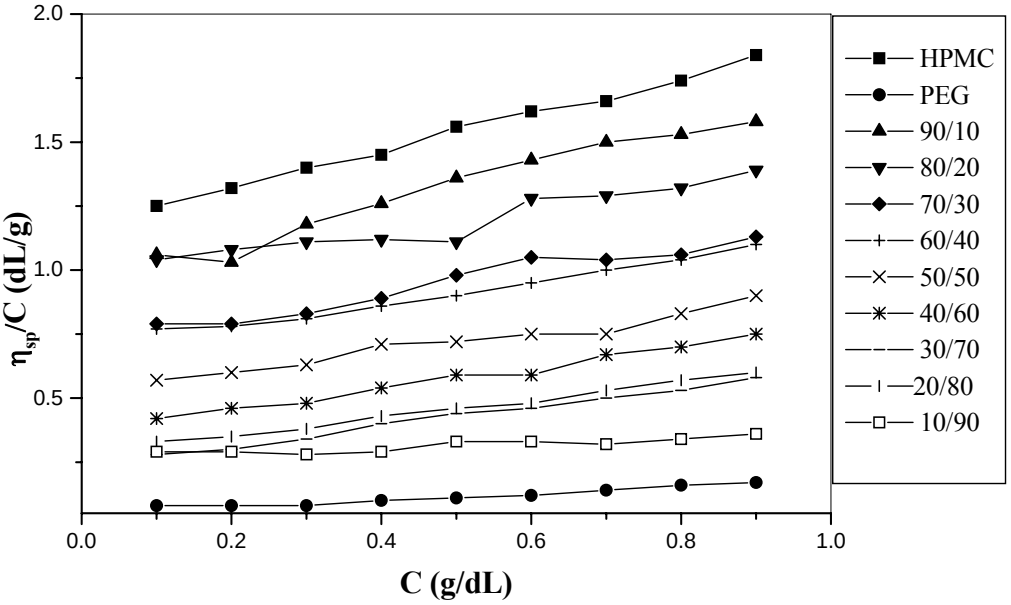

Figure 2. Huggin's plots for 1% w/v HPMC/ PEG blend in water at 50º C

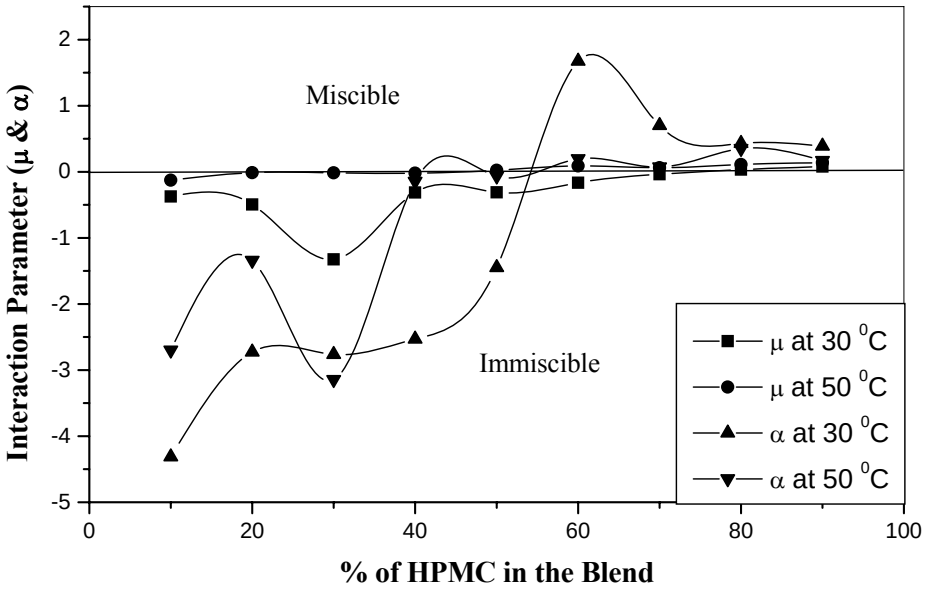

Figure 3: Effect of temperature on the interaction parameter μ and α of 1% w/v of HPMC/PEG blend in water at 30 and 50 °C

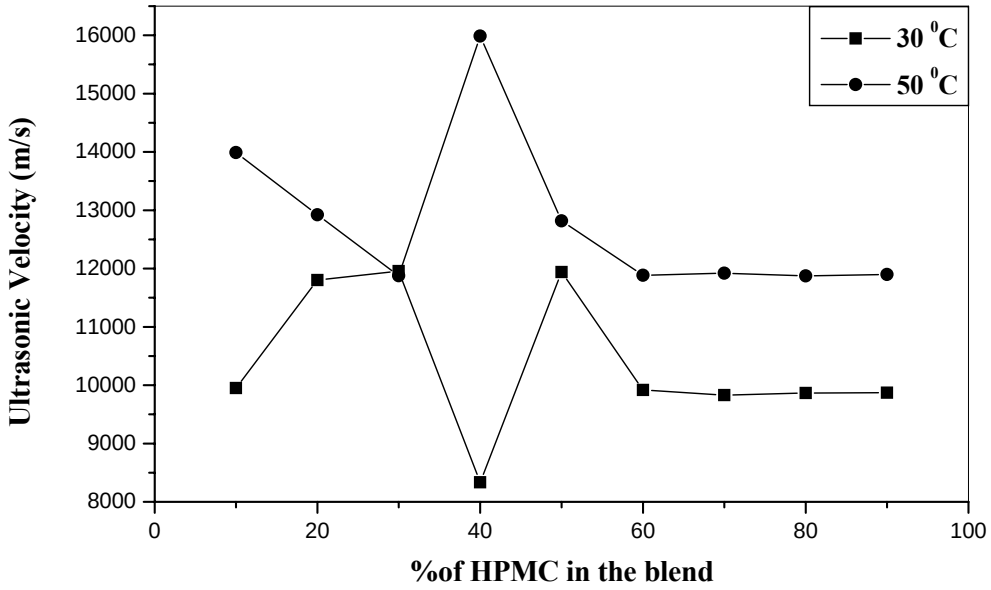

Figure 4: Effect of temperature on the variation of ultrasonic velocity of 1% w/v of HPMC/PEG blend in water at 30 and 50 °C

Kinetic studies on nanosilica production from sodium silicate in poly(vinyl alcohol) medium

***Renjanadevi.B and # K.E.George**

Department of Polymer Science and Rubber Technology, CUSAT, Kochi, India
renjana_b@rediffmail.com

Abstract

Kinetic studies on the production of silica in a nanoscale using poly(vinyl alcohol) (PVA) as surfactant was carried out in a batch reactor taking sodium silicate as raw material. The study included the effect of different process variables like sodium silicate, hydrochloric acid(HCl) and PVA concentrations, pH and drying time. All these factors have a significant effect on the nature and size of silica produced. It was found that the initial sodium silicate concentration of 15% (w/v) was the most favourable concentration producing highest yield of silica. Both acidic and basic catalysts were used in the synthesis and provided good results. A pH of 8 was found to be the most favourable. The concentration of HCl was found to be playing a critical role in the synthesis reaction and is used to determine the parameters like rate constant 'k' and reaction order 'n'. The value of the rate constant k is determined both by theoretical and experimental methods.

Key words: nanosilica, HCl, poly(vinyl alcohol), rate constant

Introduction

Nanoparticles are revolutionary materials that offer the possibility of tremendous added value. They posses large surface-to-volume ratios, high specific surface area, low bulk density and some additional properties of the actual material [1]. Silica can be manufactured in a nanoscale by a wet process by treating silicates with mineral acids in presence of a surfactant like poly vinyl alcohol(PVA) to obtain fine silica particles by precipitation [2]. The synthesis and characterization of nanosilica is of great interest as silica exhibits excellent properties. The method for obtaining amorphous types of silica could find numerous applications, particularly as polymer fillers. The tremendous applications of silica are in the fields of opto-electronics, nanocomposites, ceramics, rubber technology, biomedical materials, catalysis and chemical separations [3-5].

Several methods are used to produce nanosilica from various sources [6-12]. Bomal. et.al. reported a process for preparing precipitated silica comprising reacting a silicate with an acidifying agent to produce a suspension of precipitated silica and, then, separating and drying the suspension to obtain the precipitated silica as a dried product.The silica obtained has a good dispersibility and very satisfactory reinforcing properties. It also relates to new precipitated silicas which are in the form of powder, of substantially spherical beads or of granules, these silicas being characterized by the fact that they have a BET specific surface of between 90 and 250 m^2/g.Another study by Teofil Jesionowski studied preparation of amorphous silica via precipitation reaction from aqueous solution of sodium metasilicate and hydrochloric acid in emulsion medium, focusing on determination to optimize the dispersive and morphological properties of silicas. It is revealed that the properties of silicas precipitated from emulsion systems depend on several variables but the amount and concentration of the applied reagents and pH of the emulsion are of critical importance. Kim, Liu and Zachariah have suggested that the aerosol- assisted sol-gel method to produce nanosilica. In this method, Tetra ethoxy silane(TEOS),water and ethanol were allowed to react. Sufficient hydrolysis time was given and

then the solution was aerosolized with sodium chloride. Sodium chloride was employed both as an agent to accelerate the kinetics of silica generation and as a templating medium to support the formation and stability of pore structures. Ahamed et al, have synthesized nanosilica from rice hull. The method involved acid digestion, combustion at 700^{o}C and then milling to produce nanosilica. Kotoki et. al prepared poly vinyl alcohol/silica nanocomposite starting from sodium silicate with dilute hydrochloric acid as catalysts in poly vinyl alcohol. This is a sol-gel method in which the acid plays a catalytic role in enhancing sol-gel condensation of silicon alkoxides within the PVA. The reaction was carried out at 60^{o}C and pH maintained between 1-2.The reaction mixture was passed through cation exchange resin amberlite for the removal of sodium ions. After 24 hrs at ambient temperature it gelled and the samples were dried for 48 hrs at 47^{o}C.

Materials and Methods

Sodium silicate: Sodium silicate solution (60%) obtained from M/s Minnar chemicals, Kochi.

HCl : Hydrochloric acid(AR) manufactured by M/s Loba chemicals with an acidimetric assay of 35-38% .

Ammonia: AR grade ammonia manufactured by M/s Spectrum chemicals, Kochi, with an assay of 25% NH_3 and sp.gr. 0.91.

Poly vinyl alcohol: Poly vinyl alcohol manufactured by M/s Polex laboratories was used.

Preparation of chemicals

i) Sodium silicate Sodium silicate (15 wt %) was prepared by diluting one part of 60% solution with three parts of distilled water.

ii) Hydrochloric acid of strength 2N,3.5N,5N were prepared by diluting 5.6ml,9.7ml,13.9 ml of standard HCl to 100ml distilled water.

iii) PVA solutions of 1% & 5% were prepared by dissolving 1g and 5g of PVA in 100ml distilled water.

iv) AR grade ammonia was used as such without any dilution.

Experimental Procedure

The reaction was initially conducted on a laboratory scale with a reactor with a reactor volume of 500cm^3 for studying the kinetics and later developed into a large scale to get a more uniform product that can be used for polymer modification.

The required quantities of sodium silicate, HCl, PVA and ammonia in the volume ratio 20:14:1:1.5 were prepared.

A homogeneous mixture of 3.5N HCl, 1% PVA and ammonia in the desired ratio was made initially and it is then added to Sodium silicate solution (15%) with constant stirring and a constant heat supply of 60^{o}C.Distilled water was added to it as the solution becomes viscous and stirring becomes difficult. Stirring was continued for 2hrs and later kept at room temperature for 24 hrs. It was then filtered, washed, dried at a temperature of 100^{o}C for 5hrs and then milled to produce fine particles.

Estimation Methods

The amount of HCl reacted was estimated by titration method using NaOH solution and phenolphthalein indicator. Known volumes of sample collected from the reactor were titrated against 0.035N NaOH solution. The end point is pink colour. This procedure was continued till the concentration of HCl that remain unconverted in the reaction mixture was almost constant.

Results and Discussion

Effect of reaction parameters

Fig.1(a) &(b) shows the effect of pH on silica production. It was evident that the particle size decreased with addition of ammonia. The particle size is minimum when the pH is increased to about 8.0.After this value there is no effect of addition of ammonia as there is no change in the particle size. There is a corresponding change in the amount of impurities present in the product due to addition of ammonia. Increasing the pH results in the formation of ammonium chloride

and it remains unreacted. This will be easily removed by the wash water as it is more soluble than sodium chloride present as impurities in the system.

In the reaction between sodium silicate and HCl the rate of reaction depends on the amount of HCl converted. Hence to evaluate the rate constant k, the concentration of HCl in the reaction medium is determined at definite intervals.

The influence of acid concentration on the formation of silicais shown in Fig.2. In the reaction acid also plays a catalyst role in enhancing condensation of silica within PVA matrix. Acid provides extensive hydrogen bonding to the polymer and the developing poly-silicate network, enabling system homogeneity. Hence the acid concentration has a great influence in the uniform distribution of silica the PVA matrix. From the fig it was observed that when the acid concentration is lower, particle size is small. There is a sharp increase in the particle size as the concentration is raised from 3.5N to 5N.Thus the optimum concentration was found to be 3.5N HCl.

It was also observed that the concentration of sodium silicate also had a significant influence on the size of the silica particles obtained. Silica particles produced with 30% sodium silicate are coarser when compared to those obtained with 15% solution. Hence this concentration is found to be suitable for making nanosilica.

The impact of PVA on the particle size is given in Fig.3. It is observed that the particle size decreased with lower concentration of PVA. Hence a solution of 1% PVA is found to be suitable for producing nanosilica.

The variation of moisture with drying time for silica is given in figure 4. This was done by checking the moisture level in the cakes obtained at regular intervals of drying. It is seen that almost all the moisture was removed when a period of 5 hrs was chosen. Almost all the moisture has been removed by this time and there is no change in the moisture level if the drying time is increased further.

Determination of kinetic parameters

The information necessary for finding out the performance of the reactor used for silica synthesis are the rate constant and order of the reaction [13-15]. Based on this data the process can be scaled up to industrial level which can offer great potential for using silica for polymer modification.

The rate constant for the reaction of sodium silicate with HCl is determined based on the observation that the acid plays a significant role in the formation of silica particles. The concentration of HCl is used as a measure to find the reaction order and rate constant. The rate constant for the reaction is found out by estimating amount of HCl converted with time. The concentrations of sodium and ammonia are assumed to be constant during the course of reaction. The reaction rate is written to be of the form,

$$-r_A = k\, C_A^n \text{ ----- (1)}$$

where $-r_A$ = rate of disappearance of HCl with time = $(-dC_A/dt)$

C_A is the concentration of HCl.

k = rate constant for the reaction.

n = order of the reaction.

Taking logaritham on both sides of equation (1),

$$\ln -r_A = \ln k + n \ln C_A \text{ -------(2)}$$

A plot of $\ln -r_A$ vs $\ln C_A$ is made. The slope and intercept of the straight line obtained is determined. From these, the values of rate constant ‘k’ and reaction order ‘n’ are found out.

The $(-dC_A/dt)$ values are obtained either numerically or by graphical method[16-17]. In

the graphical method C_A vs time is plotted [18]. The slopes of the tangents drawn at various points in curve are taken as $(-dC_A/dt)$.

A plot of concentration vs time was made and is shown in Fig.5. From this graph $-dC_A/dt$ is calculated and the values are listed in Table1.

Fig.6 shows the plot of ln $(-r_{A)}$ vs ln C_A. The plot is a straight line and the slope of this line is equal to 2 which show that the reaction is of second order. Also from the intercept the value of the rate constant is found to be 0.0166 litre/mol.min.

Non-linear least squares analysis

This is a useful method to determine the rate law parameters [16-17]. In non-linear least squares analysis we search for those parameter values that minimize the sum of squares of the differences between the measured values and the calculated values for all the data points. Here we make estimates of parameter values such as reaction order and specific rate constants in order to calculate the rate of reaction, r_c. Then search for those values that minimize the sum of the squared differences of the measured reaction rate, r_m , and the calculated reaction rates,r_c. Now select the value if the parameters such that sum of $(r_m-r_{c)}^2$ is minimum. The variance is calculated according to the equation,

$$\sigma = \frac{S^2}{(N-K)} = \sum \frac{(r_{im} - r_{ic})^2}{N-K}$$

where N - is the number of runs

K - Number of parameters to be determined.

r_{im} - measured reaction rate for run i

r_{ic}- calculated reaction rate for run i

Now consider the silica synthesis reaction, the rate equation is assumed to be of the form $-r_A= k\ C_A^n$ where k is the reaction rate and n is the reaction order. For these parameters values were chosen and the rate is calculated as r_{ic} at each concentration at which an experimental point was taken. Then the sum of the squares of the difference $(r_{im}- r_{ic})$ was found out. This procedure is continued by further varying k and n until their best values, that is, those values that minimize the sum of squares. The values of k and n that minimize the sum of squares were taken as the theoretical values and the data were tabulated in table.2. It was then compared with the experimental values and the percentage error is determined. This is shown in fig.7.

Conclusion

- The concentration of HCl and sodium silicate influences the production of silica and its size.
- A pH of 8 in the reaction medium is found to be the most favourable for silica synthesis.
- The value of the reaction rate constant k is determined from a batch experiment as 0.016litre/mole.min which is found to be consistent with the theoretical methods. The reaction is found to be of second order and these data can be used for analyzing the performance of the continuous reactors used for the synthesizing silica on a large scale.

References

[1] Y.Li,J.Yu and Z.X.Guo//J.Appl.Polymer Science,84(2002),827

[2] S.K.Dolui andTapasi Kotoky, Journal of Sol-Gel Science and Technology 29, 107-114, 2004.

[3] Hideo.M;Yutaka,S;Sumio,T.Polypropylene Resin composition for automobile component parts. Japanese Patent JP 9165478

[4] Rothon, R. Particulate-Filled Polymer Composites; Longman: Essex, UK.,1995.

[5] Mizutani.Y.; Nago, S. Microporous Polypropylene Films Containing Ultrafine Silica Particles.

J. Appl. Polym. Sci.1999,72,1489.

[6] A. Krysztafkiewicz, Chemia Stosowana 28 (1984) 477.

[7] A. Krysztafkiewicz, Chemia Stosowana 31 (1987) 127.

[8] B. Marciniec, A. Krysztafkiewicz, L. Domka, Colloid Polym.Sci. 261 (1983) 306.

[9] Stober W., Fink A., Bohn E., J. Colloid Interface Sci., 26 (1968),62.

[10] Ulrich Schubert and Nichola Husing, " Synthesis of Inorganic Materials", Wiley, New York.

[11] Jal P.K., Sudarshan M. Shah A, Sabitha Patel and Mishra B.K., "Synthesis and Characterization of NanoSilica prepared by precipitation method".www.sciencedirect.com.

[12] Kenneth J. Klabunde, " NanoScale Materials in Chemistry", Wiley interscience.

[13] Smith, Chemical Engg. Kinetics, 2d ed, Mc Graw Hill, New York.

[14] Daniel and Wood, Fitting Equations to data, Wiley, New York, 1980.

[15] Frost and Pearson, Kinetics and Mechanism, 2d ed., Wiley, New York, 1961

[16] Hill, An Introduction to Chemical Engineering Kinetics and Reactor Design, Wiley,New York,1977.

[17] Mezakiki and J.R. Kittrell, AIChE J., 14, 513, 1968.

[18] J.R. Kittrell, Ind.Engg.Chem.,61, 5,76-78,1968.

[19] Octave Levenspiel, Chemical Reaction Engineering, 3d ed, Wiley, New York,1999.

[20] Weber, Chem.Eng.Prog., 49,1953,26-34.

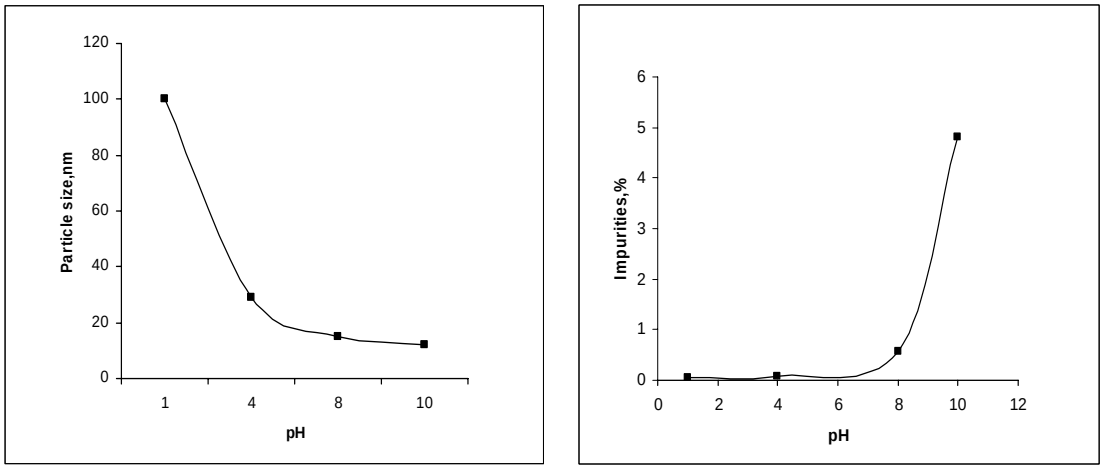

(a) **(b)**

Fig.1 (a)&(b) Effect of pH on synthesis if silica from sodium silicate.

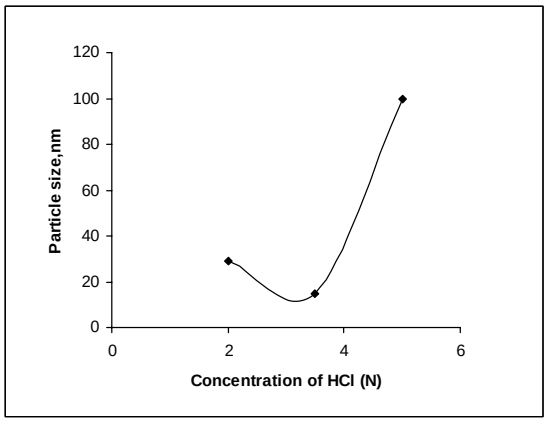

Fig.2 The influence of acid concentration on the formation of silica

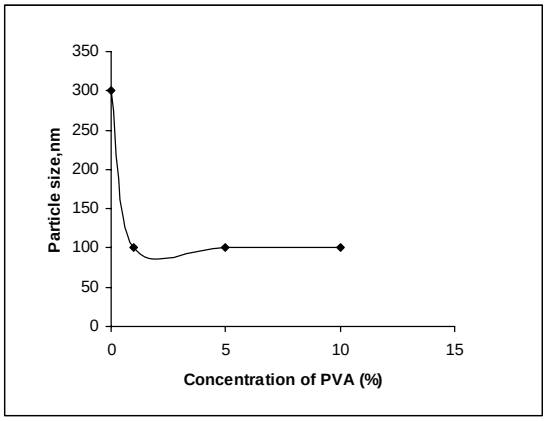

Fig.3 The impact of PVA surfactant on the particle size**.**

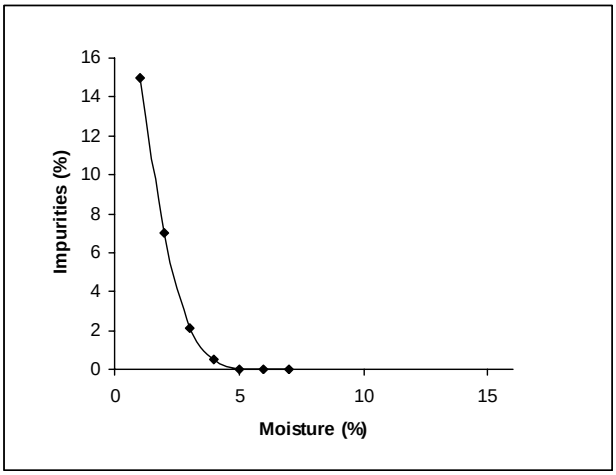

Fig.4 The variation of moisture with drying time for silica.

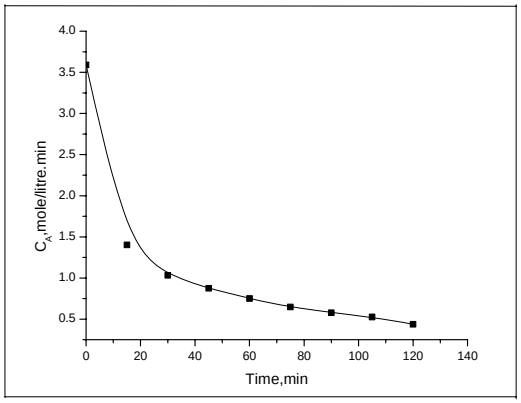

Fig.5 Plot of concentration vs time

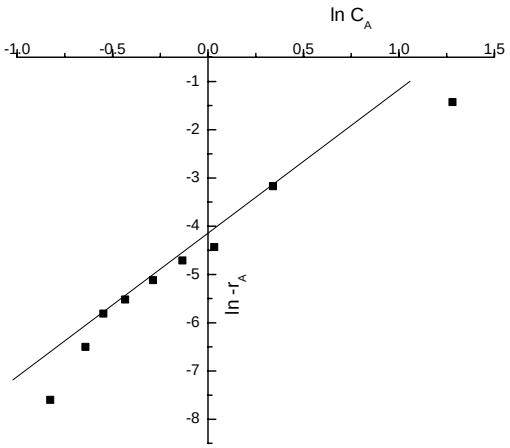

Fig.6 Plot of ln $-r_A$ vs ln C_A

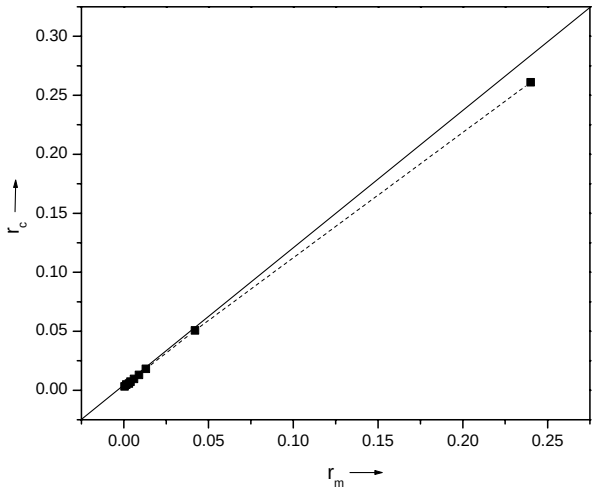

Fig.7 Plot of measured rate versus calculated rate.

Table1. Concentration-time data

Time, minutes	C_A mol/litre.min	- (dC_A/dt)
0	3.591	0.24
15	1.401	0.042
30	1.033	0.013
45	0.875	0.009
60	0.75	0.006
75	0.645	0.004
90	0.578	0.003
105	0.526	0.002
120	0.438	0.001

Table 2. Minimizing the sum of the squared differences

Data			Trial 1 k = 1, n=1 $r_c = 1 \times 3.59 = 3.59$		Trial 2 k = 0.017, n = 3		Trial3 k = 0.05, n = 3		Trial4 k =.15, n = 2		Trial 5 k = 0.017, n = 2	
Run	C_A	r_m	$r_m - r_c$	$(r_m - r_c)^2$	$r_m - r_c$	$(r_m - r_c)^2$	$r_m - r_c$	$(r_m - r_c)^2$	$r_m - r_c$	$(r_m - r_c)^2$	$r_m - r_c$	$(r_m - r_c)^2$
1	3.59	0.24	-3.35	11.22	2.073	4.299	-0.404	0.1635	-0.021	4.37×10^{-4}	-0.547	0.229
2	1.40	0.042	1.359	1.85	0.096	9.14×10^{-3}	-0.056	3.2×10^{-3}	8.6×10^{-3}	7.12×10^{-5}	4.8×10^{-3}	2.29×10^{-5}
3	1.03	0.013	1.021	1.04	0.042	1.78×10^{-3}	-0.040	1.63×10^{-3}	5.16×10^{-3}	2.66×10^{-5}	5.8×10^{-3}	3.33×10^{-5}
4.	0.88	0.009	0.866	0.75	0.025	6×10^{-4}	-0.029	8.6×10^{-4}	4.02×10^{-3}	1.61×10^{-5}	2.39×10^{-3}	5.7×10^{-6}
5.	0.75	0.006	0.744	0.55	0.015	2.28×10^{-4}	0.022	4.9×10^{-4}	3.56×10^{-3}	1.27×10^{-5}	1.17×10^{-3}	1.37×10^{-6}
6.	0.65	0.004	0.644	0.42	9.6×10^{-3}	9.23×10^{-5}	0.017	2.89×10^{-4}	3.14×10^{-3}	9.86×10^{-6}	6.28×10^{-4}	3.4×10^{-7}
7.	0.58	0.003	0.575	0.33	6.65×10^{-3}	4.43×10^{-5}	0.014	1.88×10^{-4}	2.68×10^{-3}	7.18×10^{-6}	2.83×10^{-4}	7.99×10^{-8}
8.	0.53	0.002	0.525	0.28	5.78×10^{-3}	3.34×10^{-5}	0.012	1.52×10^{-4}	3.2×10^{-3}	1.03×10^{-5}	9.74×10^{-4}	9.48×10^{-7}
9.	0.44	0.001	0.438	0.19	3.7×10^{-3}	1.37×10^{-5}	0.009	8.27×10^{-5}	2.76×10^{-3}	7.63×10^{-6}	9.28×10^{-4}	8.62×10^{-7}
				16.63		4.299		0.17		2.61×10^{-3}		0.402
			$S_1^2 = 16.63$ $\sigma_1^2 = \frac{16.63}{2}$ $= 8.315$		$S_2^2 = 4.299$ $\sigma_2^2 = 2.15$		$S_3^2 = \frac{0.17}{2}$ $\sigma_3^2 = 0.085$		$S_4^2 = 2.61 \times 10^{-3}$ $\sigma_4^2 = \frac{0.00261}{2}$ $= 0.0013$		$S_5^2 = 0.402$ $\sigma_5^2 = 0.201$	

Trial No: 4 gives the lowest value for σ^2. Hence it is chosen

$\therefore$ Theoretical value of rate constant k is takes as = 0.017 litre/mole.min

Synthesis, photopolymerization and characterization of linear alicyclic (meth)acrylates

R. Harikrishna* and C. R. Rajan
Polymer Science and Engineering Division,
National Chemical Laboratory, Pune – 411008, India.

E-mail: r.harikrishna@ncl.res.in

Abstract

A number of parameters govern the photo chemical performance of oligomeric macro monomers. The photopolymerizable macromonomers normally have an average molecular mass ranging from 1000 to 10000. They are synthesized using three major constituents: (1) A diepoxide or polyol with a molecular mass ranging from 200 to 3000, (2) aliphatic, alicyclic or aromatic diisocyanates or diacids and (3) vinyl or allyl terminated mono, di or triacrylate / methacrylate with at least one hydroxyl group or carboxylic acid group. This work describes the synthesis of linear polyurethane macro monomers with alicyclic moieties and (meth)acrylate end functionalities. Formulations made from one or more polymeric macro monomers, one or more photoinitiators were analyzed for photo curing performance using differential photocalorimetry.

The photocuring can be studied using differential photocalorimetry (DPC) , which gives the cure characteristics at applied intensity and range of wavelengths. The heat flow against time is recorded under isothermal conditions and the rates of polymerization as well as the percentage conversion are estimated. Isothermal kinetics, throws light on parameters such as the onset time, induction time and time to attain peak maximum. The synthesis as well as photopolymerization of the system is discussed.

1. Introduction

UV curable materials contain photoreactive oligomer(s)[1] and curing agents. Differential photocalorimetry[2-3] is one of the accurate methods to study the radical and cationic photopolymerizations. This method helps in optimizing photopolymerization. Formulations can have a di or multifunctional crosslinking additive with (meth)acrylate terminations added to them to facilitate cross linking. The photopolymerization kinetics has been studied extensively for many systems[4]. The order of propagation is highly influenced by the diffusion controlled polymerization which sets on after a certain limiting conversion has reached. The photopolymerization kinetics in a photo DSC measurement can depend on many factors such as concentration of photo initiator, type of monomers used, reaction temperature, nature of purge gas, type of crosslinking agent, intensity and wavelength of irradiation.

It is known that photopolymerization reactions have particular behaviours, such as autoacceleration [5], unequal functional group reactivity [6] and temporary free volume excess [7]. The temporary free volume increase during the initial stages of photopolymerization will increase the radical diffusivity with an initial increase in rate of conversion. However the polymerization rate will get reduced with time due to limitation in radical diffusion caused by an increase in viscosity of the system with conversion as well as translational, segmental and reaction diffusion associated with it [4].

2. Experimental

Materials

Isophorone diisocyanate (IPDI, from Fluka), Polytetrahydrofuran 250 (PTHF 250, from Aldrich), Polyethylene glycol 1500 (PEG 1500, from sd fine), PPG 3000 (from Aldrich) 2 – hydroxy ethyl methacrylate (HEMA, from Aldrich), 1,4-diazabicyclo[2.2.2.] octane (DABCO, from Aldrich), hydroquinone monomethyl ether (HQME, from Fluka), 2,2-dimethoxy-2-phenyl acetophenone (IRGACURE 651*, from Aldrich), diphenyl-(2,4,6-trimethylbenzoyl) phosphine oxide (IRGACURE TPO*, from Aldrich), 1-hydroxycyclohexyl phenyl ketone (IRGACURE 184*, from Aldrich), 2-hydroxy–2- methyl propiophenone (DAROCUR 1173*, from Aldrich)
* Trademark of Ciba Speciality Chemicals, Switzerland.

Synthesis of urethane acrylate macromonomer

The base prepolymer was synthesized by the addition of 9 mL (42.47 m mol) of isophorone diisocyanate in to a 100 ml three necked glass reaction vessel which was initially purged with nitrogen and connected to an over head stirrer. The stirring was done at 150 rpm. 10 mL (40 m mol) of polytetrahydrofuran 250, 1 g (0.66 m mol) of PEG 1500 and 5 mL (1.66 m mol) of PPG 3000 was added to it. The system was stirred at 70^{o}C under nitrogen atmosphere for a period of 12 hours to obtain diisocyanate terminated prepolymer. The percentage of residual isocyanate was calculated by the dibutyl amine back titration method. To the synthesized prepolymer was added 11 g (84.5 m mol) of 2 hydroxy ethyl methacrylate followed by addition of 120 mg (1.07 m mol) of DABCO as catalyst. 200ppm of HQME was added as stabilizer and the reaction was continued at 60^{o}C for 2 hours until all the isocyanate group at 2268 cm^{-1} was completely consumed by IR spectroscopy.

^{13} C NMR ($CDCl_3$): 27.56, 37.37, 41.86, 46.50 (isophorone ring), 164.70 (CH_2=C(CH_3)-<u>C</u>O-O) ppm.
IR: 1698 (C=O, urethane), 3329 and 1532 (N-H, urethane), 813 (C=C, methacrylate), 1112 and 1196 (C-O), 3000, 2943, 2959(C-H) cm^{-1}.

Formulations for photopolymerization

The photoinitiators of choice were IRGACURE 651, IRGACURE TPO, IRGACURE 184 and DAROCUR 1173. The mixing of photoinitiator with the synthesized acrylate was done on glass vials in 1g batch sizes. 0.5% of photoinitiator was homogenized with the macromonomer to obtain the photopolymerizable formulation. The isothermal photocalorimetry was studied at 30, 50 and 80^{o}C. The studies of the formulation at 18.71 and 31.19 mW/ cm^2 were also carried out.

Photopolymerization studies

DSC Q 100 differential scanning calorimeter connected to Q Series PCA was used for the online monitoring of the photopolymerization process. The formulation was homogenized in the glass sample tube using a vortex stirrer. About 10 mg of the sample was used for analysis under a nitrogen purge of 50 ml / minute. The equilibration of the system was done for a period of one minute prior to irradiation. The irradiation was done for a period of 5 minute under a constant photo flux from the machine.

3. Results and discussion

The rate of photopolymerization was calculated from the Photo DSC heat flow measurements. If ΔH_t / dt represent the heat flow per unit time, then the rate of photopolymerization is given by [2]

$Rp = (\Delta H_t / dt) / \Delta H_{total}$.

Where Rp is the rate of photopolymerization, ΔH_t / dt is the heat flow for a fractional time period and ΔH_{total} is the total heat flow for complete polymerization of the system. This was taken as the total heat flow for a period of 20 minutes of irradiation of the sample. On integration of the above expression the corresponding conversion can be obtained. Hence the percentage conversion of the monomer was calculated using the expression

Percentage Conversion = ΔH_t / ΔH_{total} x100

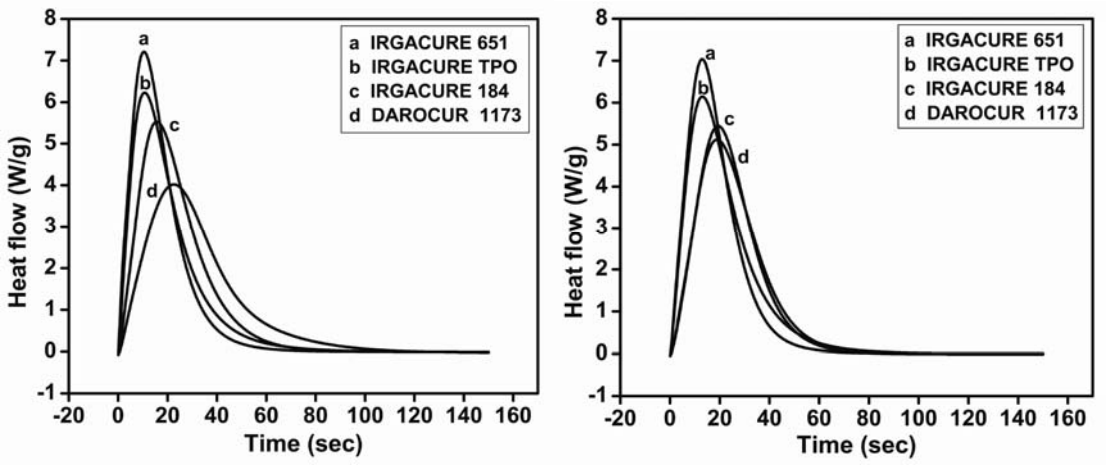

Fig-1 The heat flow Vs time profile at 50 ^oC of the formulation with 0.5% of all the four photoinitiators at (a) 18.71 and (b) 31.19 mW/ cm^2.

The above figure shows that the rate of heat flow of photopolymerization of the system consisting of IRGACURE 651 shows a higher rate than the other photoinitiators at the same concentration at 18.71 mW / cm^2. This rate is not much enhanced on increasing the intensity of irradiation. An overall increase in the concentration of the photoradicals will occur in the case of all the photoinitiators involved in the photopolymerzation studies. But a marked increased in rate is observed in the case of DAROCUR 1173 on increasing the intensity of irradiation. This is due to the increase in concentration of photoradicals which can effectively initiate photopolymerization on irradiation at higher intensites. The total number of effective free radicals which can initiate the photopolymerization is found to depend upon an optimum concentration. This concentration of effective radicals will vary for different systems due to many parameters such as autoacceleration, temporary free volume excess, segmental and reaction diffusions as well as the nature of the photopolymerizable system.

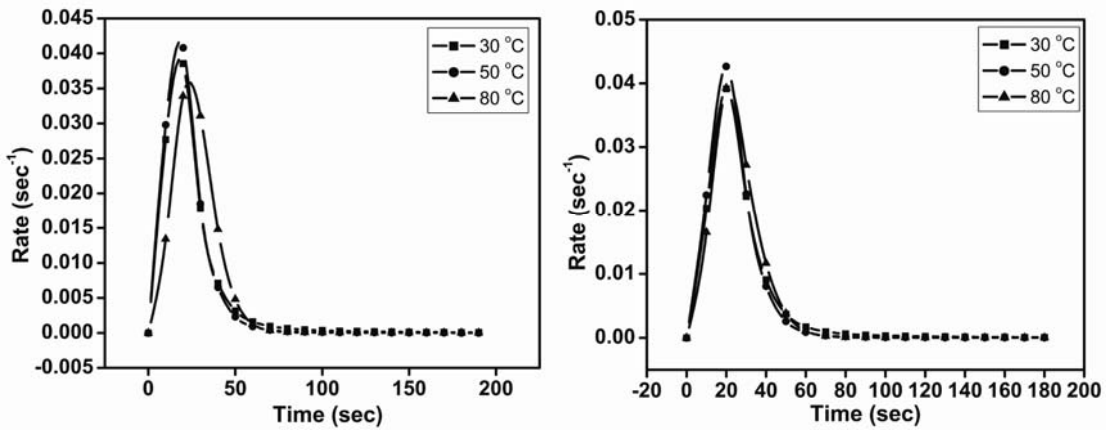

Fig-2 The time dependent rate of photopolymerization profile of the formulation containing IRGACURE 651 at three different isothermal conditions using an intensity of (a) 18.71 and (b) 31.19 mW/ cm^2.

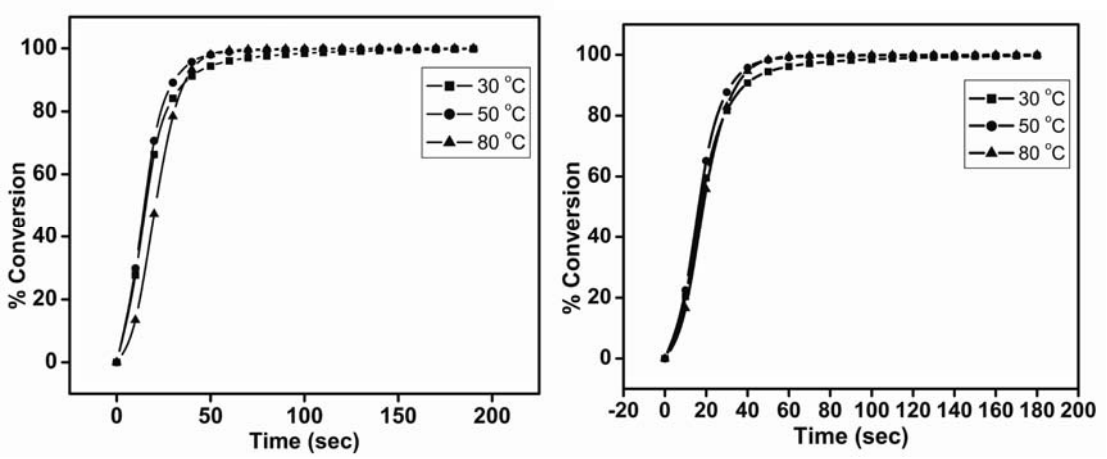

Fig-3 The time dependent percentage conversion profile of the formulation containing IRGACURE 651 at three different isothermal conditions using an intensity of (a) 18.71 and (b) 31.19 mW/ cm^2.

Figures 2 and 3 provides and analysis of IRGACURE 651 at three different isothermal conditions and two different intensities. From the plots we can infer that the rate of photopolymerization is found to increase with an increase in the isothermal condition from 30 to 50 ^{o}C. But a decrease in rate is observed instead of a further increase in rate at 80 ^{o}C. The rate of photopolymerization is found depend on the extent of concentration and diffusion of free radicals formed insitu in the reaction. If the concentration increases beyond a threshold value for a system, the matrix will allow a rapid radical radical recombination. This recombination can lead to an abrupt drop of the effective free radicals which can initiate the photopolymerization which inturn results in a reduction in the rate of photopolymerization. The rate of initiation of photopolymerization is propotional to the intensity of absorbed radiation while the rate of propagation is found to depend on the square root of the intensity of absorbed radiation [8]. As a result, from the

initial stage itself at higher intensities an abrupt increase in photopolymerization rate is observed. Hence a nearly doubling of intensity will increase the autoacceleration step and hence a higher temporary free volume is created at the initial stage of photopolymerzation for the analysis done at higher intensities. This effect will not be so much pronounced in the case of autoaccelareation which can occur in the case of increase in temperature from 50 to 80 ^{o}C.

4. References

1. Webster G (1996) Chemistry and technology of UV & EB formulation for coatings, inks and paints, Vol. 2: Prepolymers and reactive diluents, Chapter3. 1st edn. Sita Technology, London
2. Pamedytyte V, Abadie MJM, Makuska R (2002) J Appl Polym Sci 86: 579.
3. J.D.Cho, H.T.Ju, Y.S.Park and J.W.Hong., Macromol. Mater. Eng. 291 (2006) 1155 – 1163.
4. Andrzejewska E (2001) Prog Polym Sci 26: 605
5. Allen P, Simon G, Williams D, Williams E. (1989) Macromolecules 22:809
6. Bowman CN, Peppas NA (1992) Chem Engg Sci 47: 1411
7. Bowman CN, Peppas NA (1991) Macromolecules 24:1914
8. Odian G Principles of polymerization Fourth Ed. John Wiley, NY.

Initiation of cationic polymerization using allyl phosphonium salts in presence of free radical initiators

Mukesh Kumar Gupta and Raj Pal Singh*

Polymer Science and Engineering Division, National Chemical Laboratory,
Pune – 411 008, India.

E-mail: rp.singh@ncl.res.in

Abstract

The objective of present study was to examine the initiation efficiency of novel addition fragmentation agents, namely 2-(N, N-Dimethylcaboxy-propenyl) triphenylphosphonium hexafluoroantimonate (DMTPH) and 2-(Morpholinocarboxy-propenyl) triphenyl phosphonium hexafluoroantimonate (MTPH) in cationic polymerization. Thus, the present study describes the synthesis of amide based allylic phosphonium salts (DMTPH and MTPH) with hexafluoroantimonate counter anion and examines their initiation activity as an addition fragmentation agent both in the presence and the absence of added thermal radical initiator in cationic polymerization of cyclohexene oxide (CHO). The thermo-latent activity of these salts in accelerating the polymerization of CHO was investigated at 70 °C.

Keywords: cationic polymerization, addition fragmentation agent, allyl phosphonium salts, thermal initiation

Introduction

In last few decades, importance of latent cationic initiators, which show activity by external stimulation such as heat or light, have been recognized in number of different industrial applications such as microelectronics, photolithography, curing and adhesives [1]. Many technologically important monomers such as vinyl ethers and cyclic oxiranes, are polymerizable in cationic mode, therefore, development of more efficient photo and thermal latent cationic initiators are desirable [2-7]. The use of free radical sources in combination of allylic onium salt is an easy and flexible way to generate active species for cationic polymerization. The desirable features of this process involve accessibility of appropriate radical sources with broad range of absorption characteristics and temperature, which have been successfully utilized in free radical promoted cationic polymerization. Yagci et al. have employed various allylic onium salts such as sulfonium salts [8-9], pyridinium salts [10], allyloxy pyridinium salts [11-12], anilinium [13] salts etc in

* Corresponding author

photocationic polymerization. Earlier, Yagci et al. have developed acrylates based on allylic phosphonium salts as photo and thermo-latent initiators in cationic polymerization [14]. To the best of our knowledge, the chemistry of amide based phosphonium salt, as an addition fragmentation agent in thermally initiated cationic polymerization has not been studied. Therefore, the present study describes the synthesis of novel amide based phosphonium salts (**DMTPH** and **MTPH**) and examines their efficiency as an addition fragmentation agent in conjugation of thermal radical sources in cationic polymerization.

Experimental

Materials

N, N-Dimethylacrylamide, acryloylmorpholine and cyclohexene oxide (CHO), was purchased from Aldrich chemicals. All other chemicals (> 99 %) were purchased from S.D. Fine Chemicals Ltd, Mumbai, India. 2-(bromomethyl)- N, N-dimethyl acryl amide [15], 2-(bromomethyl)-acryloylmorpholine [15] and Phenyl azo triphenyl methane (PAT)[16] were prepared as reported. Monomer (CHO) was distilled over CaH_2 and used just before polymerization.

Synthesis of 2-(N, N-Dimethylcaboxy-propenyl) triphenylphosphonium hexafluoro antimonate (DMTPH)

To a solution of Ph_3P (5 mmol, 1.31 g) in toluene (10 mL), 2-(bromomethyl)- N, N-dimethyl acrylamide (**BMDMA**) (5 mmol, 1.04 g) was added and allowed to stir for 1 h. The resulting white precipitate was dissolved in H_2O and washed with *n*-hexane. Finally, $NaSbF_6$ was added to the aqueous part in one portion. The resulting white precipitate was filtered, washed with water and dried under vacuum. Yield: 2.2 g (77 %), white crystals, ^{1}H NMR (CD_3CN): δ = 7.6-8.1 (m, 15 H, Ph), 5.55 (s, 2 H, CH_2), 4.41, 4.34 (s, 2H, $=CH_2$), 2.86, 2.66 (s, 3H, $-NCH_3$) ppm.

Synthesis of 2-(Morpholinocarboxy-propenyl) triphenylphosphonium hexafluoro antimonate (MTPH)

This compound was synthesized in the similar manner as described for **DMTPH.**

Yield: 2.8 g (79 %), white crystals, ^{1}H NMR (CD_3CN): δ = 7.6-8.1 (m, 15 H, Ph), 5.53 (s, 2H, CH_2), 4.41, 4.34 (s, 2H, $=CH_2$), 3.52 (t, 4H, $-NCH_2$), 3.35 (t, 4H, $-OCH_2$) ppm.

Characterization

Molecular weight of polymers was measured by gel permeation chromatography (GPC) in chloroform as eluent (flow rate: 1 mL/min) on a setup consisting of a pump and six Ultra Styragel column (50 to 10^5 Å porosities) and detection was carried out with the aid of UV-100 and RI-150

detectors. NMR spectra were recorded on a Brüker 200 MHz instrument with $CDCl_3$ and acetonitrile (for initiators) as solvent and tetramethylsilane as internal standard.

Polymerization procedure

A mixture of monomer and initiator (with or without radical source) was placed in a flame dried ampoule equipped with three way stopcock connected to manifold and degassed for 30 min with three freeze-pump-thaw cycles and sealed off. The ampoule was immersed in an oil bath at constant temperature. After the reaction for a set temperature, polymerization mixture was dissolved in DCM and precipitated with excess methanol then dried under vacuum at ambient temperature. The conversion of monomer was determined by gravimetrically.

Results and discussion

Initiator synthesis

The allylic phosphonium salts (**DMTPH** and **MTPH**) were synthesized by reaction of corresponding allyl bromide with triphenylphosphine (Ph_3P) followed by anion exchange of bromide (Br^-) with hexafluoroantimonate (SbF_6^-) anion. The structure of initiators was well characterized by ^1H NMR, IR and elemental analysis as described in experimental section (Scheme 1).

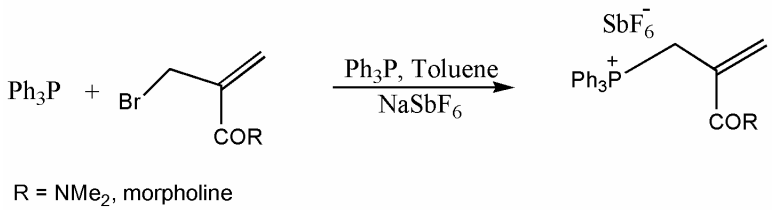

Scheme 1. Synthesis of amide based allylic phosphonium salts

Polymerization

For the polymerization reactions, CHO was used as model monomer for cationic polymerization with phosphonium salts due to non-polymerizable nature of CHO using free radicals.

Polymerization in the absence of radical sources

Figure 1 shows, temperature-conversion curve for polymerization of CHO in absence of added free radical source.

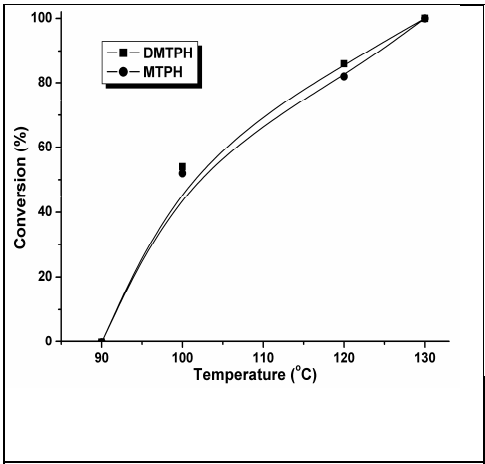

Figure 1. Temperature-conversion curve in polymerization of CHO with allylic phosphonium salts in the absence of radical sources for 2 h

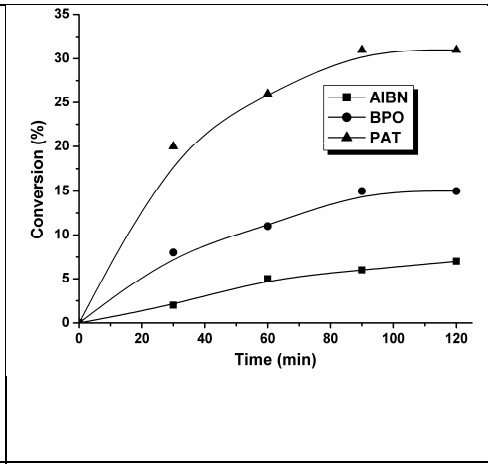

Figure 2. Time-conversion curve in polymerization of CHO with **DMTPH** in the presence of radical sources at 70 °C

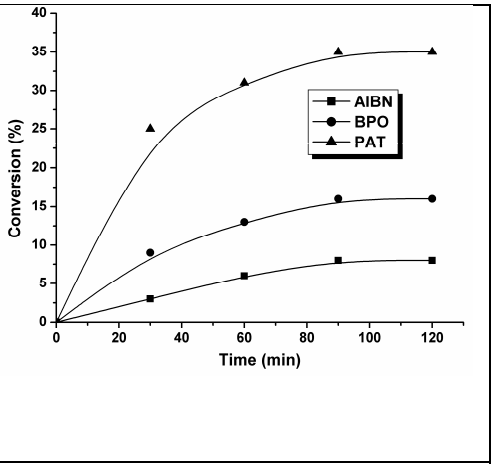

Figure 3. Time-conversion curve in polymerization of CHO with **MTPH** in the presence of radical sources at 70 °C

Polymerization in the presence of radical sources

The bulk polymerization of CHO was performed with 0.1 mol % of phosphonium salt initiators (**DMTPH** and **MTPH**) in the presence of free radical sources (namely **AIBN**, **BPO** and **PAT**) at 70 °C up to 2 h (Table 1).

Table 1. Thermal polymerization of CHO initiated by thermal radical sources [a]

Initiator	Radical source	Time (min)	Conversion[b] (%)	M_n (M_w/M_n)[c]
DMTPH	**PAT**	60	35	5600 (1.69)
	BPO	120	16	6766 (1.94)
	AIBN	120	8	6600 (1.84)
MTPH	**PAT**	60	31	6000 (1.79)
	BPO	120	16	6900 (1.81)
	AIBN	120	7	8200 (1.62)

[a]Conditions; monomer: initiator: radical source = 5 mol l^{-1} : 5 x 10^{-3} mol l^{-1}: 5.0 x 10^{-3} mol l^{-1}, [b]determined gravimetrically, [c]determined by GPC based on polystyrene standards.

Figure 2 shows the time-conversion curve for the polymerization of CHO with **DMTPH** in the presence of thermal radical source (**AIBN**, **BPO** and **PAT**). It can be seen that with increase in reaction time, polymerization of CHO proceeds with each phosphonium salt/radical source combination and attains respective limiting conversion. The limiting conversion with **PAT**, **BPO** and **AIBN** was found as 35 (60 min), 16 (120 min) and 8 (120 min), respectively. The order of initiator activity was observed as **PAT** > **BPO** > **AIBN**.

Figure 3 shows the time-conversion curve for the polymerization of CHO with **MTPH** in the presence of radical sources (Table 1). It also shows an increase in percentage conversion with the increase in reaction time. The limiting conversion with **PAT**, **BPO** and

AIBN was found as 31 (60 min), 16 (120 min) and 7 (120 min), respectively. The order of initiator activity was observed as **PAT** > **BPO** > **AIBN**. This can be explained by the difference in the decomposition rate constant and the reactivity of radical toward the double bond of phosphonium salts [17].

The molecular weight (M_n) of polymers was found in the range of 5600-8200. The above results suggest that in presence of radical source, the polymerization rate of CHO can be speed up, whereas no polymerization was observed in the absence of radical sources even at 90 ^oC.

Conclusions

The amide based allylic phosphonium salts were synthesized and successfully used as thermo-latent initiator in the presence of free radical source as addition fragmentation agent in cationic polymerization. Without use of radical source, conversion starts above 90 ^oC. The rate of polymerization can be accelerated with the use of free radical source at 70 ^oC and was observed as **PAT** > **BPO** > **AIBN**. It can also be concluded that a wide range of thermal radical source can be employed to tune the conditions to enhance the rate of polymerization.

Acknowledgement

Authors are grateful to Dr. S. Sivaram, Director, NCL, Pune for providing necessary facilities and fruitful discussions. MKG thanks CSIR, New Delhi, for the award of senior research fellowship.

References

1 S. P. Pappas *UV Curing Science and Technology*; Technology marketing corporation, Norwalk CT, **1978**.
2 J. V. Crivello, *Adv. Polym. Sci.* **1984**, 1, 62.
3 Y. Yagci, I. Reetz, *Prog. Polym. Sci.* **1998**, 23, 1485.
4 J. V. Crivello, *J. Polym. Sci, Polym Chem Ed*. **1999**, 37, 4241.
5 Y. Yagci, Y. Yuksel, D. B. Aydogan, *The Chemical Record* **2007**, 7, 78.
6 Y. Yagci, I. Reetz, *Reactive and Functional Polymers* **1999**, 42, 255.
7 Y. Yagci, A. Onen, I. Reetz, *Macromol Symposia* **2001**, 174, 255.
8 S. Denizligil, Y. Yagci, C. MacArdle, *Polymer* **1995**, 36, 3093.
9 S Denizligil, Y Yagci, C MacArdle, J P Fouassier, *Macromol. Chem. Phys*. **1996**, 197, 1233.
10 M. Onciu, A. Onen, Y. Yagci, *Polym. Int.* **2001**, 50, 144.
11 I. Reetz, V. Bacak, Y. Yagci, *Macromol. Chem. Phys*. **1997**, 198, 19.
12 I. Reetz, V. Bacak, Y. Yagci, *Polym. Int.* **1997**, 43, 27.
13 A. Onen, Y. Yagci, *Macromolecules*, **2001**, 34, 7608.
14 L. Atmaca, I. Kayihan, Y. Yagci, *Polymer* **2000**, 41, 6035.
15 M. Davoust, J-F. Briere, P. Metzner, *Org. Biomol. Chem*. **2006**, 4, 3048.
16 R. G. Kyager J. P. Lorand, N. R. Stevenes, N. R. Herron. *J. Am Chem Soc* **1977**, 99, 7589.
17 Y. Yagci, A. Onen, *J. Polym. Sci., Polym. Chem*. **1996**, 34, 3621.

Miscibility studies of HPMC/PEG blends in water by viscosity, density, refractive index and ultrasonic velocity method

Sudhir Ramswamy Illiger[1]; Chandralekha Fadnis[1]; T. Demappa[1]*; J. Jayaraju[2] and J. Keshavayya[2]

[1] Department of Post-Graduate Studies and Research in Polymer Science, University of Mysore, Sir M.V.PG .Center, Tubinakere, Mandya, 571402, Karnataka, INDIA
[2] Department of Chemistry, School of Chemical Sciences, Jnana Sahyadri, Kuvempu University, Shankaraghatta-577 451, Shimoga, Karnataka, India
Email: tdemappa2003@yahoo.co.in

ABSTRACT:

Hydroxy propyl methyl cellulose (HPMC) / Polyethylene glycol (PEG) blends are edible polymer films used for food packing and directly in foodstuffs. However they are water-soluble in ordinary temperature and have good mechanical properties. The miscibility of HPMC/PEG blend in water was studied by viscosity, ultrasonic velocity, density and refractive index techniques at 30 and 50º C. Using viscosity data, the interaction parameters μ and α were calculated. These values revealed that HPMC/PEG blend is miscible when the HPMC content is more than 60 wt-% in the blend at 30 and 50º C, below which is immiscible. Further the result was also confirmed by ultrasonic velocity, density, refractive index measurements, which also revealed that the change in temperature has no significant effect on the miscibility of HPMC/PEG polymer blend.

Keywords: **b**lend, density, hydroxy propyl methylcellulose, miscibility, poly(ethylene glycol), refractive index, ultrasonic velocity, viscosity.

1. Introduction

The importance of polymer blending has been increased in recent years, because of the preparation of polymeric materials with desired properties, low basic cost and improved process ability. Polymer blends are physical mixtures of structurally different polymers or co-polymers, which interact through secondary forces with no covalent bonding (Krause, 1978) and are miscible at molecular level. The basis of polymer-polymer miscibility may arise from any specific interactions, such as hydrogen bonding, dipole-dipole forces and charge transfer complexes for homopolymer mixtures (Varnell & Coleman, 1981; Varenell, Rant, Cdeman, 1983; Woo, Barlow & Paul, 1986). There have been various techniques of studying the miscibility of the polymer blends (Crispim, Rubira, Muniz, 1999; Patel, 2004; Ping, 1997; Jiang, Han, 1998; Cabanclas, Serrano & Baselga, 2005). Some of these techniques are complicated, costly and time consuming. Hence it is desirable to identify simple, low cost and rapid techniques to study the miscibility of polymer blends. Chee and Sun et al (Chee, 1990; Sun, 1992) have suggested a viscometric method for the study of polymer-polymer miscibility in solution. Singh and Singh (Singh, 1984; Singh, 1983) have suggested the use of ultrasonic velocity and viscosity measurements for investigating the polymer miscibility in solution. Paladhi and Singh (Palladi, 1994 a; Palladi and Singh, 1994 b) have shown that the variation of ultrasonic velocity and viscosity with blend composition is linear for miscible blends and non-linear for immiscible blends. Recently, Varada Rajulu et al (Varada Rajulu, Reddy, Ranga

Reddy, 1998) have used ultrasonic and refractometric technique to study the miscibility of polymer blend.

As part of our research work, we have studied the miscibility of HPMC/PEG blend in water at different temperatures by viscosity, ultrasonic velocity, density, and refractive index techniques (Demappa et al., 2006; 2007). We selected these polymers, because they have many pharmaceutical and biomedical applications (Zeng, Fang, 2004; Jumel, Harding, 1996). Hydroxy propyl methyl cellulose (HPMC) is a polysaccharide prepared from cellulose. It contains both methyl and hydroxy propyl substitutes. Poly (ethylene glycol) (PEG) is a synthetic water-soluble polymer with good film forming property, which offers good tensile strength (TS), flexibility and barrier properties to oxygen and aroma (Schellekens & Bastiansen, 1991). Poly (ethylene glycol) (PEG) is used in all applications of aqueous phase partitioning. For biochemical separations on the laboratory scale, the most commonly used aqueous phase system is composed of Dextron and PEG (Albertson, P.A., New York,1986) The structures of both HPMC and PEG are shown in scheme 1 and scheme 2 respectively.

2. Experimental

HPMC (E 15 LV premium; LOBA CHEMIE PVT LTD) and PEG ($\overline{M}_w = 200$; AR grade, Merck India Ltd., India) were used for this work. A dilute polymer solution of 1% w/v was prepared for viscometric studies. Stock solutions of homopolymers and the blends of HPMC/PEG of different compositions, 10/90, 20/80, 30/70, 40/60, 50/50, 60/40, 70/30, 80/20 and 90/10, were prepared in water. Viscosity measurements at 30 and 50 ºC were made using an Ubbelohde suspended level viscometer with the flow time of 98 s for distilled water. The total weight of the two components in the solution was always maintained at 1 g/dL. And the different temperatures were maintained in a thermostat bath, with a thermal stability of ± 0.05ºC. The ultrasonic velocity measurements were performed by an ultrasonic interferometric technique (Varada Rajulu, 1996). The temperatures were maintained at 30 and 50º C by circulating water from a thermostat, with a thermal stability of ± 0.05ºC, through the double–walled jacket of the ultrasonic experimental cell. The experimental frequency was 2-MHz, and the velocity measurements were accurate to better than ±0.5%. The densities of the solutions were measured at 30 and 50º C by specific gravity bottle. The refractive indices of the HPMC/PEG blend solutions were measured using an Abbe's refractometer, with a thermostat water-circulation system (Varada Rajulu, Mabusab, 1998) at 30 and 50 ºC (Singh, & Singh, 1984). The accuracy of the refractive index measurements is ± 0.02%.

3. Results and Discussion

HPMC, however, is known to be a flexible nonionic polymer, which obeys the classical Huggin's equation. The Huggin's plots for the pure components (HPMC and PEG) and their blends at 30 and 50º C are shown in figure 1, 2 & table 1, 2 respectively. The figure indicates the considerable higher slope variation for 80/20 and 60/40 HPMC/PEG blend compositions. This may be attributed to the mutual attraction of macromolecules in solution, because of the increase of hydrodynamic and thermodynamic interaction. Hence HPMC/PEG blend is found to be miscible, only when the HPMC content is more than 60 % in the blend. Below this critical concentration, a sharp decrease in the slope is observed in the Huggin's plot because of the phase separation.

To quantify the miscibility of the polymer blends Chee (Chee, 1990) suggested that the general expression for interaction parameter when polymers are mixed in weight fractions w_1 and w_2 is as follows:

$$\Delta B = \frac{b - \bar{b}}{2w_1 w_2} \qquad (1)$$

Where $\bar{b} = w_1 b_{11} + w_2 b_{22}$ in which, b_{11} *and* b_{12} are the slopes of the viscosity curves for the pure components. The coefficient b is related to the Huggin's coefficient K_H as

$$b = K_H [\eta]^2 \qquad (2)$$

for ternary systems, the coefficient b is also given by

$$b = w_1^2 b_{11} + w_2^2 b_{22} + 2w_1 w_2 b_{12} \qquad (3)$$

where b_{12} is the slope for the blend solution. Using these values, Chee (Chee, 1990) defined a more effective parameter as follows:

$$\mu = \frac{\Delta B}{\{[\eta]_2 - [\eta]_1\}^2} \qquad (4)$$

where $[\eta]_1$ and $[\eta]_2$ are the intrinsic viscosities for the pure component solutions. The blend is miscible when $\mu \geq 0$ and immiscible when $\mu < 0$ (Chee, 1990). The values of μ, calculated with the aforementioned expression at 30 and 50º C are represented in Table 3.

Recently, Sun et al (Sun, 1992) have suggested a new formula for the determination of polymer miscibility as follows:

$$\alpha = K_m - \frac{K_1 [\eta]_1^2 w_1^2 + K_2 [\eta]_2^2 w_2^2 + 2\sqrt{K_1 K_2}\,[\eta_1][\eta_2] w_1 w_2}{\{[\eta]_1 w_1 + [\eta]_2 w_2\}^2} \qquad (5)$$

where K_1, K_2 and K_m are the Huggin's constants for individual components 1, 2 and the blend, respectively. The long-range hydrodynamic interactions are considered while deriving this equation. Sun et al (Sun, 1992) have suggested that a blend will be miscible when $\alpha \geq 0$ and immiscible when $\alpha < 0$.The computed values of μ and α are found to be negative when the HPMC content is up to 50% and then positive beyond this value at 30 and 50º C, respectively and the data are given in Table 3 and Figure 3 shows the miscibility windows of the HPMC/PEG blend in water. As the long-range hydrodynamic interactions are considered in the equation for α, eq (5) is more accurate than eq (4). A similar observation was made by Varada Rajulu et al and Jayaraju et al (Varada Rajulu, 1998; Jayaraju, 2006) in case of polyvinyl pyrrolidone/ polystyrene and Chitosan/Hydroxypropyl methyl cellulose blends, where μ was found to be negative and α was found to be positive. They confirmed the miscibility of such blends by other methods. To confirm this further, we have measured the ultrasonic velocity (ν), density (ρ) and refractive index (n) of the blend under consideration at various compositions, at 30 and 50ºC. These values are presented in Table 3. The variation of the ultrasonic velocity in figure 4, density and refractive index with the blend composition is shown in fig 5 respectively. The adiabatic compressibility β_{ad} (Varada Rajulu, 1990) of different blend compositions was evaluated by using the equation.

$$\beta_{ad} = \frac{1}{v^2 \rho} \qquad (6)$$

Where v is the velocity of sound and ρ is the density of blend solutions, and the values are given in Table 3. The variation of adiabatic compressibility at 30 and 50 º C is shown in Figure 5. The graphs show both linear and nonlinear regions. It was already established (Cabanclas et al and

Sun et al) that the variation is linear for miscible blend and non-linear for immiscible blend. In the present case, the variation is found to be linear when the HPMC content is more than 60 % at 30 and 50º C respectively. This observation is in confirmation with μ and α value. So the present study indicates the existence of miscibility windows when the HPMC content is more than 60 % in the blend. This is because, the specific interaction between the polymer segments is more when the HPMC content is more than 60%, there by, leading to miscibility of the blend. And below this composition there will not be much interaction between the polymer segments, which leads to immiscibility of the polymer blend. Here, the miscibility of the blend may be due to some specific interaction like H-bonding between HPMC/PEG.

4. Conclusion

Using viscosity, Ultrasonic velocity, density and refractive index methods, it is concluded that the polymer blend of HPMC/PEG is found to be miscible, when the HPMC content is more than 60 % in the blend at 30 and 50º C respectively. Below this HPMC concentration, the blends were found to be immiscible. It is also observed that temperature has no significant effect on the miscibility of these blends even though the reduced viscosity, density, refractive index and adiabatic compressibility decreases and the ultrasonic velocity increases as the temperature increases. Thus afore mentioned techniques are simple, low cost, rapid and efficient methods in exploring the miscibility windows of HPMC/PEG blend in solution.

References

Albertson, P.A.-Partition of cell particles and macromolecules, 3rd ed; Wiley: New york, 1986.

Crispim, E.G; Rubira, A.F; Muniz, E.C. (1990).Solvent effect on the miscibility of poly(methyl methacrylate) /poly(vinyl acetae) blends : using differential scanning calorimetry and viscometry technique.*polymer 1999; 40,5129*.

Cabanclas, J.C; Serrano, B; Baselga.J (2005). Development of continous morphologies in initially heterogeneous thermosets blended with poly (methyl methacrylate). *Journal of Macromolecules, 38,961.*

Chee, K.K. Determination of polymer–polymer miscibility by viscometry. (1990). *European Polymer Journal, 26, 423.*

Demappa, T., Basavaraju, K.C and Rai, S.K. (2006). Preparation of chitosan and its miscibility studies with gelatin using viscosity, ultrasonic and refractive index. *Carbohydrate Polymers, 66,357.*

Demappa, T., Basavaraju, K.C, and Rai, S.K. (2007), Miscibility studies of Polysaccharide Xanthan gum and PEO (Polyethylene Oxide) in dilute solution. *Carbohydrate Polymers, 69,462.*

Jiang , W.H; Han, S.(1998). An improved criterion of polymer –polymer miscibility determined by viscometry. *European Polymer Journal,,34,1579.*

Jumel,K; Harding,S.E; Hayter.I. (1996).Molar mass and viscometric charecterization of hydroxy Propyl methylcellulose. *Carbohydrate Polymer, 29,105.*

Jayaraju, J., Raviprakash, S.D., Keshavayya, J., and Rai, S.K.(2006). Miscibility Studies on Chitosan/Hydroxy propyl methyl Cellulose Blend in Solution by Viscosity, Ultrasonic Velocity, Density, and Refractive Index Methods. *Journal of Applied Polymer Science,102, 2738.*

Krause, S. In Polymer–Polymer Compatibility in Polymer Blends; Paul,D.R., and

Seymour, N., Eds.; Academic Press: NewYork, 1978; Vol. 1.
Patel,M.(2004).viscoelastic properties of polystyrene using dynamic rheometry. Polymer Test, 23,107.
Ping, Z.(1997).A new criterion of polymer –polymer miscibility detected by viscometry. *European Polymer Journal, 33,411.*
Palladhi, R., Singh, R.P. (1994a). Miscibility and interaction studies on some aqueous polymer blend solution by ultrasonic and rheological techniques. *Journal of Applied Polymer Science, 51, 1559*
Palladhi, R., Singh, R.P.(1994b). Ultrasonic and rheological investigation on interacting blend solutions of poly (acrylic acid) with poly (vinyl pyrrolidone) of poly (vinyl alcohol). *European Polymer Journal, 30,251.*
Schellekens, R., Bastiansen, C.J. (1991). A drawing behaviour of polyvinyl alcohol fibers. *Journal of Applied Polymer Science, 43, 2311.*
Sun, Z., Wang, W., Fung, Z.(1992) Criterion of polymer-polymer miscibility determined by viscometry. *European Polymer Journal, 28,1259.*
Singh, Y.P., Singh, R.P.(1984)Compatibility studies on polyblends of PVC with chlororubber-20 and its graft polyblends by ultrasonic. *European Polymer Journal, 20,535*
Singh, Y.P.,Singh, R.P.(1983). Miscibility studies on polymer blends by viscometric and ultrasonic techniques. *European Polymer Journal, 19, 535*
Varnell,D.F, Coleman, M.M. (1981).FTIR, Studies of polymer blends,pt5: Further observations on polyester-poly (vinyl chloride) blends. *Polymer, 22,1324*
Varenell, D.F, Runt, J.P, Coleman, M.M.(1983), Fourier Transform infrared studies of polymer blends, further observations on the poly (bisphenol -A. carbonate) –poly (e-caprolactone) system. *Polymer, 24,37*
Varada Rajulu,A; Reddy,R.L; Ranga Reddy,R.N.V.(1998).Ultrasonic and viscometric investigation of cellulose acetate /poly (methyl methacrylate) blends in solution *Acoustica ,84,577.*
Vararda Rajulu, A., Mabusab, P.(1996). Ultrasonic studies of water/poly (ethylene glycol) mixtures. *European Polymer Journal, 32,267.*
Varada Rajulu,A;Mabusab,P.(1998). Refractometric studies in water /polethylene glycol-300 mixtures. *European Polymer Journal, 34,31*
Varada Rajulu,A; Siddaramaiah; Reddy,R.L. (1998). Ultrasonic,refractometric and viscosity studies of some polymer blends in solution. *Journal of Applied Polymer Science, 70,1823.*
Varada Rajulu, A; Rao,K.C; Naidu,S.V.(1990). Miscibility studies on chitosan/ hydroxypropyl cellulose .... *Journal of pure Applied Ultrason.. 12,115.*
Woo, E.M , Barlow, J. W.Paul, D.R. (1986). Phase behaviour of blends of aliphatic polyesters with a vinylidine chloride copolymer. *Journal of Applied Polymer Science, 32,3889.*
Zeng, M; Fang.Z;Xu,C. (2004).Novel method of preparing microporous membrane by selective dissolution of chitosan/polyethylene glycol blend membrane. *Journal of Applied Polymer Science,,91,2840.*

Table 1: The reduced viscosity data for HPMC/PEG and their blends in water at 30 °C

Concentration (g/dL)	η_{sp}/C (dL/g) at 30 °C										
			HPMC/PEG Blend composition								
	HPMC	PEG	90/10	80/20	70/30	60/40	50/50	40/60	30/70	20/80	10/90
0.1	1.40	0.09	1.22	1.16	1.11	0.90	0.69	0.58	0.38	0.33	0.21
0.2	1.54	0.12	1.38	1.25	1.42	0.96	0.72	0.64	0.42	0.33	0.22
0.3	1.67	0.12	1.39	1.32	1.20	0.99	0.79	0.64	0.42	0.36	0.25
0.4	1.79	0.15	1.51	1.37	1.25	1.05	0.82	0.68	0.45	0.41	0.23
0.5	1.93	0.17	1.58	1.42	1.27	1.07	0.83	0.72	0.52	0.42	0.25
0.6	2.07	0.18	1.65	1.50	1.31	1.19	0.86	0.73	0.55	0.43	0.29
0.7	2.21	0.20	1.78	1.61	1.38	1.21	0.95	0.76	0.57	0.42	0.28
0.8	2.33	0.20	1.98	1.64	1.46	1.26	0.95	0.80	0.58	0.42	0.29
0.9	2.46	0.23	1.99	1.74	1.49	1.30	0.99	0.85	0.62	0.47	0.29

Table 2: The reduced viscosity data for HPMC/PEG and their blends in water at 50 °C

Concentration (g/dL)	η_{sp}/C (dL/g) at 50 °C										
			HPMC/PEG Blend composition								
	HPMC	PEG	90/10	80/20	70/30	60/40	50/50	40/60	30/70	20/80	10/90
0.1	1.25	0.08	1.06	1.04	0.79	0.77	0.57	0.42	0.28	0.33	0.29
0.2	1.32	0.08	1.13	1.08	0.79	0.78	0.60	0.46	0.30	0.35	0.29
0.3	1.40	0.08	1.18	1.11	0.83	0.81	0.63	0.48	0.34	0.38	0.28
0.4	1.45	0.10	1.26	1.12	0.89	0.86	0.71	0.54	0.40	0.43	0.29
0.5	1.56	0.11	1.36	1.11	0.98	0.90	0.72	0.59	0.44	0.46	0.33
0.6	1.62	0.12	1.43	1.28	1.05	0.95	0.75	0.59	0.46	0.48	0.33
0.7	1.66	0.14	1.50	1.29	1.04	1.00	0.75	0.67	0.50	0.53	0.32
0.8	1.74	0.16	1.53	1.32	1.06	1.04	0.83	0.70	0.53	0.57	0.34
0.9	1.84	0.17	1.58	1.39	1.13	1.10	0.90	0.75	0.58	0.60	0.36

Table 3 : Interaction parameters, density, refractive index, ultrasonic velocity and adiabatic compressibility of HPMC/PEG blend at 30 and 50˚ C

Composition HPMC/PEG	Interaction Parameter				Ultrasonic velocity		Density		Refractive Index		Adiabatic Compressibi	
	μ	α	μ	α	(m/s)		(g/cm^3)		(n)		(Kg^{-1} ms^2) 1	
	30 °C		50 °C		30 °C	50 °C	30 °C	50 °C	30 °C	50 °C	30 °C	50
10/90	-0.3736	-4.3120	-0.1275	-2.6998	9950	13990	1.0337	1.0312	1.341	1.339	0.9990	0.4
20/80	-0.4942	-2.7278	-0.0140	-1.3419	11803	12923	1.0379	1.0305	1.342	1.347	0.6650	0.5
30/70	-1.3249	-2.7632	-0.0162	-3.1464	11956	11876	1.0349	1.0313	1.340	1.338	0.6760	0.6
40/60	-0.3138	-2.5312	-0.0205	-0.1469	8336	15987	1.0348	1.0290	1.341	1.339	1.3906	0.3
50/50	-0.3095	-1.4488	0.0233	-0.0660	11940	12818	1.0364	1.0308	1.340	1.337	0.6777	0.5
60/40	-0.1652	1.6743	0.0879	0.1948	9918	11886	1.0353	1.0300	1.341	1.339	0.9699	0.6
70/30	-0.0368	0.7001	0.0616	0.0715	9831	11920	1.0355	1.0305	1.341	1.339	0.9990	0.6
80/20	0.0320	0.4302	0.1105	0.3506	9865	11875	1.0359	1.0311	1.341	1.339	0.9920	0.6
90/10	0.0781	0.3880	0.1372	0.1691	9870	11899	1.0361	1.0316	1.341	1.339	0.9890	0.6

Scheme 1: structure of HPMC

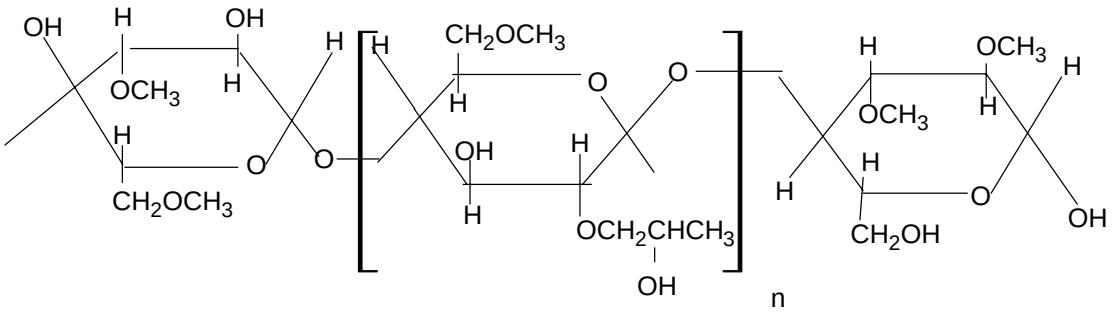

$C_8H_{16}O_8$ $(C_{10}H_{18}O_8)_n$ $C_8H_{16}O$

Scheme 2: structure of PEG

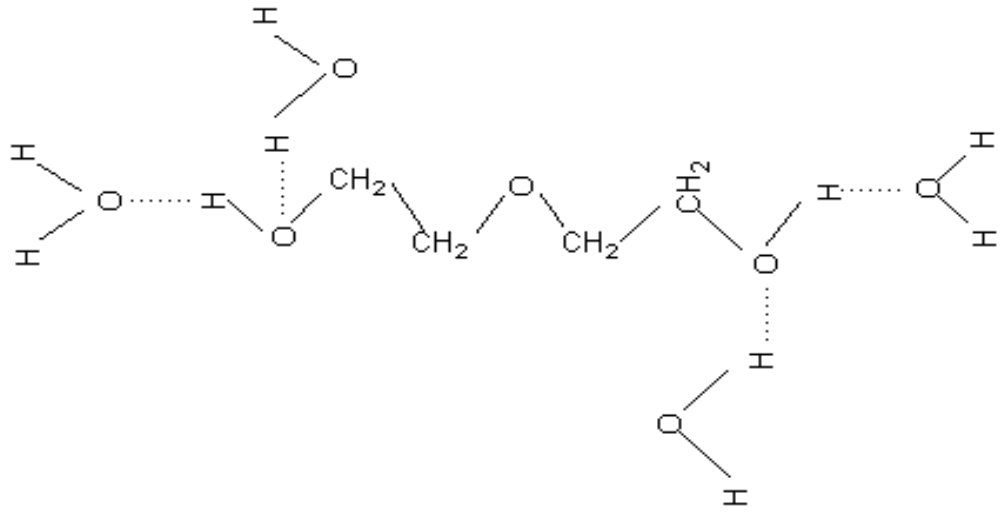

Polyethylene glycol

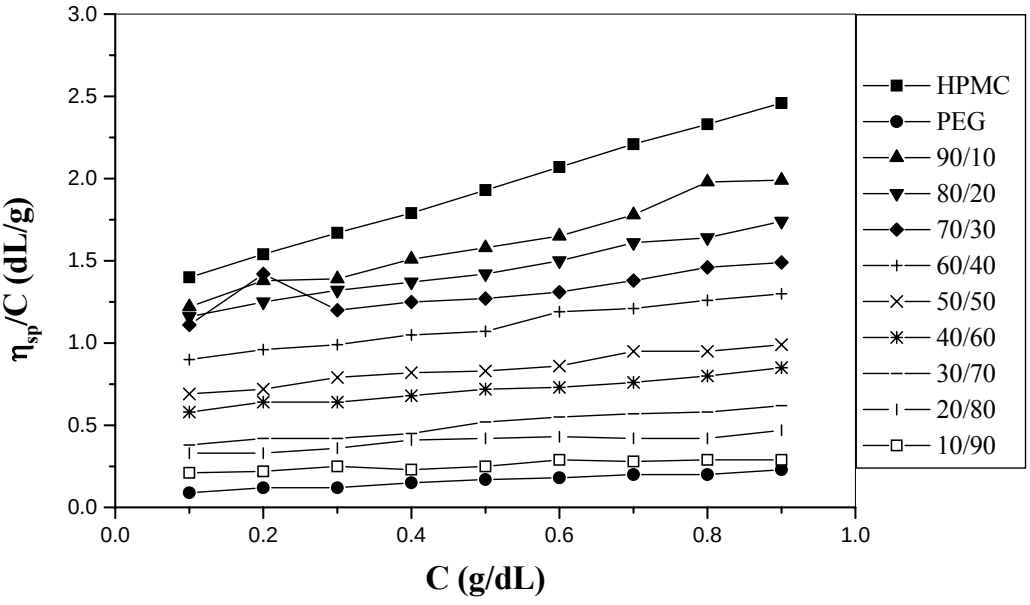

Figure 1. Huggin's plots for 1% w/v HPMC/PEG blend in water at 30ºC

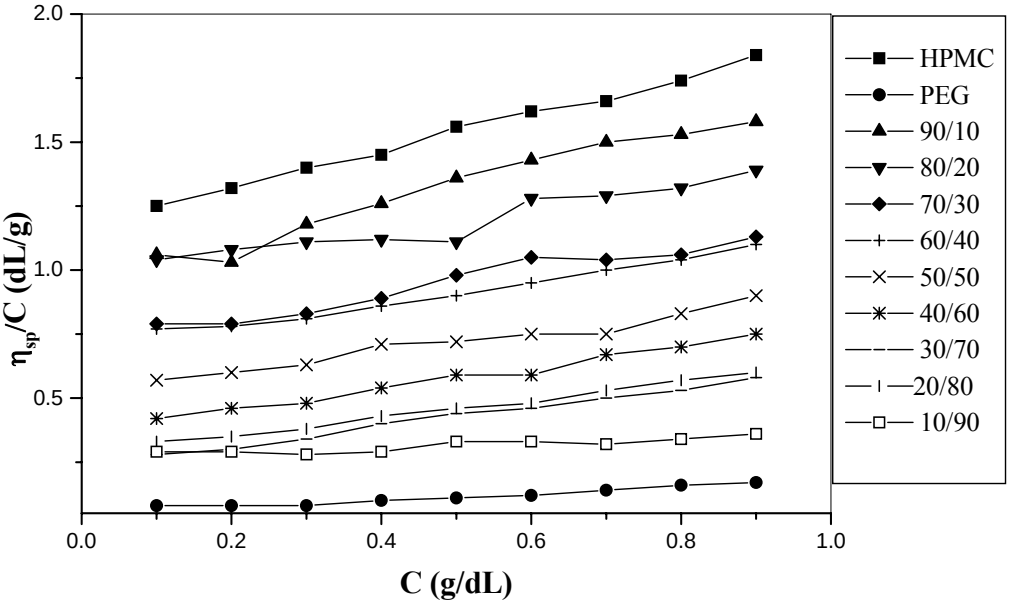

Figure 2. Huggin's plots for 1% w/v HPMC/ PEG blend in water at 50º C

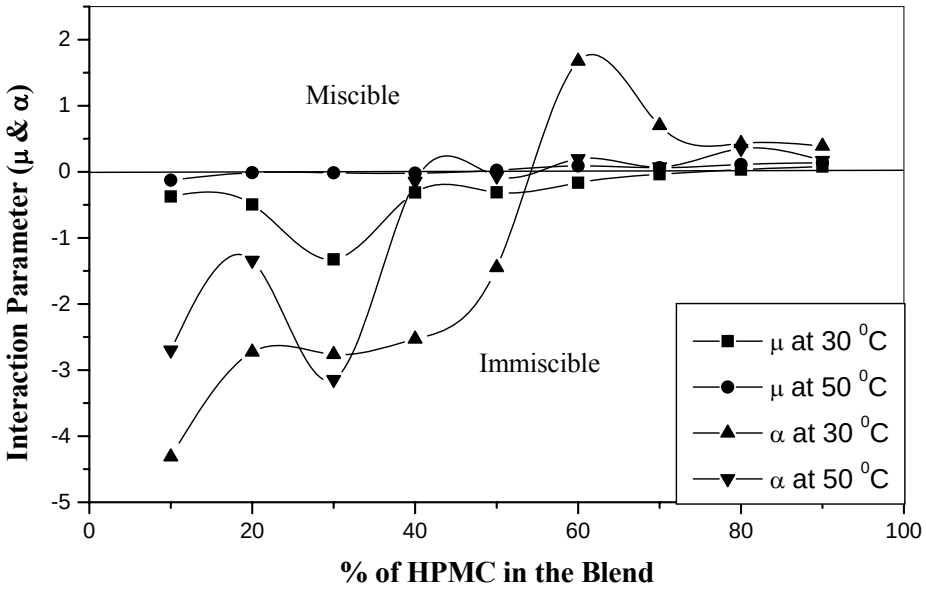

Figure 3: Effect of temperature on the interaction parameter μ and α of 1% w/v of HPMC/PEG blend in water at 30 and 50 °C

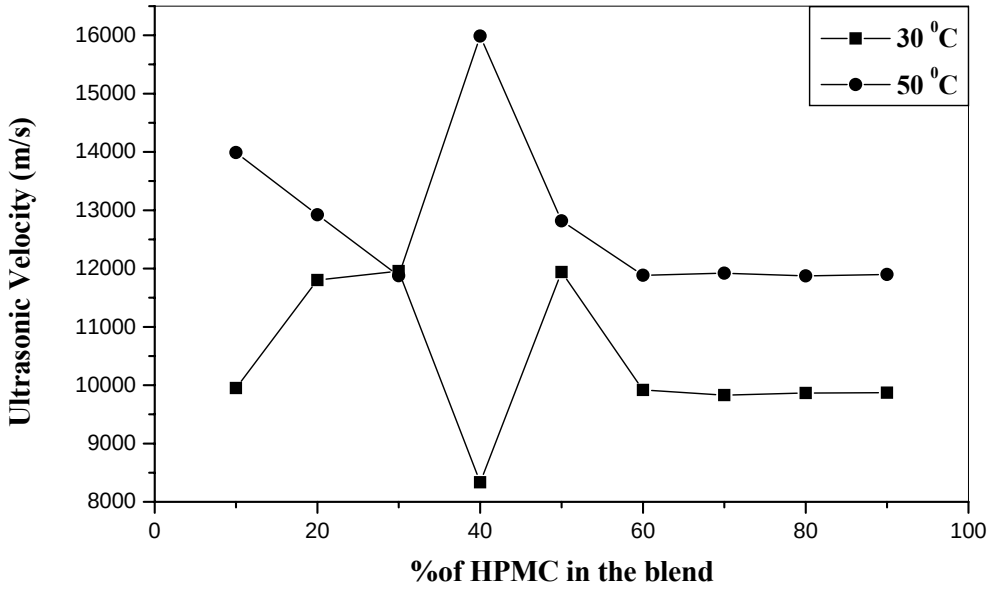

Figure 4: Effect of temperature on the variation of ultrasonic velocity of 1% w/v of HPMC/PEG blend in water at 30 and 50 °C